Fibroblast signaling pathways in regulation of mammary gland morphogenesis

Jakub Sumbal

FACULTY OF MEDICINE,
DEPARTMENT OF HISTOLOGY
AND EMBRYOLOGY

ÉCOLE DOCTORAL
COMPLEXITÉ DU VIVANT

GENETICS AND
DEVELOPMENTAL BIOLOGY
(UMR3215/U934)

Fibroblast signaling pathways in regulation of mammary gland morphogenesis

Doctoral thesis

MUDr Jakub SUMBAL

Supervisors:	Silvia FRE, PhD (Sorbonne Université)
	doc MVDr Aleš HAMPL, CSc (Masaryk University)
Reviewers:	Colinda SCHEELE, PhD (KU Leuven)
	Mariaceleste ARAGONA, Ph.D. (University of Copenhagen)
Examiners:	René Marc MEGE, PhD (Institut Jacques Monod)
	Lucie PEDUTO, PhD (Institut Pasteur)
	Peter FABIAN, PhD (Masaryk University)
President of the Jury:	Fréderic DEVAUX, PhD (Sorbonne Université)

Programme: Biomedical Sciences — Brno 2024

ED515 Complexité du Vivant — Paris 2024

Bibliographic record

Author: Jakub Sumbal
Faculty of Medicine, Masaryk University
Institut Curie, Sorbonne Université

Title of Thesis: Fibroblast signaling pathways in regulation of mammary gland morphogenesis

Degree Programme: Biomedical Sciences| Complexité du Vivant

Supervisors: Silvia FRE, PhD & doc. MVDr Aleš HAMPL, PhD

Year: 2024

Number of Pages: 181

Keywords: Fibroblasts, stroma, extracellular matrix, branching morphogenesis, mammary gland, organoid, cell contractility

Annotation

This thesis is focused on fibroblasts, cells of the mesenchyme/stroma, and their role during epithelial branching morphogenesis. The body of the thesis is composed of two manuscripts that are published and under review. The first study describes the functional role of fibroblasts in mammary gland branching morphogenesis in co-culture system *in vitro*, identifying fibroblast contractility as a novel factor influencing mammary gland branching. The follow-up study focuses on *in vivo* pubertal murine mammary morphogenesis and mainly on the newly described contractile fibroblasts. It provides a comprehensive single cell analysis of fibroblasts during mammary branching, including the characterization, spatial distribution, origin and fate of the contractile fibroblasts.

Annotation in Czech

Tato práce je zaměřena na fibroblasty, buňky mezenchymu/stromatu, a jejich roli při větvící morfogenezi epitelu. Hlavní část práce tvoří dva články, z nichž jeden je opublikován a jeden v recenzním řízení. První studie popisuje funkční úlohu fibroblastů na větvící morfogenezi mléčné žlázy v systému kokultur *in vitro* a identifikuje kontraktilitu fibroblastů jako nový faktor ovlivňující větvení mléčné žlázy. Navazující studie se zaměřuje na morfogenezi mléčné žlázy pubertálních myší *in vivo* a především na nově popsanou kontraktilitu fibroblastů. Poskytuje komplexní analýzu jednotlivých buněk fibroblastů během větvení mléčné žlázy, včetně charakterizace, prostorové distribuce, původu a osudu kontraktilních fibroblastů.

Abstract

Epithelial branching morphogenesis is a process for creating organ-specific ramified epithelial shapes that are crucial for proper organ function. It is significantly influenced by interactions between epithelial cells and their stromal microenvironment. This thesis investigates the role of fibroblast contractility in mammary epithelial branching morphogenesis using co-culture systems, time-lapse imaging, single-cell RNA sequencing, spatial mapping, and *in vivo* lineage tracing. Our *in vitro* findings reveal that physical contact between fibroblasts and epithelial cells, along with fibroblast contractility, is essential for inducing mammary epithelial branching. Inhibition of ROCK or non-muscle myosin II, or fibroblast-specific knock-out of *Myh9* disrupts this process. *In vivo*, we discovered a transient, niche-forming population of specialized contractile fibroblasts that localize around the terminal end buds (TEBs) of pubertal murine mammary glands and are recruited from the surrounding fat pad. Our exhaustive characterization using functional organoid-fibroblast co-cultures demonstrates that different fibroblast populations can acquire contractile features upon direct contact with the epithelium, promoting morphogenesis. This study provides comprehensive insights into mammary fibroblast heterogeneity, their functional relevance for branching morphogenesis, and their lineage hierarchy during mouse mammary gland development, identifying fibroblast contractility as a novel stromal factor driving mammary epithelial morphogenesis and contributing to a deeper understanding of the roles of mechanically active fibroblasts in both developmental and tumorigenic contexts.

Abstract in Czech

Větvící morfogeneze epitelu je proces vytváření orgánově specifických tvarů epitelu, které jsou klíčové pro správnou funkci orgánu, a je významně ovlivňována interakcemi mezi epitelovými buňkami a jejich stromálním mikroprostředím. Tato práce zkoumá roli kontraktility fibroblastů v morfogenezi větvení epitelu mléčné žlázy pomocí systémů společné kultivace, časosběrného zobrazování, sekvenování RNA jednotlivých buněk, prostorového mapování a sledování linií *in vivo*. Naše zjištění *in vitro* ukazují, že fyzický kontakt mezi fibroblasty a epitelovými buňkami je spolu s kontraktilitou fibroblastů nezbytný pro indukci větvení mléčného epitelu. Inhibice ROCK nebo nesvalového myosinu II, nebo vyřazení *Myh9* specificky ve fibroblastech tento proces narušuje. *In vivo* jsme objevili přechodnou, niku tvořící populaci specializovaných kontraktilních fibroblastů, které se lokalizují kolem terminálních koncových pupenů (TEB) pubertálních myších mléčných žláz a rekrutují se z okolního tukového polštáře. Naše vyčerpávající charakterizace pomocí funkčních kokultur organoidů s fibroblasty ukazuje, že různé populace fibroblastů mohou při přímém kontaktu s epitelem získat kontraktilní vlastnosti, což podporuje morfogenezi. Tato studie poskytuje komplexní pohled na heterogenitu fibroblastů mléčné žlázy, jejich funkční význam pro morfogenezi větvení a hierarchii jejich linií během vývoje myší mléčné žlázy, identifikuje kontraktilitu fibroblastů jako nový stromální faktor řídící morfogenezi mamárního epitelu a přispívá k hlubšímu pochopení role mechanicky aktivních fibroblastů ve vývojových i nádorových souvislostech.

Abstract in French

La morphogenèse des ramifications épithéliales est un processus de création de formes épithéliales spécifiques à un organe, cruciales pour le bon fonctionnement de l'organe. Elle est influencée de manière significative par les interactions entre les cellules épithéliales et leur microenvironnement stromal. Cette thèse étudie le rôle de la contractilité des fibroblastes dans la morphogenèse des ramifications de l'épithélium mammaire en utilisant des systèmes de co-culture, l'imagerie time-lapse, le séquençage de l'ARN d'une seule cellule, la cartographie spatiale et le traçage de la lignée in vivo. Nos résultats in vitro révèlent que le contact physique entre les fibroblastes et les cellules épithéliales, ainsi que la contractilité des fibroblastes, sont essentiels pour induire la ramification de l'épithélium mammaire. L'inhibition de ROCK, de la myosine II non musculaire ou le knock-out de Myh9 spécifique aux fibroblastes perturbent ce processus. In vivo, nous avons découvert une population transitoire, formant une niche, de fibroblastes contractiles spécialisés qui se localisent autour des bourgeons de l'extrémité terminale (TEB) des glandes mammaires murines pubertaires et sont recrutés à partir du coussinet adipeux environnant. Notre caractérisation exhaustive à l'aide de co-cultures fonctionnelles organoïde-fibroblaste démontre que différentes populations de fibroblastes peuvent acquérir des caractéristiques contractiles au contact direct de l'épithélium, favorisant ainsi la morphogenèse. Cette étude fournit des informations complètes sur l'hétérogénéité des fibroblastes mammaires, leur pertinence fonctionnelle pour la morphogenèse des ramifications et leur hiérarchie de lignage au cours du développement de la glande mammaire de la souris, identifiant la contractilité des fibroblastes comme un nouveau facteur stromal conduisant la morphogenèse épithéliale mammaire et contribuant à une compréhension plus profonde des rôles des fibroblastes mécaniquement actifs dans les contextes développementaux et tumorigènes.

Laymen summary

Organ shape and inner structure are important for organ function. In this thesis, I studied development of mammary gland in a mouse model, and specifically I studied interaction between different cells that together build the tissue. I focused on fibroblasts, a type of cell in connective tissue found in all organs of our bodies, and how these cells communicate with the glandular part of the organ to ensure correct development.

Using a line of state-of-the-art methods, I first probed the interaction *in vitro*, in a co-culture system, where fibroblasts are grown together with the mammary gland ducts to study their interaction. We found that fibroblasts migrate towards the ducts and use mechanical force to squeeze the ducts into budding or branched shape.

We then further focused on *in vivo* development of mammary gland of mouse. Similar to human, mouse mammary gland undertakes dramatic development during the puberty and we discovered that there is a specialized population of fibroblasts exclusively present during this developmental frame. These special fibroblasts express markers of cell contraction, hinting that the interaction that we first only observed in a laboratory could play a role in real organism as well. Moreover, we revealed that it is the interaction with the mammary ducts that induces fibroblast contractility, suggesting a bidirectional communication between the two cellular compartments. Overall, this research offers new insights into the role of fibroblasts in mammary gland development with potential implication for understanding cancer development as well.

Résumé grand public

La forme et la structure interne de l'organe sont importantes pour sa fonction. Dans cette thèse, j'ai étudié le développement de la glande mammaire dans un modèle de souris et j'ai étudié l'interaction entre les différentes cellules qui construisent ensemble le tissu. Plus précisément, je me suis concentrée sur les fibroblastes, un type de cellule du tissu conjonctif présent dans tous les organes de notre corps, et sur la manière dont ces cellules communiquent avec la partie glandulaire de l'organe pour assurer un développement correct.

En utilisant une série de méthodes de pointe, j'ai d'abord sondé l'interaction in vitro, dans un système de co-culture, où les fibroblastes sont cultivés avec les canaux de la glande mammaire pour étudier leur interaction. Nous avons constaté que les fibroblastes migrent vers les canaux et utilisent la force mécanique pour comprimer les canaux et leur donner une forme bourgeonnante ou ramifiée.

Nous nous sommes ensuite concentrés sur le développement in vivo de la glande mammaire de la souris. Comme chez l'homme, la glande mammaire de la souris connaît un développement spectaculaire pendant la puberté et nous avons découvert qu'il existe une population spécialisée de fibroblastes exclusivement pendant cette période de développement. Ces fibroblastes spéciaux expriment des marqueurs de contraction cellulaire, ce qui laisse supposer que l'interaction que nous n'avons observée qu'en laboratoire pourrait également jouer un rôle dans l'organisme réel. De plus, nous avons montré que c'est l'interaction avec les canaux mammaires qui induit la contractilité des fibroblastes, ce qui suggère une communication bidirectionnelle entre les deux compartiments cellulaires. Dans l'ensemble, cette recherche offre de nouvelles perspectives sur le rôle des fibroblastes dans le développement de la glande mammaire, avec des implications potentielles pour la compréhension du développement du cancer.

Declaration

I declare that I have written this thesis on my own, supervised by the thesis directors. All the sources used are listed in the bibliography section at the end.

I declare that I have used the following artificial intelligence tools during the thesis:

- ChatGPT model to help with coding in R,
- DeepL write to help with writing style of several parts of the thesis,
- DeepL translate to translate the abstract and laymen abstract to French.

Acknowledgements

I would like to thank the following people:

Silvia Fre, my supervisor in Paris, for her never-ending support, deep trust and empathy, and her understanding and patience in every situation that life (science) may bring;

Aleš Hampl, my supervisor in Brno, for taking over the supervision of my thesis and especially for his continuous support from the first days at the histology department;

Pavel Tomančák, member of my thesis advisory committee, for his mentorship, good advice and guidance, not only on the radwegs of Dresden;

Danijela Matič Vignjevič, member of my thesis advisory committee, for the to-the-point discussions and sharp takes on fibroblast biology;

Robin P Journot, for being a great desk mate and friend, open to discuss science 24/7 and all the members of the *Fate and Plasticity of Epithelial Stem Cells* team at the Curie Institute, especially to Marisa, Candice, Mathilde, Claudia, Calvin, Camila and Silvia jr.;

All the members of the *Histology and Embryology Department*;

And of course the biggest *Thank You* to my wife Zuzana, who handed me the passion for science, has supported me despite all the hurdles and has always been there for me;

and to Viktorie Anna, our daughter, who has brightened up all the days (and nights) with joy since the day she was born.

I acknowledge the financial support of Brno Ph.D. Talent funded by the Brno City Municipality, the Barrande fellowship and FRM grant number FDM202106013570.

Table of Contents

List of Figures

List of abbreviations

Actb, beta actin

BM, basement memebrane

BOM, basal organoid medium

BSA, bovine serum albumine

CAF, cancer associated fibroblast

Cd, cluster of differentiation

Col, collagen

CUBIC, clear unobstructed brain imaging cocktail

DAPI, 4′,6-diamidino-2-phenylindole

DMEM, Dulbecco's modified Eagle Medium

Dpp4, dipeptidyl peptidase 4

ECM, extracellular matrix

EDTA, Ethylenediaminetetraacetic acid

EdU, 5-Ethynyl-2′-deoxyuridine

Eef1g, eucaryotic elongation actor 1 γ

EGF, epidermal growth factor

Enpep, glutamyl aminopeptidase

ERK, extracellular signal-regulated kinase

ERT, estrogen receptor, tamoxifen-inducible

F3, coagullation factor 3

FACS, fluorescence-activated cell sorting

FBS, fetal bovine serum

FGF, fibroblast growth factor

FM, fibroblast medium

GFP, green fluorescent protein

iCAF, inflammatory CAF

KRT, keratin

MCF7, Michigan cancer foundation-7

MEM, minimal essential medium

Mfap, microfibril associated protein

mG, membrane GFP

MMP, matrix metalloproteinase

MOI, multiplicity of infection

mT, membrane Tomato

myCAF, myofibroblastic CAF

Myh, myosin heavy chain

NES, nestin

PBS, phosphate-buffered saline

PCR, polymerase chain reaction

PDGFR, platelet-derived growth factor receptor

PFA, paraformaldehyde

Pi16, peptidase inhibitor 16

ROCK, Rho Associated Protein Kinase

RT, room temperature

S100A4, S100 Calcium Binding Protein A4

Sca1, stem cell antigen 1

scRNAseq, single cell RNA sequencing

SDC, syndecan

SHARPIN, SHANK Associated RH Domain Interactor

TEB, termianl end bud

Thbs, thrombospondin

TIMP, tissue inhibitor of metalloproteinases

Tnc, tenascin

VIM, vimentin

αSMA, α-smooth muscle actin

R26, Rosa26 locus

RAC1, Rac Family Small GTPase 1

RNA, ribonucleic acid

List of Appendices

1 Introduction

BRANCHING MORPHOGENESIS

Branching morphogenesis is a universal building mechanism to increase the functional surface in confined volume that is used by organisms from all kingdoms. From fungal hyphae, roots and branches of plants to branched organelles, cells or whole tissues, branching is used to achieve a shape that will accommodate the desired function. Trees need to cover a large area with energy-producing leaves, while keeping the structural identity of their branches, neurons need to branch to functionally connect different parts of brain with muscular units to ensure motoric cognition and finally the ducts of the mammary gland branch to increase the area of milk-producing epithelium in order to nurture the future generation.

How the branched shape emerges is one of the most exciting questions in biology. While the scale and regulatory networks of the branching elements differ, the very basic physical principles are often shared, opening an opportunity for cross-discipline inspiration. On the following pages, I will focus on the branching morphogenesis of tubular epithelial organs with special emphasis on mammary gland, the model system used in the experimental part of my thesis.

THE BUILDING BLOCKS OF EPITHELIAL BRANCHING MORPHOGENESIS

Cellular mechanisms in branching morphogenesis

Epithelial branching morphogenesis is a highly dynamic process that depends on coordination of cell and tissue movements. Newton's second law of motion postulates that a cause of movement is a force and therefore when studying dynamic morphological processes, the underlying forces must always be considered. Indeed, biophysical principles behind branching morphogenesis have been extensively studied. It is however the advance in live-imaging of large tissue samples, techniques that directly measure small scale forces, and progress in mathematical modelling that enabled the renaissance of mechanobiology that we see in the recent years (Nelson et al., 2024).

While branching morphogenesis involves the collective behavior of a tissue on large scale, including the interaction between different tissue compartments or even interaction between different organs withing the same organism, we can simplify the process by describing the single cellular processes happening within. Please note, however, that the cellular processes work simultaneously during branching morphogenesis, interacting and influencing each other, therefore it is only scholar division in order to understand the whole complex process. Adding another layer of complexity, all cellular processes, as well as their coordination in time and space, are orchestrated by molecular signaling networks. This is a bi-directional interaction however, because molecular and biochemical signals change the mechanics and the geometry of tissues, while changes in tissue mechanics also feedback to molecular networks through mechanosensory pathways.

We can divide the cellular processes based on the forces driving the movement, either as epithelial-intrinsic, when they originate within epithelial cells, extrinsic, if forces are generated by the surrounding cells or a combination of both (Figure 1).

Epithelium-intrinsic forces

Cell growth

Cell division is often happening during morphogenesis. Growing tissue increases its volume, therefore generates forces (Figure 1A) that are applied on the surrounding tissues that respond by deformation and/or movement. Proliferation is often spatially restricted, either into the developing part of an organ, like tips of the growing mammary gland (Paine and Lewis, 2017; Paine et al., 2016; Scheele et al., 2017), hair follicles of the skin (Schneider et al., 2009) or intestinal crypts (Gehart and Clevers, 2019); or into different layers of an epithelium, that can result into folding of an epithelial sheet into a three-dimensional shape (Wang et al., 2021b). Moreover, changes in cell volume can also generate forces within tissues (Dasgupta et al., 2018).

Cell migration

Cells can generate forces with their contractile acto-myosin apparatus. Developing Drosophila trachea or mammalian vasculature are typical examples of leader-followers cell migration system applied in branching morphogenesis. Here, one or a group of specialized cells (leaders) actively migrate in a specific direction and pull along other cells (Affolter et al., 2009; Navis and Nelson, 2016). In collective migration, a cohesive group of epithelial cells migrate together, while maintaining relatively strong cell-cell contacts (Figure 1A). The mammary epithelium can elongate branches via collective migration that depends on ERK and RAC1 signaling, but is independent of cell division (Ewald et al., 2008; Huebner et al., 2016).

Apical and basal constriction

For individual and collective migration, epithelial cells need to loosen cell-cell adhesions, however acto-myosin forces can also shape fully adhesive epithelial sheets. Apical constriction is the asymmetric contraction of only the apical actomyosin network that results in bending of epithelial sheets (Figure 1A) during neural tube development, gastrulation, intestinal crypt formation or Drosophila salivary gland morphogenesis (Martin and Goldstein, 2014; Navis and Nelson, 2016). Similarly, basal constriction can bend an epithelium during optic cup development (Martinez-Morales et al., 2009; Okuda et al., 2018). Contractility-dependent cell

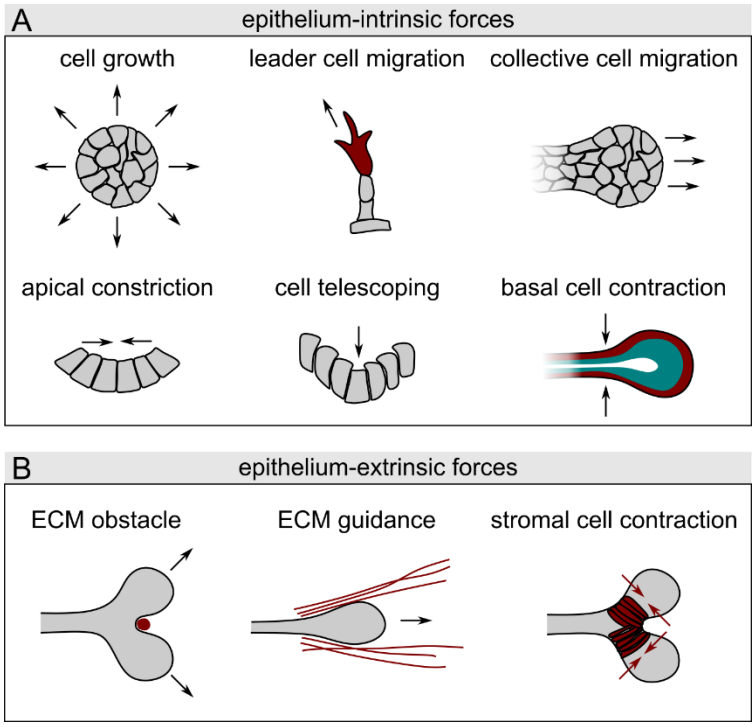

Figure 1. Forces shaping epithelial tissues. A. Schematic representations of cell behaviours that generate epithelium intrinsic forces. B. Epithelium-extrinsic factors that interfere with epithelial forces or generate forces that originate from extra-epithelial space.

telescoping is employed in epithelial invagination during salivary gland and tooth development (Figure 1A), in the latter accompanied by contraction of the apical cell layer (Li et al., 2020a). And finally, in the mammary gland, contraction of basal cells is believed to aid luminal cell intercalation at the tip-to-duct interface and therefore facilitate ductal elongation (Neumann et al., 2018, Figure 1A).

The forces that are generated by tissue growth or contraction are further propagated within the epithelium (Ruppel et al., 2023). When cells are tightly connected, the tissue is stiff, and the forces can be extensively transmitted within the tissue. Loosening of cell adhesions results in more fluid-like tissues that enable cell-cell rearrangement (Petridou et al., 2019; Tetley et al., 2019). Therefore, the combination of cell growth and division, active contraction and tissue fluidization can result in the formation of different tissue shapes in developing epithelia. These epithelial-intrinsic forces must be coordinated with external mechanical cues.

Epithelium-extrinsic forces

Passive obstacles

The extracellular matrix (ECM) plays an essential role in branching morphogenesis. The ECM is not only a rigid scaffold around the cells, but a dynamic entity that is constantly being deposited, remodeled and degraded by both epithelial and extra-epithelial cells, fibroblasts and macrophages. Historically, branching morphogenesis of the pubertal mammary gland was used as a key paradigm for studying the role of ECM on epithelial branching. The pioneering findings of the laboratories of Mina Bissel and Zena Werb were later generalized to other branched organs and today the critical role of the ECM is recognized for all branched epithelia (Díaz-de-la-Loza and Stramer, 2024; Fata et al., 2004; Lu et al., 2011; Wiseman and Werb, 2002).

The ECM defines the constraints within which epithelial branching occurs. Spatial heterogeneity of ECM mechanical properties around epithelia can affect branching by creating stiff obstacles on one hand and regions of minor resistance on the other hand, therefore pre-determining the direction of epithelial growth and driving ductal bifurcations

(Figure 1B). The forces however must come from cells since the ECM itself is not capable of contracting. The combination of epithelial cell proliferation or collective migration with local ECM accumulation can cause tissue shape changes, as shown *in vivo* in clefting of salivary gland tips by fibronectin accumulation, in Drosophila imaginal wing disk folding dictated by regionalization of the basement membrane (BM) (Harmansa et al., 2023; Sui et al., 2018) and collagen 1 accumulation and orientation leading the invasion of mammary tips (or terminal end buds, TEBs) (Brownfield et al., 2013; Nerger et al., 2021).

Similarly to ECM accumulation, there are other structures in the stroma that can affect the growth and branching of epithelium. Blood vessels develop in synchrony with branched organs, running along the branches of the lung or the mammary gland (Lazarus et al., 2011; Wang et al., 2021a). Besides their obvious function to ensure the metabolic needs of the developing organ, the blood vessels, as well as lymphatics or nerves, could also serve as mechanical landmarks that drive epithelial shaping and branching direction. At a bigger scale, other organs co-developing in the same organism can mechanically affect the shape of a developing tissue. The mechanical relation of neighboring organs is evident, for example, in the co-development of the gall bladder and the liver, or in missing the left lung lobe on the side of the developing heart or the presence of numerous sulci imprinted on bones by running blood vessels. A thorough investigation of co-development of different organs at the biomechanical and molecular level is however still missing.

It is important to note that both the ECM and blood vessels regulate morphogenesis also at the molecular level. ECM molecules bind to cell surface receptors triggering intracellular signaling and bind, accumulate and release growth factors within the extracellular space (Muncie and Weaver, 2018). Endothelial cells express signaling molecules that can directly affect epithelial morphogenesis, for example fibroblast growth factor (FGF) (Lazarus et al., 2011) or WNT (Wang et al., 2021a) ligands.

Active sculptors

In the stroma, there are also elements able to generate contractile forces, strong enough to move and deform the adjacent epithelium. A well-documented is the branching lung at the

pseudo-glandular stage, where smooth muscle cell contraction drives bifurcation of the lung epithelial buds (Goodwin et al., 2019; Kim et al., 2015, Figure 1B). Of interest, smooth muscle cell differentiation is dispensable for lung branching (Goodwin et al., 2023; Young et al., 2020). Smooth muscle contraction also shapes the lung of lizards, this time forming folds on the saccular inflating lung (Palmer et al., 2021). Other systems where contractile stromal cells shape the underlying epithelium include gut villification (Huycke et al., 2024; Shyer et al., 2013) and the formation of feather buds (Shyer et al., 2017) and hair follicles (Villeneuve et al., 2024). Lessons from pathology indicate, however, that fibroblasts of virtually any organ are able to elicit a contractile phenotype, therefore it seems important and relevant to study contractile stromal cells in other organs during their development and investigate their function in relation to branching morphogenesis. The different ways by which mesenchymal/stromal cells shape epithelial tissues into functional units are discussed in the next chapter.

MESENCHYMAL CELLS DRIVE EPITHELIAL BRANCHING

The extra-epithelial space, often referred to as mesenchyme in embryos and stroma in postnatal organisms, is composed of ECM and a plethora of non-epithelial cells. In the stroma, there are hematopoietic-derived cells forming the blood and lymphatic circulation (granulocytes, lymphocytes, monocytes and erythrocytes) and tissue resident cells, including resident immune cells, macrophages and mast cells; there are also fibroblasts, adipocytes, pericytes, smooth muscle cells, nerve cells and endothelial cells of blood and lymphatic vessels (Sumbal et al., 2021). While immune cells and endothelium come from separate lineages, the rest of the mesenchymal cells showcase a great deal of plasticity (Plikus et al., 2021), that will be further described later.

The stromal cells play vital roles during tissue development. The first evidence of the inductive role of mesenchyme/stroma in epithelial morphogenesis was brought by studies on embryonic mammary and salivary gland explants. By transplanting the epithelial bud from one organ's mesenchyme to the other, it was demonstrated that it was the mesenchyme that dictated the final shape of the organ (Kratochwil, 1969; Figure 2A). Similarly, the cross-

transplantation of kidney embryonic epithelium into lung mesenchyme lead to lung-like branching of the kidney epithelium (Lin et al., 2003; Figure 2A). This pioneering research demonstrated that epithelial-stromal interactions play important roles in organ morphogenesis, although the results from salivary-to-mammary transplantations were recently contested by a similar experiment with a more quantitative approach, which revealed that the frequency of side branching was epithelium-intrinsic, while the overall growth was dictated by the mesenchyme (Lan et al., 2024), and thus showed that epithelial morphogenesis is dictated by a combination of epithelial-intrinsic and -extrinsic cues.

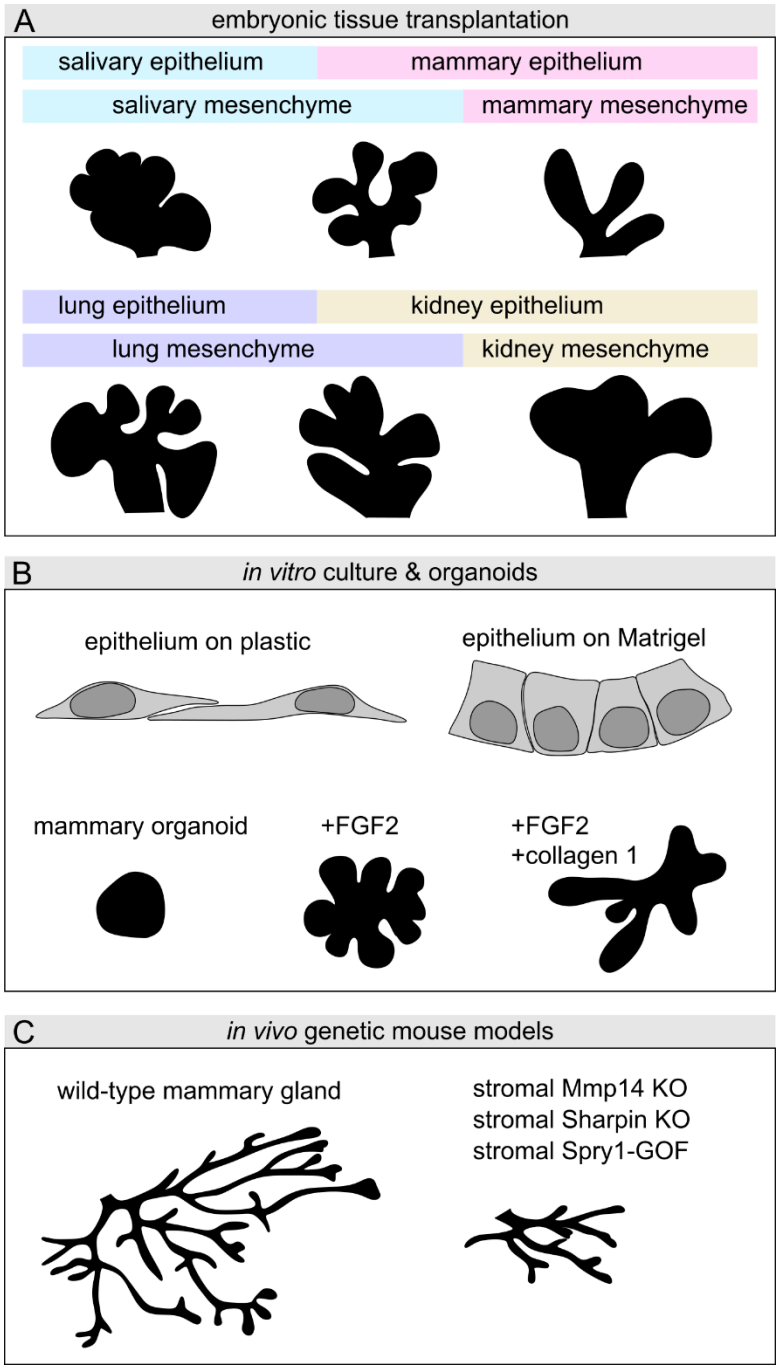

Figure 2. Key experiments demonstrating the power of stromal/mesenchymal influence on epithelial morphogenesis. A. Embryonic tissue recombination experiments. B. In vitro cultured epithelium achieve in vivo-like architecture and polarity when cultured on Matrigel ECM and ECM composition changes the shape of mammary organoid branching. C. Fibroblast-specific genetic alternations with indirect effect on epithelial morphogenesis.

Another experimental system that clearly demonstrated the importance of the stroma for epithelial morphogenesis is represented by organoids, *in vitro* cultured tissue pieces able to self-

organize and recapitulate several features and the cellular heterogeneity of their tissue of origin when grown in an ECM-like matrix (Matrigel). With the emergence of organoids in the 70's and 80's of the last century, it was shown that it is the ECM that is crucial for proper 3D organization of epithelium (Barcellos-Hoff et al., 1989; Li et al., 1987, Figure 2B). Further experiments varying the composition of the matrix or the medium led to the development of more complex organoids, self-organized structures that faithfully recapitulate the morphogenesis of many organs, including the intestinal epithelium, the brain, the pancreas or mammary gland. In mammary organoids, the ratio between collagen 1 (an ECM fibrillar protein produced by fibroblasts) and Matrigel (BM-like protein mixture) controls the formation and elongation of organoid branches (Nguyen-Ngoc and Ewald, 2013; Figure 2B). The presence of paracrine signals can induce proliferation and budding of epithelium. Moreover, changes of dynamics of growth factor availability affect branch shape (Sumbal et al., 2020b) and elongation (Caruso et al., 2022). This shows that proteins that are *in vivo* produced by stromal/mesenchymal cells can dictate epithelial morphogenesis, at least *in vitro.* Finally, co-culture of epithelial organoids with fibroblasts further shows the morphogenetic capacity of stromal cells (Koledova and Lu, 2017; Koledova et al., 2016; Sumbal and Koledova, 2019).

Genetic mouse models are further pointing to the important role of mesenchyme, and especially fibroblasts, in epithelial morphogenesis. Diphtheria toxin-mediated depletion of mesenchymal cells leads to serious defects in embryonic pancreas morphogenesis (Landsman et al., 2011). Overactivation of mammary fibroblasts by knocking out ERK pathway inhibitor *Spry1* leads to increased ductal growth in puberty (Koledova et al., 2016). Moreover, the fibroblast-specific knock-out of the ECM remodeling enzyme matrix metalloproteinase (*Mmp14*) stalled mammary pubertal morphogenesis (Feinberg et al., 2018; Figure 2C).

Altogether, the results from transplantation experiments, organoid cultures and genetic mouse models support a model in which stromal cells represent a driving morphogenetic force shaping the branching epithelium.

FIBROBLASTS

Fibroblasts are stromal cells of mesenchymal origin, present in all organs of our bodies. Fibroblasts were first discovered by Rudolf Wirchof in 1858 as "spindle-shaped cells of connective tissue" (Wirchof, 1858) but it was almost forty years later that the term "fibroblast" was used to describe cells that produce ECM upon wounding (Ziegler, 1895; Figure 3). It is until today, that the nomenclature of fibroblasts is still not unified, despite an effort is being made to find a consensus (Plikus et al., 2021; Sahai et al., 2020). Fibroblasts are cells that express components of the ECM, are found in the connective tissue, are of mesenchymal or neural crest origin and can contribute to other mesenchymal cells and are

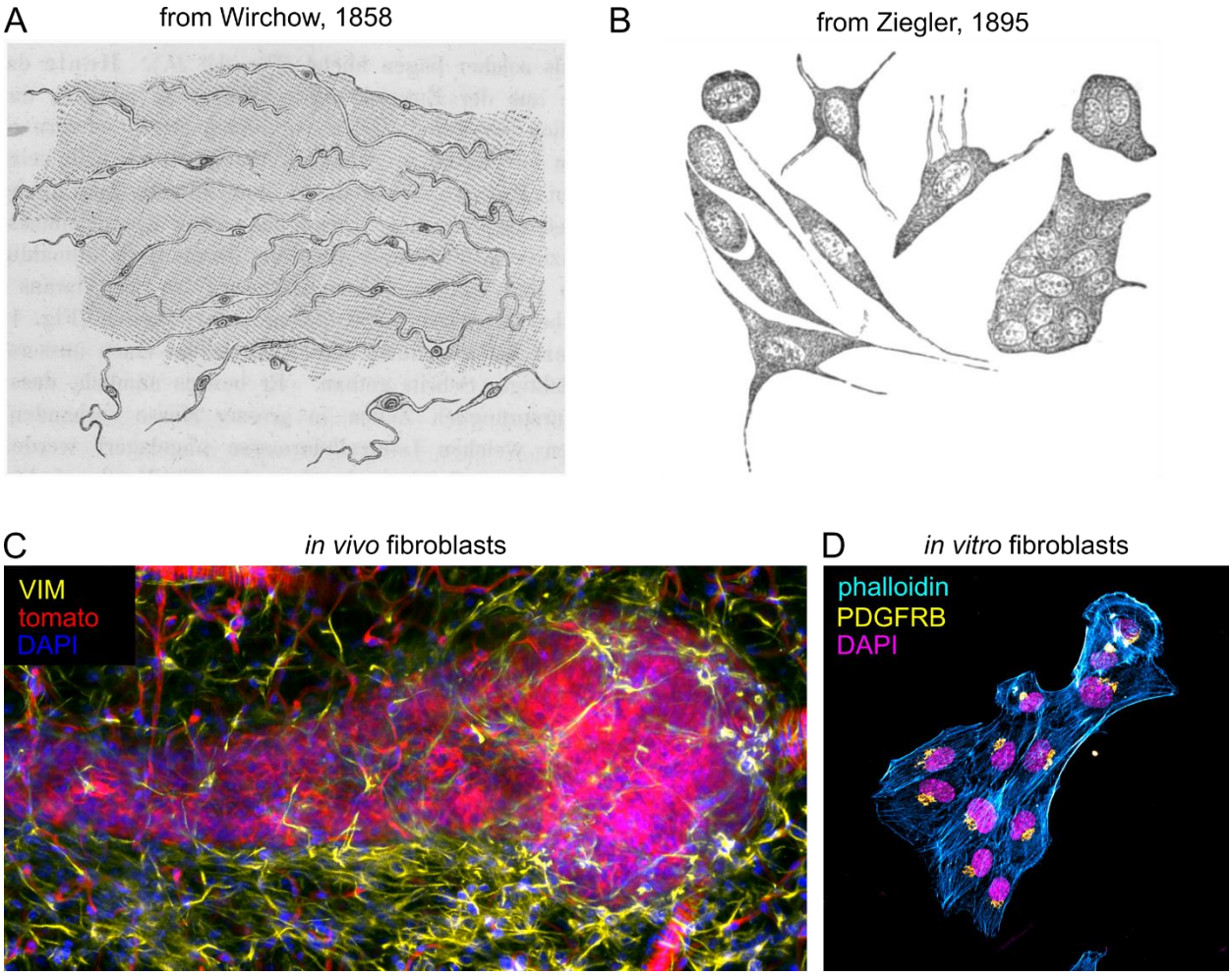

Figure 3. Fibroblast morphology. A. Illustration of spindle-shaped cell of connective tissue by R. Wirchow. B. Ilustration of fibroblasts in culture by Ziegler. C. A z-stack of mammary gland epithelium (red) surrounded by fibroblasts (yellow). D. A group of mammary fibroblasts in vitro in culture.

defined by stellate or spindle-like shape (Plikus et al., 2021; Sahai et al., 2020). In specific contexts, other names are used to describe the same cells, like pre-adipocytes or mesenchymal stem cells, based on the presumed ability of fibroblasts to differentiate into adipocytes or other mesenchymal cells, respectivelly.

Fibroblast definition

Using molecular markers to define fibroblasts is a hurdle, because the most used markers are often not universal for all fibroblasts or not specific to fibroblasts, since they are expressed by other cell types as well. For example, the PDGFRα is not expressed by myofibroblasts in skin wounds but is expressed by neural glial cells (Rivers et al., 2008). S100A4, by other name the fibroblast-specific protein 1, is in fact very unspecific, expressed only by a subset of fibroblasts but also expressed by some immune cell types including macrophages (Österreicher et al., 2011). Vimentin (VIM) marks all fibroblasts but, but is also expressed by endothelial cells, macrophages, lymphocytes (Evans, 1998; Ye et al., 2015) and at low level by myoepithelial cells (Peuhu et al., 2017b). In wound healing or cancer, alpha smooth muscle actin (αSMA) is commonly used as fibroblast marker, but is not expressed by quiescent fibroblasts while being expressed by smooth muscle cells, pericytes or myoepithelium. There are more examples like that, so it is common to use negative selection criteria to define fibroblasts (especially in flow cytometry and gene expression analyses), like a lack of epithelial, endothelial or immune cell marker expression (Plikus et al., 2021; Sumbal et al., 2021). To make it even more complicated, epithelial cells can undergo full or partial epithelial-to-mesenchymal transition and acquire expression of several markers otherwise specific to fibroblasts. Therefore, the identification of fibroblasts should always be considered in the specific context, including organ, developmental frame or disease stage.

Fibroblast functions: Matrisome and secretome

Fibroblasts have many functions (Figure 4) that are combined to achieve context-specific goals ranging from supporting tissue development, through maintaining homeostasis, protecting against foreign objects to aiding pathological processes. The function that gave fibroblasts their name is their pivotal role in producing, maintaining, remodeling and degrading the ECM. Although other stromal cells are involved in maintaining ECM

homeostasis, too (Wang et al., 2020), fibroblasts are major producers of fibrillar and non-fibrillar collagens, elastin, fibronectin, laminins and other structural ECM component as well as glycosaminoglycans and hyaluronic acid that regulate tissue hydration (Hynes and Naba, 2012; Lu et al., 2011). They also produce matrix metalloproteinases and tissue inhibitors of metalloproteinases to regulate the ECM turnover. Finally, fibroblasts exert contractile forces that further remodel the ECM (Huang et al., 2012). Altogether fibroblasts regulate both chemical and mechanical characteristics of the connective tissue to accommodate specific needs of different organ from elastic lungs to resistant skin (Plikus et al., 2021). Moreover, the chemical and mechanical composition as well as the topology of the ECM are paramount factors regulating epithelial morphogenesis (Goodwin and Nelson, 2020; Lang et al., 2021).

Another key function of fibroblasts is secretion of active molecules – growth factors, cytokines, adipokines and metabolites that facilitate the communication within fibroblasts or between fibroblasts and other cell types. Probably the best described is the necessity of fibroblast-produced paracrine ligands for the epithelial stem cell niche – intestinal fibroblasts produce R-spondins (Goto et al., 2022; Maimets et al., 2022), fibroblasts in lung (Jones et al., 2019), mammary gland (Parsa et al., 2008; Zhang et al., 2014) and pancreas (Miralles et al., 1999) produce FGFs that act on epithelial FGF receptors. Similarly, developmental pathways can be employed to support epithelial tissue regeneration upon damage or cancer growth. Besides that, fibroblast secretome can mediate communication with immune cells (Arwert et al., 2020; Ferrer et al., 2017; McGee et al., 2013; Van Linthout et al., 2014), carry anti-microbial function (Zhang et al., 2015; Zhang et al., 2019), regulate adipose tissue homeostasis (Schwalie et al., 2018; Zachara et al., 2022) and is a key determinant of senescent tissues (Zhang et al., 2024).

Fibroblast functions: contractility

Upon activation, typically caused by tissue injury, fibroblasts acquire a highly contractile phenotype characterized by expression of αSMA, a state in which the cells are called "myofibroblasts" (Hinz, 2010). Myofibroblast contractility is necessary for the initial steps of wound healing, while later, when the tension in the healed wound relaxes, myofibroblasts disappear. However, in the case of chronic injury, persistent activation of myofibroblasts can occur and leads to a non-reversible positive feedback loop of fibroblast activation – a pathological state called fibrosis (Desmoulière et al., 2005). During fibrosis, the traction forces and aberrant ECM deposition caused by myofibroblasts hyperactivation alters the tissue micro-architecture and biomechanical properties that leads to a loss of other cell types, cease in organ-specific function and in some cases, tumorigenesis. Fibrosis is a leading cause of death in developed world, being involved in more than 50 % of deaths (Friedman et al., 2013). Therefore, understanding the molecular cues that regulate fibroblast activation is an outstanding need in biomedical research. Much less is known about the involvement of fibroblast contractility in normal organ development. Recently, fascinating studies reported the mechanical role of contractile fibroblasts in the developing hair follicle (Villeneuve et al., 2024) and in folding the fetal intestinal epithelium (Huycke et al., 2024). More research is needed, however, to unravel the existence and role of contractile fibroblasts during normal development of branched epithelial tissues.

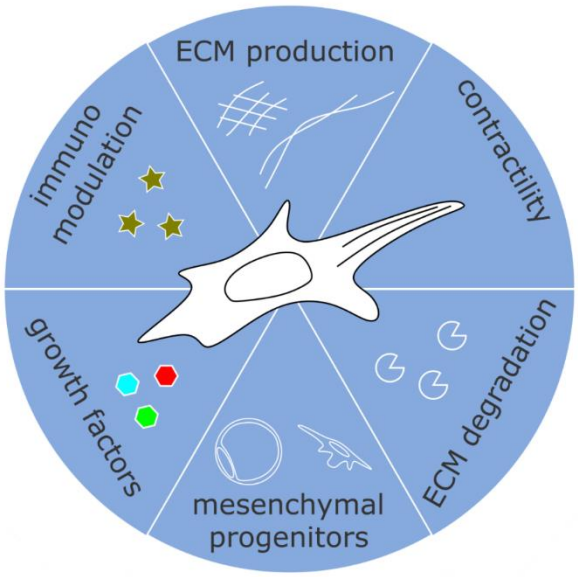

Figure 6. Fibroblast functions. Schematic depiction of various functions executed by fibroblasts.

Fibroblast functions: progenitors

Fibroblasts are cells of remarkable plasticity, that can change into other mesenchymal cell types. In fact this ability, led to the term *mesenchymal stem cells* being used to describe

fibroblasts in the stroma of blood vessels (Pittenger et al., 2019). *In vitro*, the ability of fibroblasts to differentiate into osteoblasts, chondrocytes, myoblasts or adipocytes, depending on the media composition and substrate mechanical properties, is well documented (Pittenger et al., 2019). The situation *in vivo* is far more complex and only recently began to be elucidated. *In vivo*, the model of mesenchymal stem cells that differentiate into different types of specialized stromal cells is less clear, whereas it appears that different stromal cell types display extensive plasticity allowing them to change state depending on the needs of the tissue. For example, fibroblasts change into adipocytes during development of skin (Driskell et al., 2014) and interscapular, inguinal (Sun et al., 2017), mesenteric and gonadal fat pad (Stefkovich et al., 2021). Adipocytes, however, can de-differentiate back to fibroblasts upon skin healing (Shook et al., 2020) or fibrosis (Marangoni et al., 2015). Similarly, adipocytes of the mammary fat pad change into fibroblasts during pregnancy, a process that is reversed during involution and repeated with every pregnancy (Wang et al., 2021a; Zwick et al., 2018). Fibroblasts can also give rise to pericytes, which seems to be irreversible in normal conditions (Goss et al., 2021), but pericytes can reverse into fibroblasts during fibrosis (Hung et al., 2013). Moreover, in the developing lung, there is no evident mesenchymal stem cell, but fibroblasts can give rise to smooth muscle cells during airway development (Goodwin et al., 2022). Of note, there is a controversial report about the alleged differentiation of fibroblasts into mammary epithelial cells (Joshi et al., 2019), a result that has not however been reproduced. To sum up, *in vitro* studies indicate the remarkable plasticity of fibroblasts that have the potential to switch into other mesenchymal cell types. *In vivo*, fibroblasts are also very plastic, but the developmental and tissue context is critical in inferring lineage relationships. The degree of fibroblast plasticity, the signals that govern changes in stromal cell states and the conservation of such processes across organs and in pathology warrant further *in vivo* studies.

Fibroblasts, however, are more than just a quiescent or activated cell state. Single cell genomic techniques brought insights into fibroblast heterogeneity both within and across organs in terms of transcriptome (Buechler et al., 2021; Muhl et al., 2020) and lipidome (Capolupo et al., 2022). While there are universal fibroblast subtypes, specialized fibroblast

exist in almost all organs (Buechler et al., 2021), with their matrisome signature being the dominant factor differentiating the tissue-specific subtypes (Muhl et al., 2020). The two most universal fibroblast subtypes found in normal tissues are the adventitial *Pi16+/Dpp4+* fibroblasts, characterized by the expression of canonical progenitor markers like *Cd34* or *Sca1* and the parenchymal *Col15a1+* fibroblasts that express BM genes (Buechler et al., 2021). However, there is no sharp distinction of the two clusters however, suggesting their developmental relation (Buechler et al., 2021). The heterogeneity of normal fibroblasts is reflected in breast cancer associated fibroblasts (CAFs), with two major CAFs subtypes: inflammatory CAFs (iCAFs) and myofibroblastic CAFs (myCAFs), sharing similarities with adventitial and parenchymal fibroblasts, respectively (Bartoschek et al., 2018; Croizer et al., 2024; Foster et al., 2022; Houthuijzen et al., 2023). It is however, yet to be determined, how the heterogeneity of normal fibroblasts relates to the heterogeneity of CAFs, which signaling pathways are involved and whether druggable targets could be identified for anti-cancer therapy. Given the immense plasticity of fibroblasts, it is likely that the identified transcriptomic subtypes are rather cell states that can change dynamically to accommodate the needs of the surrounding tissue, although certain level of hierarchy may exist, as demonstrated in the developing fat pad (Merrick et al., 2019; Stefkovich et al., 2021) or skin (Driskell et al., 2013). The relation between fibroblast heterogeneity and epithelial branching morphogenesis remains rather unexplored, but it is reasonable to speculate that distinct fibroblast subtypes may be spatially distributed and dynamically adjusted to support the needs of the developing epithelium in terms of ECM, growth factors as well as tissue mechanics and geometry.

STROMAL CELLS DURING MAMMARY GLAND DEVELOPMENT

The mammary gland is an exocrine ramified gland whose main function is to provide nutrition for the offspring. The development of mammary gland happens in three consecutive stages. First, rudimentary epithelial tree is derived from the embryonic surface ectoderm and stays relatively quiescent after birth (Cowin and Wysolmerski, 2010; Macias and Hinck, 2012; Watson and Khaled, 2008). Then a massive wave of branching morphogenesis re-starts at puberty, in response to a spike in female sex hormones, and involves the invasion

of the surrounding fat pad driven by the TEBs (Hinck and Silberstein, 2005; Macias and Hinck, 2012; Paine and Lewis, 2017; Sternlicht, 2006). Later in adulthood, the mammary gland undergoes cycles of proliferation, side branching and branch disappearance with each estrous cycle and more dramatic cycles designed to specify functional mammary differentiation during pregnancy and lactation (Anderson et al., 2007), followed by gland involution that restores a virgin-like tissue architecture (Watson, 2006). Finally, the epithelial tree of the mammary gland is terminally involuted after the end of reproductive age, due to the cease in sex hormone cycling at menopause.

Embryonic development

Morphogenesis of the mammary epithelium during all developmental stages is accompanied by changes in the mesenchyme/stroma. The first stage of mammary embryonic development is a formation of the milk line on embryonic day 10.5 (E10.5), followed at E11.5 by placode formation, a thickening of embryonic ectoderm, that is formed upon paracrine signals from

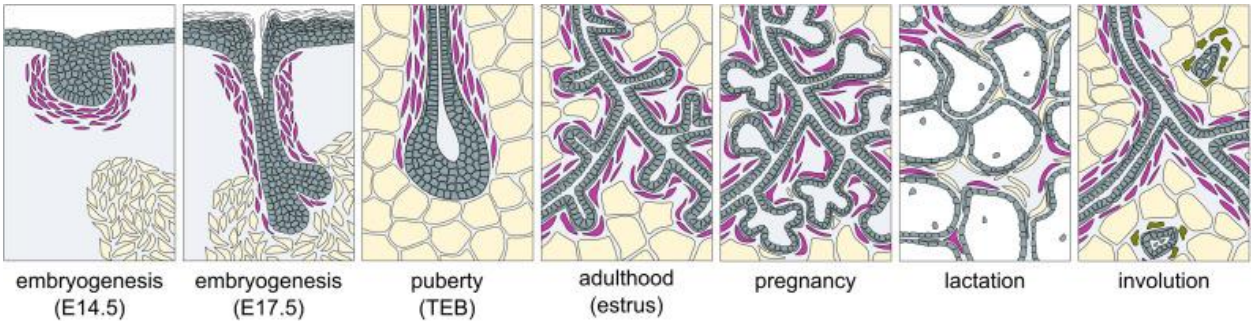

Figure 7. Fibroblasts during mammary gland development. Schematic depiction of fibroblasts (pink), preadipocytes and adipocytes (yellow) during mammary developmental stages. Epithelium is in grey. From Sumbal et al. 2021, SemCellDevBiol.

the underlying mesenchyme and somites, mainly WNTs and FGFs (Eblaghie et al., 2004; Veltmaat et al., 2004; Veltmaat et al., 2006). The placode then invaginates into a mammary bud and starts to sink into the underlying mesenchyme. At this stage (E13.5-E14.5), the bud is surrounded by mammary mesenchyme (Figure 5), a specific layer of fibroblasts marked by expression of hormone receptors and active WNT signaling (Boras-Granic and Wysolmerski, 2008; Sakakura et al., 1982). There are however other fibroblasts a bit further from epithelium that can communicate with the bud by sending paracrine signals – dermal mesenchyme (Carabaña et al., 2024) and fat pad precursor (Sakakura et al., 1982). On E15.5-E16.5 the

epithelial bud elongates, forming a primary sprout which will start branching a few days later. Interestingly, the onset of epithelial branching corresponds with the epithelium reaching and invading the fat pad precursor (Cowin and Wysolmerski, 2010; Figure 5). Heterotypic recombination of embryonic mammary epithelium with either mammary mesenchyme or fat pad precursor revealed a distinct morphogenetic capacity of these two mesenchymal tissues, promoting epithelial proliferation or ductal elongation, respectively (Sakakura et al., 1982). Therefore, we can hypothesize that it is the contact with the developing fat pad that promotes epithelial branching. It however remains to be investigated in the native *in vivo* environment. Also, the developmental relation between the embryonic mesenchymal tissues and postnatal mammary stroma is not clear. While most of the adipose tissue is derived from the fat pad precursor, it is yet to be investigated by lineage tracing whether the postnatal periductal fibroblasts are a derivate of the mammary mesenchyme that would migrate together with epithelium into the fat pad, or of the fat pad precursor. Recent single cell analysis of embryonic mammary fibroblasts (Carabaña et al., 2024) may help in developing tools to facilitate this endeavor.

Pubertal branching morphogenesis

Pubertal morphogenesis of the mammary gland starts with the peak of female sex hormone at the onset of puberty, roughly between 3 and 4 weeks of age in mice. In response to estrogen, TEBs are formed at the tips of the branches of the rudimentary epithelial tree formed during embryogenesis. TEBs are specialized epithelial structures that drive pubertal mammary gland morphogenesis (Hinck and Silberstein, 2005; Paine and Lewis, 2017). TEBs are highly proliferative, composed of a stratified epithelium with several layers of body (internal) luminal-like cells with decreased cell polarity and adhesion, compared to ductal luminal cells. The maintenance of the proliferative state of TEBs crucially depends on FGF (Lu et al., 2008; Parsa et al., 2008) and WNT signaling (Badders et al., 2009; Lindvall et al., 2009; Roarty et al., 2015), signals secreted by mammary fibroblasts (Bühler et al., 1993; Kouros-Mehr and Werb, 2006; Zhang et al., 2014). While genetic disruption of fibroblasts affects mammary branching *in vivo* (Hammer et al., 2017; Koledova et al., 2016; Peuhu et al., 2017a), the mechanistic understanding of the role of fibroblasts in mammary branching is unknown.

At the whole organ scale, the branching pattern of mammary glands is not stereotypical and differs between animals or even between the left and right side of each animal. Moreover, when the endogenous gland is excised before puberty and a new piece of gland is grafted, the gland still repopulates the whole fat pad (Deome et al., 1959; Lawson et al., 2015). This suggests that there is no predetermination in the whole organ level in terms of growth factor gradient or collagen fiber orientation but instead arises from stochastic local interactions. Indeed, the branching pattern of mammary gland can be faithfully reproduced by simulating

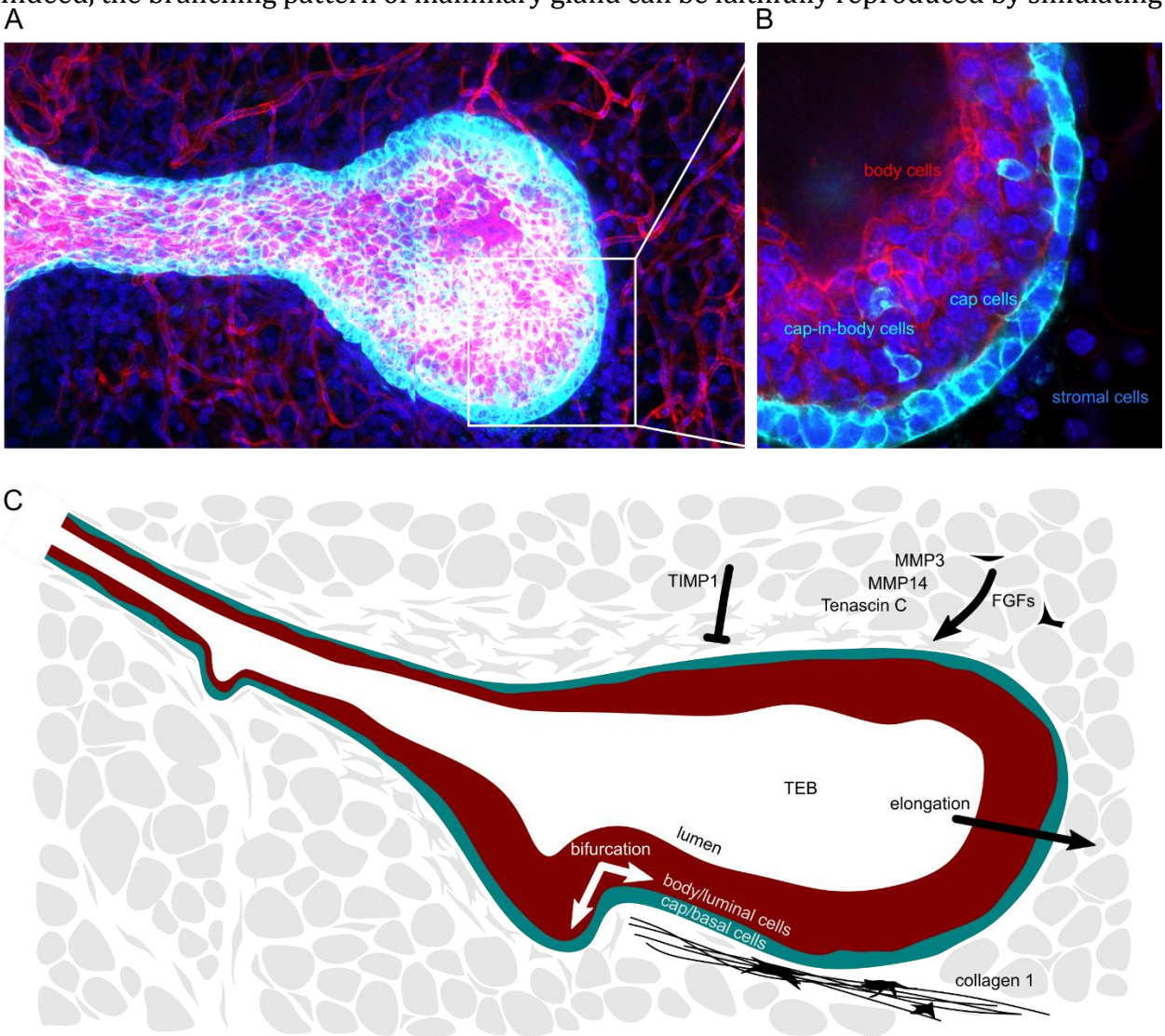

Figure 8. Terminal end bud (TEB) – the miniorgan that drives pubertal mammary morphogenesis. A, B. A z-stack (A) and a section in detail (B) of TEB of pubertal mouse, showing basal (cyan) and luminal(red) cells. C. A schematic representation of TEB with the stromal influence on TEB growth – growth factors, ECM deposition and ECM remodeling.

the gland as a framework of branching and annihilating random walks, using three simple rules of bifurcation of the tip, elongation and annihilation (Hannezo et al., 2017).

On a local tissue level, however, the branching pattern appears less random, with all the TEBs oriented in one direction which they tend to keep even after bifurcation (Nerger et al., 2021; Paine et al., 2016). Due to the relative inaccessibility of the organ *in vivo*, many mechanistic insights into mammary branching morphogenesis come from organoids, epithelial structures grown in 3D ECM gels with the proper cellular architecture capable of lactation (Caruso et al., 2024; Sumbal et al., 2020a; Sumbal et al., 2020c). Similarly to *in vivo*, budding of mammary organoids relies on receptor tyrosine kinase signaling, activated by ligands of FGF (Ewald et al., 2008; Huebner et al., 2016) or EGF family (Fata et al., 2007; Jardé et al., 2016). Organoids, however, fail to reproduce the same branching pattern of the *in vivo* gland. Despite recent significant advances in organoid technology (Caruso et al., 2022; Nguyen-Ngoc and Ewald, 2013; Yuan et al., 2023), it is still not possible to achieve the same geometry of the *in vivo* branched network in organoids.

One critical feature that is normally missing in epithelial organoid cultures are stromal cells. Fibroblasts *in vivo* dynamically secrete and remodel the ECM as the gland growths, ensuring the proper chemical and biomechanical ECM composition at the right place and time. Collagen 1 accumulation correlates with TEB cleft and bifurcation (Nerger et al., 2021) and collagen 1 fibers align with the TEB invasion direction, although this is disputed (Brownfield et al., 2013; Nerger et al., 2021). Tenascin C, an anti-adhesive ECM molecule that promotes epithelial proliferation is accumulated around TEBs and embryonic bud and is absent in adult gland (Chiquet-Ehrismann et al., 1986; Inaguma et al., 1988; Midwood et al., 2011). Moreover, genetic disruption of ECM remodeling by interfering with MMP3 (Sympson et al., 1994; Witty et al., 1995), TIMP1 (Fata et al., 1999) or MMP14 (Feinberg et al., 2018) impedes the gland morphogenesis. Finally, stromal knock-out of SHARPIN leads to decrease in fibroblast contractility resulting in dysfunctional collagen remodeling and stalled epithelial invasion (Peuhu et al., 2017a). This further demonstrates that not only the right composition, but also dynamic degradation and remodeling of ECM by the stromal cells is crucial to ensure proper morphogenesis. Matrisome expression is a major feature that

distinguishes fibroblast subtypes in many organs (Muhl et al., 2020), therefore connecting fibroblast heterogeneity, dynamic in time and space, with epithelial morphogenesis is an attractive research avenue. Despite several recent studies that aimed to understand the heterogeneity of postnatal mammary fibroblasts (Houthuijzen et al., 2023; Kanaya et al., 2019; Li et al., 2020b; Li et al., 2024; Yoshitake et al., 2022), the spatial mapping of mammary fibroblasts in pubertal gland was not performed (Houthuijzen et al., 2023; Li et al., 2024), therefore the connection between fibroblast heterogeneity and epithelial morphogenesis is still missing. Moreover, other stromal cells that have been implicated in mammary development are macrophages, eosinophils (Gouon-Evans et al., 2000; Gouon-Evans et al., 2002), mast cells (Lilla and Werb, 2010) and endothelial cells (Wang et al., 2021a).

2 Results

PREFACE 1: SQUEEZING MORPHOGENESIS: HOW FIBROBLASTS SHAPE ORGANOIDS

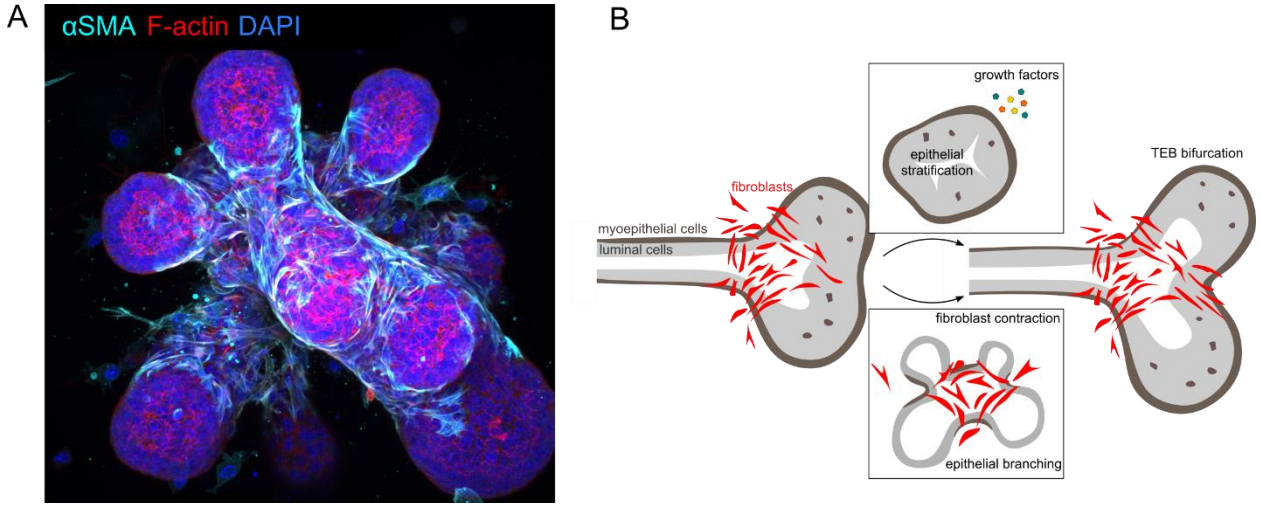

Figure 9. Fibroblast contractility-dependent induction of epithelial organoid budding. A. A representative image of organoid-firboblast co-culture. B. A scheme showing the dissection of two ways fibroblasts could influence epithleial morphogenesis. From Sumbal et al., 2024, PLOS Biology.

In the first manuscript, recently published in *PLOS Biology* (Sumbal et al., 2024a) and available in appendix A, we studied the *in vitro* phenomenon of mammary organoid budding in co-culture with primary mammary fibroblasts (Figure 7). When mixed with fibroblasts and ECM, mammary organoids undergo simple morphogenetic events of growth and budding (Koledova and Lu, 2017; Koledova et al., 2016; Sumbal and Koledova, 2019; Sumbal and Sumbalova Koledova, 2024). While this was traditionally attributed to paracrine signaling between epithelium and fibroblasts, especially FGF signaling, we described several crucial morphometric and temporal differences between organoid budding induced by FGF2 or promoted by the co-culture with fibroblasts. By setting a range of co-culture set-ups (Sumbal and Sumbalova Koledova, 2024) we demonstrated that fibroblasts must be in direct contact with the organoid, otherwise no morphogenesis occurs and organoids remain in simple cystic state. To further investigate the contact points we used fluorescent live imaging, electron microscopy and developed a method for high-end confocal imaging of big samples (Sumbal and Koledova, 2022). We found that fibroblasts form contacts before the budding occurs and once buds are formed, fibroblasts populate rather the necks than tips of the

epithelial buds. Those observations led us to the hypothesis that fibroblasts wrap the epithelial organoid and „squeeze“ it into its budded shape. To test it, we treated the co-cultures with myosin II and ROCK inhibitors or genetically knocked-out myosin heavy chain 9 (*Myh9*) in fibroblasts prior the co-culture. And we observed dramatic decrease in organoid budding when fibroblast contractility was hindered, suggesting that similarly to smooth muscle cells shaping the lung (Goodwin et al., 2019; Kim et al., 2015), mammary gland fibroblasts generate contractile forces to instruct epithelial branching. Interestingly, we observed conservation of the same mechanism when fibroblasts where co-cultured with breast cancer spheroids, similarly to recent findings in colon cancer (Barbazan et al., 2023).

The biggest limitation of this study is of course the *in vitro* character of the studied phenomena. However, we for the first time reported the presence of αSMA positive fibroblasts in the stroma surrounding the TEBs in pubertal mammary gland. Altogether, the functional *in vitro* experiments with histological *in vivo* findings are opening a path for further discoveries in the role of contractile fibroblasts in epithelial morphogenesis *in vivo*.

PREFACE 2: TERMINAL END BUD: CHANGE YOUR NICHE - AID YOUR GROWTH

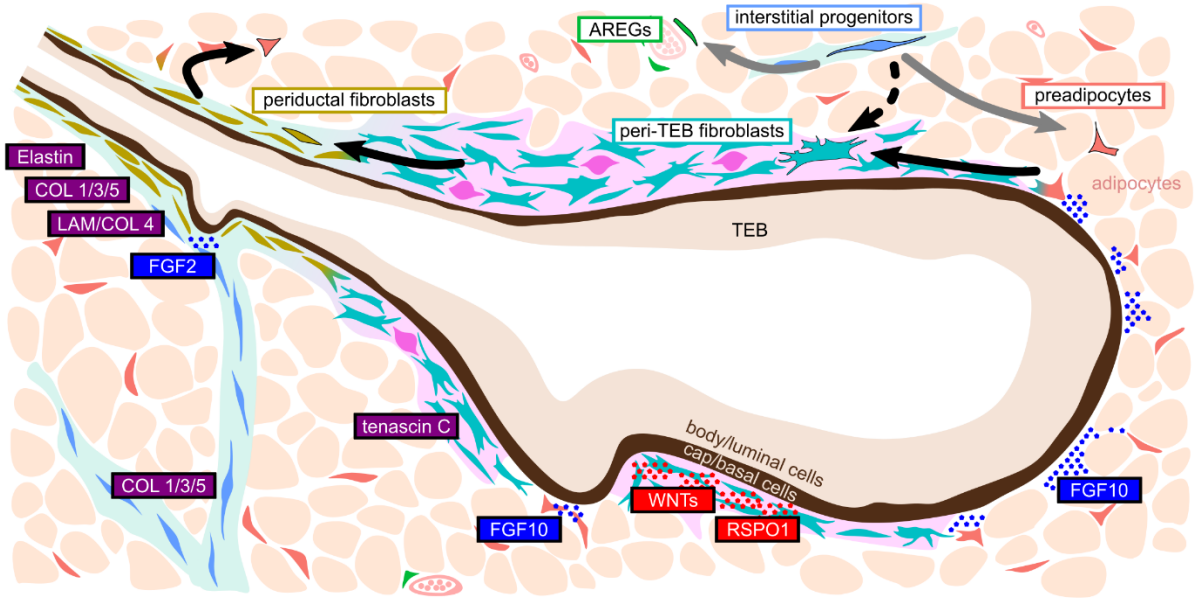

Figure 10. Mammary fibroblast heterogeneity in puberty. A schmatic summary of the main findings, showing spatial distribution of the described fibroblast population, changes of cell states (arrows), paracrine signals and ECM they produce. From Sumbal et al. 2024, Biorxiv.

In a follow up study, now posted on bioRxiv (Sumbal et al., 2024b), available as Appendix B to this thesis and under revision, we have revealed the heterogeneity and hierarchy of fibroblasts in the developing mouse mammary gland at puberty, demonstrating that the epithelium coordinates its growth and branching by activating adjacent fibroblasts in a spatially controlled manner, reminiscent of the activation of CAFs.

The comprehensive investigation of pubertal mammary fibroblasts *in vivo* in this study allowed us to identify distinct populations of fibroblasts that are spatially organized within specific tissue domains and, importantly, to characterize the population of contractile fibroblasts located just around the growing tips of the mammary epithelium. By scRNAseq, we found that these specialized fibroblasts produce specific growth factors and ECM components, which, together with their contractile characteristics, make them essential players of epithelial morphogenesis. Notably, *in vivo* lineage tracing of these contractile fibroblasts uncovered that they are activated at the growing tips of the epithelium (the TEBs); however, they do not clonally expand, and they lag behind the growing ducts rather

than escorting the invading epithelial tips. Analysis of the fate of these cells *in vivo* during pubertal growth indicated that, once the epithelium moves forward, these fibroblasts give rise to peri-ductal fibroblasts and to preadipocytes, showing that mammary activated contractile fibroblasts represent a transient cell state induced by proximity to the growing epithelium (Figure 8).

The results reported in this manuscript not only advance our knowledge of epithelial-microenvironment interactions and fibroblast plasticity, but also offer an original perspective on the role of cell-niche interactions in shaping the branching mammary epithelium. We demonstrate that fibroblast activation, a process typically associated with cancer or wound healing, is a crucial mechanism in normal organ development. This insight bridges developmental biology with cancer research, fibrosis, and regenerative medicine, highlighting that conserved mechanisms acting in fibroblasts can be re-used in different tissue contexts to establish organ shape, but also maintain it and restore it after damage. The conclusions of our study provoke further questions about the conservation of fibroblast plasticity, state transition and activation in normal versus pathological settings and lay a promise for future identification of druggable molecular regulators of niche cells for cancer and fibrosis therapy.

3 Methods

MOUSE MODELS

Housing, breeding and experimentation with mice were performed under the approval of the Ministry of Education, Youth and Sports of the Czech Republic (license # MSMT-9232/2020-2), supervised by the Expert Committee for Laboratory Animal Welfare of the Faculty of Medicine, Masaryk University, at the Laboratory Animal Breeding and Experimental Facility of the Faculty of Medicine, Masaryk University (LABEFMU, facility license #58013/2017-MZE-17214), or under the approval of the ethics committee of the Institut Curie and the French Ministry of Research (reference #34364-202112151422480) in the Animal Facility of Institut Curie (facility license #C75–05–18). The list of used mouse strains and genetic models is in the following table.

The mice were kept in individually ventilated cages with controlled temperature of 22°C and 12/12 h light/dark cycle. The food and water were administrated ad libitum. The mice were genotyped at age of 3-4 weeks, by PCR on DNA obtained from ear punch biopsies. For induction of the *CreERT* construct, mice were injected with 2 mg of tamoxifen diluted in corn oil per 10 g of mouse weight at the indicated time-point, via intraperitoneal injection. For proliferation assessment, mice were injected with EdU 10 nmol/1 g of mouse, delivered via intraperitoneal injection; if not indicated otherwise, mice were injected at 5 weeks of age and sacrificed 2 hours after for tissue collection.

The list of animal models

Genetic model	**Reference**	**Source**
Wild-type ICR	N/A	LABEFMU
Wild-type C57BL/6	N/A	LABEFMU
R26-mT/mG	(Muzumdar et al., 2007)	The Jackson Laboratory
Acta2-CreERT2	(Wendling et al., 2009)	The Jackson Laboratory
LifeAct-GFP	(Riedl et al., 2010)	Wedlich-Söldner team
Myh9fl/fl	(Conti et al., 2004)	Sara Wickström

Nu/J	(Flanagan, 1966)	LABEFMU
Notch1-CreERT2	(Fre et al., 2011)	Our team

MAMMARY GLAND DISSECTION AND FIXATION

Mice were euthanized by cervical dislocation and pinned by extremities to the dissection bord. The ventral skin was washed with 70% ethanol and the skin was cut by making one longitudinal cut and four cuts towards the extremities. Then, the skin was gently separated from the body by cotton swab and pinned to the dissection board to expose the inner surface with the mammary glands. For primary cell isolation, all five pairs of mammary glands were dissected and placed in sterile dish with PBS, with special attention not to collect the muscle between mammary gland #2 and #3 and the lymph node from mammary gland #4 was excised and discarded. For histology, mammary glands #4 and/or #5 were dissected and spread on a microscopy glass slide, let to stick to the glass for a minute on air and then submerged into 4% paraformaldehyde (PFA) at 4°C overnight. For whole-mount carmine staining, mammary gland #4 were dissected, spread on a glass slide, let to stick to the glass for a minute and submerged in Carnoy's fixative overnight at room temperature (RT). For whole-mount CUBIC clearing, mammary gland #2 and #3 were dissected, spread on a microscopy glass slide and fixed in 4% PFA at 4°C overnight.

4% PFA	
16% PFA (*Electron Microscopy*)	10 ml
PBS	30 ml

Carnoy's fixative	
100% ethanol	600 g
Glacial acetic acid	100 g
Chloroform	300 g

FIBROBLAST/ORGANOID ISOLATION

Mammary glands in sterile PBS were transferred into cell culture laminar flow box and transferred on a sterile lid of a 10 cm petri dish and chopped with 3 scalpels held in one hand for ~5 minutes, until the tissue was chopped to 0.5 mm pieces and formed a cohesive mass. Then the chopped tissue was transferred into 50 ml centrifuge tube with pre-warmed collagenase solution and incubated on an orbital shaker for 30-60 minutes at 37°C, 120 RPM with the level of digestion optically controlled.

The tube with digested tissue was then spun down for 5 minutes, 500 rcf at 4°C, resulting in separation in 3 layers – pellet (cells/organoids), supernatant and fatty layer (adipocytes). From now on, the tissue was only processed with BSA-coated serological pipettes, pipette tips and tubes. The supernatant and fatty layer were pipetted into15 ml tubes, spun down for 5 minutes, 500 rcf at 4°C and the supernatant was discarded. All the pellets were resuspended with DMEM/F12 and merged in one 15 ml tube, spun down for 5 minutes, 500 rcf at 4°C and the supernatant was discarded. The pellet was resuspended in 4 ml of DMEM/F12 and 40 µl of DNase stock (2000 U/ml) and incubated at RT for 5 minutes, handshaking occasionally. Then, 6 ml of DMEM/F12 was added and the tube was spun down for 5 minutes, 500 rcf at 4°C and the supernatant was discarded.

Multicellular epithelial fragments (organoids) and stromal cells were separated by five rounds of differential centrifugation. At each round, the pellet was resuspended in 10 ml of DMEM/F12, spun down for 10 seconds at 500 rcf and the supernatant containing single cells was transferred to new 50 ml tubes, while the pellet containing organoids was used for another round of differential centrifugation. After five rounds, the pellet was resuspended in 1 ml of basal organoid medium (BOM). The number of organoids in suspension was counted under microscope by pipetting 20 µl of the freshly resuspended solution on a glass slide and counting the number of organoids. The average number from two countings was multiplied by 50 to calculate the number of organoids per 1 ml of media. For the processing of the single cell suspension please refer to the section *'2D culture of mammary fibroblasts'*.

Collagenase stock (50 mg/ml)	
Collagenase A from *C. histolyticum* (Roche #65518621)	500 mg
DMEM/F12	10 ml
Mix well, prepare 400/800/1200 µl aliquots and keep at -20°C for several months	

Trypsin stock (50 mg/ml)	
Trypsin (Gibco #27250-018)	500 mg
DMEM/F12	10 ml
Mix well, prepare 400/800/1200 µl aliquots and keep at -20°C for several months	

Collagenase solution (10 ml for tissue from one mouse)	
Collagenase stock	400 µl
Trypsin stock	400 µl
Gentamycin 40 mg/ml	12 µl
Insulin-transferrin-selenium (ITS; 1 mg/ml insulin, 0.55 mg/ml transferrin, 0.67 µg/ml selenium)	100 µl
Fetal bovine serum (FBS)	500 µl
DMEM/F12	8.6 ml

BSA coating solution (2.5 % in PBS)	
Bovine serum albumin (BSA)	1 g
PBS	40 ml
Keep at 4°C, after each use, sterilize by 0.22 µm filtration.	

Basal organoid medium (BOM)	
DMEM/F12 with HEPES	49 ml
Penicilin /Streptomycin (10,000 U penicillin, 10,000 µg streptomycin per 1 ml)	500 µl
Insulin-transferrin-selenium (ITS)	500 µl

FLUORESCENT ASSISTED CELL SORTING (FACS)

For flow cytometry and/or fluorescent assisted cell sorting (FACS), the mammary glands were processed as described in *'fibroblast/organoid isolation'* chapter with the following changes. First, the tissue was digested by incubation for 90-120 minutes at 37°C, 150 RPM. Then, after the DNase treatment, the differential centrifugation was not performed and instead the pellet was resuspended in 500-1500 µl of red blood cell (RBC) lysis buffer and filtered through a 40 µm cell strainer to obtain single cell suspension. After centrifugation for 2 minutes, 600 rcf at 4°C and the supernatant was discarded and the pellet was resuspended in 100-500 µl of FACS staining medium with fluorophore-conjugated antibodies. The cells were incubated with antibodies for 20 minutes in dark at 4°C while shaking. Then, the cells were washed twice with ice-cold PBS and finally resuspended in 300-1000 µl of Flow buffer and filtered through the tube cap 30 µm cell strainer directly into the FACS tube and kept on ice.

The reading on flow cytometer was done no more than 30 minutes after staining. Cells were sorted on either BD ARIA III or BD Fusion with the set up in the table below. The cells were sorted in 1.5 ml tubes with 500 µl of 10% FBS in CO_2 independent media.

RBC lysis buffer	
NH_4Cl	8.02 g
$NaHCO_3$	1 g
EDTA	0.0372 g
Distilled H_2O (dH_2O)	1000 ml

Add the solid chemicals in 800 mL of dH_2O and mix, adjust pH to 7.2-7.4. Add dH_2O until the volume is 1000 ml, filter sterilize and store at RT.

FACS staining medium	
CO_2 independent medium	17.8 ml
FBS	2 ml
Penicilin/Streptomycin	200 µl

Flow buffer	
EDTA 0.5 M pH8	500 µl
BSA 10% in PBS	5 ml
FBS	500 µl
DMEM/F12 without phenol red, with HEPES	44 ml
Sterilize by 0.22 filtration, keep at 4°C.	

FACS antibodies

Target	**Spec**	**clone**	**conjugation**	**Manuf.**	**REF #**	**dilution**
CD45	Rat	30-F11	APC-Cy7	BD	#561037	1:200
CD31	Rat	390	APC-Cy7	BioLegend	#102439	1:200
CD24	Rat	M1/69	APC-Cy7	BioLegend	#101849	1:200
CD49F	Rat	GoH3	APC-Cy7	BioLegend	#313628	1:200
CD140A	Rat	APA5	BV421	BioLegend	#135923	1:50
CD39	Rat	24DMS1	PE-Cy7	eBioscience	25-0391-80	1:200
SCA1	Rat	D7	PerCP-Cy5.5	BioLegend	#108123	1:200
DPP4	Rat	H194-112	APC	BioLegend	#137807	1:200

FACS set up		
fluorophore	**Excitation laser**	**Emission filter (center/band)**
BV421	405 nm	450/40 nm or 450/50 nm
GFP	488 nm	530/30 nm
PerCP-Cy5.5	488 nm	695/40 nm
tdTomato	561 nm	582/15 nm
PE-Cy7	561 nm	780/60 nm
APC	640 nm	660/20 nm
APC-Cy7	640 nm	780/60 nm

2D CULTURE OF MAMMARY FIBROBLASTS

The supernatant containing the single cell fraction from the differential centrifugation steps was spun down for 2 minutes, at 600 rcf at 4°C and the supernatant was discarded. The cells were resuspended in 10 ml of pre-warmed fibroblast medium (FM) and seeded on 10 cm tissue culture dishes. Fibroblasts were enriched by differential attachment. The cells were incubated at 37°C, 5 % CO2 for 30 minutes, after that the cells were inspected on inverted tissue culture microscope to see successful attachment of fibroblasts to the bottom of the dish. Then the medium was discarded and the cells were washed two times with PBS before the addition of new FM. This dish was marked as passage #1.

The cells were kept at 37°C, 5 % CO_2 and inspected daily. When ~80 % confluency was reached, the cells were split. For that, the medium was discarded, the cells were washed two times with PBS and 2 ml of Trypsin/EDTA or TryplE was added before an incubation at 37°C, 5 % CO_2 for 5 minutes. After that the cells were inspected on the microscope to check successful detachment. Then 5 ml of FBS/PBS solution was added, well mixed with the cells and collected in a tube. The dish was then washed with 4 ml of PBS to collect any remaining cells and it was added to the tube with cells, spun down for 2 minutes, 600 rcf at 4°C and the supernatant was discarded. The pellet was resuspended in FM and distributed to new cell culture petri dishes in 1:4 ratio and with the passage # increased by one.

Alternatively, the cells were frozen when reaching 80 % confluency. The same procedure was followed as for splitting the cells, but at the end, the pellet was resuspended in 1 ml of freezing medium, transferred into freezing tube and frozen in freezing chamber in -80°C freezer. The next day, cells were moved to liquid nitrogen for long-term storage or kept in -80°C freezer for short term.

Fibroblast medium (FM)	50 ml	200 ml
DMEM, 1 g/ml glucose	44 ml	176 ml
FBS	5 ml	20 ml
Penicilin/Streptomycin	500 µl	2 ml
Insulin-transferrin-selenium (ITS)	500 µl	2 ml

FBS/PBS solution (10 % FBS)	
FBS	5 ml
PBS	45 ml

Freezing medium	
FBS	9 ml
DMSO	1 ml

KNOCKDOWN AND KNOCKOUT OF *MYH9* IN MAMMARY FIBROBLASTS

For *Myh9* knock-down experiment, wild-type fibroblasts subcultured for maximum of three passages were used. The cells were treated with pre-designed Silencer Select siRNAs targeted against *Myh9* gene Myh9 (IDs s70267 and s70268, Myh9si#1 and Myh9si#2, respectively) and scrambled negative control siRNA (Silencer Select negative control or Stealth negative control siRNA). The transfection was mediated with Lipofectamine 3000 reagent according to the manufacturer's instructions, with 20 nM siRNA used.

Myh9 knock-out was performed on subcultured fibroblasts from genetic mouse model *Myh9*$^{fl/fl}$ by adeno-cre adenovirus transduction. The adenoviruses (adeno-Cre-GFP and control Adeno-GFP) used were purchased from Vector Biolabs and the cells were treated at 200 MOI for 4 hours. Fibroblasts were used for co-culture 1 day after the transfection/transduction, while fibroblasts were also collected 72 hours after treatment for knock-down/knock-out efficiency determination by qPCR of immunostaining.

LIFEACT ADENOVIRAL TRANSDUCTION

To visualize the fibroblast-organoid contact in co-culture, wild-type subcultured fibroblasts were transduced with LifeAct-GFP adenovirus (IBIDI). The viruses at 500 MOI were incubated with fibroblasts for 4 hours at 37°C in fibroblast medium. The cells were harvested the next day and used for co-culture experiment.

3D ORGANOID-FIBROBLAST CO-CULTURE WITH SUB-CULTURED FIBROBLASTS (MIXED SETTING)

For the 3D co-culture of organoids with sub-cultured fibroblasts, fibroblasts were trypsinized as described in *'2D culture of mammary fibroblasts'*, resuspended in 1 ml of BOM and counted using the Bürker chamber and freshly isolated organoids were counted (see *'Fibroblast/organoid isolation'*). For 1 well of co-culture, 200 organoids were mixed with 50,000 fibroblasts and 50 µl of Matrigel for bright-field imaging in a 24 well-plate or 120 organoids, 30,000 fibroblasts and 30 µl of Matrigel for confocal imaging on IBIDI 8-well µ-Slide.

15 minutes prior plating, the wells of the cell culture vessel were coated by 10 µl of Matrigel to create a bottom patch. The desired number of organoids and fibroblasts were transferred into BSA-coated 1.5 tube and spun down at 500 rcf for 5 minutes at 4°C. The supernatant was carefully aspirated with a pipette, then the pellet was resuspended in 10 µl of cold BOM before adding Matrigel. From this point onward, both the tube with cells and the tube with Matrigel were kept on ice and the pipette tips were cooled down by pipetting up and down ice-cold PBS. After carefully mixing with Matrigel to avoid any air bubbles, the

mixture was transferred on warm cell culture plates, directly onto the prepared Matrigel patches. The cultures were incubated for 45 min in a cell culture incubator (at 37°C, 5% CO_2) to allow Matrigel gelation. Afterwards the cell culture medium (pre-warmed BOM) was added to the wells and the cells were further incubated at 37°C, 5% CO_2.

3D ORGANOID-FIBROBLASTS CO-CULTURES (DIFFERENT SETTINGS)

The set-up of different 3D co-cultures of mammary fibroblasts and organoids to test the requirement of cell-cell contact is in detail described in a published methodology chapter (Sumbal and Sumbalova Koledova, 2024). Briefly, the fibroblasts and organoids were isolated as described in *'3D organoid-fibroblast co-culture with sub-cultured fibroblasts (mixed setting)'*.

For conditioned medium, fibroblasts were seeded in tissue culture vessel in FM and the next day, the medium was changed to BOM and incubated with the cells for 24 hours. After that, the conditioned medium was collected, filtered through 0.22 μm filter and used immediately for an experiment. Organoids were seeded in Matrigel droplet as in previous chapter and overlayed with the conditioned medium after Matrigel solidification.

For a transwell co-culture, fibroblasts were seeded on the plastic of 24-well plate, while organoids were plated in Matrigel droplet in the cell culture insert with the transwell membrane of 8 μm pore size.

For a sandwich co-culture, fibroblasts were seeded in Matrigel as a round patch (50,000 fibroblasts in 30 μl of Matrigel). After 10 minutes, the patch was overlayed with 10 μl of Matrigel and after another 10 minutes with Matrigel with organoids (30 μl of Matrigel and 200 organoids).

For an aggregate co-culture, 2000 organoids were mixed with $5*10^5$ fibroblasts, plated on non-adherent poly-HEMA treated well of a 6 well plate and incubated in BOM overnight. The next day, 3 rounds of differential centrifugation were performed to eliminate single cells, aggregates were counted and seeded in density of 200 aggregates in 50 μl of Matrigel.

3D ORGANOID-FIBROBLASTS CO-CULTURE WITH FACS-SORTED FIBROBLASTS

For the 3D co-culture of organoids with FACS-sorted fibroblasts the following changes were made compared to *'3D organoid-fibroblast co-culture with sub-cultured fibroblasts (mixed setting)'*. The ratio of cells used was 100 organoids, 80,000 fibroblasts and 25 µl of ECM mixture and ECM mixture was used instead of Matrigel.

Extracellular matrix Collagen Matrigel (ECM) mixture, collagen I concentration 2.5 mg/ml (500 µl)	
MEM, 10x	35 µl
NaOH, 1 M	8.21 µl
H_2O (distilled, sterile)	36.79 µl
Collagen 1 from rat tail, 4.63 mg/ml (Corning)	270 µl
Mix well in 2 ml tube, optically control for the change of phenol red from yellow to pink. Keep on ice for 1 hour for collagen cross-linking before mixing with Matrigel and use immediately.	
Matrigel	150 µl

MCF7-RAS CELL LINE SPHEROID-FIBROBLAST CO-CULTURE WITH SUB-CULTURED FIBROBLASTS

The MCF7-ras cells were kindly provided by Dr. Ula Polanska. The cells were expanded in FM under daily microscopy surveillance. To form spheroids, the cells were incubated in high density in non-adherent polyHEMA-coated dish for 24 hours. The next day, 3 rounds of differential centrifugation were performed to eliminate single cells, spheroids were counted and used for experimentation. Co-culture experiments with MCF7-ras spheroids were performed the same way as with organoids and are described in appropriate sections.

IMMUNOCYTOCHEMISTRY OF FIBROBLASTS

For immunocytochemistry, fibroblasts were plated on IBIDI 8-well plates. At the desired time-point, the cells were fixed with 4% PFA for 30 minutes. After washing 3 times with PBS, the cells were permeabilized with 0.5% Triton X-100 in PBS for 30 minutes and blocked with 3D blocking solution (3DBS) for 30 minutes. The cells were incubated with primary antibodies diluted in 3DBS for 2 hours at RT or overnight at 4°C. Then the cells were washed 3 times with 0.05% Tween20 in PBS before incubating with secondary antibodies and DAPI diluted in PBS for 2 hours at RT. The cells were washed 3 times with 0.05% Tween 20 in PBS and stored in PBS at 4°C until imaging.

3D blocking solution (3DBS)	5 ml
10% BSA in PBS	1,000 µl
FBS	250 µl
PBS	3,750 µl
Triton X-100	25 µl
Store at 4°C and use in a week.	

Antibodies for fibroblast immunocytochemistry

Target	**Species**	**clone**	**Conjugation**	**Manufacturer**	**REF #**	**Dilution**
αSMA	Mouse	1A4	-	Sigma	A2547	1:400
αSMA	Mouse	1A4	Cy3	Sigma	C6198	1:400
B-catenin	Mouse	14	-	BD	610154	1:50
NES	Mouse	Rat-401	-	Merck/Milipore	MAB353	1:100
MYH9	Rabbit	Polyclonal	-	BioLegend	# 909801	1:1000
MYH10	Rabbit	Polyclonal	-	BioLegend	#19099	1:1000
VIM	Rabbit	D21H3	-	CellSignalling	#5741	1:200
Various secondary antibodies coupled with AF488, Cy3, AF594, Cy5 (ThermoFisher), 1:200						

IMMUNOCYTOCHEMISTRY OF 3D CO-CULTURES

Cell culture IBIDI plates were fixed with RT 4% PFA for 30 minutes at RT, before washing 3 times 10 minutes with PBS. The cultures were permeabilized with 1% Triton x-100 in PBS for 1 h, blocked with 3DBS for 1 hour and then incubated with primary antibodies diluted in 3DBS overnight at 4°C. The next day, the co-cultures were washed 3 times for 1 h with 0.05 Tween 20 in PBS. Then, the co-cultures were incubated with secondary antibodies and DAPI overnight. After that, they were washed 3 times for 1 h with 0.05 Tween 20 in PBS, cleared with 80% glycerol in PBS or CUBIC2 (see below) and imaged on a laser scanning confocal microscope (LSM780, 800, 880, 900; Zeiss).

DROPLET-BASED IMMUNOCYTOCHEMISTRY OF 3D CO-CULTURES

The method for droplet-based staining of single organoids is described in detail in a published methodology chapter (Sumbal and Koledova, 2022). Briefly, the co-cultures were fixed in 4% PFA for an hour at RT and washed 3 times with PBS. Then, single organoids were cut out of the gel with a layer of surrounding ECM with 25G needle under the control of stereoscope, transferred on a parafilm-covered 10 cm plastic dish, and overlayed with 20 µl of PBS. The staining steps are the same as in 'Immunocytochemistry of 3D co-cultures', but all are 20 µl in volume and all solution changes are done under stereoscope control. At the end, the co-cultures are cleared with CUBIC2 overnight and mounted in CUBIC 2 between microscopy slide and coverslip with three layers of a double-sided tape used as a spacer. Then the co-cultures were imaged using a laser scanning confocal microscope(LSM780, 800, 880, 900; Zeiss).

WHOLE-MOUNT MAMMARY GLAND CLEARING AND IMAGING

For whole-mount clearing and imaging, we followed the Clear Unobstructed Brain Imaging Cocktails (CUBIC) protocol (Lloyd-Lewis et al., 2016; Susaki et al., 2014). The harvested mammary glands #2 and #3 were fixed in 4% PFA overnight, washed in PBS and incubated in CUBIC-1 at RT, shaking (all steps for whole-mount staining are performed while shaking at 120 rpm), for four days, changing the solution after 2 days. Then the tissues were washed

with PBS for 1 hour and incubated in 3DBS overnight at RT, shaking. Then, the mammary glands were incubated with primary antibodies diluted in 3DBS for three days at 4°C. After washing with IHC washing buffer 3 times for 1 hour, the tissues were incubated with secondary antibodies, fluorescent dye-conjugated primary antibodies and 1 µg/ml DAPI diluted in 3DBS for three days at 4°C. After washing with IHC washing buffer 3 times for 1 hour, the tissues were cleared in CUBIC-2 solution for at least 2 days at RT, changing the solution after 1 day. Finally, the samples were mounted in CUBIC-2 solution between 2 coverslips using double-sided tape as a spacer.

CUBIC-1	100 g
Urea	25 g
N,N,N',N'-tetrakis(2-hydroxypropyl)ethylenediamine	25 g
Triton X-100	15 g
dH_2O	35 ml
Mix well with a magnetic stirrer overnight, store at RT protected from light.	

CUBIC-2	100 g
Urea	25 g
Sucrose	50 g
2,2',2''-nitrilotriethanol	10 g
Triton X-100	100 µl
dH_2O	15 ml
Mix well with a magnetic stirrer overnight, store at RT protected from light.	

Antibodies for whole-mount staining

Target	**Species**	**Clone**	**Conjugate**	**Manufacturer**	**REF #**	**Dilution**
αSMA	Rabbit	1A4	-	Novus Biol	NB600-531	1:200
αSMA	Mouse	1A4	Cy3	Sigma	C6198	1:200
VIM	Rabbit	D21H3	-	Cell Signaling	#5741	1:200

Goat anti-rabbit secondary antibody coupled with Cy5 (ThermoFisher), 1:200

REAL-TIME QUANTITATIVE PCR

For qPCR analysis of gene expression in sub-cultured fibroblasts, RNA was isolated using the RNeasy Mini Kit (Qiagen) using the manufacturer's instructions. RNA concentration was then measured using nanodrop and RNA was transcribed into cDNA using the Transcriptor First Strand cDNA Synthesis Kit (Roche) or TaqMan Reverse Transcription kit (Life Technologies) using manufacturer's instructions. The real-time qPCR was performed with 5 ng of cDNA and 5 pmol of gene-specific reverse and forward primers using the Light Cycler SYBR Green I Master Mix on LighCycler 480 II (both Roche). Relative gene expression was calculated using the ΔΔCt method and normalized to housekeeping genes. The list of primers used is below.

Gene symbol	Forward primer (5'-3')	Reverse primer (5'-3')	Length [bp]
Actb	GGCTGTATTCCCCTCCATCG	CCAGTTGGTAACAATGCCATGT	154
Eef1g	TTCCTGCCGGCAAGGTTCCA	TGCCGCCTCTGGCGTACTTC	119
Myh9	GGCCCTGCTAGATGAGGAGT	CTTGGGCTTCTGGAACTTGG	106
Myh10	GGAATCCTTTGGAAATGCGAAGA	GCCCCAACAATATAGCCAGTTAC	102
Myh14	CAGTGACCATGTCCGTGTCTG	CGTAGAGGAACGATTGGGCTG	81

TRANSMISSION ELECTRON MICROSCOPY OF 3D CO-CULTURES

For transmission electron microscopy, the co-cultures were fixed with 3% glutaraldehyde in pH 7.4 100 mM sodium cacodylate buffer for 45 minutes and postfixed in 1% osmium tetroxide before washing in the cacodylate buffer. The samples were embedded in 1% agar blocks, dehydrated in increasing ethanol series finishing in 100% p.a. ethanol, treated in 100% acetone and then embedded in Durcupan resin. The samples were sectioned on LKB

8802A ultramicrotome, stained with uranyl acetate and Reynold's lead citrate. The ultrathin sections were examined on transmission electron microscope FEI Morgagni 286(D).

MICRODISSECTION OF TEB/DUCTAL REGIONS

5 weeks old R26-mT/mG females were used for TEB/duct microdissection. Mammary glands #3 and #4 were harvested and spread on plastic 10 cm petri dish. Under the control of fluorescent stereoscope, the regions of gland containing either ducts or TEBs were cut and collected in CO_2-independent medium on ice.

SINGLE CELL RNA SEQUENCING

The samples containing either ducts or TEBs were digested in a 3 mg/ml collagenase A and 100 U/ml hyaluronidase with 5% FBS in CO2-independent medium for 2 hours at 37°C on an orbital shaker at 120 rpm. Then the tissue fragments were treated with 0.25% trypsin, 5 mg/ml dispase II and 100 μg/ml DNase I. Then the cells were treated with RBC lysis buffer and filtered through a 40 μm cell strainer to eliminate cell clumps. The resulting single cell suspension was frozen in freezing medium by slow temperature decrease at -80°C and moved to liquid nitrogen the day after. The frozen cells were shipped to Single Cell Discoveries, BV, Netherlands for sequencing. The sequencing was done on the 10x Genomics platform using the 3'v3 chemistry, targeting 5000 cells per sample and sequencing depth of 50,000 reads per cell.

SCRNASEQ DATA ANALYSIS – DATA PREPROCESSING

The raw data were preprocessed and aligned by the Single Cell Discoveries, BV using the Cell Ranger version 6.1.2 and aligned to mouse genome mm10-2020-A. The estimated number of cells, mean reads per cell and median genes per cell were 6,361/33,917/1,364 and 6,727/30,889/1,493 for the TEB and duct sample, respectively. The analysis of the data was performed using R and the Seurat package. The following filters were applied to the data to remove doublets and damaged cells: genes with expression in < 3, *nCount_RNA* < 3000 or > 60000, *nFeature_RNA* < 1000 or with a percentage of mitochondrial reads > 20 were removed. The data were normalized with the *SCTransform* function. Uniform Manifold

Approximation and Projection and neighbors identification were computed using the *RunUMAP* and *FindNeighbors* function on the first 9 PCs Clusters were defined using the *FindClusters* function with a resolution set to 0.2. Fibroblast, epithelial and leukocyte populations were then identified based on canonical markers (*Col1a1*, *Col3a1*, *Pdgfra* for fibroblasts; *Ptprc* for leukocytes; *Epcam*, *Cdh1* for epithelium).

SCRNASEQ DATA ANALYSIS – SUBPOPULATION ANALYSIS

The fibroblast, epithelial and leukocyte subsets of cells were then merged together and reanalyzed using the first 10 PCs for *RunUMAP* and 0.3 resolution for *FindClusters*. Possible lymphocyte-containing doublets within fibroblast cluster were identified by *Ptprc* expression and excluded from the analysis. Cluster markers were calculated using the *FindAllMarkers* function. The expression scores were calculated using the *AddModuleScore* function. For the fat pad fibroblasts (Merrick et al., 2019) the following markers were used: Group 1 (*Ark1c18, Cd55, Anxa3, Pi16, Sema3c, Gap43, Bmp7, Dect2, Dpp4, Wnt2*), group 2 (*Ggt5, Fabp4, Pparg, Vcam1, Bmper, Cd36, Rarres2, Apoe, Icam1*) and group 3 (*Fmo2, Vit, Ifitm1, Gdf10, Clec11a, F3*). For the adult mammary fibroblasts (Yoshitake et al., 2022) the following marker genes were used: Fib_0 (*Pi16, Anxa3, Sema3c, Myoc, Igfbp5, Akr1c18, Cd55, Smpd3, Ackr3, Dpp4*), Fib_1 (*Fabp4, Lpl, Col4a1, Sparcl1, Cxcl14, Hmgcs1, Col6a3, Smoc2, Col5a3, Col4a2*), Fib_2 (*Postn, Mfap4, Scg3, Penk, Tnc, Apoe, Enpp2, Mdk, Srpx, Thbs1*) and Fib_3 (*Gdf10, F3, Gas6, Cxcl12, Cst3, Tmem176b, Fmo2, Inmt, Mgp, Il6*).

SCRNASEQ DATA ANALYSIS – CELLCHAT

Communication link between cell populations were identified using the CellChat R package. Only epithelial and fibroblast clusters were used for this analysis. Interactions between the different clusters were identified based on the mouse *Secreted Signaling* internal CellChat database. Interactions identified in less than 5 cells per group were filtered out. Interactions between groups were visualized using the *netVisual_chord_gene* function.

IMMUNOHISTOCHEMISTRY

For immunohistochemistry, the harvested mammary glands were fixed with 4% PFA overnight, washed with PBS 6 times for 10 minutes each and transferred into 70% ethanol. The tissues were further processed by histopathological platform of Institut Curie or Faculty of Medicine of Masaryk University. Briefly, the tissues were dehydrated in series of ethanol, transferred into xylene and melted paraffin and cooled down in paraffin in histological molds. 5 μm tissue sections were cut on microtome and transferred on Superfrost glass slides for routine histology or Superfrost plus for immunohistochemistry. The slides were let to dry completely at 60°C overnight before storage at RT.

Before staining, the slides were rehydrated by dipping 2 times for 5 minutes each in xylene and then in a series of ethanol of decreasing concentration (2 times 100%, 95%, 70%) for 5 minutes each, while rocking occasionally before transferring into dH_2O for 10 minutes. Next the antigen retrieval was performed by transferring the slides into pH6 or pH9 antigen retrieval buffer and incubating them in a water bath at 96°C for 25 minutes. The slides were left to cool down in the antigen retrieval buffer for at least 40 minutes. The slides were washed in PBS for 5 minutes and then the hydrophobic barrier was created with a histological marker, carefully avoiding the section to dry.

The sections were incubated in IHC blocking buffer for 30 minutes at RT in a wet chamber. Then primary antibodies diluted in blocking buffer were applied and incubated overnight at 4°C in the wet chamber. The next day the slides were washed 3 times for 10 minutes with IHC wash buffer while shaking. Then, secondary antibodies diluted in PBS were applied together with 1 μg/ml DAPI and incubated for 2 hours at RT in the wet chamber in dark. After that the slides were washed 3 times for 10 minutes with IHC wash buffer while shaking, rinsed in PBS and mounted with aqueous mounting medium.

pH6 antigen retrieval buffer	250 ml
0.1 M sodium citrate	24 ml
0.1 M citric acid	1 ml

dH_2O	225 ml
Store at RT and use within a month. May be reused 3 times.	

pH9 antigen retrieval buffer	1000 ml
1 M Tris	10 ml
1 M EDTA	1 ml
dH2O	989 ml
Adjust the pH to 9 and store at RT; use within a month. May be reused 3 times.	

IHC blocking buffer	5 ml
FBS	250 µl
10% BSA in PBS	1000 µl
PBS	3750 µl
Always prepare fresh.	

IHC wash buffer	1000 ml
Tween20	500 µl
PBS	Up to 1000 ml
Mix well and store at RT.	

Antibodies for IHC

Target	**Species**	**Clone**	**Conj.**	**Manufacturer**	**REF #**	**Retrieval**	**Dilution**
αSMA	Mouse	1A4	-	Sigma	A2547	pH6	1:400
αSMA	Mouse	1A4	Cy3	Sigma	C6198	pH6	1:400
β-catenin	Mouse	14	-	BD	610154	pH9	1:50
NES	Mouse	Rat-401	-	Millipore	MAB353	pH6	1:100

MYH10	Rabbit	Polyclonal	-	BioLegend	#19099	pH6	1:200
VIM	Rabbit	D21H3	-	Cell Signaling	#5741	pH6	1:300
CD34	Rat	MEC 14.7	-	Abcam	ab8185	pH6	1:50
PDGFRα	Rabbit	D1E1E	-	Cell Signaling	#3174	pH9	1:200
COL1A1	Rabbit	E8F4L	-	Cell Signaling	#72026	pH6	1:100
SDC1	Rat	281-2	-	BD	#553712	pH6	1:400
TNC	Rat	MAB2138	-	R&D	#578	pH6	1:30
DPP4	Rabbit	EPR18215	-	Abcam	ab187048	pH6	1:200
CD39	Rabbit	E2X6B	-	Cell Signaling	#14481	pH6	1:200
KRT8	Rat	TROMA-I	-	DSHB	TROMA-I	pH6	1:200
GFP	Chicken	-	-	Novus Biol	NB100-1614	pH6	1:300
SCA1	Rat	E13-161.7	biotin	Beckton Dick co.	553334	pH6	1:100
Various secondary antibodies coupled with AF488, Cy3, AF594, Cy5 (ThermoFisher), 1:200							

IN SITU HYBRIDIZATION

In situ hybridization was performed on formalin fixed, paraffin embedded samples using the RNA Scope kit (ACD/Bio-Techne) following the manufacturer's instructions. The commercially available probes used are listed below. The stained sections were mounted with polymount medium and examined on a laser scanning confocal microscope. The quantification was performed manually in Image J, using DAPI as a marker of cells, and determining positive cells as 3 or more dots for *Enpep*, *Thbs1* and *Ly6a,* and cytoplasm full of dots for *F3*, *Tnc*, *Pi16* and *Mfap4*.

RNA Scope probes

Target	**Manufacturer**	**Reference #**	**channel**
Mfap4	ACD	421391	C1
Tnc	ACD	465021-C2	C2

Pi16	ACD	451311-C3	C3
F3	ACD	448691	C1
Enpep	ACD	862211-C3	C3
Thbs1	ACD	457891-C3	C3

MAMMARY FRAGMENT TRANSPLANTATION

For the transplantation assay, the grafts were a 0.5x0.5 mm pieces of the mammary gland containing epithelial duct harvested by microdissection of #4 mammary gland from 5 weeks old R26-mT/mG female under the control of a stereoscope with fluorescence. The tissue for engraftment was kept in CO_2 independent medium on ice before transplantation for no longer than 6 hours. 3 weeks old nude mice were used as host. The mice were anesthetized with isoflurane, disinfected and a reverse Y-shaped cut was made on the abdomen, exposing both #4 mammary glands. Next, the supplying blood vessels were cauterized and the proximal part of the gland (from nipple to lymph node, containing the rudimental epithelial tree) was cut out. In the remaining fat pad, a small pocket was incised using iris scissors and the graft was transplanted into it. Immediately after that the skin was overlayed and closed with a biodegradable suture (vicryl). The mice were observed daily and supplied with 0.2 mg/ml ibuprofen in drinking water for the first two weeks for analgesia. 3.5 weeks after transplantation, the mice were sacrificed and the mammary glands harvested for analysis.

STATISTICAL ANALYSIS

Sample size was not determined *a priori* and investigators were not blinded to experimental conditions. In the manuscript 1, statistical analysis was carried out in GraphPad Prism software in manuscript 2 in R using *stat_compare_means* function or *geom_signif* function of ggplot2 package. For comparing percentage, the *chisq.test* was used. N denotes number of samples used for statistical analysis, n denotes number of independent biological replicates, n.s. means not significant, *p < 0.05, **p < 0.01, ***p < 0.001, ****p < 0.0001. The box plots show median, the box borders are Q2-Q3, the whiskers are minimum to maximum, big points are predicted outliers, dots show single samples.

4 Discussion

Contractile (myo)fibroblasts in development

The results I obtained during my PhD have demonstrated that mammary fibroblasts can acquire a contractile phenotype. I observed this initially in vitro, when I found that contractile fibroblasts promote epithelial organoid budding in co-cultures (Sumbal et al., 2024a). Then, we further probed the heterogeneity of mammary fibroblasts *in vivo* and discovered the existence of contractile fibroblasts. This was only possible due to the microdissection that enriched for cells close to the epithelial TEBs, because peri-TEB fibroblasts are temporally and spatially associated with the growing tips of the mammary epithelium (TEBs) (Sumbal et al., 2024b). While contractile fibroblasts are commonly found in healing wounds, fibrosis or cancer, the presence and function of contractile fibroblasts in normal organ development is much less investigated. In fact, contractile fibroblasts could be easily mistaken for other cell types like pericytes if only probed by single cell sequencing and, therefore, we made a big effort to test that peri-TEB fiborblasts are indeed fibroblasts by immunohistochemical methods as well.

Contractile fibroblasts have been associated with chicken feather bud patterning (Shyer et al., 2017) and recently, concomitantly with our findings in the mammary gland, two important studies discovered a crucial mechanical role of fibroblasts in hair follicle development (Villeneuve et al., 2024) and intestinal villi formation (Huycke et al., 2024). In mammary gland development , however, it remains to be determined what is the mechanical role of contractile fibroblasts and if they are necessary for branching. Based on the drop-like shape of TEBs and the positioning of contractile fibroblasts around the neck of the growing ductal tips, we hypothesize that fibroblasts encircle the growing epithelium and squeeze it to propel it forward in a toothpaste-like manner. Our *in vitro* data from organoids (Sumbal et al., 2024a) and similar studies from embryonic lung branching (Kim et al., 2015; Palmer et al., 2021) indeed suggest that fibroblasts can generate mechanical forces able to deform or displace epithelia. For such a compressive role, fibroblasts would need to create a supracellular structure akin to intestinal CAFs (Barbazan et al., 2023) and indeed we found

that the peri-TEB fibroblasts create a histologically specific stroma composed of several layers of concentric fibroblasts and express a specific set of ECM proteins and integrins that could instruct and direct their function.

Fibroblast heterogeneity

The recognition of cell heterogeneity sky-rocketed with the recent advancement in single-cell genomic techniques. The need to describe stromal cell heterogeneity is evident in the mammary gland from the growing number of recent articles describing different mammary fibroblast populations in the normal gland (Houthuijzen et al., 2023; Kanaya et al., 2019; Li et al., 2020b; Li et al., 2024; Yoshitake et al., 2022) and in breast cancer (Bartoschek et al., 2018; Croizer et al., 2024; Foster et al., 2022; Kieffer et al., 2020) determined by scRNAseq. The novelty of our study lies in the analysis of fibroblasts in the specific developmental window of puberty: an active morphogenetic stage in mammary branching development that we further refined by enriching our samples with TEB-containing parts by manual microdissection. Moreover, we generated a detailed spatial atlas, positioning all the fibroblast clusters we identified by single cell RNA sequencing, including previously described ones, in relation to their position within the mammary gland histology. Altogether, our pubertal-specific single cell transcriptome with spatial information opens the perspectives of further advanced studies about mammary fibroblasts. For example, using mammary fibroblasts in co-culture notoriously gives heterogenous results (Koledova and Lu, 2017; Sumbal and Koledova, 2019; Sumbal and Sumbalova Koledova, 2024; Yuan et al., 2023), that even led to their replacement with non-mammary feeder cells in recent co-culture systems (Yuan et al., 2023), therefore hindering the faithful recapitulation of *in vivo* physiology. With the new knowledge that our experiments provide, new lines of research may be able to use specific fibroblast populations from defined developmental times to obtain more robust and reproducible results. Moreover, the new insight into fibroblast heterogeneity warrant further research into functional relationship within the different fibroblasts clusters and between fibroblast cluster and other cells, including epithelium and immune cells.

Fibroblast origins and fate

Hand-in-hand with the recognition of fibroblast heterogeneity comes our effort to understand the lineage relation of different fibroblast populations across developmental stages. Similar lineage tracing experiments have been performed to investigate epithelial stem cell lineages in many tissues, resulting in our deep understanding of clonal relationships and hierarchies of stem cells that promises future improvement of clinical management of cancer, including patient stratification and treatment, and tissue engineering. While some studies have tried to genetically track normal fibroblasts that become CAFs to uncover the origin of CAFs from specific fibroblast populations (Houthuijzen et al., 2023), the unequivocal interpretation of the results from these studies suffered from the use of mouse Cre lines which were not sufficiently specific or exclusive of a defined cell cluster. Similarly, the specificity of the Cre lines we have used remains one of the limitations of our study, due to promiscuous expression of the Cre drivers. The *αSMA-CreERT2* line is not only expressed in peri-TEB fibroblasts but also in mammary myoepithelial basal cells, pericytes and other mural cells; similarly, the *Notch1-CreERT2* line is expressed by peri-TEB and peri-ductal fibroblasts but also by luminal epithelial cells and endothelial cells and pericytes. Despite these limitations, our results do not suggest the existence of rigid lineage relationships but rather reveal the extensive plasticity of fibroblasts. To fully understand the hierarchical relationships between fibroblast populations found during mammary embryonic development (Carabaña et al., 2024), puberty (Houthuijzen et al., 2023; Li et al., 2024; Sumbal et al., 2024b), adult homeostasis, different oestrus cycle, lactation and involution (Kanaya et al., 2019; Li et al., 2020b; Yoshitake et al., 2022) or breast cancer (Bartoschek et al., 2018; Foster et al., 2022), the generation of novel Cre lines specific for defined fibroblast populations is of paramount importance, and we are currently undertaking this research direction. Moreover, further elucidation of signaling pathways that govern changes in fibroblast states should bring more insights into how the heterogeneity of fibroblasts is regulated.

Stromal influence on epithelial biology

Taken together, our studies generated a paradigm shift in fibroblast biology, considering these cells as mechanically active units able to generate forces that shape epithelial development, via secretion of growth factors and ECM components, as well as providing signaling positional cues and generating forces acting on developing epithelia. Moreover, we described the relationships between different populations of fibroblasts in mammary development, showing that the contractile phenotype is specifically acquired by fibroblasts neighboring the growing epithelial TEBs. We foresee that further studies into mammary fibroblast biology will help to elucidate the relations between normal and pathological fibroblasts, identify potentially druggable signaling pathways that govern changes in fibroblast phenotypes and enable ways to indirectly impact epithelial biology by changing the surrounding fibroblasts. Such a possibility would be beneficial for basic research as well as cancer therapy or tissue engineering.

Summary of publications and research activities

PUBLICATIONS DURING THE TIME OF THESIS

Original research

1. **Sumbal J**, Fre S, Sumbalova Koledova Z. Fibroblast-induced mammary epithelial branching depends on fibroblast contractility. PLoS Biol. 2024 Jan 10;22(1):e3002093. doi: 10.1371/journal.pbio.3002093. PMID: 38198514; PMCID: PMC10805323.

   Bibliometrics: Q1 in WoS category BIOLOGY, IF 9.8, citations: 1 in WoS

   My contribution: conceptualization of the work, performing the experiments, data analysis, creating figures and writing the original manuscript

2. **Sumbal, J**, Journot, R P, Faraldo, M M, Koledova Sumbalova Z. and Fre, S. Contractile fibroblasts are recruited to the growing mammary epithelium to support branching morphogenesis. Biorxiv 2024 doi: 10.1101/2024.06.05.597593.

   Bibliometrics: NA

   My contribution: conceptualization of the work, performing the experiments, data analysis, creating figures and writing the original manuscript

3. Hradecka L, Wiesner D**, Sumbal J**, Koledova ZS, Maska M. Segmentation and Tracking of Mammary Epithelial Organoids in Brightfield Microscopy. IEEE Trans Med Imaging. 2023 Jan;42(1):281-290. doi: 10.1109/TMI.2022.3210714. Epub 2022 Dec 29. PMID: 36170389.

   Bibliometrics: Q1 in WoS category COMPUTER SCIENCE, INTERDISCIPLINARY APPLICATIONS, IF 10.6, citations: 4 in WoS

   My contribution: Providing the biological data, running the wet lab experiments including organoid culture and time-lapse microscopy, providing expert annotation of the microscopy data.

Methodology chapters

1. **Sumbal J**, Sumbalova Koledova Z. Fibroblast-Epithelium Co-culture Methods Using Epithelial Organoids and Cell Line-Derived Spheroids. Methods Mol Biol. 2024;2764:107-129. doi: 10.1007/978-1-0716-3674-9_8. PMID: 38393591.
   My contribution: Performing the experiment, writing the manuscript.

2. **Sumbal J**, Gudjonsson T, Traustadottir GA, Koledova Z. An Organotypic Assay to Study Epithelial-Fibroblast Interactions in Human Breast. Methods Mol Biol. 2022;2471:283-299. doi: 10.1007/978-1-0716-2193-6_16. PMID: 35175604.
   My contribution: Performing the experiment, writing the manuscript.

3. **Sumbal J**, Koledova Z. Single Organoids Droplet-Based Staining Method for High-End 3D Imaging of Mammary Organoids. Methods Mol Biol. 2022;2471:259-269. doi: 10.1007/978-1-0716-2193-6_14. PMID: 35175602.
   My contribution: Performing the experiment, writing the manuscript.

Conference reports

1. Twigger AJ*, **Sumbal J***, Bentires-Alj M, Howard BA. Thirteenth Annual ENBDC Workshop: Methods in Mammary Gland Biology and Breast Cancer. J Mammary Gland Biol Neoplasia. 2022 Dec;27(3-4):233-239. doi: 10.1007/s10911-022-09526-6. Epub 2022 Oct 15. PMID: 36242657; PMCID: PMC9568960.
   *co-first authors
   My contribution: Writing the manuscript.

REMAINING PUBLICATIONS OF THE THESIS AUTHOR

Original research

1. **Sumbal J**, Chiche A, Charifou E, Koledova Z, Li H. Primary Mammary Organoid Model of Lactation and Involution. Front Cell Dev Biol. 2020 Mar 19;8:68. doi: 10.3389/fcell.2020.00068. PMID: 32266252; PMCID: PMC7098375.

Bibliometrics: Q1 in WoS category DEVELOPMENTAL BIOLOGY, IF 6.684, citations: 44 in WoS

My contribution: conceptualization of the work, performing the experiments, data analysis, creating figures and writing the original manuscript.

2. Koledova Z, **Sumbal J**, Rabata A, de La Bourdonnaye G, Chaloupkova R, Hrdlickova B, Damborsky J, Stepankova V. Fibroblast Growth Factor 2 Protein Stability Provides Decreased Dependence on Heparin for Induction of FGFR Signaling and Alters ERK Signaling Dynamics. Front Cell Dev Biol. 2019 Dec 12;7:331. doi: 10.3389/fcell.2019.00331. PMID: 31921844; PMCID: PMC6924264.

   Bibliometrics: Q1 in WoS category DEVELOPMENTAL BIOLOGY, IF 5.186, citations: 26 in WoS

   My contribution: performing the experiments (cell culture), data analysis, creating figures.

3. **Sumbal J**, Koledova Z. FGF signaling in mammary gland fibroblasts regulates multiple fibroblast functions and mammary epithelial morphogenesis. Development. 2019 Dec 2;146(23):dev185306. doi: 10.1242/dev.185306. PMID: 31699800.

   Bibliometrics: Q1 in WoS category DEVELOPMENTAL BIOLOGY, IF 5.611, citations: 29 in WoS

   My contribution: performing the experiments, data analysis, creating figures and writing the original manuscript.

Reviews

1. **Sumbal J,** Budkova Z, Traustadóttir GÁ, Koledova Z. Mammary Organoids and 3D Cell Cultures: Old Dogs with New Tricks. J Mammary Gland Biol Neoplasia. 2020 Dec;25(4):273-288. doi: 10.1007/s10911-020-09468-x. Epub 2020 Nov 18. PMID: 33210256.

   Bibliometrics: Q4 in WoS category ONCOLOGY, IF 2.673, citations: 15 in WoS

My contribution: conceptualization of the work, creating figures and writing the manuscript.

2. **Sumbal J,** Belisova D, Koledova Z. Fibroblasts: The grey eminence of mammary gland development. Semin Cell Dev Biol. 2021 Jun;114:134-142. doi: 10.1016/j.semcdb.2020.10.012. Epub 2020 Nov 4. PMID: 33158729.
   Bibliometrics: Q1 in WoS category DEVELOPMENTAL BIOLOGY, IF 7.499, citations: 9 in WoS
   My contribution: conceptualization of the work, creating figures, writing the manuscript.

Methodology chapters

1. Charifou E, **Sumbal J,** Koledova Z, Li H, Chiche A. A Robust Mammary Organoid System to Model Lactation and Involution-like Processes. Bio Protoc. 2021 Apr 20;11(8):e3996. doi: 10.21769/BioProtoc.3996. PMID: 34124297; PMCID: PMC8160540.
   Bibliometrics: Q4 in WoS category BIOLOGY, IF 0.8, citations: 4 in WoS
   My contribution: experimentation, writing the manuscript.

Note on impact factor

I personally do not consider impact factor as a reliable metric to assess the quality, merit or performance of individual articles or authors and I fully support the San Francisco Declaration on Research Assessment (DORA).

RESEARCH ACTIVITIES RELATED TO THE THESIS

1. Talk in main section at conference *15th ENBDC workshop "Methods in mammary gland biology…",* Weggis, Switzerland, 2024;
2. Invited plenary talk, Max Plank Institute of Molecular Cell Biology and Genetics, Dresden, Germany, 2024;
3. Talk in main section at conference, *Gordon research seminar on Mammary Gland Biology* 2023, West Dover, VT, USA, 2023;

4. Talk in main section at conference, *SY-Stem – Symposium for next generation of stem cell researchers*, Vienna, Austria, 2023;
5. Talk in main section at conference, *the 2nd Crick Beddington Developmental Biology Symposium*, London, UK, 2023.

Bibliography

Affolter, M., Zeller, R. and Caussinus, E. (2009). Tissue remodelling through branching morphogenesis. *Nat Rev Mol Cell Biol* **10**, 831–842.

Anderson, S. M., Rudolph, M. C., McManaman, J. L. and Neville, M. C. (2007). Key stages in mammary gland development. Secretory activation in the mammary gland: it's not just about milk protein synthesis! *Breast Cancer Res* **9**, 204.

Arwert, E. N., Milford, E. L., Rullan, A., Derzsi, S., Hooper, S., Kato, T., Mansfield, D., Melcher, A., Harrington, K. J. and Sahai, E. (2020). STING and IRF3 in stromal fibroblasts enable sensing of genomic stress in cancer cells to undermine oncolytic viral therapy. *Nat Cell Biol* **22**, 758–766.

Badders, N. M., Goel, S., Clark, R. J., Klos, K. S., Kim, S., Bafico, A., Lindvall, C., Williams, B. O. and Alexander, C. M. (2009). The Wnt receptor, Lrp5, is expressed by mouse mammary stem cells and is required to maintain the basal lineage. *PLoS One* **4**, e6594.

Barbazan, J., Pérez-González, C., Gómez-González, M., Dedenon, M., Richon, S., Latorre, E., Serra, M., Mariani, P., Descroix, S., Sens, P., et al. (2023). Cancer-associated fibroblasts actively compress cancer cells and modulate mechanotransduction. *Nat Commun* **14**, 6966.

Barcellos-Hoff, M. H., AGGELER, J., RAM, T. G. and BISSELL, M. J. (1989). Functional differentiation and alveolar morphogenesis of primary mammary cultures on reconstituted basement membrane. *Development* **105**, 223–235.

Bartoschek, M., Oskolkov, N., Bocci, M., Lövrot, J., Larsson, C., Sommarin, M., Madsen, C. D., Lindgren, D., Pekar, G., Karlsson, G., et al. (2018). Spatially and functionally distinct subclasses of breast cancer-associated fibroblasts revealed by single cell RNA sequencing. *Nat Commun* **9**, 5150.

Boras-Granic, K. and Wysolmerski, J. J. (2008). Wnt signaling in breast organogenesis. *Organogenesis* **4**, 116–122.

Brownfield, D. G., Venugopalan, G., Lo, A., Mori, H., Tanner, K., Fletcher, D. A. and Bissell, M. J. (2013). Patterned Collagen Fibers Orient Branching Mammary Epithelium through Distinct Signaling Modules. *Current Biology* **23**, 703–709.

Buechler, M. B., Pradhan, R. N., Krishnamurty, A. T., Cox, C., Calviello, A. K., Wang, A. W., Yang, Y. A., Tam, L., Caothien, R., Roose-Girma, M., et al. (2021). Cross-tissue organization of the fibroblast lineage. *Nature* **593**, 575–579.

Bühler, T. A., Dale, T. C., Kieback, C., Humphreys, R. C. and Rosen, J. M. (1993). Localization and Quantification of Wnt-2 Gene Expression in Mouse Mammary Development. *Developmental Biology* **155**, 87–96.

Capolupo, L., Khven, I., Lederer, A. R., Mazzeo, L., Glousker, G., Ho, S., Russo, F., Montoya, J. P., Bhandari, D. R., Bowman, A. P., et al. (2022). Sphingolipids control dermal fibroblast heterogeneity. *Science* **376**, eabh1623.

Carabaña, C., Sun, W., Veludo Ramos, C., Huyghe, M., Perkins, M., Maillot, A., Journot, R., Hartani, F., Faraldo, M. M., Lloyd-Lewis, B., et al. (2024). Spatially distinct epithelial and mesenchymal cell subsets along progressive lineage restriction in the branching embryonic mammary gland. *EMBO J* **43**, 2308–2336.

Caruso, M., Huang, S., Mourao, L. and Scheele, C. L. G. J. (2022). A Mammary Organoid Model to Study Branching Morphogenesis. *Front. Physiol.* **13**,.

Caruso, M., Saberiseyedabad, K., Mourao, L. and Scheele, C. L. G. J. (2024). A Decision Tree to Guide Human and Mouse Mammary Organoid Model Selection. In *3D Cell Culture: Methods and Protocols* (ed. Sumbalova Koledova, Z.), pp. 77–105. New York, NY: Springer US.

Chiquet-Ehrismann, R., Mackie, E. J., Pearson, C. A. and Sakakura, T. (1986). Tenascin: an extracellular matrix protein involved in tissue interactions during fetal development and oncogenesis. *Cell* **47**, 131–139.

Conti, M. A., Even-Ram, S., Liu, C., Yamada, K. M. and Adelstein, R. S. (2004). Defects in cell adhesion and the visceral endoderm following ablation of nonmuscle myosin heavy chain II-A in mice. *J Biol Chem* **279**, 41263–41266.

Cowin, P. and Wysolmerski, J. (2010). Molecular Mechanisms Guiding Embryonic Mammary Gland Development. *Cold Spring Harb Perspect Biol* **2**, a003251.

Croizer, H., Mhaidly, R., Kieffer, Y., Gentric, G., Djerroudi, L., Leclere, R., Pelon, F., Robley, C., Bohec, M., Meng, A., et al. (2024). Deciphering the spatial landscape and plasticity of immunosuppressive fibroblasts in breast cancer. *Nat Commun* **15**, 2806.

Dasgupta, A., Merkel, M., Clark, M. J., Jacob, A. E., Dawson, J. E., Manning, M. L. and Amack, J. D. (2018). Cell volume changes contribute to epithelial morphogenesis in zebrafish Kupffer's vesicle. *Elife* **7**, e30963.

Deome, K. B., Faulkin, L. J., Bern, H. A. and Blair, P. B. (1959). Development of mammary tumors from hyperplastic alveolar nodules transplanted into gland-free mammary fat pads of female C3H mice. *Cancer Res* **19**, 515–520.

Desmoulière, A., Chaponnier, C. and Gabbiani, G. (2005). Tissue repair, contraction, and the myofibroblast. *Wound Repair Regen* **13**, 7–12.

Díaz-de-la-Loza, M.-C. and Stramer, B. M. (2024). The extracellular matrix in tissue morphogenesis: No longer a backseat driver. *Cells & Development* **177**, 203883.

Driskell, R. R., Lichtenberger, B. M., Hoste, E., Kretzschmar, K., Simons, B. D., Charalambous, M., Ferron, S. R., Herault, Y., Pavlovic, G., Ferguson-Smith, A. C., et al. (2013). Distinct fibroblast lineages determine dermal architecture in skin development and repair. *Nature* **504**, 277–281.

Driskell, R. R., Jahoda, C. A. B., Chuong, C.-M., Watt, F. M. and Horsley, V. (2014). Defining dermal adipose tissue. *Experimental Dermatology* **23**, 629–631.

Eblaghie, M. C., Song, S.-J., Kim, J.-Y., Akita, K., Tickle, C. and Jung, H.-S. (2004). Interactions between FGF and Wnt signals and Tbx3 gene expression in mammary gland initiation in mouse embryos. *J Anat* **205**, 1–13.

Evans, R. M. (1998). Vimentin: the conundrum of the intermediate filament gene family. *Bioessays* **20**, 79–86.

Ewald, A. J., Brenot, A., Duong, M., Chan, B. S. and Werb, Z. (2008). Collective Epithelial Migration and Cell Rearrangements Drive Mammary Branching Morphogenesis. *Developmental cell* **14**, 570.

Fata, J. E., Leco, K. J., Moorehead, R. A., Martin, D. C. and Khokha, R. (1999). Timp-1 is important for epithelial proliferation and branching morphogenesis during mouse mammary development. *Dev Biol* **211**, 238–254.

Fata, J. E., Werb, Z. and Bissell, M. J. (2004). Regulation of mammary gland branching morphogenesis by the extracellular matrix and its remodeling enzymes. *Breast Cancer Res* **6**, 1–11.

Fata, J. E., Mori, H., Ewald, A. J., Zhang, H., Yao, E., Werb, Z. and Bissell, M. J. (2007). The MAPKERK-1,2 pathway integrates distinct and antagonistic signals from TGFα and FGF7 in morphogenesis of mouse mammary epithelium. *Dev Biol* **306**, 193–207.

Feinberg, T. Y., Zheng, H., Liu, R., Wicha, M. S., Yu, S. M. and Weiss, S. J. (2018). Divergent Matrix-Remodeling Strategies Distinguish Developmental from Neoplastic Mammary Epithelial Cell Invasion Programs. *Dev Cell* **47**, 145-160.e6.

Ferrer, R. A., Saalbach, A., Grünwedel, M., Lohmann, N., Forstreuter, I., Saupe, S., Wandel, E., Simon, J. C. and Franz, S. (2017). Dermal Fibroblasts Promote Alternative Macrophage Activation Improving Impaired Wound Healing. *J Invest Dermatol* **137**, 941–950.

Flanagan, S. P. (1966). "Nude", a new hairless gene with pleiotropic effects in the mouse. *Genet Res* **8**, 295–309.

Foster, D. S., Januszyk, M., Delitto, D., Yost, K. E., Griffin, M., Guo, J., Guardino, N., Delitto, A. E., Chinta, M., Burcham, A. R., et al. (2022). Multiomic analysis reveals conservation of cancer-associated fibroblast phenotypes across species and tissue of origin. *Cancer Cell* **40**, 1392-1406.e7.

Fre, S., Hannezo, E., Sale, S., Huyghe, M., Lafkas, D., Kissel, H., Louvi, A., Greve, J., Louvard, D. and Artavanis-Tsakonas, S. (2011). Notch lineages and activity in intestinal stem cells determined by a new set of knock-in mice. *PLoS One* **6**, e25785.

Friedman, S. L., Sheppard, D., Duffield, J. S. and Violette, S. (2013). Therapy for fibrotic diseases: nearing the starting line. *Sci Transl Med* **5**, 167sr1.

Gehart, H. and Clevers, H. (2019). Tales from the crypt: new insights into intestinal stem cells. *Nat Rev Gastroenterol Hepatol* **16**, 19–34.

Goodwin, K. and Nelson, C. M. (2020). Branching morphogenesis. *Development* **147**, dev184499.

Goodwin, K., Mao, S., Guyomar, T., Miller, E., Radisky, D. C., Košmrlj, A. and Nelson, C. M. (2019). Smooth muscle differentiation shapes domain branches during mouse lung development. *Development* **146**, dev181172.

Goodwin, K., Jaslove, J. M., Tao, H., Zhu, M., Hopyan, S. and Nelson, C. M. (2022). Patterning the embryonic pulmonary mesenchyme. *iScience* **25**, 103838.

Goodwin, K., Lemma, B., Zhang, P., Boukind, A. and Nelson, C. M. (2023). Plasticity in airway smooth muscle differentiation during mouse lung development. *Dev Cell* **58**, 338-347.e4.

Goss, G., Rognoni, E., Salameti, V. and Watt, F. M. (2021). Distinct Fibroblast Lineages Give Rise to NG2+ Pericyte Populations in Mouse Skin Development and Repair. *Front Cell Dev Biol* **9**, 675080.

Goto, N., Goto, S., Imada, S., Hosseini, S., Deshpande, V. and Yilmaz, Ö. H. (2022). Lymphatics and fibroblasts support intestinal stem cells in homeostasis and injury. *Cell Stem Cell* **29**, 1246-1261.e6.

Gouon-Evans, V., Rothenberg, M. E. and Pollard, J. W. (2000). Postnatal mammary gland development requires macrophages and eosinophils. *Development* **127**, 2269–2282.

Gouon-Evans, V., Lin, E. Y. and Pollard, J. W. (2002). Requirement of macrophages and eosinophils and their cytokines/chemokines for mammary gland development. *Breast Cancer Res* **4**, 155–164.

Hammer, A. M., Sizemore, G. M., Shukla, V. C., Avendano, A., Sizemore, S. T., Chang, J. J., Kladney, R. D., Cuitiño, M. C., Thies, K. A., Verfurth, Q., et al. (2017). Stromal

PDGFR-α Activation Enhances Matrix Stiffness, Impedes Mammary Ductal Development, and Accelerates Tumor Growth. *Neoplasia* **19**, 496–508.

Hannezo, E., Scheele, C. L. G. J., Moad, M., Drogo, N., Heer, R., Sampogna, R. V., van Rheenen, J. and Simons, B. D. (2017). A Unifying Theory of Branching Morphogenesis. *Cell* **171**, 242-255.e27.

Harmansa, S., Erlich, A., Eloy, C., Zurlo, G. and Lecuit, T. (2023). Growth anisotropy of the extracellular matrix shapes a developing organ. *Nat Commun* **14**, 1220.

Hinck, L. and Silberstein, G. B. (2005). Key stages in mammary gland development: the mammary end bud as a motile organ. *Breast Cancer Res* **7**, 245–251.

Hinz, B. (2010). The myofibroblast: paradigm for a mechanically active cell. *J Biomech* **43**, 146–155.

Houthuijzen, J. M., de Bruijn, R., van der Burg, E., Drenth, A. P., Wientjens, E., Filipovic, T., Bullock, E., Brambillasca, C. S., Pulver, E. M., Nieuwland, M., et al. (2023). CD26-negative and CD26-positive tissue-resident fibroblasts contribute to functionally distinct CAF subpopulations in breast cancer. *Nat Commun* **14**, 183.

Huang, X., Yang, N., Fiore, V. F., Barker, T. H., Sun, Y., Morris, S. W., Ding, Q., Thannickal, V. J. and Zhou, Y. (2012). Matrix stiffness-induced myofibroblast differentiation is mediated by intrinsic mechanotransduction. *Am J Respir Cell Mol Biol* **47**, 340–348.

Huebner, R. J., Neumann, N. M. and Ewald, A. J. (2016). Mammary epithelial tubes elongate through MAPK-dependent coordination of cell migration. *Development* **143**, 983–993.

Hung, C., Linn, G., Chow, Y.-H., Kobayashi, A., Mittelsteadt, K., Altemeier, W. A., Gharib, S. A., Schnapp, L. M. and Duffield, J. S. (2013). Role of lung pericytes and resident fibroblasts in the pathogenesis of pulmonary fibrosis. *Am J Respir Crit Care Med* **188**, 820–830.

Huycke, T. R., Häkkinen, T. J., Miyazaki, H., Srivastava, V., Barruet, E., McGinnis, C. S., Kalantari, A., Cornwall-Scoones, J., Vaka, D., Zhu, Q., et al. (2024). Patterning and folding of intestinal villi by active mesenchymal dewetting. *Cell* **187**, 3072-3089.e20.

Hynes, R. O. and Naba, A. (2012). Overview of the matrisome--an inventory of extracellular matrix constituents and functions. *Cold Spring Harb Perspect Biol* **4**, a004903.

Inaguma, Y., M, K., Ej, M., Ca, P., R, C.-E. and T, S. (1988). Epithelial induction of stromal tenascin in the mouse mammary gland: from embryogenesis to carcinogenesis. *Developmental biology* **128**,.

Jardé, T., Lloyd-Lewis, B., Thomas, M., Kendrick, H., Melchor, L., Bougaret, L., Watson, P. D., Ewan, K., Smalley, M. J. and Dale, T. C. (2016). Wnt and Neuregulin1/ErbB

signalling extends 3D culture of hormone responsive mammary organoids. *Nat Commun* **7**, 13207.

Jones, M. R., Dilai, S., Lingampally, A., Chao, C.-M., Danopoulos, S., Carraro, G., Mukhametshina, R., Wilhelm, J., Baumgart-Vogt, E., Al Alam, D., et al. (2019). A Comprehensive Analysis of Fibroblast Growth Factor Receptor 2b Signaling on Epithelial Tip Progenitor Cells During Early Mouse Lung Branching Morphogenesis. *Front Genet* **9**, 746.

Joshi, P. A., Waterhouse, P. D., Kasaian, K., Fang, H., Gulyaeva, O., Sul, H. S., Boutros, P. C. and Khokha, R. (2019). PDGFRα+ stromal adipocyte progenitors transition into epithelial cells during lobulo-alveologenesis in the murine mammary gland. *Nat Commun* **10**, 1760.

Kanaya, N., Chang, G., Wu, X., Saeki, K., Bernal, L., Shim, H.-J., Wang, J., Warden, C., Yamamoto, T., Li, J., et al. (2019). Single-cell RNA-sequencing analysis of estrogen- and endocrine-disrupting chemical-induced reorganization of mouse mammary gland. *Commun Biol* **2**, 406.

Kieffer, Y., Hocine, H. R., Gentric, G., Pelon, F., Bernard, C., Bourachot, B., Lameiras, S., Albergante, L., Bonneau, C., Guyard, A., et al. (2020). Single-Cell Analysis Reveals Fibroblast Clusters Linked to Immunotherapy Resistance in Cancer. *Cancer Discov* **10**, 1330–1351.

Kim, H. Y., Pang, M.-F., Varner, V. D., Kojima, L., Miller, E., Radisky, D. C. and Nelson, C. M. (2015). Localized Smooth Muscle Differentiation Is Essential for Epithelial Bifurcation during Branching Morphogenesis of the Mammalian Lung. *Dev Cell* **34**, 719–726.

Koledova, Z. and Lu, P. (2017). A 3D Fibroblast-Epithelium Co-culture Model for Understanding Microenvironmental Role in Branching Morphogenesis of the Mammary Gland. *Methods Mol Biol* **1501**, 217–231.

Koledova, Z., Zhang, X., Streuli, C., Clarke, R. B., Klein, O. D., Werb, Z. and Lu, P. (2016). SPRY1 regulates mammary epithelial morphogenesis by modulating EGFR-dependent stromal paracrine signaling and ECM remodeling. *Proceedings of the National Academy of Sciences* **113**, E5731–E5740.

Kouros-Mehr, H. and Werb, Z. (2006). Candidate regulators of mammary branching morphogenesis identified by genome-wide transcript analysis. *Dev Dyn* **235**, 3404–3412.

Kratochwil, K. (1969). Organ specificity in mesenchymal induction demonstrated in the embryonic development of the mammary gland of the mouse. *Dev Biol* **20**, 46–71.

Lan, Q., Trela, E., Lindström, R., Satta, J. P., Kaczyńska, B., Christensen, M. M., Holzenberger, M., Jernvall, J. and Mikkola, M. L. (2024). Mesenchyme instructs growth while epithelium directs branching in the mouse mammary gland. *Elife* **13**, e93326.

Landsman, L., Nijagal, A., Whitchurch, T. J., VanderLaan, R. L., Zimmer, W. E., MacKenzie, T. C. and Hebrok, M. (2011). Pancreatic Mesenchyme Regulates Epithelial Organogenesis throughout Development. *PLoS Biol* **9**, e1001143.

Lang, C., Conrad, L. and Iber, D. (2021). Organ-Specific Branching Morphogenesis. *Front Cell Dev Biol* **9**, 671402.

Lawson, D. A., Werb, Z., Zong, Y. and Goldstein, A. S. (2015). The Cleared Mammary Fat Pad Transplantation Assay for Mammary Epithelial Organogenesis. *Cold Spring Harb Protoc* **2015**, pdb.prot078071.

Lazarus, A., Del-Moral, P. M., Ilovich, O., Mishani, E., Warburton, D. and Keshet, E. (2011). A perfusion-independent role of blood vessels in determining branching stereotypy of lung airways. *Development* **138**, 2359–2368.

Li, M. L., Aggeler, J., Farson, D. A., Hatier, C., Hassell, J. and Bissell, M. J. (1987). Influence of a reconstituted basement membrane and its components on casein gene expression and secretion in mouse mammary epithelial cells. *Proc Natl Acad Sci U S A* **84**, 136–140.

Li, J., Economou, A. D., Vacca, B. and Green, J. B. A. (2020a). Epithelial invagination by a vertical telescoping cell movement in mammalian salivary glands and teeth. *Nat Commun* **11**, 2366.

Li, C. M.-C., Shapiro, H., Tsiobikas, C., Selfors, L. M., Chen, H., Rosenbluth, J., Moore, K., Gupta, K. P., Gray, G. K., Oren, Y., et al. (2020b). Aging-Associated Alterations in Mammary Epithelia and Stroma Revealed by Single-Cell RNA Sequencing. *Cell Rep* **33**, 108566.

Li, J., Ma, R., Wang, X., Lu, Y., Chen, J., Feng, D., Zhou, J., Xia, K., Klein, O., Xie, H., et al. (2024). Sprouty genes regulate activated fibroblasts in mammary epithelial development and breast cancer. *Cell Death Dis* **15**, 1–15.

Lilla, J. N. and Werb, Z. (2010). Mast cells contribute to the stromal microenvironment in mammary gland branching morphogenesis. *Dev Biol* **337**, 124–133.

Lin, Y., Zhang, S., Tuukkanen, J., Peltoketo, H., Pihlajaniemi, T. and Vainio, S. (2003). Patterning parameters associated with the branching of the ureteric bud regulated by epithelial-mesenchymal interactions. *Int J Dev Biol* **47**, 3–13.

Lindvall, C., Zylstra, C. R., Evans, N., West, R. A., Dykema, K., Furge, K. A. and Williams, B. O. (2009). The Wnt co-receptor Lrp6 is required for normal mouse mammary gland development. *PLoS One* **4**, e5813.

Lloyd-Lewis, B., Davis, F. M., Harris, O. B., Hitchcock, J. R., Lourenco, F. C., Pasche, M. and Watson, C. J. (2016). Imaging the mammary gland and mammary tumours in 3D: optical tissue clearing and immunofluorescence methods. *Breast Cancer Res* **18**, 127.

Lu, P., Ewald, A. J., Martin, G. R. and Werb, Z. (2008). Genetic mosaic analysis reveals FGF receptor 2 function in terminal end buds during mammary gland branching morphogenesis. *Developmental Biology* **321**, 77–87.

Lu, P., Takai, K., Weaver, V. M. and Werb, Z. (2011). Extracellular matrix degradation and remodeling in development and disease. *Cold Spring Harb Perspect Biol* **3**, a005058.

Macias, H. and Hinck, L. (2012). Mammary gland development. *Wiley Interdiscip Rev Dev Biol* **1**, 533–557.

Maimets, M., Pedersen, M. T., Guiu, J., Dreier, J., Thodberg, M., Antoku, Y., Schweiger, P. J., Rib, L., Bressan, R. B., Miao, Y., et al. (2022). Mesenchymal-epithelial crosstalk shapes intestinal regionalisation via Wnt and Shh signalling. *Nat Commun* **13**, 715.

Marangoni, R. G., Korman, B. D., Wei, J., Wood, T. A., Graham, L. V., Whitfield, M. L., Scherer, P. E., Tourtellotte, W. G. and Varga, J. (2015). Myofibroblasts in murine cutaneous fibrosis originate from adiponectin-positive intradermal progenitors. *Arthritis Rheumatol* **67**, 1062–1073.

Martin, A. C. and Goldstein, B. (2014). Apical constriction: themes and variations on a cellular mechanism driving morphogenesis. *Development* **141**, 1987–1998.

Martinez-Morales, J. R., Rembold, M., Greger, K., Simpson, J. C., Brown, K. E., Quiring, R., Pepperkok, R., Martin-Bermudo, M. D., Himmelbauer, H. and Wittbrodt, J. (2009). ojoplano-mediated basal constriction is essential for optic cup morphogenesis. *Development* **136**, 2165–2175.

McGee, H. M., Schmidt, B. A., Booth, C. J., Yancopoulos, G. D., Valenzuela, D. M., Murphy, A. J., Stevens, S., Flavell, R. A. and Horsley, V. (2013). IL-22 promotes fibroblast-mediated wound repair in the skin. *J Invest Dermatol* **133**, 1321–1329.

Merrick, D., Sakers, A., Irgebay, Z., Okada, C., Calvert, C., Morley, M. P., Percec, I. and Seale, P. (2019). Identification of a mesenchymal progenitor cell hierarchy in adipose tissue. *Science* **364**, eaav2501.

Midwood, K. S., Hussenet, T., Langlois, B. and Orend, G. (2011). Advances in tenascin-C biology. *Cell Mol Life Sci* **68**, 3175–3199.

Miralles, F., Czernichow, P., Ozaki, K., Itoh, N. and Scharfmann, R. (1999). Signaling through fibroblast growth factor receptor 2b plays a key role in the development of the exocrine pancreas. *Proceedings of the National Academy of Sciences* **96**, 6267–6272.

Muhl, L., Genové, G., Leptidis, S., Liu, J., He, L., Mocci, G., Sun, Y., Gustafsson, S., Buyandelger, B., Chivukula, I. V., et al. (2020). Single-cell analysis uncovers fibroblast heterogeneity and criteria for fibroblast and mural cell identification and discrimination. *Nat Commun* **11**, 3953.

Muncie, J. M. and Weaver, V. M. (2018). The Physical and Biochemical Properties of the Extracellular Matrix Regulate Cell Fate. *Curr Top Dev Biol* **130**, 1–37.

Muzumdar, M. D., Tasic, B., Miyamichi, K., Li, L. and Luo, L. (2007). A global double-fluorescent Cre reporter mouse. *Genesis* **45**, 593–605.

Navis, A. and Nelson, C. M. (2016). Pulling together: Tissue-generated forces that drive lumen morphogenesis. *Semin Cell Dev Biol* **55**, 139–147.

Nelson, C. M., Xiao, B., Wickström, S. A., Dufrêne, Y. F., Cosgrove, D. J., Heisenberg, C.-P., Dupont, S., Shyer, A. E., Rodrigues, A. R., Trepat, X., et al. (2024). Mechanobiology: Shaping the future of cellular form and function. *Cell* **187**, 2652–2656.

Nerger, B. A., Jaslove, J. M., Elashal, H. E., Mao, S., Košmrlj, A., Link, A. J. and Nelson, C. M. (2021). Local accumulation of extracellular matrix regulates global morphogenetic patterning in the developing mammary gland. *Current Biology* **31**, 1903-1917.e6.

Neumann, N. M., Perrone, M. C., Veldhuis, J. H., Huebner, R. J., Zhan, H., Devreotes, P. N., Brodland, G. W. and Ewald, A. J. (2018). Coordination of receptor tyrosine kinase signaling and interfacial tension dynamics drive radial intercalation and tube elongation. *Dev Cell* **45**, 67-82.e6.

Nguyen-Ngoc, K.-V. and Ewald, A. J. (2013). Mammary ductal elongation and myoepithelial migration are regulated by the composition of the extracellular matrix. *J Microsc* **251**, 212–223.

Okuda, S., Takata, N., Hasegawa, Y., Kawada, M., Inoue, Y., Adachi, T., Sasai, Y. and Eiraku, M. (2018). Strain-triggered mechanical feedback in self-organizing optic-cup morphogenesis. *Sci Adv* **4**, eaau1354.

Österreicher, C. H., Penz-Österreicher, M., Grivennikov, S. I., Guma, M., Koltsova, E. K., Datz, C., Sasik, R., Hardiman, G., Karin, M. and Brenner, D. A. (2011). Fibroblast-specific protein 1 identifies an inflammatory subpopulation of macrophages in the liver. *Proc Natl Acad Sci U S A* **108**, 308–313.

Paine, I. S. and Lewis, M. T. (2017). The Terminal End Bud: the Little Engine that Could. *J Mammary Gland Biol Neoplasia* **22**, 93–108.

Paine, I. S., A, C., J, L., A, S., V, C., J, R. and Mt, L. (2016). A Geometrically-Constrained Mathematical Model of Mammary Gland Ductal Elongation Reveals Novel Cellular Dynamics within the Terminal End Bud. *PLoS computational biology* **12**,.

Palmer, M. A., Nerger, B. A., Goodwin, K., Sudhakar, A., Lemke, S. B., Ravindran, P. T., Toettcher, J. E., Košmrlj, A. and Nelson, C. M. (2021). Stress ball morphogenesis: How the lizard builds its lung. *Sci Adv* **7**, eabk0161.

Parsa, S., Ramasamy, S. K., De Langhe, S., Gupte, V. V., Haigh, J. J., Medina, D. and Bellusci, S. (2008). Terminal end bud maintenance in mammary gland is dependent upon FGFR2b signaling. *Dev Biol* **317**, 121–131.

Petridou, N. I., Grigolon, S., Salbreux, G., Hannezo, E. and Heisenberg, C.-P. (2019). Fluidization-mediated tissue spreading by mitotic cell rounding and non-canonical Wnt signalling. *Nat Cell Biol* **21**, 169–178.

Peuhu, E., Kaukonen, R., Lerche, M., Saari, M., Guzmán, C., Rantakari, P., De Franceschi, N., Wärri, A., Georgiadou, M., Jacquemet, G., et al. (2017a). SHARPIN regulates collagen architecture and ductal outgrowth in the developing mouse mammary gland. *The EMBO Journal* **36**, 165–182.

Peuhu, E., Virtakoivu, R., Mai, A., Wärri, A. and Ivaska, J. (2017b). Epithelial vimentin plays a functional role in mammary gland development. *Development* **144**, 4103–4113.

Pittenger, M. F., Discher, D. E., Péault, B. M., Phinney, D. G., Hare, J. M. and Caplan, A. I. (2019). Mesenchymal stem cell perspective: cell biology to clinical progress. *npj Regen Med* **4**, 1–15.

Plikus, M. V., Wang, X., Sinha, S., Forte, E., Thompson, S. M., Herzog, E. L., Driskell, R. R., Rosenthal, N., Biernaskie, J. and Horsley, V. (2021). Fibroblasts: Origins, definitions, and functions in health and disease. *Cell* **184**, 3852–3872.

Riedl, J., Flynn, K. C., Raducanu, A., Gärtner, F., Beck, G., Bösl, M., Bradke, F., Massberg, S., Aszodi, A., Sixt, M., et al. (2010). Lifeact mice for studying F-actin dynamics. *Nat Methods* **7**, 168–169.

Rivers, L. E., Young, K. M., Rizzi, M., Jamen, F., Psachoulia, K., Wade, A., Kessaris, N. and Richardson, W. D. (2008). PDGFRA/NG2 glia generate myelinating oligodendrocytes and piriform projection neurons in adult mice. *Nat Neurosci* **11**, 1392–1401.

Roarty, K., Shore, A. N., Creighton, C. J. and Rosen, J. M. (2015). Ror2 regulates branching, differentiation, and actin-cytoskeletal dynamics within the mammary epithelium. *J Cell Biol* **208**, 351–366.

Ruppel, A., Wörthmüller, D., Misiak, V., Kelkar, M., Wang, I., Moreau, P., Méry, A., Révilloud, J., Charras, G., Cappello, G., et al. (2023). Force propagation between epithelial cells depends on active coupling and mechano-structural polarization. *eLife* **12**, e83588.

Sahai, E., Astsaturov, I., Cukierman, E., DeNardo, D. G., Egeblad, M., Evans, R. M., Fearon, D., Greten, F. R., Hingorani, S. R., Hunter, T., et al. (2020). A framework for advancing our understanding of cancer-associated fibroblasts. *Nat Rev Cancer* **20**, 174–186.

Sakakura, T., Sakagami, Y. and Nishizuka, Y. (1982). Dual origin of mesenchymal tissues participating in mouse mammary gland embryogenesis. *Developmental Biology* **91**, 202–207.

Scheele, C. L. G. J., E, H., Mj, M., A, Z., Ns, L., A, van O., Bd, S. and J, van R. (2017). Identity and dynamics of mammary stem cells during branching morphogenesis. *Nature* **542**,.

Schneider, M. R., Schmidt-Ullrich, R. and Paus, R. (2009). The hair follicle as a dynamic miniorgan. *Curr Biol* **19**, R132-142.

Schwalie, P. C., Dong, H., Zachara, M., Russeil, J., Alpern, D., Akchiche, N., Caprara, C., Sun, W., Schlaudraff, K.-U., Soldati, G., et al. (2018). A stromal cell population that inhibits adipogenesis in mammalian fat depots. *Nature* **559**, 103–108.

Shook, B. A., Wasko, R. R., Mano, O., Rutenberg-Schoenberg, M., Rudolph, M. C., Zirak, B., Rivera-Gonzalez, G. C., López-Giráldez, F., Zarini, S., Rezza, A., et al. (2020). Dermal Adipocyte Lipolysis and Myofibroblast Conversion Are Required for Efficient Skin Repair. *Cell Stem Cell* **26**, 880-895.e6.

Shyer, A. E., Tallinen, T., Nerurkar, N. L., Wei, Z., Gil, E. S., Kaplan, D. L., Tabin, C. J. and Mahadevan, L. (2013). Villification: how the gut gets its villi. *Science* **342**, 212–218.

Shyer, A. E., Rodrigues, A. R., Schroeder, G. G., Kassianidou, E., Kumar, S. and Harland, R. M. (2017). Emergent cellular self-organization and mechanosensation initiate follicle pattern in the avian skin. *Science* **357**, 811–815.

Stefkovich, M., Traynor, S., Cheng, L., Merrick, D. and Seale, P. (2021). Dpp4+ interstitial progenitor cells contribute to basal and high fat diet-induced adipogenesis. *Mol Metab* **54**, 101357.

Sternlicht, M. D. (2006). Key stages in mammary gland development: the cues that regulate ductal branching morphogenesis. *Breast Cancer Res* **8**, 201.

Sui, L., Alt, S., Weigert, M., Dye, N., Eaton, S., Jug, F., Myers, E. W., Jülicher, F., Salbreux, G. and Dahmann, C. (2018). Differential lateral and basal tension drive folding of Drosophila wing discs through two distinct mechanisms. *Nat Commun* **9**, 4620.

Sumbal, J. and Koledova, Z. (2019). FGF signaling in mammary gland fibroblasts regulates multiple fibroblast functions and mammary epithelial morphogenesis. *Development* **146**, dev185306.

Sumbal, J. and Koledova, Z. (2022). Single Organoids Droplet-Based Staining Method for High-End 3D Imaging of Mammary Organoids. *Methods Mol Biol* **2471**, 259–269.

Sumbal, J. and Sumbalova Koledova, Z. (2024). Fibroblast-Epithelium Co-culture Methods Using Epithelial Organoids and Cell Line-Derived Spheroids. *Methods Mol Biol* **2764**, 107–129.

Sumbal, J., Chiche, A., Charifou, E., Koledova, Z. and Li, H. (2020a). Primary Mammary Organoid Model of Lactation and Involution. *Front Cell Dev Biol* **8**, 68.

Sumbal, J., Vranova, T. and Koledova, Z. (2020b). FGF signaling dynamics regulates epithelial patterning and morphogenesis. 2020.11.17.386607.

Sumbal, J., Budkova, Z., Traustadóttir, G. Á. and Koledova, Z. (2020c). Mammary Organoids and 3D Cell Cultures: Old Dogs with New Tricks. *J Mammary Gland Biol Neoplasia* **25**, 273–288.

Sumbal, J., Belisova, D. and Koledova, Z. (2021). Fibroblasts: The grey eminence of mammary gland development. *Semin Cell Dev Biol* **114**, 134–142.

Sumbal, J., Fre, S. and Sumbalova Koledova, Z. (2024a). Fibroblast-induced mammary epithelial branching depends on fibroblast contractility. *PLoS Biol* **22**, e3002093.

Sumbal, J., Journot, R. P., Faraldo, M. M., Koledova, Z. S. and Fre, S. (2024b). Contractile fibroblasts are recruited to the growing mammary epithelium to support branching morphogenesis. 2024.06.05.597593.

Sun, C., Berry, W. L. and Olson, L. E. (2017). PDGFRα controls the balance of stromal and adipogenic cells during adipose tissue organogenesis. *Development* **144**, 83–94.

Susaki, E. A., Tainaka, K., Perrin, D., Kishino, F., Tawara, T., Watanabe, T. M., Yokoyama, C., Onoe, H., Eguchi, M., Yamaguchi, S., et al. (2014). Whole-brain imaging with single-cell resolution using chemical cocktails and computational analysis. *Cell* **157**, 726–739.

Sympson, C. J., Talhouk, R. S., Alexander, C. M., Chin, J. R., Clift, S. M., Bissell, M. J. and Werb, Z. (1994). Targeted expression of stromelysin-1 in mammary gland provides evidence for a role of proteinases in branching morphogenesis and the requirement

for an intact basement membrane for tissue-specific gene expression. *J Cell Biol* **125**, 681–693.

Tetley, R. J., Staddon, M. F., Heller, D., Hoppe, A., Banerjee, S. and Mao, Y. (2019). Tissue fluidity promotes epithelial wound healing. *Nat. Phys.* **15**, 1195–1203.

Van Linthout, S., Miteva, K. and Tschöpe, C. (2014). Crosstalk between fibroblasts and inflammatory cells. *Cardiovasc Res* **102**, 258–269.

Veltmaat, J. M., Van Veelen, W., Thiery, J. P. and Bellusci, S. (2004). Identification of the mammary line in mouse by Wnt10b expression. *Dev Dyn* **229**, 349–356.

Veltmaat, J. M., Relaix, F., Le, L. T., Kratochwil, K., Sala, F. G., van Veelen, W., Rice, R., Spencer-Dene, B., Mailleux, A. A., Rice, D. P., et al. (2006). Gli3-mediated somitic Fgf10 expression gradients are required for the induction and patterning of mammary epithelium along the embryonic axes. *Development* **133**, 2325–2335.

Villeneuve, C., Hashmi, A., Ylivinkka, I., Lawson-Keister, E., Miroshnikova, Y. A., Pérez-González, C., Myllymäki, S.-M., Bertillot, F., Yadav, B., Zhang, T., et al. (2024). Mechanical forces across compartments coordinate cell shape and fate transitions to generate tissue architecture. *Nat Cell Biol* **26**, 207–218.

Wang, Y., Chaffee, T. S., LaRue, R. S., Huggins, D. N., Witschen, P. M., Ibrahim, A. M., Nelson, A. C., Machado, H. L. and Schwertfeger, K. L. (2020). Tissue-resident macrophages promote extracellular matrix homeostasis in the mammary gland stroma of nulliparous mice. *eLife* **9**, e57438.

Wang, J., Song, W., Yang, R., Li, C., Wu, T., Dong, X. B., Zhou, B., Guo, X., Chen, J., Liu, Z., et al. (2021a). Endothelial Wnts control mammary epithelial patterning via fibroblast signaling. *Cell Reports* **34**, 108897.

Wang, S., Matsumoto, K., Lish, S. R., Cartagena-Rivera, A. X. and Yamada, K. M. (2021b). Budding epithelial morphogenesis driven by cell-matrix versus cell-cell adhesion. *Cell* **184**, 3702-3716.e30.

Watson, C. J. (2006). Involution: apoptosis and tissue remodelling that convert the mammary gland from milk factory to a quiescent organ. *Breast Cancer Res* **8**, 203.

Watson, C. J. and Khaled, W. T. (2008). Mammary development in the embryo and adult: a journey of morphogenesis and commitment. *Development* **135**, 995–1003.

Wendling, O., Bornert, J.-M., Chambon, P. and Metzger, D. (2009). Efficient temporally-controlled targeted mutagenesis in smooth muscle cells of the adult mouse. *Genesis* **47**, 14–18.

Wiseman, B. S. and Werb, Z. (2002). Stromal effects on mammary gland development and breast cancer. *Science* **296**, 1046–1049.

Witty, J. P., Wright, J. H. and Matrisian, L. M. (1995). Matrix metalloproteinases are expressed during ductal and alveolar mammary morphogenesis, and misregulation of stromelysin-1 in transgenic mice induces unscheduled alveolar development. *Mol Biol Cell* **6**, 1287–1303.

Ye, X., Tam, W. L., Shibue, T., Kaygusuz, Y., Reinhardt, F., Ng Eaton, E. and Weinberg, R. A. (2015). Distinct EMT programs control normal mammary stem cells and tumour-initiating cells. *Nature* **525**, 256–260.

Yoshitake, R., Chang, G., Saeki, K., Ha, D., Wu, X., Wang, J. and Chen, S. (2022). Single-Cell Transcriptomics Identifies Heterogeneity of Mouse Mammary Gland Fibroblasts With Distinct Functions, Estrogen Responses, Differentiation Processes, and Crosstalks With Epithelium. *Frontiers in Cell and Developmental Biology* **10**,.

Young, R. E., Jones, M.-K., Hines, E. A., Li, R., Luo, Y., Shi, W., Verheyden, J. M. and Sun, X. (2020). Smooth Muscle Differentiation Is Essential for Airway Size, Tracheal Cartilage Segmentation, but Dispensable for Epithelial Branching. *Dev Cell* **53**, 73-85.e5.

Yuan, L., Xie, S., Bai, H., Liu, X., Cai, P., Lu, J., Wang, C., Lin, Z., Li, S., Guo, Y., et al. (2023). Reconstruction of dynamic mammary mini gland in vitro for normal physiology and oncogenesis. *Nat Methods* **20**, 2021–2033.

Zachara, M., Rainer, P. Y., Hashimi, H., Russeil, J. M., Alpern, D., Ferrero, R., Litovchenko, M. and Deplancke, B. (2022). Mammalian adipogenesis regulator (Areg) cells use retinoic acid signalling to be non- and anti-adipogenic in age-dependent manner. *EMBO J* **41**, e108206.

Zhang, X., D, M., Z, K., G, Q., Ch, S. and P, L. (2014). FGF ligands of the postnatal mammary stroma regulate distinct aspects of epithelial morphogenesis. *Development (Cambridge, England)* **141**,.

Zhang, L., Guerrero-Juarez, C. F., Hata, T., Bapat, S. P., Ramos, R., Plikus, M. V. and Gallo, R. L. (2015). Innate immunity. Dermal adipocytes protect against invasive Staphylococcus aureus skin infection. *Science* **347**, 67–71.

Zhang, L.-J., Chen, S. X., Guerrero-Juarez, C. F., Li, F., Tong, Y., Liang, Y., Liggins, M., Chen, X., Chen, H., Li, M., et al. (2019). Age-Related Loss of Innate Immune Antimicrobial Function of Dermal Fat Is Mediated by Transforming Growth Factor Beta. *Immunity* **50**, 121-136.e5.

Zhang, J., Yu, H., Man, M.-Q. and Hu, L. (2024). Aging in the dermis: Fibroblast senescence and its significance. *Aging Cell* **23**, e14054.

Zwick, R. K., Rudolph, M. C., Shook, B. A., Holtrup, B., Roth, E., Lei, V., Van Keymeulen, A., Seewaldt, V., Kwei, S., Wysolmerski, J., et al. (2018). Adipocyte hypertrophy and lipid dynamics underlie mammary gland remodeling after lactation. *Nat Commun* **9**, 3592.

Appendix A: Fibroblast-induced mammary epithelial branching depends on fibroblast contractility

The first appendix is the published article in PLOS Biology. The paper is described and discussed in the preface 1. For the best possible experience, I recommend you to visit the publisher's website at doi.org/10.1371/journal.pbio.3002093, that contains supplementary information including movies of the time-lapse experiments.

PLOS BIOLOGY

RESEARCH ARTICLE

Fibroblast-induced mammary epithelial branching depends on fibroblast contractility

Jakub Sumbal[1,2,3], **Silvia Fre**[2], **Zuzana Sumbalova Koledova**[1¤*]

1 Masaryk University, Faculty of Medicine, Department of Histology and Embryology, Brno, Czech Republic, **2** Institut Curie, Laboratory of Genetics and Developmental Biology, INSERM U934, CNRS UMR3215, PSL Université Paris, Paris, France, **3** Sorbonne Université, Collège Doctoral, Paris, France

¤ Current address: Institute of Molecular Genetics of the Czech Academy of Sciences, Prague, Czech Republic
* koledova@med.muni.cz, zuzana.sumbalova-koledova@img.cas.cz

OPEN ACCESS

Citation: Sumbal J, Fre S, Sumbalova Koledova Z (2024) Fibroblast-induced mammary epithelial branching depends on fibroblast contractility. PLoS Biol 22(1): e3002093. https://doi.org/10.1371/journal.pbio.3002093

Academic Editor: Emma Rawlins, University of Cambridge, UNITED KINGDOM

Received: March 13, 2023

Accepted: November 24, 2023

Published: January 10, 2024

Peer Review History: PLOS recognizes the benefits of transparency in the peer review process; therefore, we enable the publication of all of the content of peer review and author responses alongside final, published articles. The editorial history of this article is available here: https://doi.org/10.1371/journal.pbio.3002093

Data Availability Statement: All relevant data are within the paper and its Supporting Information files.

Funding: This work was supported by grants from the Grant Agency of Masaryk University (MU)

Abstract

Epithelial branching morphogenesis is an essential process in living organisms, through which organ-specific epithelial shapes are created. Interactions between epithelial cells and their stromal microenvironment instruct branching morphogenesis but remain incompletely understood. Here, we employed fibroblast-organoid or fibroblast-spheroid co-culture systems and time-lapse imaging to reveal that physical contact between fibroblasts and epithelial cells and fibroblast contractility are required to induce mammary epithelial branching. Pharmacological inhibition of ROCK or non-muscle myosin II, or fibroblast-specific knockout of *Myh9* abrogate fibroblast-induced epithelial branching. The process of fibroblast-induced branching requires epithelial proliferation and is associated with distinctive epithelial patterning of yes associated protein (YAP) activity along organoid branches, which is dependent on fibroblast contractility. Moreover, we provide evidence for the in vivo existence of contractile fibroblasts specifically surrounding terminal end buds (TEBs) of pubertal murine mammary glands, advocating for an important role of fibroblast contractility in branching *in vivo*. Together, we identify fibroblast contractility as a novel stromal factor driving mammary epithelial morphogenesis. Our study contributes to comprehensive understanding of overlapping but divergent employment of mechanically active fibroblasts in developmental versus tumorigenic programs.

Introduction

Efficient formation of large epithelial surfaces in limited organ volumes is achieved through branching morphogenesis [1]. The underlying processes of epithelial morphogenesis, including epithelial cell proliferation, migration, intercalation, differentiation, and death, are regulated by both internal genetic programs as well as external cues provided by systemic signals (such as hormones) and local organ-specific microenvironment [1–3]. The mammary gland is the ideal tissue paradigm for stochastically branching epithelia. Mammary morphogenesis starts in the embryo, but the majority of branch bifurcations and ductal elongation takes place postnatally during puberty. During this time epithelial morphogenesis is driven by terminal

(https://gamu.muni.cz/; grants no. MUNI/G/1446/2018, MUNI/G/1775/2020 to Z.S.K., MUNI/A/1398/2021 and MUNI/A/1301/2022), from Internal Grant Agency of Faculty of Medicine MU (MUNI/11/SUP/06/2022 to Z.S.K. and MUNI/IGA/1314/2021 to J. S.), from Foundation pour la Recherche Médicale (FRM) (https://www.frm.org/; grant no. "FRM Equipes" EQU201903007821 to S.F., the Association for Research against Cancer (ARC) (https://www.fondation-arc.org/the-fondation-arc/; grant no. ARCPGA2021120004232_4874) to S.F., and from Czech Science Foundation (GAČR) (https://gacr.cz/; grant no. GA23-04974S to Z.S.K.). J.S. is supported by Barrande Fellowship (Ministry of Education, Youth and Sports; https://www.msmt.cz/), Fondation pour la Recherche Médicale (https://www.frm.org/; grant no. FDM202106013570), and by Brno PhD. Talent Scholarship, funded by the Brno City Municipality (https://www.jcmm.cz/projekt/brno_phd_talent/). The funders had no role in study design, data collection and analysis, decision to publish, or preparation of the manuscript.

Competing interests: The authors have declared that no competing interests exist.

Abbreviations: 3SB, 3D staining buffer; CAF, cancer-associated fibroblast; ECM, extracellular matrix; FBS, fetal bovine serum; FGF2, fibroblast growth factor 2; FGFR, FGF receptor; IHC-IF, immunohistochemistry-immunofluorescence; ROI, region of interest; TEB, terminal end bud; YAP, yes associated protein.

end buds (TEBs), bulb-shaped structures containing proliferative stratified epithelium that invades the surrounding mammary stroma [4].

The microenvironment of the mammary epithelium is a dynamic entity that consists of extracellular matrix (ECM) and stromal cells, including fibroblasts. Fibroblasts lay adjacent to the epithelium and have been well recognized as master regulators of mammary epithelial morphogenesis during puberty through production of growth factors [5–9] and ECM molecules [5,7,9–14] necessary for mammary epithelial growth and branching [15]. However, the dynamics of the epithelial–fibroblast interactions during mammary branching morphogenesis as well as whether fibroblasts contribute to shaping of mammary epithelium through additional mechanisms have remained unknown.

Microenvironment of several developing organs has been shown to govern epithelial patterning by dynamic cues of mechanically active cells. Dermal cells in chick skin determine feather buds by mechanical contraction [16], intestinal vilification is dependent on compression by smooth muscle cells [17], and embryonic lung mesenchyme promotes epithelial bifurcation by mechanical forces [18–20]. However, it has not been elucidated whether the mammary microenvironment contains an instructive component of mechanically active cells as well.

To answer this question, we performed live imaging and functional analysis of co-cultures of primary mammary epithelial organoids (isolated epithelial fragments with in vivo like architecture consisting of inner luminal and outer myoepithelial (basal) cells) with primary mammary fibroblasts. Analogously to primary mammary organoids treated with fibroblast growth factor 2 (FGF2), a well-established model of mammary branching morphogenesis driven by paracrine signals [21], our in vitro co-culture model provides a unique window into fibroblast–epithelial interactions during pubertal mammary branching morphogenesis. It enables visualization of stromal fibroblasts during dynamic morphogenetic processes, which are otherwise largely inaccessible in vivo due to light-scattering properties of mammary adipose tissue. In this work, we show that physical contact between fibroblasts and epithelial cells, and actomyosin-dependent contractility of fibroblasts are required for branching morphogenesis. We demonstrate successful reconstitution of budding morphogenesis by 3D co-culture of contractile fibroblasts in breast cancer spheroids that normally do not form buds. Moreover, by combining contractile fibroblasts with strong proliferative signals we reproduce TEB-like branching morphogenesis in organoid cultures and reveal localization of contractile fibroblasts around TEBs in the mammary glands, suggesting a role for fibroblast contractility in vivo. Our results reveal a novel role of fibroblast contractility in driving epithelial branching morphogenesis.

Results

Fibroblast-induced branching of organoids does not reproduce FGF2-induced budding

To uncover the role of fibroblasts in epithelial morphogenesis, we investigated differences between organoid budding induced solely by paracrine factors (using primary mammary organoids exposed to exogenous FGF2) and organoid branching induced by fibroblasts (using organoids co-cultured with primary mammary fibroblasts in the absence of any exogenous growth factor). Addition of FGF2 or fibroblasts to mammary organoid cultures both induced branching of epithelial organoids (Fig 1A and 1B and S1 Movie) but examination of the resulting organoid morphogenesis revealed important differences in dynamics and epithelial architecture in the 2 conditions. First, organoids co-cultured with fibroblasts developed bigger branches, but the branches were less numerous (Fig 1A, 1C and 1D). Second, they branched

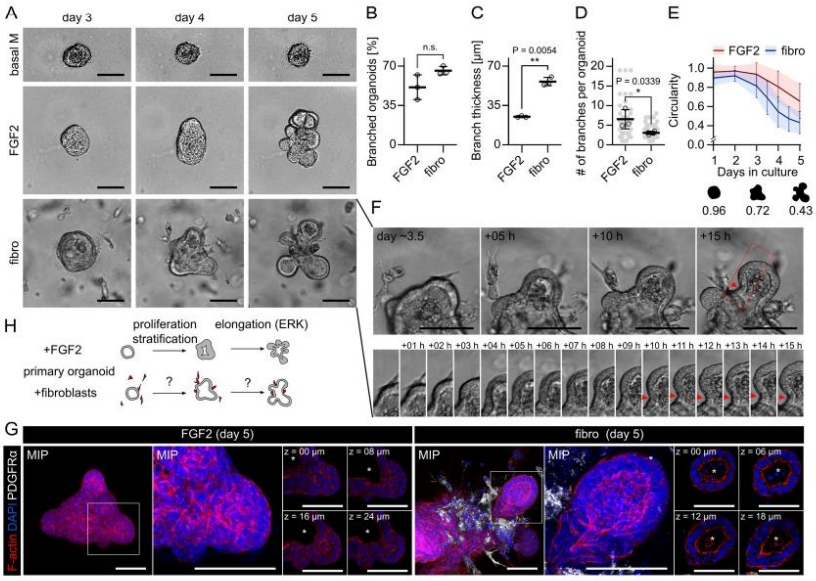

Fig 1. Fibroblast-induced branching of organoids does not reproduce FGF2-induced budding. **(A)** Snapshots from time-lapse imaging of primary mammary organoids in basal organoid medium (basal M) without any FGF supplementation (top), basal M with FGF2 (middle), or co-cultured with primary mammary fibroblasts (fibro) in basal M with no FGF supplementation (bottom). Scale bar: 100 μm. Full videos are presented in S1 Movie. **(B)** Quantification of percentage of branched organoids per all organoids in the conditions from **(A)**. The plot shows mean ± SD, each dot represents biologically independent experiment, $n = 3$. Statistical analysis: Two-tailored t test. **(C)** Quantification of branch thickness from experiments in **(A)**. The plot shows mean ± SD, each dot represents a biologically independent experiment, $n = 3$. Statistical analysis: Two-tailored t test. **(D)** Quantification of number of branches per branched organoids in conditions from **(A)**. The plot shows mean ± SD, each lined dot shows mean from each experiment, each faint dot shows single organoid measurement, $n = 3$ biologically independent experiments, $N = 20$ organoids per experiment. Statistical analysis: Two-tailored t test. **(E)** Quantification of organoid circularity in conditions from **(A)**. The lines represent mean, the shadows and error bars represent ± SD, $n = 3$ biologically independent experiments, $N = 20$ organoids per experiment. The schemes show representative shape of indicated circularity. **(F)** Detailed images of branch development in co-culture with fibroblasts from **(A)**. Scale bar: 20 μm. **(G)** MIP of F-actin (red), DAPI (blue), and PDGFRα (white) in organoid with exogenous FGF2 or with fibroblasts (fibro). Zoom-in area from the box is depicted as MIP and single z slices. The asterisks denote lumen. Scale bar: 100 μm. **(H)** A scheme depicting differences between organoid budding induced by exogenous FGF2 and organoid branching in a co-culture with fibroblasts. The data underlying the graphs shown in the figure can be found in S1 Data. FGF2, fibroblast growth factor 2; MIP, maximum intensity projection.

https://doi.org/10.1371/journal.pbio.3002093.g001

half-day to 1 day earlier than organoids treated with FGF2 (Fig 1A and 1E) and the branches were developed rapidly, including the development of negative curvature at the root of the branch (Fig 1F). Third, while FGF2-induced epithelial branching involved epithelial stratification as previously reported [21], co-culture with fibroblasts did not perturb the epithelial bilayer with its lumen (Fig 1A and 1G). These results suggest that fibroblasts and exogenous FGF2 drive organoid branching by different mechanisms.

While the mechanism of FGF2-induced organoid budding was previously described in detail to begin with epithelial proliferation and stratification [22] followed by budding and ERK-dependent and proliferation-independent bud elongation [23], how fibroblasts induce organoid branching remains unanswered (Fig 1H).

Endogenous paracrine signals are not sufficient to induce organoid branching in co-cultures

The ability of exogenous FGF2 to promote organoid budding [21] (Fig 1A) well demonstrates the importance of paracrine signals for epithelial branching, although FGF2 amount used in in vitro branching assays likely exceeds physiological values in vivo. Therefore, we sought to determine, whether endogenous FGFs or other paracrine signals produced by fibroblasts in co-cultures [5,7] are sufficient to drive organoid branching. First to test the involvement of FGF signaling, we inhibited either FGF receptors (FGFRs) using SU5402, or ERK, a common signaling node of all receptor tyrosine kinases using U0126. As expected, both inhibitors abolished branching induced by exogenous FGF2 (Fig 2A and 2B). However, in the co-cultures with fibroblasts, the same concentration of inhibitors did not abolish branching, albeit slightly reduced organoid growth (Fig 2A and 2B), suggesting that paracrine signaling via FGFR-ERK pathway is not the only mechanism driving organoid branching.

To probe the involvement of other paracrine signaling pathways in fibroblast-induced organoid branching, namely to test if fibroblast paracrine signaling alone is sufficient to induce organoid branching, or if other mechanisms involving fibroblast–epithelial proximity or contact are involved, we performed an array of different types of organoid (co-)culture set-ups (Fig 2C, top). When we provided unidirectional fibroblasts-to-epithelium paracrine signals by culture of organoids in fibroblast-conditioned medium, no organoid branching was observed (Fig 2C and 2D). When we allowed bidirectional paracrine signals by co-culture of organoids with fibroblasts in the same well but the organoids and fibroblasts were separated by a transwell membrane or by a thick layer of Matrigel, no organoid branching was observed either (Fig 2C and 2D). However, when we allowed both paracrine signals and physical contact between organoids and fibroblasts by co-culturing them together either dispersed in Matrigel or as aggregates of fibroblasts on top of organoids embedded in Matrigel, we observed organoid branching (Fig 2C–2E). These results demonstrated an essential requirement of fibroblast–epithelium contact for fibroblast-induced organoid branching, thus revealing that fibroblast-secreted paracrine factors are not sufficient to initiate branching.

MCF7-ras spheroids recapitulate fibroblast-induced branching of organoids

To further test the requirement of fibroblast–epithelium contact for fibroblast-induced epithelial branching, we developed a simpler co-culture system, where mammary fibroblasts were co-cultured with MCF7-ras breast cancer cell line spheroids (Fig 2F) instead of organoids from normal mammary epithelium. The advantage of MCF7-ras spheroids is that the spheroids grow constantly due to constitutively active RAS GTPase and unlike normal epithelium they do not respond to exogenous FGF2 (Fig 2G) or EGF (S1A Fig) by branching. We found that similarly to normal epithelium, MCF7-ras spheroids remained round in fibroblast co-cultures, which did not allow physical contact with fibroblasts, but developed numerous buds when physical contact with fibroblasts was allowed (Fig 2H and S1B Fig). These results demonstrated that fibroblasts are able to promote epithelial budding even in a system that is morphogenetically unresponsive to paracrine signals.

Fibroblasts form physical contact with organoids

To gain more insights into the mechanism of fibroblast-induced organoid branching, we examined organoid branching in the dispersed co-cultures in more detail. A day-by-day analysis of the contacts between fibroblasts and organoids revealed that the contacts are established

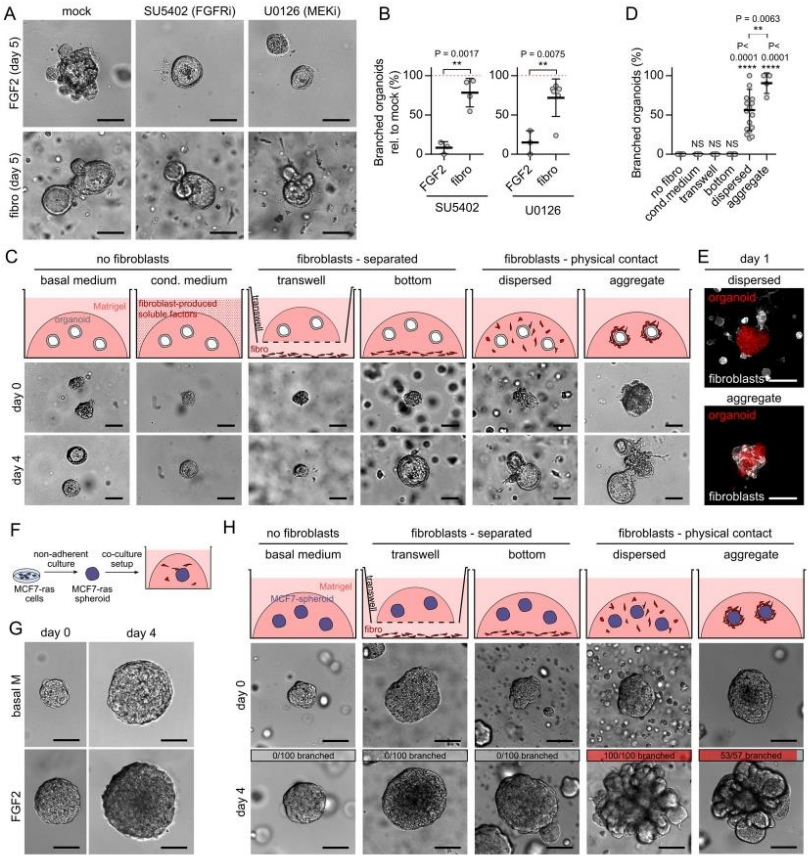

Fig 2. Endogenous paracrine signals are not sufficient to induce organoid branching. (A) Representative organoids cultured with exogenous FGF2 or with fibroblasts (fibro), treated with inhibitors of FGFR (SU5402) and MEK (U0126). Scale bar: 100 μm. **(B)** Quantification of branched organoid per all organoids, relative to mock. The plots show mean ± SD, each dot represents biologically independent experiment, $n = 3–5$, $N = 20$ organoids per experiment. Statistical analysis: Two-tailored *t* test. **(C)** Schemes and images on day 0 and day 4 of different organoid-fibroblast co-culture set-ups. Scale bar: 100 μm. **(D)** Quantification of organoid branching in different co-culture set-ups. The plot shows mean ± SD, each dot represents biologically independent experiment, $n = 16$ independent experiments for "no fibro," 5 for "cond. medium," 5 for "transwell," 12 for "bottom," 16 for "dispersed," and 4 for "aggregate," $N = 20$ organoids per experiment. Statistical analysis: Multiple *t* tests compared to control "no fibro," or indicated by the line. **(E)** Dispersed and aggregated co-culture of LifeAct-GFP fibroblast (white) and tdTomato organoid (red) at the beginning of the culture. Scale bar: 100 μm. **(F)** A scheme of MCF7-ras spheroid co-culture setup. **(G)** Representative MCF7-ras spheroids cultured in basal organoid medium (basal M) or basal M with exogenous FGF2. Scale bar: 100 μm. **(H)** Schemes and images on day 0 and day 4 of different spheroid-fibroblast co-culture set-ups. Top gray and red bars indicate proportion of branched spheroids out of all spheroids per condition, $n = 3–5$ independent experiments, $N = 20$ spheroids per experiment. Scale bar: 100 μm. The data underlying the graphs shown in the figure can be found in S1 Data. FGF2, fibroblast growth factor 2; FGFR, FGF receptor.

https://doi.org/10.1371/journal.pbio.3002093.g002

from the first day and thus precede the branching events that occur on days 3 and 4 (S2A–S2C Fig). To corroborate this finding, we performed a co-culture experiment with organoids labeled by tdTomato and GFP-tagged fibroblasts. The time-lapse movies confirmed that

fibroblasts came in close contact with the epithelium early during the co-culture and remained there during branching (Fig 3A and S2 Movie). Confocal imaging analysis revealed that fibroblasts (marked by PDGFRα) came in contact with all organoids (100% of 59 organoids analyzed in 3 independent biological replicates, S2D Fig) and contacted a larger proportion of the organoid middle sectional perimeter in round organoids than in branched organoids (S2E Fig).

On the branched organoids, fibroblasts were predominantly located around the necks of the nascent branches and sat directly in contact with the epithelium (Fig 3B and 3C). Immunofluorescence staining of epithelial markers revealed that fibroblasts formed contacts with KRT5 positive myoepithelial cells (Fig 3D and 3E). Transmission electron microscopy of the co-cultures confirmed the close proximity between the fibroblasts and the epithelium, with a thin layer of ECM in between (Fig 3F). Using immunostaining we detected laminin 5, a basal membrane component, between the organoid and the adjacent fibroblast (Fig 3G and 3H). These data suggest that fibroblasts form contacts with epithelium via ECM.

Fibroblast-induced epithelial branching depends on fibroblast contractility

Based on observations from the time-lapse videos of organoids branched by fibroblasts (S1 and S2 Movies), we hypothesized that fibroblasts could constrict epithelium, folding it into branches. Immunofluorescence investigation of fibroblast-branched organoids revealed that fibroblasts in contact with the organoid formed a cellular loop, encircling the branch neck (Figs 4A and S3A–S3C and S3 Movie), and contained F-actin cables oriented mostly perpendicularly to the branch longitudinal axis (Fig 4A). Moreover, the fibroblasts stained positively for phosphorylated myosin light chain 2 (P-MLC2), a marker of active non-muscle myosin II (Fig 4B). Therefore, we examined the involvement of fibroblast contractility in fibroblast-induced organoid branching using small molecule inhibitors of non-muscle myosin II (blebbistatin) or ROCK1/2 (Y27632), 2 major nodes of cell contractility. The contractility inhibitors abrogated branching in co-cultures but did not inhibit organoid budding induced by exogenous FGF2 (Fig 4C and 4D; ROCK inhibition in FGF2-induced organoids even led to hyperbranched phenotype as previously described [21]). Similarly to organoid co-cultures, in the MCF7-ras spheroid co-culture model, spheroid budding was inhibited by addition of contractility inhibitors (S4A–S4D Fig). Importantly, the contractility inhibitors did not diminish the capability of fibroblasts to migrate towards and contact the organoid (S5A–S5D Fig), in agreement with previous reports that showed that fibroblast migration in 3D is not abrogated by non-muscle myosin II inhibition [7]. Noteworthy, addition of the contractility inhibitors on day 3 of the co-culture, when branches were already formed, led to retraction of formed branches (S6A–S6D Fig), suggesting a role of contractility in branch maintenance as well as initiation.

Because exogeneous treatment with pharmacological inhibitors in the culture medium affects both epithelial cells and fibroblasts, we genetically targeted exclusively in fibroblasts the contractility machinery gene myosin heavy chain 9 (*Myh9*), one of the 2 non-muscle myosin II heavy chain genes expressed in mammary fibroblasts (S7A and S7B Fig). Both siRNA-mediated *Myh9* knock-down in wild-type fibroblasts and adenoviral Cre-mediated knock-out in $Myh9^{fl/fl}$ fibroblasts led to a decrease of organoid branching in co-cultures (Figs 4E, 4F and S8A–S8E and S4 and S5 Movies). To analyze if *Myh9* knock-out affected the ability of fibroblasts to migrate towards and contact the organoid, we took advantage of the mosaic nature of the adenovirus-mediated gene delivery. We quantified the amount of GFP+ fibroblasts (transduced by either Ad-Cre-GFP or Ad-GFP) and GFP-fibroblasts (not transduced by either of the adenoviruses) and compared their migration towards and contact with epithelium. We found no differences in their migration and epithelium-contacting abilities (S9A and S9B Fig). These

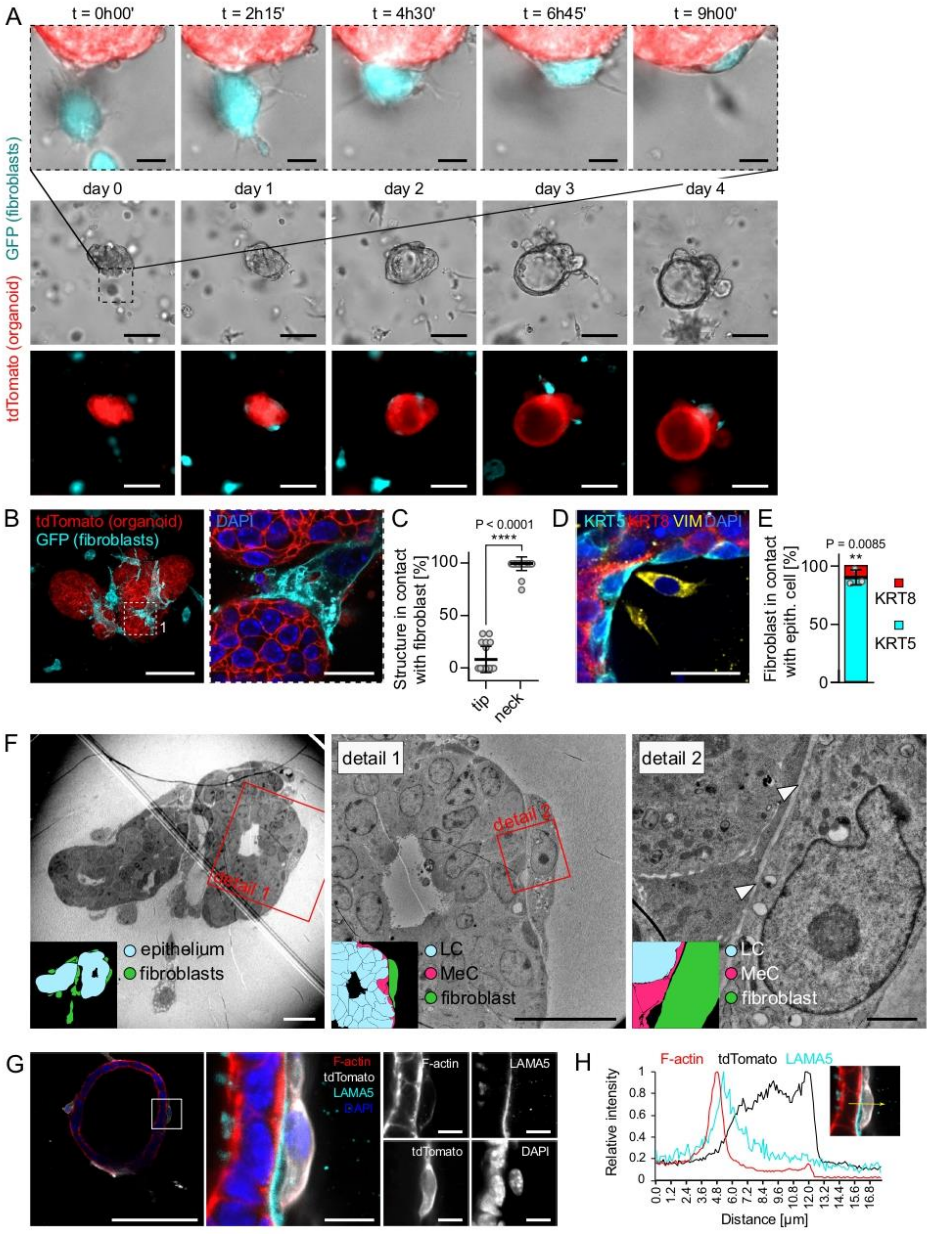

Fig 3. Fibroblasts in co-cultures are in physical contact with the epithelium. (A) Snapshots from time-lapse brightfield and fluorescence imaging of organoid (tdTomato) and fibroblast (GFP) co-culture (dispersed culture). Scale bar: 100 μm. Top line shows detail of fibroblast-organoid close interaction. Scale bar: 20 μm. **(B, C)** Images (**B**) and quantification (**C**) of the contact point between organoid (tdTomato) and

fibroblasts (GFP) on day 4 of co-culture (dispersed culture). Scale bar: 100 μm, scale bar in detail: 20 μm. **(C)** The plot shows mean ± SD, each dot represents 1 organoid, $n = 5$ experiments, $N = 21$ organoids. Statistical analysis: Two-tailored t test. **(D)** Images of the contact point between organoid (luminal (KRT8) and myoepithelial (KRT5) cells) and fibroblasts (VIM) on day 5 of co-culture (dispersed culture). Scale bar: 20 μm. **(E)** Quantification of fibroblasts in contact with KRT5+ or KRT8+ epithelial cells. The plot shows mean ± SD, each dot represents average from 1 biological replicate, $n = 3$ experiments, $N = 14$ organoids, 219 fibroblasts. Statistical analysis: Two-tailored t test. **(F)** Transmission electron micrographs and scheme (inset) of the contact point between luminal (LC, blue) and myoepithelial (MeC, magenta) cells and fibroblasts (green) on day 4 of co-culture (dispersed culture). Scale bar: 20 μm, scale bar in detail: 2 μm. In agreement with a published study (Ewald and colleagues), luminal cells are defined as lumen-facing cells, which present microvilli and numerous vesicles and granules. Myoepithelial cells are basally oriented, more elongated cells with less vesicles, granules, and organelles in the cytoplasm and they show a different electron density in their cytoplasm (it appears darker than the cytoplasm of luminal cells). The white arrowheads denote ECM between fibroblast and organoid. **(G)** Optical slice of organoid-fibroblast co-culture (dispersed culture), laminin 5 (cyan), DAPI (blue), F-actin (red), fibroblasts were isolated from *R26-mT/mG* mice (tdTomato, white). Scale bar: 100 μm, scale bar in detail: 10 μm. **(H)** A representative 1D relative fluorescence intensity plot. The measurement line is depicted in yellow (right). The data underlying the graphs shown in the figure can be found in S1 Data. ECM, extracellular matrix.

https://doi.org/10.1371/journal.pbio.3002093.g003

results demonstrate that fibroblast contractility is not necessary for fibroblast migration towards organoids but is required to induce organoid branching in co-cultures.

The need of fibroblast contractility for inducing epithelial branching suggests a mechanical signal transduction from fibroblasts to epithelium; therefore, we examined the subcellular localization of yes associated protein (YAP), a mechano-sensor that in a resting cell resides in the cytoplasm but translocates to the nucleus upon mechanical stress [24]. We found that YAP specifically accumulated in the nuclei of epithelial cells in the neck region of epithelial branch of the co-culture, the region in contact with contractile fibroblasts (Fig 4G and 4H). Importantly, this pattern was not present in branches induced with FGF2 (Fig 4G and 4I), indicating that YAP activation in epithelial cells at the necks of elongating buds is induced by the contact with contractile fibroblasts and not simply by the overall shape of the epithelial bud. However, knockout of *Myh9* in fibroblasts resulted in round organoids with no branching and a homogeneous distribution of nuclear YAP (Fig 4J). Our results show that while fibroblast contractility is necessary for the formation of branch with patterned YAP signal, the nuclear translocation of YAP can happen even in the absence of fibroblast contractility.

Fibroblast-induced epithelial branching requires epithelial proliferation

Activation of YAP signaling followed by its nuclear translocation is often associated with cell proliferation [24]. To investigate if such association is manifested in the organoids, we performed EdU labeling for proliferative cells. In the co-cultures, we detected highest cell proliferation in the stalks of the branches (S10A–S10C Fig), i.e., in the areas of YAP nuclear localization (Fig 4G). In contrast, in the FGF2-treated organoids, no such pattern of EdU+ cells was observed (S10A, S10B and S10D Fig).

To test whether epithelial proliferation (and thus expansion) plays a role in organoid branching in co-cultures, we inhibited cell proliferation using aphidicolin (DNA polymerase inhibitor), upon which we observed a severe defect in organoid branching (S10E–S10G Fig). To test for the possibility that the observed effect could be caused by inhibition of fibroblast proliferation, we performed the experiment also with fibroblasts pretreated with mitomycin C, an irreversible DNA synthesis blocker (S10E Fig). The pretreatment of fibroblast with mitomycin C had no effect on the result (S10E–S10G Fig), demonstrating that fibroblast proliferation is dispensable while epithelial proliferation is necessary for organoid branching in co-cultures. In concordance with the results from organoid co-cultures, in the MCF7-ras spheroid co-culture model the blockage of spheroid proliferation by mitomycin C pretreatment of spheroids decreased spheroid size expansion and dramatically decreased branching of the MCF7-ras spheroids (S11A and S11B Fig).

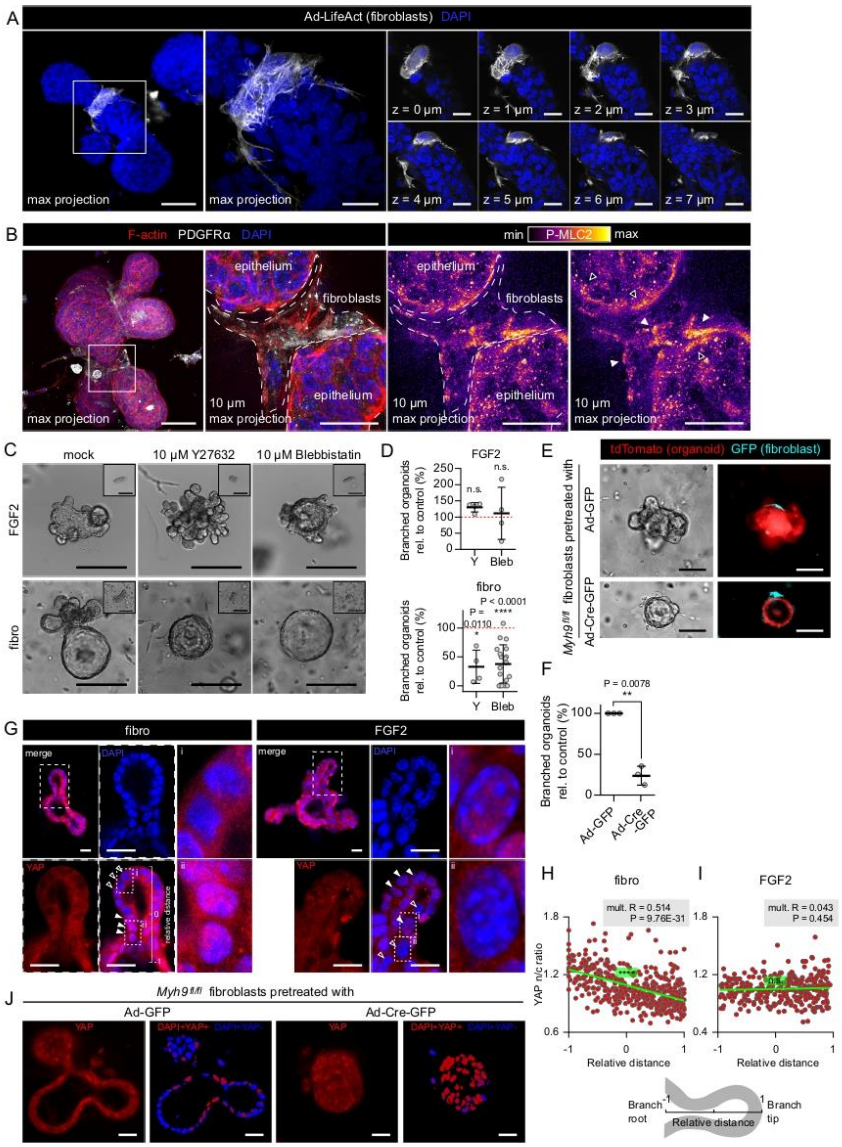

Fig 4. Fibroblast-induced branching requires fibroblast contractility. (A) Maximum projection (left), detailed maximum projection (middle), and detail optical sections (right) of organoid branch induced in co-culture with fibroblasts (day 4 of dispersed culture). DAPI (blue), fibroblasts prelabeled with Ad-LifeAct-GFP (white). Scale bar: 50 μm, scale bar in detail: 20 μm. **(B)** Full maximum projection (left) and 10 μm maximum projection (both middle and right) of organoid co-cultured with fibroblasts (dispersed culture). F-actin (red), PDGFRα (white), DAPI (blue), and phosphorylated myosin light chain 2 (P-MLC2, fire LUT). Scale bar: 50 μm, scale bar in detail: 20 μm. **(C)** Images of organoids on day 5 of culture (with day 0 insets) with FGF2 or

with fibroblasts (dispersed culture) and treated with mock (DMSO) or contraction inhibitors (ROCK1/2 inhibitor Y27632 or non-muscle myosin II inhibitor blebbistatin). Scale bar: 100 μm. **(D)** The plots show organoid branching with contraction inhibitors as mean ± SD. Statistical analysis: Multiple *t* tests between each treatment and the mock-treated control; $n = 4–18$ (each dot represents a biologically independent experiment), $N = 20$ organoids per experiment. **(E)** Images of tdTomato organoids on day 5 of co-culture with control or *Myh9* knock-out fibroblasts (dispersed culture). Scale bar: 100 μm. Videos from the 5-day experiment are presented in S5 Movie. **(F)** The plot shows organoid branching with control of *Myh9* knock-out fibroblasts from experiment in (**E**) as mean ± SD. Statistical analysis: two-tailored paired *t* test; $n = 3$ (each dot represents a biologically independent experiment), $N = 20$ organoids per experiment. **(G)** Staining of YAP in an organoid co-cultured with fibroblasts (dispersed culture) or with FGF2. Scale bar: 20 μm. Full arrowheads point to cells with nuclearly localized YAP, empty arrowheads point to cells with cytoplasmic YAP. **(H, I)** Quantification of YAP nuclear/cytoplasmic signal ratio. The scheme explains relative distance: −1 is branch root, +1 is branch tip. Each dot represents a single cell, $n = 436$ cells from 19 branches of 10 organoids (fibro, **H**); $n = 306$ cells from 12 branches of 10 organoids (FGF2, **I**). Statistical analysis: Linear regression, mult. R indicates correlation coefficient; P is the result of ANOVA F-test. **(J)** Staining of organoids co-cultured with control or *Myh9* knock-out fibroblasts. Scale bar: 200 μm. The data underlying the graphs shown in the figure can be found in S1 Data. FGF2, fibroblast growth factor 2; YAP, yes associated protein.

https://doi.org/10.1371/journal.pbio.3002093.g004

Evidence for the role of fibroblast contractility in epithelial morphogenesis in vivo

During puberty, the period of major mammary epithelial growth and branching, new primary mammary epithelial branches arise through bifurcation of TEBs. Could contractile fibroblasts play a role in this process? TEBs are large and highly proliferative stratified epithelial structures consisting of multiple (5–10) layers of luminal cells (called body cells) and an outer layer of basal cells (or cap cells). Such structures are not replicated in our co-culture model because we model only a part of the complex in vivo microenvironment—the effect of fibroblasts. In vivo the TEBs are surrounded by a complex stroma, which provides instructions for epithelial morphogenesis, including besides fibroblasts several more stromal cell types (adipocytes, immune cells) that secrete paracrine signals for epithelial proliferation [25–30]. While our reductionist in vitro co-culture model (consisting of fibroblasts and epithelial organoids in basal medium with no exogenous morphogenetic growth factors) was essential for untangling the importance of the contact versus paracrine signaling in fibroblast-induced branching, to model TEBs we needed to modify our co-culture model to promote epithelial proliferation.

The classic mammary organoid model cultured in Matrigel with FGF2 [21] mimics epithelial stratification to some extent (reaching 3–4 layers of luminal cells in TEB-like ends of the branches) but does not support full myoepithelial coverage of branches [31]. We revealed that a stabilized form of FGF2 (FGF2-STAB; [32,33]) induces several TEB-like features in the organoids, including highly proliferative phenotype, multiple layers of luminal cells, and full myoepithelial cell coverage [34]. When we exposed the dispersed organoid-fibroblast co-cultures to FGF2-STAB, the organoids developed large branches with a set of features typical of TEBs in vivo, including stratified luminal cells, full myoepithelial coverage, and presence of basal-in-luminal cells (similar to cap-in-body cells in vivo [4]) (Fig 5A–5G). These results demonstrate that combination of contractile fibroblasts and strong proliferative signals can reproduce several aspects typical for TEB branching in organoid cultures (Fig 5H).

Finally, we sought to determine whether the contractility-dependent mechanism of fibroblast-induced branching could take place in vivo. We found fibroblasts expressing a contractility marker alpha smooth muscle actin (αSMA) in developing mammary glands during puberty (Fig 6A). The αSMA+ fibroblasts specifically populate the stroma surrounding the TEBs (Fig 6A and 6B), the actively growing part of epithelium, which produces new branches. Importantly, the fibroblasts in co-cultures do express αSMA as well (Fig 6C). To visualize the organization of fibroblasts in the peri-TEB stroma, we performed whole organ immunostaining, clearing and imaging of the mammary gland. We observed that fibroblasts (stained for their cytoskeletal marker vimentin) were organized perpendicularly to the nascent bud in

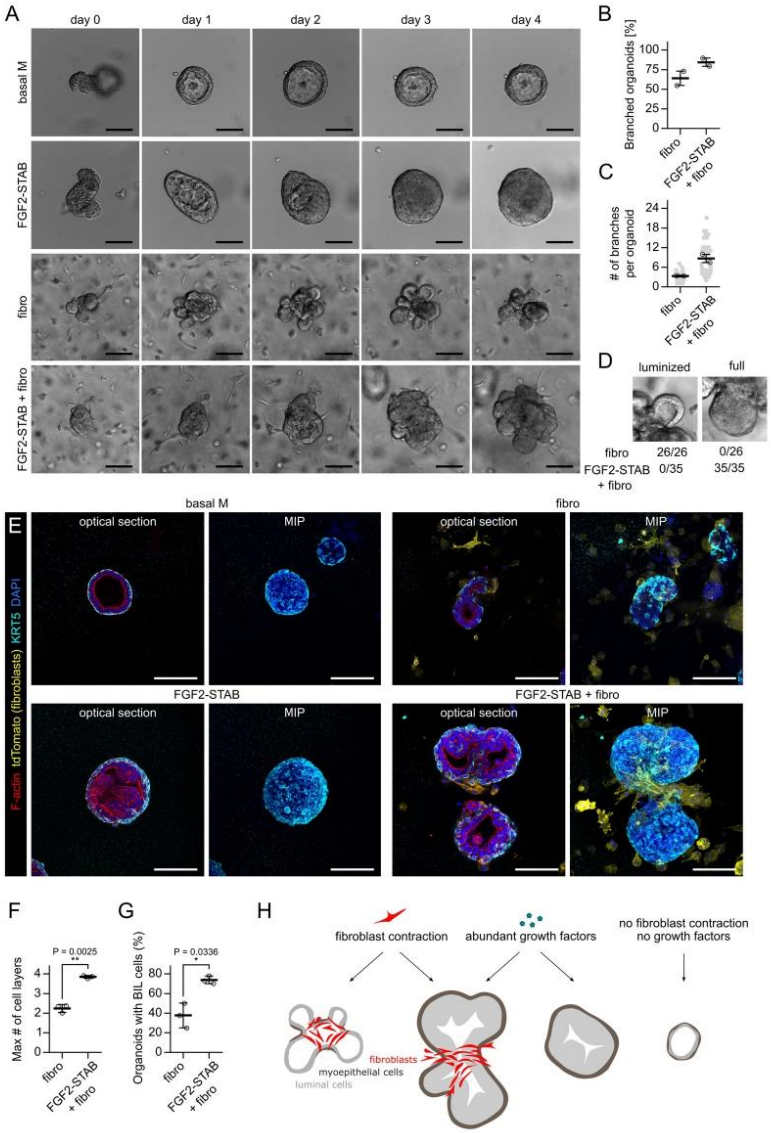

Fig 5. Combination of fibroblasts and FGF2-STAB induces TEB-like phenotype of organoids. (A) Time-lapse snap-shots of organoids grown in basal organoid medium with no exogenous growth factors (basal M), with FGF2-STAB, co-cultured with fibroblasts or co-cultured with fibroblasts with FGF2-STAB. Scale bar: 100 μm. **(B)** Quantification of organoid branching. The plot shows mean ± SD. $n = 2$ independent biological replicates, $N = 20$ organoids per experiment. **(C)** Quantification of number of branches per branched organoid. The plot shows mean ± SD. $n = 2$ independent biological replicates, $N = 12–19$ branching organoids per experiment. **(D)** Examples of luminized and full branch on bright-field imaging and quantification of the branch phenotypes. $n = 2$ independent biological replicates, $N = 12–19$ branching organoids per experiment. **(E)** Representative confocal images of organoids

on day 5 of culture with FGF2-STAB or fibroblasts. Scale bar: 100 μm. **(F)** Quantification of maximum number of cell layers in a branch in confocal images. The plot shows mean ± SD. The dots represent averages from individual experiments. Statistical analysis: two-tailored *t* test; $n = 3$ independent biological replicates, $N = 9–13$ organoids per experiment. **(G)** Quantification of the percentage of organoids with KRT5+ cells present within the layers of KRT5-cells (basal-in-luminal, BIL cells) in confocal images. The plot shows mean ± SD. Statistical analysis: two-tailored *t* test; $n = 3$ independent biological replicates, $N = 9–13$ organoids per experiment. **(H)** A schematic representation of uncoupling fibroblast contraction and growth factor signaling in organoids. The data underlying the graphs shown in the figure can be found in S1 Data. FGF2, fibroblast growth factor 2; TEB, terminal end bud.

https://doi.org/10.1371/journal.pbio.3002093.g005

bifurcating TEB (Fig 6D–i and S6 Movie) and perpendicularly to the epithelial growth direction at the TEB neck (Fig 6D-ii-1 and 6E and S7 Movie), forming loops similar to those observed in in vitro co-cultures (Figs 4A and 6F). On the other hand, fibroblasts surrounding subtending duct formed a less organized, mesh-like structure (Fig 6D-ii-2 and 6E). Together, our findings suggest that contractile fibroblasts could play a role in bifurcation of TEBs during branching morphogenesis in puberty.

Discussion

Mechanical forces are an integral part and a driving factor of tissue morphogenesis. However, the sources of mechanical forces in different tissues are still unclear and little is understood of how force sensing is translated into cell fate during organ formation. Our work reveals the critical role of fibroblast-derived mechanical forces in regulation of mammary epithelial branching morphogenesis. It demonstrates that mammary fibroblasts generate mechanical forces via their actomyosin apparatus and transmit them to the epithelium, which leads to epithelial deformation and patterning of epithelial intracellular signaling, resulting in epithelial folding into branched structures.

Fibroblast-generated mechanical forces as part of complex tissue mechanics

The role of intraepithelial forces in morphogenetic processes involving tissue folding, such as gastrulation, tubulogenesis, or buckling has been long recognized and intensively studied [35]. Similarly, the instructive role of mechanical properties and 3D organization of the ECM in determination of cell fate and behavior during organ formation, including mammary epithelial branching morphogenesis, has been well established [10,31,36]. However, the evidence for regulation of epithelial morphogenesis by mechanical stimuli from mesenchymal cells was discovered only recently and has been scarce, limited to the morphogenesis of feather buds in chick skin by mechanically active dermal cells [16], gut villification [17], and lung epithelial bifurcation and alveologenesis induced by smooth muscle cells or myofibroblasts [18–20,37].

Fibroblasts as central regulators of epithelial morphogenesis and homeostasis: Evidence for mechanically active fibroblasts in vivo

Fibroblasts accompany mammary epithelial cells from early development through homeostasis to aging and disease and employ different functions to meet epithelial needs [15]. The multiple fibroblast functions are facilitated by fibroblast heterogeneity, which has only recently begun to be resolved using single-cell RNA sequencing approaches [38,39]. These studies confirmed well-established fibroblast roles in epithelial development and tissue homeostasis via production of paracrine signals and ECM, and fibroblast roles in regulation of immune landscape of the mammary gland. Though they did not detect mechanically active fibroblasts. However, these studies included only adult and aged mammary glands and omitted puberty, the stage of active mammary epithelial branching morphogenesis. Using immunostaining on mammary

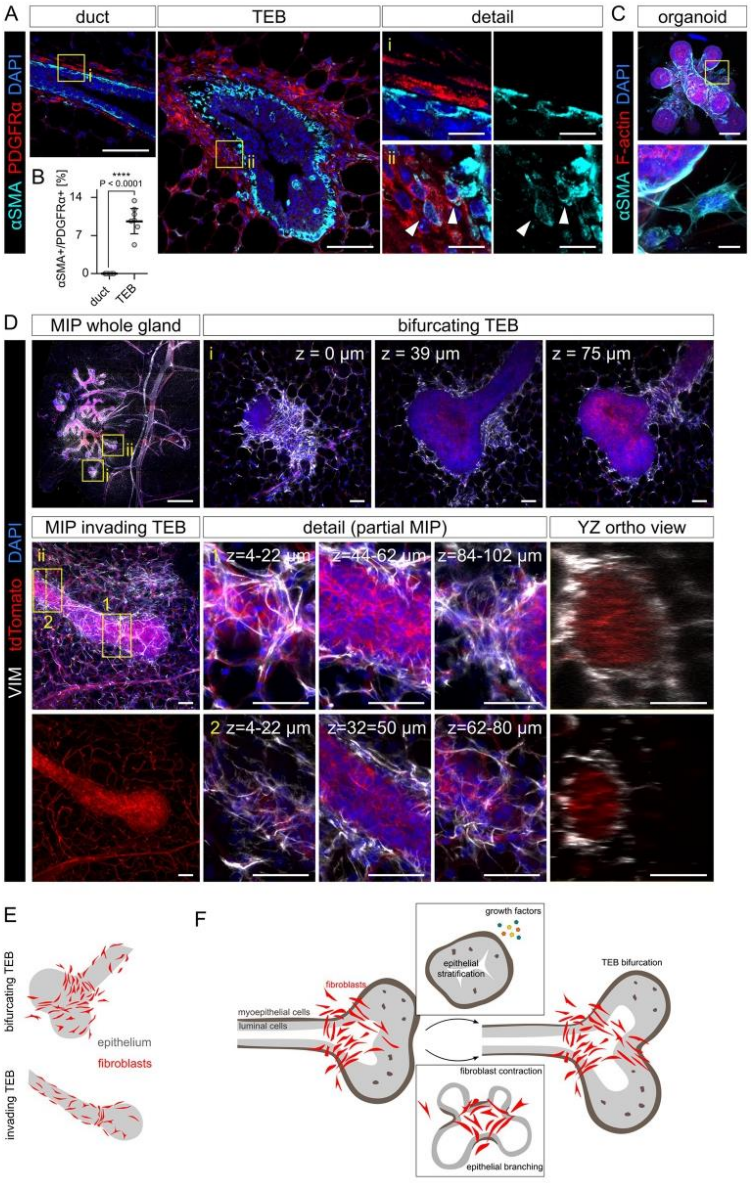

Fig 6. Contractile fibroblasts surround mammary TEBs in vivo. (A) PDGFRα and αSMA staining on pubertal mammary gland sections and detail of peri-ductal and peri-TEB fibroblasts. Scale bar: 50 μm and 10 μm in detail. **(B)** Quantification of αSMA+ cells out of PDGFRα+ fibroblasts. The plot shows mean ± SD, each dot represents 1 field of view, $n = 7$ TEBs and 8 ducts; statistical analysis: t test. **(C)** αSMA staining in a dispersed co-culture (day 5) and a detail of an αSMA+ fibroblast in contact with the organoid. Scale bar: 50 μm; scale bar in detail 10 μm. **(D)** Whole-mount

imaging of pubertal mammary gland stained for vimentin (VIM, a fibroblast marker). Detail (i) shows a bifurcating TEB. Detail (ii) shows an invading TEB, with close-up showing partial MIPs of upper, middle, and lower part of the TEB neck (1) and a subtending duct (2). The positions of the orthogonal YZ views are indicated with dashed yellow lines. Scale bar: 1 mm in the whole gland MIP, 50 μm in other images. **(E)** A schematic representation of fibroblasts surrounding TEBs in vivo and an organoid in vitro. Schemes were drawn from Figs 6D and 3B. **(F)** A schematic representation of our hypothesis on the role of contractile fibroblasts in TEB branching. Two mechanisms, paracrine signaling (growth factors) and mechanical cues (fibroblast contractility), which we uncoupled in vitro, work together to support mammary branching morphogenesis (TEB bifurcation) in vivo. The data underlying the graphs shown in the figure can be found in S1 Data. MIP, maximum intensity projection; TEB, terminal end bud.

https://doi.org/10.1371/journal.pbio.3002093.g006

glands in puberty, we discovered that mechanically active fibroblasts (contractile fibroblasts expressing αSMA, myofibroblasts) are localized specifically around TEBs, the main structures of epithelial branching during puberty, where they organize into structures similar to the loops observed in our fibroblast-organoid co-culture models. These data suggest that fibroblast contractility could play a role in mammary epithelial branching in vivo. Future studies employing myofibroblast-specific mouse models are needed to determine functional requirement of fibroblast contractility for mammary epithelial branching. Importantly, the presence and function of αSMA+ fibroblasts has been well documented in other developing or homeostatic organs, such as lung [40,41], intestine [42–44], or dermal sheath of the hair follicle [45,46]. While in the intestine the αSMA+ fibroblasts serve as a source of paracrine niche signals [42,44,47], the contractility of myofibroblasts is actively employed in alveolar septation [37] or relocation of the stem cell niche during hair cycle regression [45].

The mechanism of fibroblast-induced mammary morphogenesis: Connection to ECM remodeling

It was previously proposed that mechanical forces generated by mesenchymal/stromal cells regulate epithelial morphogenesis indirectly via changes of ECM mechanics, including collagen I remodeling in embryonic gut [48] and postnatal mammary gland [5,14,15], or elastin deposition in the lung [40]. However, while not excluding contribution of such mechanism to mammary epithelial branching in vivo, our investigations in vitro in organoid-fibroblast co-cultures devoid of collagen I demonstrate that collagen I fibers are not required for induction of epithelial folding by fibroblast contractility. Mammary fibroblasts form direct, highly dynamic contacts with mammary epithelial cells and induce a mechanosensitive response in the epithelium, resulting in patterning of a key morphogenetic regulator YAP. The direct contact between mammary fibroblasts and epithelial cells in vivo could be enabled by immature, thin basement membrane of TEBs [49], the highly proliferative epithelial structures, which drive pubertal mammary branching morphogenesis, and active remodeling of ECM by matrix metalloproteinases produced by both epithelial cells and fibroblasts [50], which is essential for mammary branching morphogenesis [50,51]. Our work does not exclude the importance of ECM remodeling by fibroblast mechanical forces in epithelial branching. We speculate that in vivo the highly dynamic mechanically active fibroblasts could initiate formation of epithelial clefts and further reinforce them by subsequent deposition and remodeling of ECM. Recently published simulations suggest that mammary pubertal branching is highly stochastic; however, its overall shape depends on the angle of TEB bifurcation [13,52]. Thus, the local effect of fibroblast contractility could affect the random branching pattern.

The intimate relationship between fibroblasts and epithelium

Although our co-culture experiments demonstrate the need for direct contact between fibroblasts and epithelium for epithelial branching, paracrine interactions between the 2 are also

likely to be involved. Particularly at the beginning of the co-culture, as the fibroblasts migrate towards the organoid, they may follow epithelial signals such as PDGF or FGF ligands, which have been shown to be produced by epithelial cells [53,54] and to stimulate the directional migration of fibroblasts in vitro [7,53]. The degree of fibroblast motility in vivo and their directed migration to the epithelium during mammary development remains an open question, and the use of intravital imaging may shed light on this issue.

Direct molecular contact via heterotypic adhesions has been reported to promote cancer cell migration and invasion [55,56], but it has been less studied in normal epithelium. In our co-culture, we did not observe fibroblasts promoting invasive behavior in either normal organoids or cancer cell spheroids and we detected an ECM layer separating organoid from fibroblasts, suggesting that a different mode of cell–cell contact takes place. Moreover, the ability of fibroblasts to promote contact-dependent branching regardless whether in contact with myoepithelial cells of organoids or luminal cells of cancer spheroids suggest that fibroblasts could promote organoid branching without a proper molecular connection, just by forming a supracellular fibroblast structure that envelops the epithelium and applies contractile forces, as it was suggested for cancer-associated fibroblasts (CAFs) interacting with intestinal tumors [57].

The mechanism of fibroblast-induced mammary morphogenesis: Requirement of paracrine signaling

Importantly, our results do not rule out the importance of fibroblast-secreted factors in mammary epithelial morphogenesis. However, we demonstrate that paracrine signals are not sufficient to drive organoid branching in the 3D in vitro cultures of organoids with fibroblasts without addition of any branching-inducing growth factors and show the importance of fibroblast-epithelium contact, so short-distance paracrine or juxtacrine signals could be important in the process. Several growth factors, including FGF2, FGF7, EGF, or TGFα can induce organoid branching in the absence of fibroblasts when added to the medium in nanomolar concentrations [58], including bifurcation of the organoid branches [59]. However, the evidence for requirement of those growth factors' expression in mammary fibroblasts for mammary epithelial branching in vivo is missing.

The mechanism of fibroblast-induced mammary morphogenesis: Epithelial response

Our work reveals that the mechanical strain imposed on mammary epithelial cells by fibroblasts results in epithelial folding with negative curvature in the epithelial–fibroblast contact points. The part of epithelium with negative curvature, the stalk of the branch shows presence of epithelial cells with nuclear YAP and increased epithelial proliferation. In contrast, the organoids that branched in response to exogenous FGF2 did not show patterned cell proliferation or YAP nuclear localization, further accentuating different mechanisms underlying epithelial branching in response to growth factors and contractile fibroblasts. It remains unclear though whether fibroblasts induce YAP activation to promote epithelial proliferation at the neck and thus bud elongation, or if the patterned YAP activation in epithelial buds reflects the proliferative status of cells located in different regions of the organoid. Our data suggest that epithelial proliferation in the co-cultures is mechanistically linked to the contact with the fibroblasts and/or to the mechanical stress imposed by the contractile fibroblasts in the underlying epithelium and in its vicinity, possibly through juxtacrine signaling or mechanochemical interplay. Budding morphogenesis of stratified epithelium, such as in the FGF2-induced mammary organoids, might employ self-organizing mechanisms, including preferential cell-ECM adhesion versus cell–cell adhesion as demonstrated in salivary gland organoids [60]. We propose that in

vivo, in the complex microenvironment of the stroma-invading, growing and bifurcating TEB, it is the combined action of contractile fibroblasts and strong proliferative signals from the stroma that governs the morphogenetic process. It was demonstrated that although the whole TEB contains proliferative cells, it is the cells localized in the neck of the TEB, which will mainly contribute to the growth of the adjacent duct, not the cells localized in the TEB tip [61]. Because contractile fibroblasts surround specifically the neck region of the TEB, we speculate that they play an essential role in this process.

Importantly, the direct interactions between mammary epithelium (including both organoids from normal epithelium and spheroids from breast cancer cells) and fibroblasts do not lead to invasive dissemination of epithelial cells, unlike in co-cultures of squamous cell carcinoma with CAFs [55]. Interestingly, a recent study described mechanical compression of intestinal tumors by CAFs forming a mechanically active tumor capsule [57], providing further evidence for context-dependent employment of fibroblast-derived mechanical forces in tissue morphogenesis and tumorigenesis. In conclusion, we find that fibroblasts drive branching morphogenesis in mammary organoids by exerting mechanical forces on epithelial cells. These observations support the hypothesis that contractile fibroblasts drive pubertal mammary branching; however, future in vivo studies will be needed to formally demonstrate this. It is conceivable that such conserved mechanism could be used to regulate morphogenesis of other branched organs, providing a comprehensive understanding of overlapping but divergent employment of mechanically active fibroblasts in developmental versus tumorigenic programs.

Materials and methods

Animals

All procedures involving animals were performed under the approval of the Ministry of Education, Youth and Sports of the Czech Republic (license # MSMT-9232/2020-2), supervised by the Expert Committee for Laboratory Animal Welfare of the Faculty of Medicine, Masaryk University, at the Laboratory Animal Breeding and Experimental Facility of the Faculty of Medicine, Masaryk University (facility license #58013/2017-MZE-17214), or under the approval of the ethics committee of the Institut Curie and the French Ministry of Research (reference #34364–202112151422480) in the Animal Facility of Institut Curie (facility license #C75–05–18). ICR mice were obtained from the Laboratory Animal Breeding and Experimental Facility of the Faculty of Medicine, Masaryk University. *R26-mT/mG* [62] and *Acta2-CreERT2* mice [63] were acquired from the Jackson Laboratories. LifeAct-GFP mice [64] were created by Wedlich-Söldner team, $Myh9^{fl/fl}$ mice [65] were kindly provided by Dr. Sara Wickström. Transgenic animals were maintained on a C57/BL6 background. Experimental animals were obtained by breeding of the parental strains, the genotypes were determined by genotyping. The mice were housed in individually ventilated or open cages, all with ambient temperature of 22˚C, a 12 h:12 h light:dark cycle, and food and water ad libitum. Female 4 to 8 weeks old virgin mice were used in the experiments. Mice were euthanized by cervical dislocation and mammary gland tissues were collected immediately.

Primary mammary organoid and fibroblast isolation and culture

Primary mammary fibroblasts and organoids were isolated from 6 to 8 weeks old female virgin mice (ICR, unless otherwise specified) as previously described [66]. The mammary glands were chopped and partially digested in a solution of collagenase and trypsin [2 mg/ml collagenase A, 2 mg/ml trypsin, 5 μg/ml insulin, 50 μg/ml gentamicin (all Merck), 5% fetal bovine serum (FBS; Hyclone/GE Healthcare) in DMEM/F12 (Thermo Fisher Scientific)] for 30 min

at 37˚C. Resulting tissue suspension was treated with DNase I (20 U/ml; Merck) and submitted to 5 rounds of differential centrifugation (450 × g for 10 s) to separate epithelial (organoid) and stromal fractions. The organoids were resuspended in basal organoid medium [1 × ITS (10 μg/ml insulin, 5.5 μg/ml transferrin, 6.7 ng/ml sodium selenite), 100 U/ml of penicillin, and 100 μg/ml of streptomycin in DMEM/F12] and kept on ice until co-culture setup. The cells from the stromal fraction were pelleted by centrifugation, suspended in fibroblast cultivation medium (10% FBS, 1× ITS, 100 U/ml of penicillin, and 100 μg/ml of streptomycin in DMEM) and incubated on cell culture dishes at 37˚C, 5% CO_2 for 30 min. Afterwards, the unattached (non-fibroblast) cells were washed away, the cell culture dishes were washed with PBS and fresh fibroblast medium was provided for the cells. The cells were cultured until about 80% confluence. During the first cell subculture by trypsinization, a second round of selection by differential attachment was performed, when the cells were allowed to attach only for 15 min at 37˚C and 5% CO_2. The fibroblasts were expanded and used for the experiments until passage 5.

To inhibit fibroblast proliferation for specific assays, the fibroblasts were treated with 10 μg/ml mitomycin C in fibroblast medium for 3 h at 37˚C, 5% CO_2. Afterwards, the fibroblasts were washed 3 times with PBS and 1 time with basal organoid medium, trypsinized and used to set up co-cultures.

To prepare fibroblast-conditioned medium, the fibroblasts were seeded in cell culture dishes in fibroblast medium and the next day, the cells were washed 3 times with PBS and incubated with basal organoid medium for 24 h. Afterwards, the medium was collected from the dishes, sterile-filtered through a 0.22 μm filter, and used immediately in the experiment, or aliquoted, stored at −20˚C and used within 5 days of conditioned medium preparation.

3D culture of mammary organoids and fibroblasts

3D culture of mammary organoids and fibroblasts was performed as previously described [67]. Freshly isolated mammary organoids were embedded in Matrigel either alone (300 organoids in 45 μl of Matrigel per well) or with 5×10^4 mammary fibroblasts per well and plated in domes in 24-well plates. For transwell experiments, organoids were plated in domes in the transwell (8 μm pore size, Falcon-Corning), fibroblasts were plated in lower chamber. After setting the gel for 45 to 60 min at 37˚C, the cultures were overlaid with basal organoid medium (1× ITS, 100 U/ml of penicillin, and 100 μg/ml of streptomycin in DMEM/F12), not supplemented or supplemented with growth factors [2.5 nM FGF2 (Enantis) or 2.5 nM FGF2-STAB (Enantis)] or small molecule inhibitors (S1 Table) according to the experiment. The cultures were incubated in humidified atmosphere of 5% CO_2 at 37˚C on Olympus IX81 microscope equipped with Hamamatsu camera and CellR system for time-lapse imaging. The organoids/co-cultures were photographed every 60 min for 5 days with manual refocusing every day (high-detail imaging) or photographed only once per day for 5 days (low-detail imaging). The images were exported and analyzed using Image J. Organoid branching and retraction was evaluated from videos and it was defined as formation (or loss) of a new bud/branch from the organoid. Organoids that fused with another organoid or collapsed after attachment to the bottom of the dish were excluded from the quantification. Quantification of fibroblast-organoid contacts was performed manually in ImageJ. Quantification of branch thickness was performed on images from day 5 of culture, manually in ImageJ.

For fluorescent time-lapse imaging, organoids were isolated from *R26-mT/mG* mammary glands on day of the experiment. Fibroblasts were isolated from *Acta2-CreERT2;mT/mG* mice, cultured to passage 2–3 and induced in vitro by 0.5 mM 4-OH-tamoxifen (Sigma) treatment for 4 days prior to trypsinization and experimental use. Before experiment, the GFP

fluorescence of fibroblasts was assessed using a microscope and when it was > 95%, the cells were used for co-culture. Co-cultures were seeded on coverslip-bottom 24-well plate (IBIDI) and imaged on Cell Discoverer 7 equipped with PLAN-APOCHROMAT 20×/0.95 autocorr with 0.5× magnification lens. GFP was imaged with 470/40 nm excitation, 525/50 nm emission, tdTomato was imaged with 545/25 nm excitation, 605/70 nm emission filter (all Zeiss). The samples were incubated in a humidified atmosphere of 5% CO_2 at 37˚C during the imaging.

3D culture of spheroids and fibroblasts

MCF7-ras cells ([68] kindly provided by Dr. Ula Polanska) were expanded in DMEM/F12 supplemented with 10% FBS, 100 U/ml of penicillin, and 100 μg/ml of streptomycin and incubated in non-adherent PolyHEMA-coated dish overnight to form spheroids. Next day, the spheroids were embedded either alone (200 spheroids in 45 μl of Matrigel per well) or with 5×10^4 mammary fibroblasts per well and plated in domes in 24-well plates. After setting the gel for 45 to 60 min at 37˚C, the cultures were overlaid with basal organoid medium, supplemented with growth factors [2.5 nM FGF2 (Enantis) or EGF (Peprotech)] small molecule inhibitors (S1 Table) according to the experiment. The (co-)cultures were incubated in a humidified atmosphere of 5% CO_2 at 37˚C on Olympus IX81 microscope equipped with Hamamatsu camera and CellR system for time-lapse imaging and photographed every 60 min for 5 days with manual refocusing every day (high-detail imaging) or photographed only once per day for 5 days (low-detail imaging). The images were exported and analyzed using Image J. Spheroid budding was evaluated from the videos and it was defined as formation of a new bud from the spheroid. Spheroids that fused with other spheroids were excluded from the quantification.

Knockdown and knockout of *Myh9* in mammary fibroblasts

For *Myh9* knockdown, the pre-designed Silencer Select siRNAs against *Myh9* (IDs s70267 and s70268, Myh9si#1 and Myh9si#2, respectively) and the scrambled negative control siRNA (Silencer Select negative control or Stealth negative control siRNA), all from Thermo Fisher Scientific, were transfected into wild-type (ICR) fibroblasts with Lipofectamine 3000 Reagent (Thermo Fisher Scientific) according to manufacturer's instructions at 20 nM siRNA. For *Myh9* knockout, $Myh9^{fl/fl}$ fibroblasts were transduced with adenoviruses Adeno-Cre-GFP (Ad-Cre-GFP) or Adeno-GFP (Ad-GFP) from Vector Biolabs at 200 MOI for 4 h. Next day, the transfected/transduced fibroblasts were put in co-culture with organoids and submitted to bright-field or fluorescent time-lapse imaging. A part of the fibroblasts was further cultured and knockdown/knockout efficiency was determined 72 h after transfection/transduction by qPCR analysis of *Myh9* mRNA levels, normalized to housekeeping genes *Actb* and *Eef1g*, and by immunostaining for MYH9.

LifeAct adenoviral transduction

For imaging experiments with LifeAct, fibroblasts were infected with LifeAct adenoviral particles (IBIDI) according to the manufacturer's instructions prior to co-culture set-up. Briefly, the adenovirus particles were reconstituted in fibroblast cultivation medium at concentration of 500 MOI and incubated with adherent fibroblasts at 37˚C for 4 h. After that, adenovirus-containing medium was washed out, and the cells were kept overnight in fibroblast cultivation medium. The next day, GFP fluorescence was checked under the microscope and when >50% of cells appeared green, fibroblasts were used for co-culture.

Immunofluorescence staining of 2D fibroblasts

For immunofluorescent analysis, fibroblasts were cultured directly on glass coverslips, fixed with 10% neutral buffered formalin, permeabilized with 0.05% Triton X-100 in PBS and blocked with PBS with 10% FBS. Then, the coverslips were incubated with primary antibodies (S2 Table) for 2 h at RT or overnight at 4˚C. After washing, the coverslips were incubated with secondary antibodies and phalloidin AlexaFluor 488 (S2 Table) for 2 h at RT. Then, the coverslips were washed, stained with DAPI (1 μg/ml; Merck) for 10 min and mounted in Mowiol (Merck). The cells were photographed using Axio Observer Z1 microscope with laser scanning confocal unit LSM 800 with 405, 488, 561, and 640 nm lasers, GaAsp PMT detector and objective Plan-Apochromat 40×/1.20 and C-Apochromat 63× /1.20 with water immersion (all Zeiss). The brightness of each channel was linearly enhanced in Zen Blue software (Zeiss) and pictures were cropped to final size in Photo Studio 18 (Zoner).

Immunofluorescence staining of 3D co-cultures

For immunofluorescent analysis of 3D co-cultures, the co-cultures were fixed with 10% neutral buffered formalin, washed, and stored in PBS. Next, organoid co-cultures were stained according to the droplet-based method as described [69]. Briefly, the fixed co-cultures were placed on stereoscope (Leica FM165C) and pieces containing an organoid with approximately 100 μm of surrounding Matrigel with fibroblasts were manually cut out with 25G needles and moved on parafilm-covered cell culture dish for staining. All the staining steps were done on the parafilm in 20 μl drops, and all solutions were changed under direct visual control using the stereoscope. The co-cultures were permeabilized with 0.5% Triton X-100 in PBS, blocked with 8% FBS and 0.1% Triton X-100 in PBS (3D staining buffer, 3SB) and incubated with primary antibodies (S2 Table) in 3SB over 1 to 3 nights at 4˚C. Then, the co-cultures were washed for 3 h with 0.05% Tween-20 in PBS and incubated with secondary antibodies, phalloidin AlexaFluor 488 (S2 Table) and DAPI (1 μg/ml; Merck) in 3SB over 1 to 2 nights at 4˚C in dark. Then, the co-cultures were washed for 3 h with 0.05% Tween-20 in PBS, cleared with 60% glycerol and 2.5 M fructose solution overnight at RT in dark and mounted between slide and coverslip with double-sided tape as a spacer. The co-cultures were imaged using inverted microscope Axio Observer 7 with laser scanning confocal unit LSM 880 with 405, 488, 561, and 633 nm lasers, GaAsp PMT spectral detector and objective C-Apochromat 40×/1.20 or C-Apochromat 63×/1.20 with water immersion (all Zeiss). The co-cultures were photographed either as one optical slice or as 3D z-stacks of various z-step as required per experiment. The brightness of each channel was linearly enhanced in Zen Blue software (Zeiss) and pictures were cropped to final size in Photo Studio 18 (Zoner). Image analysis was done manually in ImageJ. Contact of fibroblasts and organoids in confocal images was analyzed in organoid middle section by measuring the perimeter of the organoid in contact with PDGFRα signal and without it. Fibroblast loop was defined as crescent shaped tdTomato signal that wrapped at least half of organoid branch. EdU signal was quantified in 3 to 5 optical sections of organoid 20 μm apart to avoid multiple counts from the same cell. Contact between fibroblast and KRT5/KRT8 cells, number of basal-in-luminal cells was counted manually in ImageJ. Number of cell layers in organoids was counted manually in the thickest part of a branch. LAMA5 signal along a line was measured in ImageJ.

EdU incorporation assay

For proliferation analysis, 5-ethynyl-2′-deoxyuridine (EdU) incorporation click-it kit (Thermo Fisher Scientific) was used. EdU was administered to the organoid co-cultures 2 h prior to fixation and the EdU signal was developed according to the manufacturer's instructions prior to immunofluorescence staining. The volumes were adjusted for the droplet-based staining as above.

Immunohistochemistry-immunofluorescence (IHC-IF)

Mammary glands #4 were harvested from 6 weeks old females, fixed in 10% neutral buffered formalin overnight, dehydrated in ethanol with increasing concentration and xylene and embedded in paraffin, and 5 μm sections were cut on rotational microtome (Thermo Scientific, Microm HM340E). After rehydration, sections were boiled in pH9 Tris-EDTA buffer to retrieve antigens, blocked in 10% FBS and incubated with primary and secondary antibodies, mounted (Aqua Poly/Mount, Polysciences) and imaged on laser scanning confocal microscope (LSM780/880, Zeiss). The quantification of PDGFRα and αSMA positive cells was done manually in ImageJ, considering DAPI signal to distinguish single cells and continuous αSMA signal as a border of epithelium. The fields of view were scored "duct" or "TEB" based on morphology of the structures (TEBs: stratified epithelium, bulb-like shape, presence of cap-in-body cells, cuboidal cap cells; duct: one layer of luminal cells, elongated myoepithelial cells) and on the position of the structure at the distal part of the mammary epithelium (invasive front).

Immunofluorescence staining of whole-mount cleared mammary gland

Staining and clearing of mammary glands was done following clear, unobstructed brain imaging cocktails (CUBIC) protocol [70,71]. Briefly, mammary glands #3 of 4 weeks old females were harvested and fixed in 10% neutral buffered formalin overnight, washed and incubated in CUBIC reagent 1 (25% (w/w) urea, 25% (w/w) N,N,N',N'-tetrakis(2-hydroxypropyl)ethylenediamine, 15% (w/w) Triton X-100 in distilled water) for 4 days shaking at RT. After washing, the glands were blocked using blocking buffer (5% FBS, 2% BSA, 1% Triton X-100, 0.02% sodium azide in PBS) overnight at RT, incubated with primary antibodies diluted in blocking buffer for 3 days at RT with rocking, washed 3 times for 2 h (0.05% Tween 20 in PBS) and incubated with secondary antibodies and DAPI (1 μg/ml) in blocking buffer. Then, the glands were transferred to CUBIC reagent 2 (50% (w/w) sucrose, 25% (w/w) urea, 10% (w/w) 2,2',2"-nitrilotriethanol, 0.1% (w/w) Triton X-100 in distilled water) for 2 days at RT with rocking. The samples were mounted with CUBIC reagent 2 between 2 coverslips with double-sided tape as a spacer to enable imaging from both sides and they were imaged on laser scanning confocal microscope LSM780 (Zeiss).

Image analysis of signal distribution

The analysis of YAP nuclear to cytoplasmic ratio was done in ImageJ (NIH). Cells in optical section in the middle of an organoid branch were manually annotated and segmented for target protein signal (YAP channel) and nuclei (DAPI channel) and density of pixels in YAP channel in the regions of interest (ROIs) was measured. The nuclear to cytoplasmic ratio of YAP was calculated in Excel (Microsoft). The spatial information of each ROI was manually measured on a line parallel to the branch longitudinal axis and normalized, with the value "1" set for the tip of the branch and the value "−1" set for the root of the branch. The graphs and linear regression line were created in Prism 6 (GraphPad) or Excel. Colocalization analysis of YAP and DAPI channels was done in Zen Black (Zeiss) and presented as color-coded (blue DAPI+YAP- and red DAPI+YAP+). The same cut-off for the colocalization analysis was applied for all images from the same experiment.

Real-time quantitative PCR (qPCR)

RNA from fibroblasts was isolated using RNeasy Mini Kit (Qiagen) according to the manufacturer's instruction. RNA concentration was measured using NanoDrop 2000 (Thermo Fisher Scientific). RNA was transcribed into cDNA by using Transcriptor First Strand cDNA

Synthesis Kit (Roche) or TaqMan Reverse Transcription kit (Life Technologies). Real-time qPCR was performed using 5 ng cDNA, 5 pmol of the forward and reverse gene-specific primers each (primer sequences are shown in S3 Table) in Light Cycler SYBR Green I Master mix (Roche) on LightCycler 480 II (Roche). Relative gene expression was calculated using the ΔΔCt method and normalization to 2 housekeeping genes, β-actin (*Actb*) and eukaryotic elongation factor 1 γ (*Eef1g*).

Transmission electron microscopy

The 3D co-cultures were fixed with 3% glutaraldehyde in 100 mM sodium cacodylate buffer, pH 7.4 for 45 min, postfixed in 1% OsO_4 for 50 min, and washed with cacodylate buffer. After embedding in 1% agar blocks, the samples were dehydrated in increasing ethanol series (50, 70, 96, and 100%), treated with 100% acetone, and embedded in Durcupan resin (Merck). Ultrathin sections were prepared using LKB 8802A Ultramicrotome, stained with uranyl acetate and Reynold's lead citrate (Merck), and examined with FEI Morgagni 286(D) transmission electron microscope. The cells in the schematics were segmented manually.

Statistical analysis

Sample size was not determined a priori and investigators were not blinded to experimental conditions. Statistical analysis was performed using GraphPad Prism software. Student's *t* test (unpaired, two-tailed) was used for comparison of 2 groups. Bar plots were generated by GraphPad Prism and show mean ± standard deviation (SD). $^{*}P < 0.05$, $^{**}P < 0.01$, $^{***}P < 0.001$, $^{****}P < 0.0001$. The number of independent biological replicates is indicated as *n*.

Limitations of the study

The critical experiment that demonstrates the need of fibroblasts' physical contact with the epithelium for epithelial branching does not allow to distinguish between direct physical contact and potential juxtacrine or very short-distance paracrine signaling between the epithelium and fibroblasts, which may contribute to epithelial morphogenesis.

Supporting information

S1 Fig. MCF7-ras spheroids do not respond to exogenous growth factors by branching. (A) Time-lapse snapshots of MCF7-ras spheroids cultured in basal medium with no exogenous growth factors (basal M) or with FGF2 or EGF. Scale bar: 100 μm. **(B)** Time-lapse snapshots of MCF7-ras spheroids co-cultured with no stromal cells (basal M) or with fibroblasts (fibro). Scale bar: 100 μm.
(TIFF)

S2 Fig. Fibroblast-organoid contacts precede organoid branching. (A) Time-lapse snapshots of an organoid-fibroblast co-culture. Scale bar: 100 μm. **(B)** Detailed snapshots of 3 examples of fibroblast-organoid contact establishment in the co-cultures shown in **(A)** on days 1, 2, and 3. Red arrowheads indicate fibroblasts of interest. Scale bar: 50 μm. **(C)** Quantification of organoid circularity (data from Fig 1), number of new branches and number of established fibroblast-organoid contacts from matched experiments. The plot shows mean ± SD; $n = 3$ (each dot represents the average from a biologically independent experiment, $N = 20$ organoids per experiment). **(D)** Maximum intensity projection (MIP) and optical section images of a dispersed co-culture on day 2.5, representative images of cystic and budding organoids (tdTomato). Fibroblasts were detected by immunostaining for PDGFRα. Scale bar: 100 μm. **(E)** Quantification of organoid middle section perimeter in contact with PDGFRα signal. The plot

shows mean ± SD. Each dot represents an average from 1 experiment. Statistical analysis: two-tailored *t* test; $n = 3$ independent biological samples, $N = 15–24$ organoids per sample. The data underlying the graphs shown in the figure can be found in S1 Data.
(TIFF)

S3 Fig. Quantification of fibroblast loops. (A) A representative confocal image of a dispersed co-culture on day 4. Scale bar: 20 μm, scale bar in detail: 10 μm. **(B)** A representative confocal image of a dispersed organoid-fibroblast co-culture on day 3. The arrowhead indicates the fibroblast loop at the branch neck. Scale bar: 50 μm. **(C)** Quantification of the presence of fibroblast loops around organoid branches in dispersed co-cultures. The plot shows mean ± SD. Statistical analysis: two-tailored *t* test; $n = 3$ independent biological replicates, $N = 5–12$ organoids per experiment; 56 branches in total. The data underlying the graphs shown in the figure can be found in S1 Data.
(TIFF)

S4 Fig. MCF7-ras spheroid budding in co-cultures requires cell contractility. (A, C) Photographs of spheroids on day 4 of dispersed co-culture with fibroblasts upon treatment with no inhibitor (mock), with blebbistatin (Bleb, **A**) or with Y27632 (**C**). Top gray and red bars indicate proportion of branched spheroids out of all spheroids per condition. Scale bar: 100 μm. **(B, D)** Quantification of number of branches/buds per branched spheroid in conditions from **(A)**. The plot shows mean ± SD, each lined dot shows mean from each experiment, each faint dot shows single spheroid measurement, $n = 4$ (**B**) or 5 (**D**) biologically independent experiments, $N = 20$ spheroids per experiment. Statistical analysis: two-tailored *t* test. The data underlying the graphs shown in the figure can be found in S1 Data.
(TIFF)

S5 Fig. Contractility inhibitors do not impede fibroblast motility. (A) Representative endpoint images of organoids in dispersed co-cultures with contractility inhibitors. Scale bar: 100 μm. **(B)** Detailed time-lapse snapshots of fibroblast-organoid contact establishment in co-cultures with or without the inhibitors. Scale bar: 50 μm. White arrowhead indicates the fibroblast of interest. **(C, D)** Quantification of fibroblast-organoid contacts established in co-cultures with inhibitors (Y = 10 μM Y27632, **C**; Bleb = 10 μM Blebbistatin, **D**) within the first 2 days. The plots show mean ± SD. Statistical analysis: two-tailored *t* test; $n = 3$ independent biological replicates, $N = 10$ organoids per experiment. The data underlying the graphs shown in the figure can be found in S1 Data.
(TIFF)

S6 Fig. Fibroblast contractility is necessary for branch maintenance. (A) Experimental scheme (top) and time-lapse snapshots of dispersed co-cultures treated with contractility inhibitors on day 3 of culture. Scale bar: 100 μm. White arrowheads indicate organoid branches. **(B–D)** Quantification of organoids with retracted branches (**B**), number of formed branches per branched organoids (**C**) and number of retracted branches per organoid (**D**). The plots show mean ± SD. Statistical analysis: two-tailored *t* test; $n = 4$ independent biological replicates, $N = 20$ organoids per experiment. The data underlying the graphs shown in the figure can be found in S1 Data.
(TIFF)

S7 Fig. Mammary fibroblasts express MYH9 and MYH10. (A) Real-time qPCR analysis of non-muscle myosin II heavy chain genes *Myh9*, *Myh10*, and *Myh14* in mammary fibroblasts (fib) and epithelium (organoids, org). Plots show mean ± SD. Statistical analysis: two-tailored *t* test; $n = 3$ independent biological samples. **(B)** Representative images of MYH9 and MYH10

immunostaining in mammary fibroblasts in the first passage. Scale bar: 50 μm. The data underlying the graphs shown in the figure can be found in S1 Data.
(TIFF)

S8 Fig. Knockdown of *Myh9* in mammary fibroblasts abrogates fibroblast-induced branching of mammary organoids. (A, B) Representative images (day 5 of culture) **(A)** and quantification **(B)** of organoid branching in dispersed co-cultures with wild-type fibroblasts pretreated with nonsense (siNC) or *Myh9* targeting (siMyh9) siRNA. Plot indicates mean ± SD. Statistical analysis: two-tailored paired *t* test; $n = 6$ independent *Myh9* knockdown experiments; $N = 20$ organoids per each treatment of each independent experiment. Videos from the 5-day experiment are presented in S4 Movie. **(C–E)** Quantification of MYH9 down-regulation in *Myh9* KO fibroblasts by immunofluorescence. The plot (**C**) shows mean ± SD, $n = 2$ independent experiments. Representative images (**D**) show MYH9 (cyan) and F-actin (phalloidin, magenta) staining in cultured primary mammary fibroblasts from $Myh9^{fl/fl}$ mice, treated with adeno-GFP (Ad-GFP) or adeno-Cre-GFP (Ad-Cre-GFP) vector, including details (**E**) of cytoskeleton organization. Scale bars: 1 mm (**D**), 20 μm (**E**, first and third row), and 5 μm (**E**, second and fourth row). The data underlying the graphs shown in the figure can be found in S1 Data.
(TIFF)

S9 Fig. *Myh9* knock-out does not impede fibroblast motility. (A) Detailed time-lapse snapshots of fibroblast-organoid contact establishment in dispersed co-cultures with control or *Myh9*-KO fibroblasts and tdTomato+ organoids. Scale bar: 50 μm. **(B)** Quantification of fibroblast-organoid contacts established in the first 3 days of co-culture, comparing GFP+ and GFP- fibroblasts (GFP is a marker of adenoviral transduction). The plot shows mean ± SD. Statistical analysis: two-tailored *t* test; $n = 3$ independent biological replicates, $N = 20$ organoids per experiment. The data underlying the graphs shown in the figure can be found in S1 Data.
(TIFF)

S10 Fig. Proliferation in co-culture system. (A) Representative images of organoids on day 4 of culture in basal medium (basal M), in dispersed co-culture with fibroblasts or with FGF2, EdU administered 2 h pre-fix, EPCAM (red), DAPI (blue), EdU (cyan), fibroblasts were isolated from *R26-mT/mG* mice (tdTomato, white). Scale bar: 100 μm. **(B)** Optical section of a branch from **(A)** (top), a scheme of branch regions (bottom). **(C, D)** Quantification of percentage of EdU+ cells from epithelial cells in different branch regions in fibroblast-organoid dispersed co-culture (**C**) and in FGF2-treated organoid (**D**). The box and whiskers plot shows minimum, median, and maximum values, and second and third quartiles of data distribution. $n = 3$ independent experiments, $N = 6$ organoids, 2,202 analyzed cells in **(C)**; $N = 11$ organoids, 3,104 analyzed cells in **(D)**. Statistical analysis: Multiple *t* tests. **(E)** A scheme of the proliferation-inhibition experiment. **(F)** Co-cultures at day 5 (dispersed culture), fibroblasts pretreated with +/- mitomycin C (MMC), co-cultures treated with +/- aphidicolin (Aph). Scale bar: 100 μm. **(G)** Quantification of the percentage of branched organoids from experiment in **(F)**. The plot shows mean ± SD, each dot represents a biologically independent experiment, $n = 2$, $N = 51–77$ organoids per sample, statistical analysis: *t* test. The data underlying the graphs shown in the figure can be found in S1 Data.
(TIFF)

S11 Fig. Spheroid proliferation is necessary for its branching in co-culture with fibroblasts. (A) Representative images of MCF7-ras spheroids in dispersed co-culture with fibroblasts on day 4 with spheroids formed from mock- or mitomycin C-treated MCF7-ras cells. The insets

(top red bars) show proportion of branched spheroids out of all spheroids per condition. Scale bar: 100 μm. **(B)** The plot shows number of spheroid branches/buds formed, with mean ± SD. Each lined dot represents mean of each experiment, each faint dot represents 1 spheroid, $n = 4$ independent experiments (coded by dot colors), $N = 15–20$ spheroids per experiment. Statistical analysis: two-tailored t test. The data underlying the graphs shown in the figure can be found in S1 Data.
(TIFF)

S1 Movie. Mammary epithelial branching morphogenesis upon FGF2 treatment or fibroblast co-culture. The video is composed of time-lapse videos capturing 5 days of epithelial morphogenesis in 3D organoid culture with no growth factor in the basal organoid medium (left), with FGF2 in the basal organoid medium (middle), or in fibroblast-organoid co-culture without addition of any growth factors to the basal organoid medium. Snapshots from the videos are depicted in Fig 1A.
(AVI)

S2 Movie. Fibroblasts dynamically interact with the epithelium. Time-lapse video (bright-field and fluorescence imaging) shows 4 days of epithelial morphogenesis in fibroblast (cyan)-organoid (red) co-culture (day 0–4). Scale bar: 100 μm. Snapshots from the movie are depicted in Fig 3A.
(AVI)

S3 Movie. Fibroblasts form close contacts with epithelium in the organoid branching points. 3D structure of organoid-fibroblast interaction. Single images are shown in Fig 3D. Luminal cells (KRT8), red; basal cells (KRT5), blue; all cells (F-actin), white.
(AVI)

S4 Movie. *Myh9* knock-down in fibroblasts decreases their morphogenetic potential. Time-lapse videos show 5 days of epithelial morphogenesis in co-culture with either control (left) or *Myh9* knocked-down fibroblasts (siRNA-mediated knockdown; si*Myh9*; right). Time is in hours. Snapshots from the video are depicted in Fig 4.
(AVI)

S5 Movie. *Myh9* knock-out in fibroblast decreases their morphogenetic potential. Time-lapse video captures 4 days of epithelial morphogenesis in fibroblast (cyan)-organoid(red) co-culture with either control (Ad-GFP; left) or *Myh9* knocked-out fibroblasts (adeno-Cre-mediated knock-out; Ad-Cre-GFP; right). Snapshots from the video are depicted in Fig 4. Scale bar: 100 μm.
(AVI)

S6 Movie. Fibroblasts organization around bifurcating TEB. Z-stack scroll-through of mammary gland whole-organ imaging, showing a bifurcating TEB. DAPI in blue, vimentin in white, tdTomato in red. MIP and appropriate scale bar are depicted in Fig 6.
(AVI)

S7 Movie. Fibroblasts organization around invading TEB. Z-stack scroll-through of mammary gland whole-organ imaging, showing an invading TEB. MIP and appropriate scale bar are depicted in Fig 6.
(AVI)

S1 Data. Excel spreadsheet with individual numerical data underlying plots and statistical analyses. The data are organized into separate sheets corresponding to the following figure panels: 1B, 1C, 1D, 1E, 2B, 2D, 3C, 3G, 4D, 4F, 4H, 4I, 5B, 5C, 5F, 5G, 6B, S2C, S2E, S3B, S4B,

S4D, S5C, S5D, S6B, S6C, S6D, S7A, S8B, S8C, S9B, S10C, S10D, S10G, and S11B.
(XLSX)

S1 Table. The list of pharmacological and viral compounds.
(DOCX)

S2 Table. The list of detection agents used in this study.
(DOCX)

S3 Table. The list of primers used for qPCR in this study.
(DOCX)

Acknowledgments

We are grateful to Danijela Matic Vignjevic for critical review of the manuscript, to Denisa Belisova for mouse husbandry, and to Maria Luisa Martin Faraldo for the LAMA5 antibody. We are thankful to Enantis for providing FGF2 and FGF2-STAB. We acknowledge the core facility CELLIM of CEITEC, supported by the Czech-BioImaging large RI project (LM2023050 funded by MEYS CR), for their support with obtaining scientific data presented in this paper. We gratefully acknowledge the Cell and Tissue Imaging Platform (PICT-IBiSA) at Institut Curie, member of the French National Research Infrastructure France-BioImaging (ANR-10-INBS-04).

Author Contributions

Conceptualization: Jakub Sumbal, Zuzana Sumbalova Koledova.

Funding acquisition: Jakub Sumbal, Silvia Fre, Zuzana Sumbalova Koledova.

Investigation: Jakub Sumbal, Zuzana Sumbalova Koledova.

Methodology: Jakub Sumbal, Zuzana Sumbalova Koledova.

Project administration: Zuzana Sumbalova Koledova.

Resources: Silvia Fre, Zuzana Sumbalova Koledova.

Supervision: Silvia Fre, Zuzana Sumbalova Koledova.

Validation: Jakub Sumbal.

Writing – original draft: Jakub Sumbal, Zuzana Sumbalova Koledova.

Writing – review & editing: Jakub Sumbal, Silvia Fre, Zuzana Sumbalova Koledova.

References

1. Affolter M, Zeller R, Caussinus E. Tissue remodelling through branching morphogenesis. Nat Rev Mol Cell Biol. 2009; 10:831–842. https://doi.org/10.1038/nrm2797 PMID: 19888266
2. Goodwin K, Nelson CM. Branching morphogenesis. Development. 2020; 147:dev184499. https://doi.org/10.1242/dev.184499 PMID: 32444428
3. Wang S, Sekiguchi R, Daley WP, Yamada KM. Patterned cell and matrix dynamics in branching morphogenesis. J Cell Biol. 2017; 216:559–570. https://doi.org/10.1083/jcb.201610048 PMID: 28174204
4. Paine IS, Lewis MT. The Terminal End Bud: the Little Engine that Could. J Mammary Gland Biol Neoplasia. 2017; 22:93–108. https://doi.org/10.1007/s10911-017-9372-0 PMID: 28168376
5. Koledova Z, Zhang X, Streuli C, Clarke RB, Klein OD, Werb Z, et al. SPRY1 regulates mammary epithelial morphogenesis by modulating EGFR-dependent stromal paracrine signaling and ECM remodeling. Proc Natl Acad Sci U S A. 2016; 113:E5731–5740. https://doi.org/10.1073/pnas.1611532113 PMID: 27621461

6. Kouros-Mehr H, Werb Z. Candidate regulators of mammary branching morphogenesis identified by genome-wide transcript analysis. Dev Dyn. 2006; 235:3404–3412. https://doi.org/10.1002/dvdy.20978 PMID: 17039550
7. Sumbal J, Koledova Z. FGF signaling in mammary gland fibroblasts regulates multiple fibroblast functions and mammary epithelial morphogenesis. Development. 2019; 146. https://doi.org/10.1242/dev.185306 PMID: 31699800
8. Wiseman BS, Werb Z. Stromal effects on mammary gland development and breast cancer. Science. 2002; 296:1046–1049. https://doi.org/10.1126/science.1067431 PMID: 12004111
9. Zhao C, Cai S, Shin K, Lim A, Kalisky T, Lu W-J, et al. Stromal Gli2 activity coordinates a niche signaling program for mammary epithelial stem cells. Science. 2017; 356. https://doi.org/10.1126/science.aal3485 PMID: 28280246
10. Brownfield DG, Venugopalan G, Lo A, Mori H, Tanner K, Fletcher DA, et al. Patterned collagen fibers orient branching mammary epithelium through distinct signaling modules. Curr Biol. 2013; 23:703–709. https://doi.org/10.1016/j.cub.2013.03.032 PMID: 23562267
11. Hammer AM, Sizemore GM, Shukla VC, Avendano A, Sizemore ST, Chang JJ, et al. Stromal PDGFR-α Activation Enhances Matrix Stiffness, Impedes Mammary Ductal Development, and Accelerates Tumor Growth. Neoplasia. 2017; 19:496–508. https://doi.org/10.1016/j.neo.2017.04.004 PMID: 28501760
12. Jones CE, Hammer AM, Cho Y, Sizemore GM, Cukierman E, Yee LD, et al. Stromal PTEN Regulates Extracellular Matrix Organization in the Mammary Gland. Neoplasia. 2019; 21:132–145. https://doi.org/10.1016/j.neo.2018.10.010 PMID: 30550871
13. Nerger BA, Jaslove JM, Elashal HE, Mao S, Košmrlj A, Link AJ, et al. Local accumulation of extracellular matrix regulates global morphogenetic patterning in the developing mammary gland. Curr Biol. 2021 [cited 2021 Mar 19]. https://doi.org/10.1016/j.cub.2021.02.015 PMID: 33705716
14. Peuhu E, Kaukonen R, Lerche M, Saari M, Guzmán C, Rantakari P, et al. SHARPIN regulates collagen architecture and ductal outgrowth in the developing mouse mammary gland. EMBO J. 2017; 36:165–182. https://doi.org/10.15252/embj.201694387 PMID: 27974362
15. Sumbal J, Belisova D, Koledova Z. Fibroblasts: The grey eminence of mammary gland development. Semin Cell Dev Biol. 2020. https://doi.org/10.1016/j.semcdb.2020.10.012 PMID: 33158729
16. Shyer AE, Rodrigues AR, Schroeder GG, Kassianidou E, Kumar S, Harland RM. Emergent cellular self-organization and mechanosensation initiate follicle pattern in the avian skin. Science. 2017; 357:811–815. https://doi.org/10.1126/science.aai7868 PMID: 28705989
17. Shyer AE, Tallinen T, Nerurkar NL, Wei Z, Gil ES, Kaplan DL, et al. Villification: how the gut gets its villi. Science. 2013; 342:212–218. https://doi.org/10.1126/science.1238842 PMID: 23989955
18. Goodwin K, Mao S, Guyomar T, Miller E, Radisky DC, Košmrlj A, et al. Smooth muscle differentiation shapes domain branches during mouse lung development. Development. 2019; 146. https://doi.org/10.1242/dev.181172 PMID: 31645357
19. Kim HY, Pang M-F, Varner VD, Kojima L, Miller E, Radisky DC, et al. Localized Smooth Muscle Differentiation Is Essential for Epithelial Bifurcation during Branching Morphogenesis of the Mammalian Lung. Dev Cell. 2015; 34:719–726. https://doi.org/10.1016/j.devcel.2015.08.012 PMID: 26387457
20. Palmer MA, Nerger BA, Goodwin K, Sudhakar A, Lemke SB, Ravindran PT, et al. Stress ball morphogenesis: How the lizard builds its lung. Sci Adv. 2021 [cited 2022 Jan 15]. https://doi.org/10.1126/sciadv.abk0161 PMID: 34936466
21. Ewald AJ, Brenot A, Duong M, Chan BS, Werb Z. Collective epithelial migration and cell rearrangements drive mammary branching morphogenesis. Dev Cell. 2008; 14:570–581. https://doi.org/10.1016/j.devcel.2008.03.003 PMID: 18410732
22. Huebner RJ, Lechler T, Ewald AJ. Developmental stratification of the mammary epithelium occurs through symmetry-breaking vertical divisions of apically positioned luminal cells. Development. 2014; 141:1085–1094. https://doi.org/10.1242/dev.103333 PMID: 24550116
23. Huebner RJ, Neumann NM, Ewald AJ. Mammary epithelial tubes elongate through MAPK-dependent coordination of cell migration. Development. 2016; 143:983–993. https://doi.org/10.1242/dev.127944 PMID: 26839364
24. Panciera T, Azzolin L, Cordenonsi M, Piccolo S. Mechanobiology of YAP and TAZ in physiology and disease. Nat Rev Mol Cell Biol. 2017; 18:758–770. https://doi.org/10.1038/nrm.2017.87 PMID: 28951564
25. Gouon-Evans V, Rothenberg ME, Pollard JW. Postnatal mammary gland development requires macrophages and eosinophils. Development. 2000; 127:2269–2282. https://doi.org/10.1242/dev.127.11.2269 PMID: 10804170

26. Gouon-Evans V, Lin EY, Pollard JW. Requirement of macrophages and eosinophils and their cytokines/chemokines for mammary gland development. Breast Cancer Res. 2002; 4:155–164. https://doi.org/10.1186/bcr441 PMID: 12100741

27. Gyorki DE, Asselin-Labat M-L, van Rooijen N, Lindeman GJ, Visvader JE. Resident macrophages influence stem cell activity in the mammary gland. Breast Cancer Res. 2009; 11:R62. https://doi.org/10.1186/bcr2353 PMID: 19706193

28. Lilla JN, Werb Z. Mast cells contribute to the stromal microenvironment in mammary gland branching morphogenesis. Dev Biol. 2010; 337:124–133. https://doi.org/10.1016/j.ydbio.2009.10.021 PMID: 19850030

29. Parsa S, Ramasamy SK, De Langhe S, Gupte VV, Haigh JJ, Medina D, et al. Terminal end bud maintenance in mammary gland is dependent upon FGFR2b signaling. Dev Biol. 2008; 317:121–131. https://doi.org/10.1016/j.ydbio.2008.02.014 PMID: 18381212

30. Sferruzzi-Perri AN, Robertson SA, Dent LA. Interleukin-5 transgene expression and eosinophilia are associated with retarded mammary gland development in mice. Biol Reprod. 2003; 69:224–233. https://doi.org/10.1095/biolreprod.102.010611 PMID: 12620930

31. Nguyen-Ngoc K-V, Ewald AJ. Mammary ductal elongation and myoepithelial migration are regulated by the composition of the extracellular matrix. J Microsc. 2013; 251:212–223. https://doi.org/10.1111/jmi.12017 PMID: 23432616

32. Dvorak P, Bednar D, Vanacek P, Balek L, Eiselleova L, Stepankova V, et al. Computer-assisted engineering of hyperstable fibroblast growth factor 2. Biotechnol Bioeng. 2018; 115:850–862. https://doi.org/10.1002/bit.26531 PMID: 29278409

33. Koledova Z, Sumbal J, Rabata A, de La Bourdonnaye G, Chaloupkova R, Hrdlickova B, et al. Fibroblast Growth Factor 2 Protein Stability Provides Decreased Dependence on Heparin for Induction of FGFR Signaling and Alters ERK Signaling Dynamics. Front Cell Dev Biol. 2019; 7:331. https://doi.org/10.3389/fcell.2019.00331 PMID: 31921844

34. Sumbal J, Vranova T, Koledova Z. FGF signaling dynamics regulates epithelial patterning and morphogenesis. bioRxiv; 2020. p. 2020.11.17.386607. https://doi.org/10.1101/2020.11.17.386607

35. Heisenberg C-P, Bellaïche Y. Forces in tissue morphogenesis and patterning. Cell. 2013; 153:948–962. https://doi.org/10.1016/j.cell.2013.05.008 PMID: 23706734

36. Bonnans C, Chou J, Werb Z. Remodelling the extracellular matrix in development and disease. Nat Rev Mol Cell Biol. 2014; 15:786. https://doi.org/10.1038/nrm3904 PMID: 25415508

37. Li R, Li X, Hagood J, Zhu M-S, Sun X. Myofibroblast contraction is essential for generating and regenerating the gas-exchange surface. J Clin Invest. 2020; 130:2859–2871. https://doi.org/10.1172/JCI132189 PMID: 32338642

38. Li CM-C, Shapiro H, Tsiobikas C, Selfors LM, Chen H, Rosenbluth J, et al. Aging-Associated Alterations in Mammary Epithelia and Stroma Revealed by Single-Cell RNA Sequencing. Cell Rep. 2020; 33:108566. https://doi.org/10.1016/j.celrep.2020.108566 PMID: 33378681

39. Yoshitake R, Chang G, Saeki K, Ha D, Wu X, Wang J, et al. Single-Cell Transcriptomics Identifies Heterogeneity of Mouse Mammary Gland Fibroblasts With Distinct Functions, Estrogen Responses, Differentiation Processes, and Crosstalks With Epithelium. Front Cell Dev Biol. 2022; 10:850568. https://doi.org/10.3389/fcell.2022.850568 PMID: 35300413

40. Li R, Bernau K, Sandbo N, Gu J, Preissl S, Sun X. Pdgfra marks a cellular lineage with distinct contributions to myofibroblasts in lung maturation and injury response. Morrisey E, Dietz HC, editors. Elife. 2018; 7:e36865. https://doi.org/10.7554/eLife.36865 PMID: 30178747

41. Branchfield K, Li R, Lungova V, Verheyden JM, McCulley D, Sun X. A three-dimensional study of alveologenesis in mouse lung. Dev Biol. 2016; 409:429–441. https://doi.org/10.1016/j.ydbio.2015.11.017 PMID: 26632490

42. McCarthy N, Manieri E, Storm EE, Saadatpour A, Luoma AM, Kapoor VN, et al. Distinct Mesenchymal Cell Populations Generate the Essential Intestinal BMP Signaling Gradient. Cell Stem Cell. 2020; 26:391–402.e5. https://doi.org/10.1016/j.stem.2020.01.008 PMID: 32084389

43. Powell DW, Pinchuk IV, Saada JI, Chen X, Mifflin RC. Mesenchymal cells of the intestinal lamina propria. Annu Rev Physiol. 2011; 73:213–237. https://doi.org/10.1146/annurev.physiol.70.113006.100646 PMID: 21054163

44. Xiang J, Guo J, Zhang S, Wu H, Chen Y-G, Wang J, et al. A stromal lineage maintains crypt structure and villus homeostasis in the intestinal stem cell niche. BMC Biol. 2023; 21:169. https://doi.org/10.1186/s12915-023-01667-2 PMID: 37553612

45. Heitman N, Sennett R, Mok K-W, Saxena N, Srivastava D, Martino P, et al. Dermal sheath contraction powers stem cell niche relocation during hair cycle regression. Science. 2020; 367:161–166. https://doi.org/10.1126/science.aax9131 PMID: 31857493

46. Ahlers JMD, Falckenhayn C, Holzscheck N, Solé-Boldo L, Schütz S, Wenck H, et al. Single-Cell RNA Profiling of Human Skin Reveals Age-Related Loss of Dermal Sheath Cells and Their Contribution to a Juvenile Phenotype. Front Genet. 2022; 12:797747. https://doi.org/10.3389/fgene.2021.797747 PMID: 35069694

47. Shoshkes-Carmel M, Wang YJ, Wangensteen KJ, Tóth B, Kondo A, Massasa EE, et al. Subepithelial telocytes are an important source of Wnts that supports intestinal crypts. Nature. 2018; 557:242–246. https://doi.org/10.1038/s41586-018-0084-4 PMID: 29720649

48. Hughes AJ, Miyazaki H, Coyle MC, Zhang J, Laurie MT, Chu D, et al. Engineered Tissue Folding by Mechanical Compaction of the Mesenchyme. Dev Cell. 2018; 44:165–178.e6. https://doi.org/10.1016/j.devcel.2017.12.004 PMID: 29290586

49. Silberstein GB, Daniel CW. Glycosaminoglycans in the basal lamina and extracellular matrix of the developing mouse mammary duct. Dev Biol. 1982; 90:215–222. https://doi.org/10.1016/0012-1606(82)90228-7 PMID: 6800862

50. Feinberg TY, Zheng H, Liu R, Wicha MS, Yu SM, Weiss SJ. Divergent Matrix-Remodeling Strategies Distinguish Developmental from Neoplastic Mammary Epithelial Cell Invasion Programs. Dev Cell. 2018; 47:145–160.e6. https://doi.org/10.1016/j.devcel.2018.08.025 PMID: 30269950

51. Fata JE, Werb Z, Bissell MJ. Regulation of mammary gland branching morphogenesis by the extracellular matrix and its remodeling enzymes. Breast Cancer Res. 2004; 6:1–11. https://doi.org/10.1186/bcr634 PMID: 14680479

52. Hannezo E, Clgj S, Moad M, Drogo N, Heer R, Sampogna RV, et al. A Unifying Theory of Branching Morphogenesis. Cell. 2017; 171. https://doi.org/10.1016/j.cell.2017.08.026 PMID: 28938116

53. Joshi PA, Waterhouse PD, Kasaian K, Fang H, Gulyaeva O, Sul HS, et al. PDGFRα+ stromal adipocyte progenitors transition into epithelial cells during lobulo-alveologenesis in the murine mammary gland. Nat Commun. 2019; 10:1760. https://doi.org/10.1038/s41467-019-09748-z PMID: 30988300

54. Macias H, Moran A, Samara Y, Moreno M, Compton JE, Harburg G, et al. SLIT/ROBO1 signaling suppresses mammary branching morphogenesis by limiting basal cell number. Dev Cell. 2011; 20:827–840. https://doi.org/10.1016/j.devcel.2011.05.012 PMID: 21664580

55. Labernadie A, Kato T, Brugués A, Serra-Picamal X, Derzsi S, Arwert E, et al. A mechanically active heterotypic E-cadherin/N-cadherin adhesion enables fibroblasts to drive cancer cell invasion. Nat Cell Biol. 2017; 19:224–237. https://doi.org/10.1038/ncb3478 PMID: 28218910

56. Omelchenko T, Fetisova E, Ivanova O, Bonder EM, Feder H, Vasiliev JM, et al. Contact interactions between epitheliocytes and fibroblasts: formation of heterotypic cadherin-containing adhesion sites is accompanied by local cytoskeletal reorganization. Proc Natl Acad Sci U S A. 2001; 98:8632–8637. https://doi.org/10.1073/pnas.151247698 PMID: 11447275

57. Barbazan J, Pérez-González C, Gómez-González M, Dedenon M, Richon S, Latorre E, et al. Cancer-associated fibroblasts actively compress cancer cells and modulate mechanotransduction. Nat Commun. 2023; 14:6966. https://doi.org/10.1038/s41467-023-42382-4 PMID: 37907483

58. Sternlicht MD, Sunnarborg SW, Kouros-Mehr H, Yu Y, Lee DC, Werb Z. Mammary ductal morphogenesis requires paracrine activation of stromal EGFR via ADAM17-dependent shedding of epithelial amphiregulin. Development. 2005; 132:3923–3933. https://doi.org/10.1242/dev.01966 PMID: 16079154

59. Neumann NM, Kim DM, Huebner RJ, Ewald AJ. Collective cell migration is spatiotemporally regulated during mammary epithelial bifurcation. J Cell Sci. 2023; 136:jcs259275. https://doi.org/10.1242/jcs.259275 PMID: 36602106

60. Wang S, Matsumoto K, Lish SR, Cartagena-Rivera AX, Yamada KM. Budding epithelial morphogenesis driven by cell-matrix versus cell-cell adhesion. Cell. 2021; 184:3702–3716.e30. https://doi.org/10.1016/j.cell.2021.05.015 PMID: 34133940

61. Scheele CLGJ, Hannezo E, Muraro MJ, Zomer A, Langedijk NSM, van Oudenaarden A, et al. Identity and dynamics of mammary stem cells during branching morphogenesis. Nature. 2017; 542:313–317. https://doi.org/10.1038/nature21046 PMID: 28135720

62. Muzumdar MD, Tasic B, Miyamichi K, Li L, Luo L. A global double-fluorescent Cre reporter mouse. Genesis. 2007; 45:593–605. https://doi.org/10.1002/dvg.20335 PMID: 17868096

63. Wendling O, Bornert J-M, Chambon P, Metzger D. Efficient temporally-controlled targeted mutagenesis in smooth muscle cells of the adult mouse. Genesis. 2009; 47:14–18. https://doi.org/10.1002/dvg.20448 PMID: 18942088

64. Riedl J, Flynn KC, Raducanu A, Gärtner F, Beck G, Bösl M, et al. Lifeact mice for studying F-actin dynamics. Nat Methods. 2010; 7:168–169. https://doi.org/10.1038/nmeth0310-168 PMID: 20195247

65. Conti MA, Even-Ram S, Liu C, Yamada KM, Adelstein RS. Defects in cell adhesion and the visceral endoderm following ablation of nonmuscle myosin heavy chain II-A in mice. J Biol Chem. 2004; 279:41263–41266. https://doi.org/10.1074/jbc.C400352200 PMID: 15292239

66. Koledova Z. 3D Coculture of Mammary Organoids with Fibrospheres: A Model for Studying Epithelial-Stromal Interactions During Mammary Branching Morphogenesis. Methods Mol Biol. 2017; 1612:107–124. https://doi.org/10.1007/978-1-4939-7021-6_8 PMID: 28634938

67. Koledova Z, Lu P. A 3D Fibroblast-Epithelium Co-culture Model for Understanding Microenvironmental Role in Branching Morphogenesis of the Mammary Gland. Methods Mol Biol. 2017; 1501:217–231. https://doi.org/10.1007/978-1-4939-6475-8_10 PMID: 27796955

68. Kasid A, Lippman ME, Papageorge AG, Lowy DR, Gelmann EP. Transfection of v-rasH DNA into MCF-7 human breast cancer cells bypasses dependence on estrogen for tumorigenicity. Science. 1985; 228:725–728. https://doi.org/10.1126/science.4039465 PMID: 4039465

69. Sumbal J, Koledova Z. Single Organoids Droplet-Based Staining Method for High-End 3D Imaging of Mammary Organoids. Methods Mol Biol. 2022; 2471:259–269. https://doi.org/10.1007/978-1-0716-2193-6_14 PMID: 35175602

70. Susaki EA, Tainaka K, Perrin D, Kishino F, Tawara T, Watanabe TM, et al. Whole-brain imaging with single-cell resolution using chemical cocktails and computational analysis. Cell. 2014; 157:726–739. https://doi.org/10.1016/j.cell.2014.03.042 PMID: 24746791

71. Lloyd-Lewis B, Davis FM, Harris OB, Hitchcock JR, Lourenco FC, Pasche M, et al. Imaging the mammary gland and mammary tumours in 3D: optical tissue clearing and immunofluorescence methods. Breast Cancer Res. 2016; 18:127. https://doi.org/10.1186/s13058-016-0754-9 PMID: 27964754

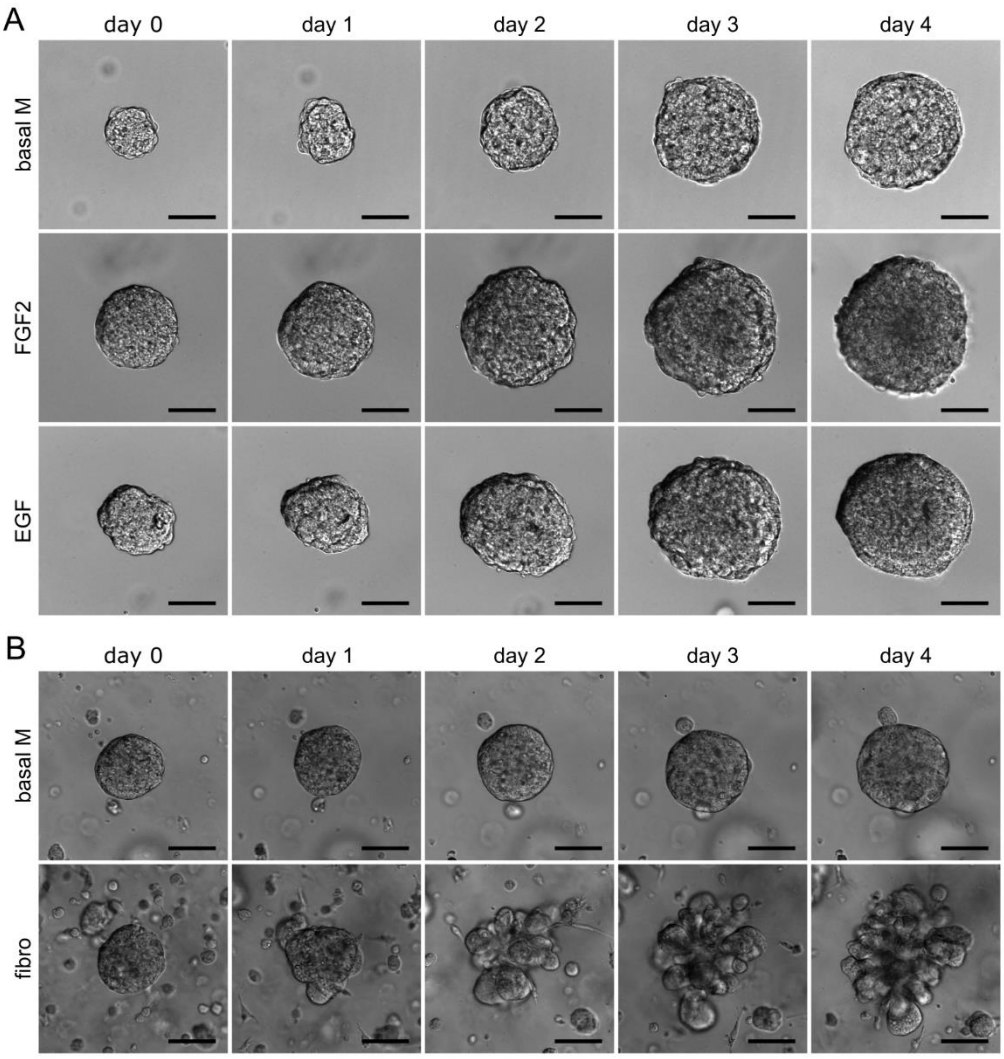
A
day 0
day 1
day 2
day 3
day 4
basal M
FGF2
EGF
B
day 0
day 1
day 2
day 3
day 4
basal M
fibro

S1 Fig.

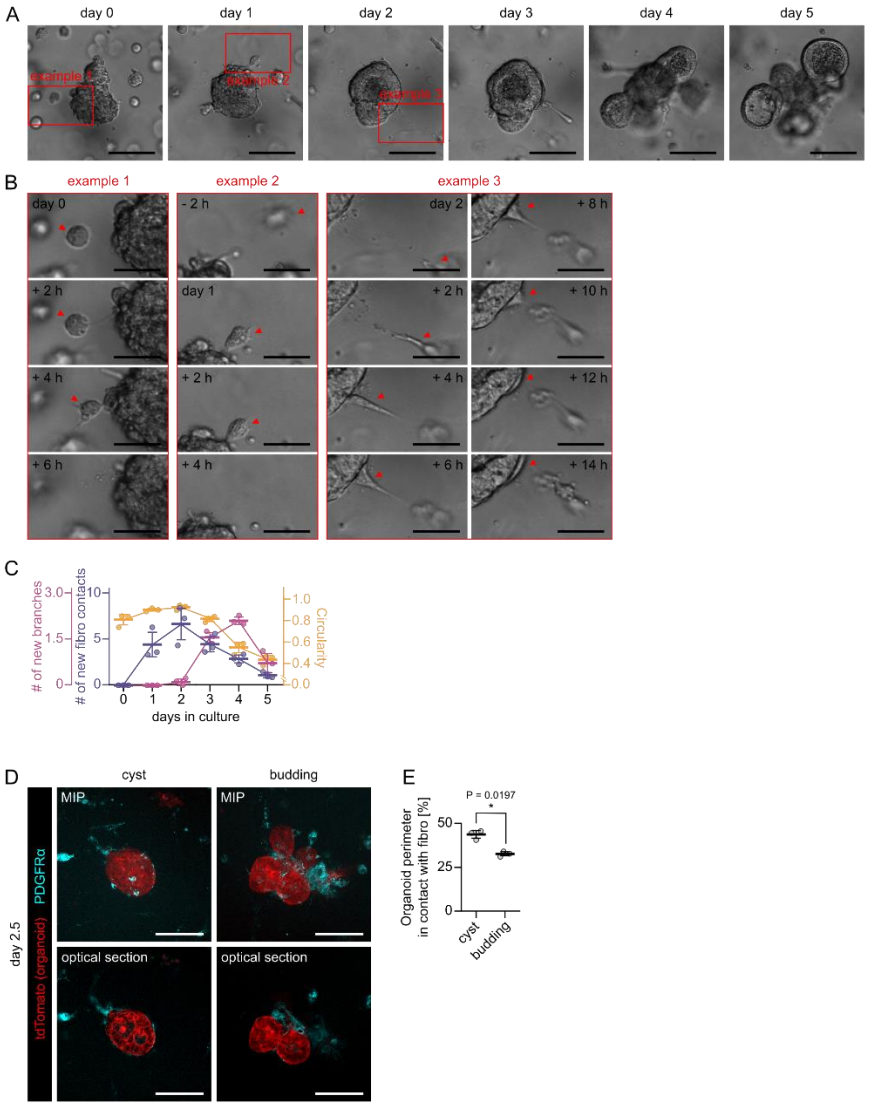
A
day 0
day 1
day 2
day 3
day 4
day 5
example 1
example 2
example 3
B
example 1
example 2
example 3
day 0
+ 2 h
+ 4 h
+ 6 h
- 2 h
day 1
+ 2 h
+ 4 h
day 2
+ 2 h
+ 4 h
+ 6 h
+ 8 h
+ 10 h
+ 12 h
+ 14 h
C
# of new branches
# of new fibro contacts
Circularity
days in culture
D
cyst
budding
day 2.5
PDGFRα
tdTomato (organoid)
MIP
optical section
E
P = 0.0197
Organoid perimeter in contact with fibro [%]
cyst
budding

S2 Fig.

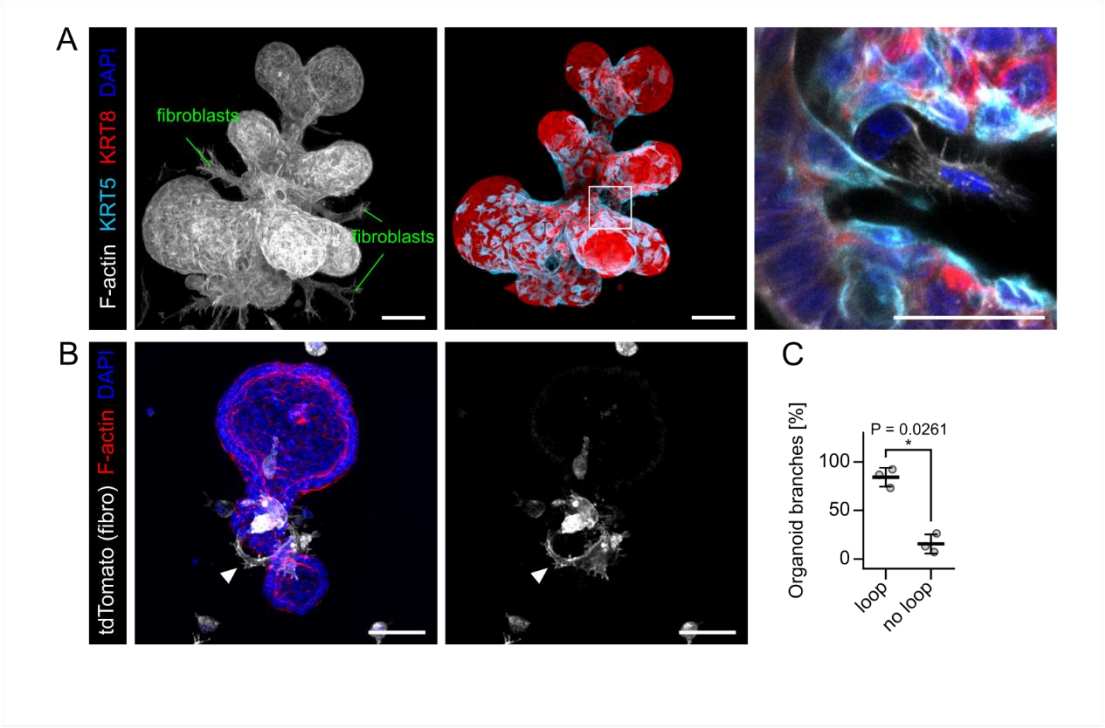
A
F-actin KRT5 KRT8 DAPI
fibroblasts
fibroblasts
B
tdTomato (fibro) F-actin DAPI
C
Organoid branches [%]
P = 0.0261
*
100
50
0
loop
no loop

S3 Fig.

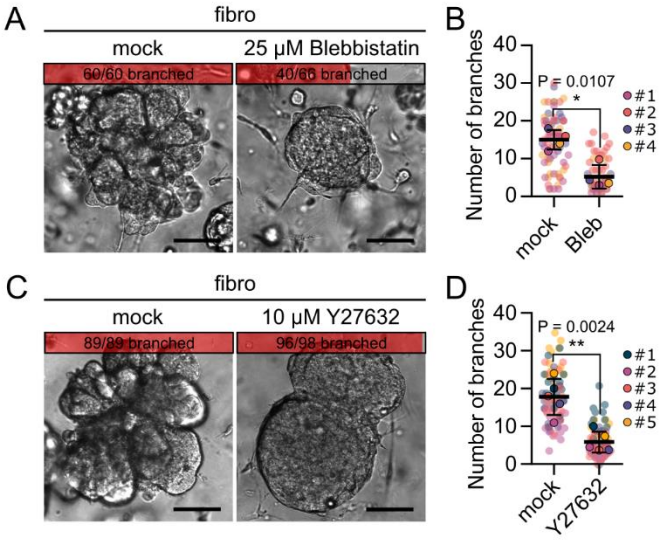
A
fibro
mock
25 μM Blebbistatin
60/60 branched
40/66 branched
B
Number of branches
P = 0.0107
*
#1
#2
#3
#4
mock
Bleb
C
fibro
mock
10 μM Y27632
89/89 branched
96/98 branched
D
Number of branches
P = 0.0024
**
#1
#2
#3
#4
#5
mock
Y27632

S4 Fig.

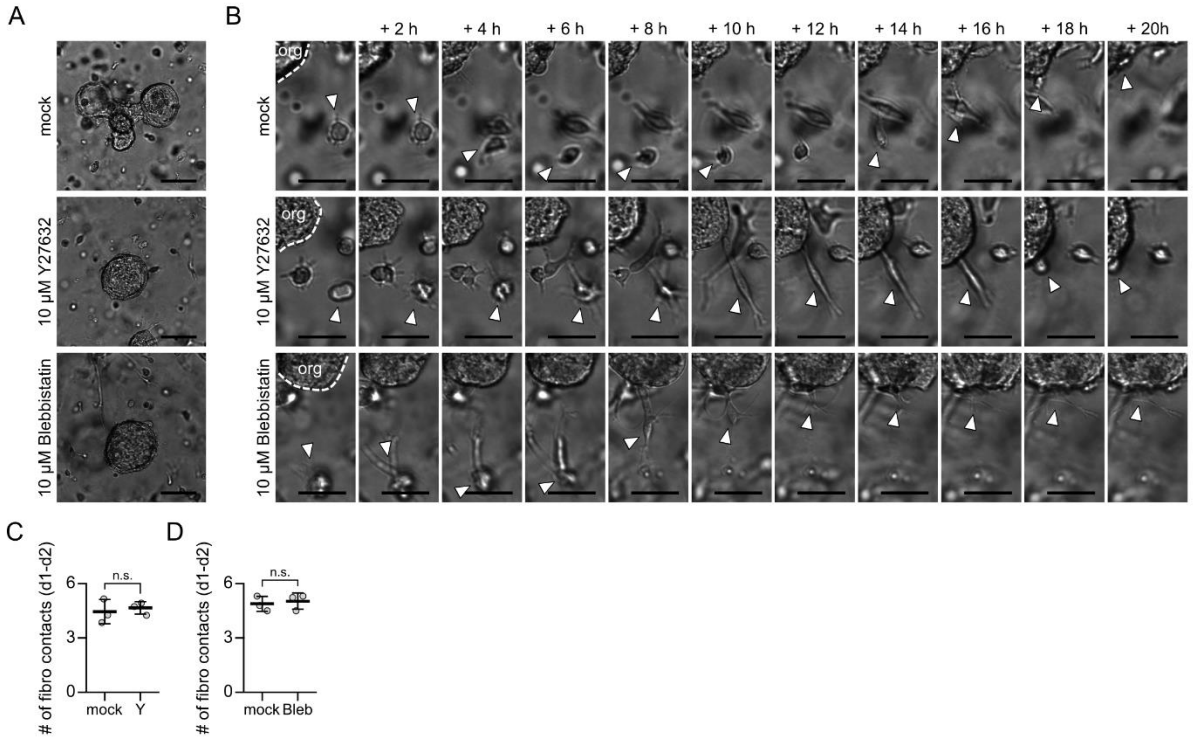
A
B
+ 2 h
+ 4 h
+ 6 h
+ 8 h
+ 10 h
+ 12 h
+ 14 h
+ 16 h
+ 18 h
+ 20h
mock
10 µM Y27632
10 µM Blebbistatin
org
C
D
# of fibro contacts (d1-d2)
n.s.
mock
Y
Bleb

S5 Fig.

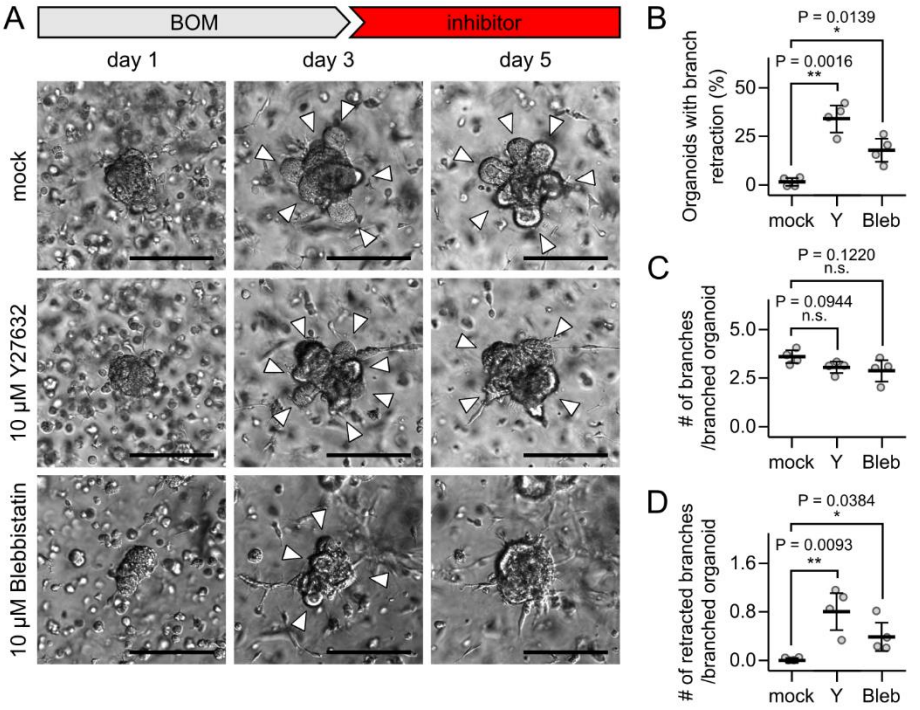
A
BOM
inhibitor
day 1
day 3
day 5
mock
10 µM Y27632
10 µM Blebbistatin
B
P = 0.0139
*
P = 0.0016
**
Organoids with branch retraction (%)
50
25
0
mock
Y
Bleb
C
P = 0.1220
n.s.
P = 0.0944
n.s.
# of branches /branched organoid
5.0
2.5
0.0
mock
Y
Bleb
D
P = 0.0384
*
P = 0.0093
**
# of retracted branches /branched organoid
1.6
0.8
0.0
mock
Y
Bleb

S6 Fig.

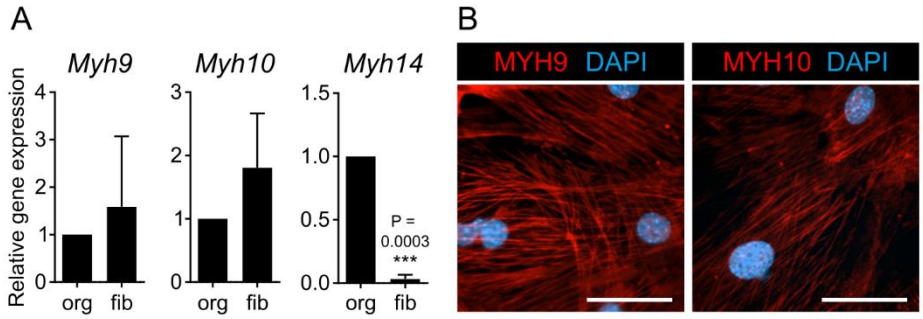
A
Myh9
Myh10
Myh14
Relative gene expression
4
3
2
1
0
3
2
1
0
1.5
1.0
0.5
0.0
P = 0.0003
***
org
fib
org
fib
org
fib
B
MYH9 DAPI
MYH10 DAPI

S7 Fig.

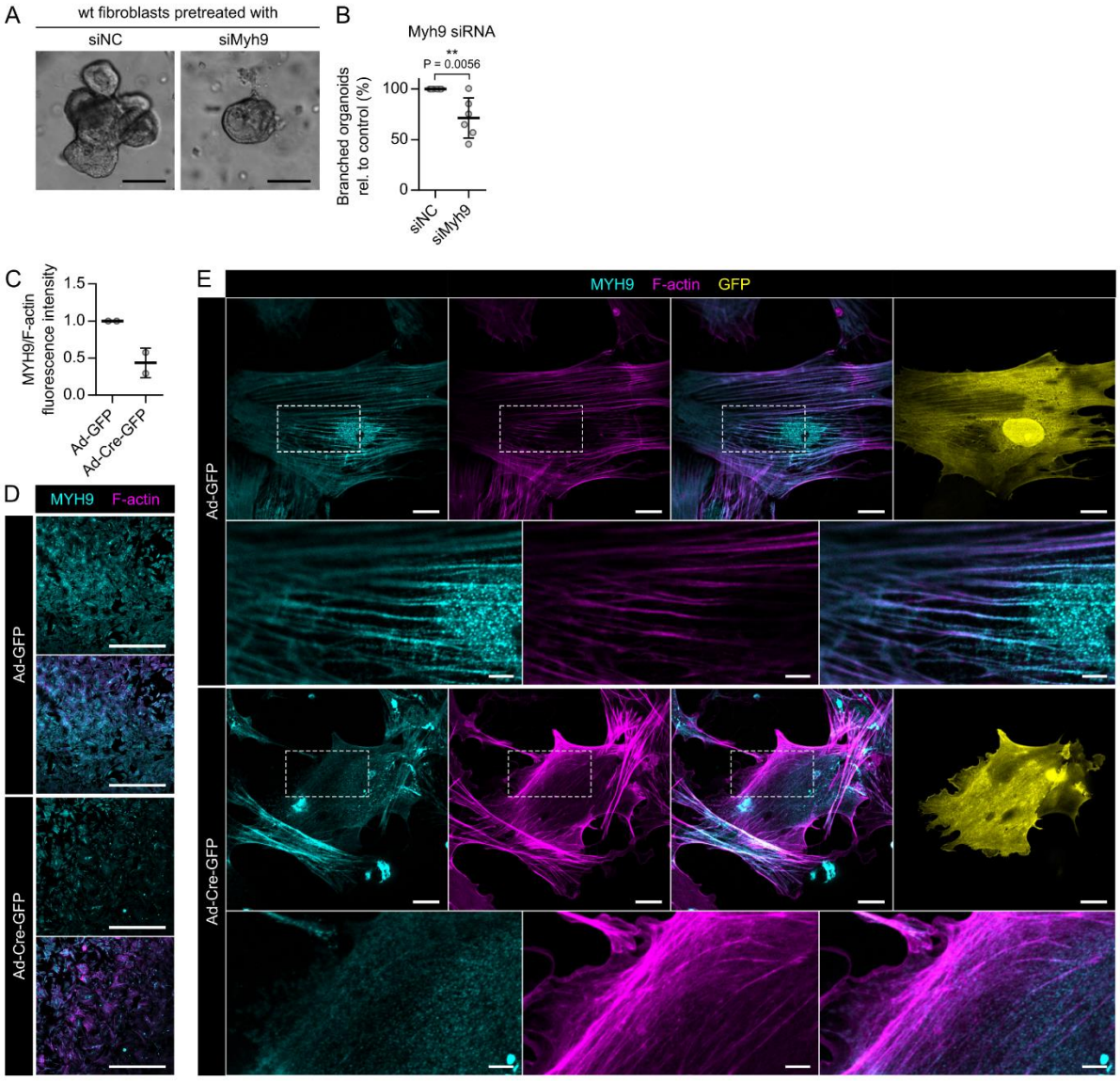
A
wt fibroblasts pretreated with
siNC
siMyh9
B
Myh9 siRNA
**
P = 0.0056
Branched organoids rel. to control (%)
100
50
0
siNC
siMyh9
C
MYH9/F-actin fluorescence intensity
1.5
1.0
0.5
0.0
Ad-GFP
Ad-Cre-GFP
D
MYH9
F-actin
Ad-GFP
Ad-Cre-GFP
E
MYH9
F-actin
GFP
Ad-GFP
Ad-Cre-GFP

S8 Fig.

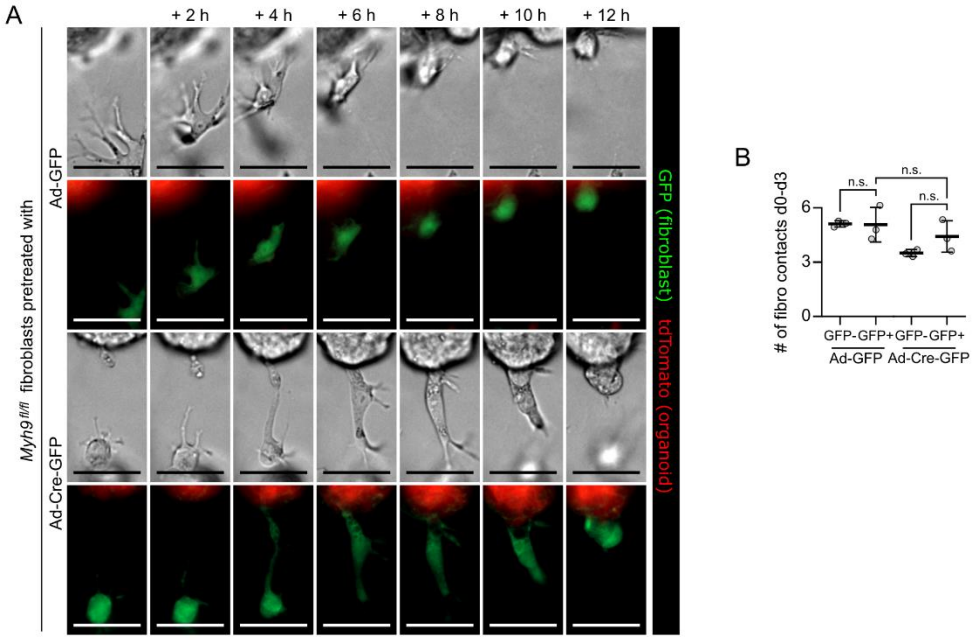

S9 Fig.

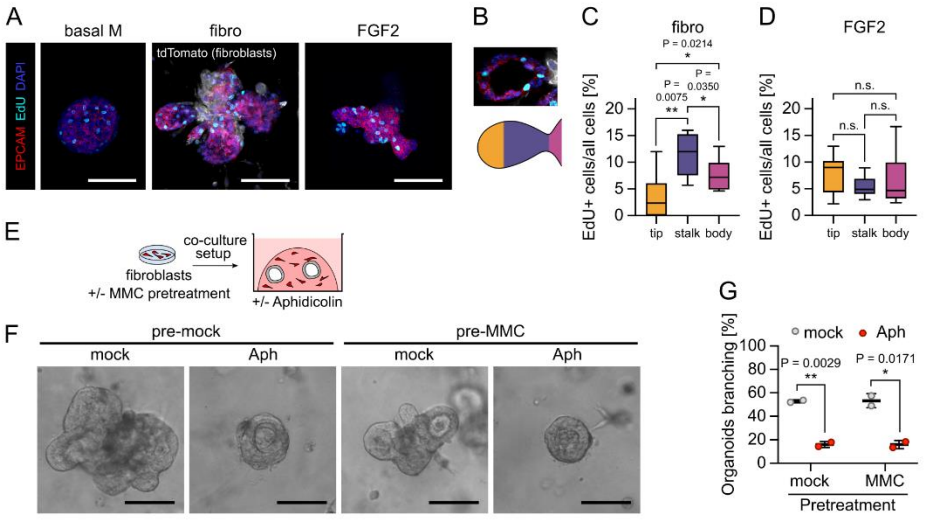

S10 Fig.

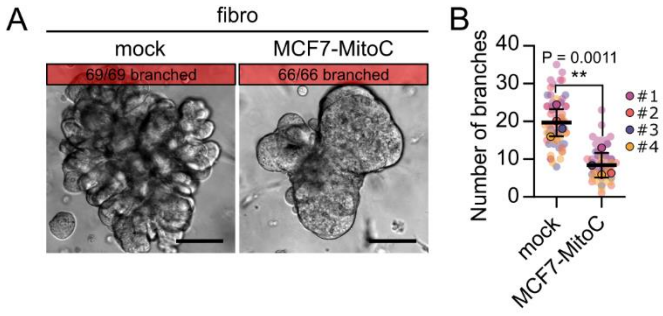
A
fibro
mock
MCF7-MitoC
69/69 branched
66/66 branched
B
Number of branches
40
30
20
10
0
P = 0.0011
**
#1
#2
#3
#4
mock
MCF7-MitoC

S11 Fig.

Appendix 2: Contractile fibroblasts are recruited to the growing mammary epithelium to support branching morphogenesis

The second appendix is a bioRxiv preprint, currently under revision.

Sumbal et al.

Contractile fibroblasts are recruited to the growing mammary epithelium to support branching morphogenesis

Authors:

Jakub Sumbal[1,2,3], Robin P. Journot[1], Marisa M. Faraldo[1], Zuzana Sumbalova Koledova[4*#], Silvia Fre[1*#]

Affiliations:

[1] Institut Curie, Laboratory of Genetics and Developmental Biology, INSERM U934, CNRS UMR3215, 75248 Paris, France

[2] Masaryk University, Faculty of Medicine, Department of Histology and Embryology, Kamenice 3, Brno, 625 00, Czech Republic

[3] Sorbonne Université, Collège Doctoral, F-75005 Paris, France

[4] Institute of Molecular Genetics of the Czech Academy of Sciences, Laboratory of Tissue Morphogenesis and Cancer, Prague, Czech Republic

Running title: Contractile fibroblasts in mammary gland

ORCID IDs:

JS: 0000-0003-3700-4518;

RPJ: 0000-0002-1967-2400;

MMF: 0000-0001-9497-1171;

SF: 0000-0002-7209-7636;

Sumbal et al.

ZSK: 0000-0002-9333-1399.

# equal contribution

*Corresponding authors and lead contacts:

SF: silvia.fre@curie.fr, ZSK: zuzana.sumbalova-koledova@img.cas.cz

Abstract

Fibroblasts are stromal cells found in connective tissue that are critical for organ development, homeostasis, and disease. Single-cell transcriptomic analyses have revealed a high level of inter- and intra-organ heterogeneity of fibroblasts. However, the functional implications and lineage relations of different fibroblast subtypes remain unexplored, especially in the mammary gland. Here we provide a comprehensive characterization of pubertal mammary fibroblasts, achieved using single-cell RNA sequencing, spatial mapping, and in vivo lineage tracing. Notably, we discovered a transient niche-forming population of specialized contractile fibroblasts that exclusively localize around the tips of the growing mammary epithelium and are recruited from the surrounding fat pad. Using functional organoid-fibroblast co-cultures we reveal that different fibroblast populations can acquire contractile features when in direct contact with the epithelium, promoting morphogenesis. In summary, our exhaustive characterization of these specialized cells provides new insights into mammary fibroblast heterogeneity and implicates their functional relevance for branching morphogenesis and lineage hierarchy during mouse mammary gland development.

Introduction

Fibroblasts are cells of mesenchymal origin that form the soft connective tissue, and they are extremely pleiotropic in their function. They secrete, remodel, and degrade components of the extracellular matrix (ECM), produce signaling molecules to communicate with other stromal cells, immune cells or organ parenchyma, act as a source of other mesenchymal cells and can become contractile and generate mechanical forces within tissues[1–3]. Through a delicate spatiotemporal orchestration of the aforementioned functions, fibroblasts guide development, maintain homeostasis and support pathological changes in many organs[1]. Recent studies employing single-cell transcriptomics suggest that fibroblasts represent a heterogenous cell population with distinct cell types or cell states specialized for different functions, presenting inter-organ conserved as well as divergent behavior and functions[4,5]. It is not yet understood, however, how fibroblast heterogeneity is linked to their plasticity and their origin.

Epithelial ductal elongation and branching in the mammary gland occurs mostly postnatally, when a peak of estrogen during puberty awakens the rudimentary mammary epithelium formed during embryogenesis, and the mammary epithelium actively proliferates and invades the surrounding fat pad stroma to generate a highly branched ductal network[6]. This morphogenetic function is executed by terminal end buds (TEBs), bulb-shaped and highly proliferative epithelial structures that form at the tips of the ducts and invade the surrounding stroma at the astonishing speed of 0.5 mm per day[7]. In a stochastic pattern, TEBs bifurcate to generate new branches[8,9]. The cellular and physical mechanisms that drive *in vivo* branching morphogenesis, TEB bifurcation and ductal elongation have not been thoroughly explored.

The importance of the stroma, in particular of fibroblasts, to support mammary branching morphogenesis is well recognized[2,10]. Mammary fibroblasts secrete growth factors[11] that can induce epithelial branching[12]. Fibroblasts also secrete and remodel collagen 1[13] that supports ductal elongation in organoids[14]. Likewise, *in vivo* collagen deposition correlates with the direction of ductal elongation[15] and with TEB bifurcations[16]. Importantly, we have recently demonstrated that contractile mammary fibroblasts

are instrumental to the induction of mammary epithelial organoid branching[17], similarly to smooth muscle cells in the budding embryonic lung[18]. We have also reported the presence of contractile α-smooth muscle actin (αSMA, encoded by *Acta2*) positive (αSMA+) fibroblasts *in vivo,* around TEBs in the pubertal mammary gland undergoing branching morphogenesis[17]. Fibroblast contractility is an important marker of their biology, often linked with their function and activation state during organ development[18,19], wound healing, fibrosis[20] as well as in cancer[21,22].

The transcriptional and functional heterogeneity of mammary fibroblasts during the prominent epithelial remodeling underlying pubertal branching morphogenesis *in vivo* has not been explored. Although single cell RNA sequencing (scRNAseq) datasets of mammary fibroblasts were generated[23–26], these studies only analyzed the mammary gland under homeostatic conditions and lacked spatial analysis. In this study, we have rigorously characterized the diversity of pubertal fibroblasts and identified a specialized subset of spatially restricted contractile fibroblasts that exist only in proximity of growing TEBs. We have thus analyzed their behavior, function and relation to other mammary fibroblasts using scRNAseq, spatial mapping, transplantations, in vitro co-cultures with organoids and in vivo lineage tracing approaches.

Results

Single cell analysis of the growing tips and the subtending ductal regions of the pubertal mammary gland reveals the existence of contractile peri-TEB fibroblasts

TEBs of developing mammary glands are surrounded by a stromal niche with a thickened peri-epithelial fibroblast layer[27] (Figure 1A, B), and we recently found that peri-TEB fibroblasts express the contractility marker αSMA (Figure 1C, Movie 1)[17]. To characterize the αSMA+ peri-TEB fibroblasts in more depth, we performed scRNAseq on cells dissociated from micro-dissected regions of pubertal mammary glands, containing either mainly TEBs or subtending ducts (Figure 1D). We purposedly chose not to FACS sort cells to prevent sample biasing and proceeded to a comparative analysis of the cell types derived from the two distinct anatomical sites, one enriched in TEBs (hence in peri-TEB fibroblasts) and one deprived of

them. In both samples, we identified distinct fibroblast clusters based on generic markers (*Col1a1, Col1a2, Pdgfra,* Supplementary figure 1A, B) and merged them to create a collective UMAP graph representing all pubertal mammary fibroblasts (Figure 1E, F). Of note, our dataset did not contain pericytes (Supplementary figure 1B) but included epithelial cells (Supplementary figure 1C-E) and leukocytes, mainly T cells, B cells, macrophages, and dendritic cells (Supplementary figure 1F-H).

Unsupervised clustering of merged fibroblasts identified six separate clusters (Figure 1E-G, Supplementary figure 2A), with clusters #3 and #5 predominantly derived from the TEB-containing sample (Figure 1F). To annotate these newly discovered fibroblast clusters, we created transcriptional scores for published fibroblasts from the developing fat pad[28,29] and we found their enrichment in specific clusters in our dataset (Figure 1H). This comparative analysis with other single cell analyses allowed us to annotate clusters #0, #2, #4 as preadipocytes, adipocyte regulatory cells (AREGs) and interstitial progenitors, respectively (Figure 1I). Cells of cluster #3 and #5 were enriched in TEB sample and cells of cluster #5 expressed typical markers of proliferation (*Mki67*, *Top2a*, *Cdk1*, Figure 1G, Supplementary figure 2A) and were therefore annotated as peri-TEB and proliferative peri-TEB fibroblasts, respectively (Figure 1I). Finally, cells belonging to cluster #1 were predominantly derived from the ductal sample, were clearly distinct from fat pad fibroblasts but showed similarity to one fibroblast cluster previously identified in the adult mammary gland (Supplementary figure 2B)[26]; therefore, we annotated them as peri-ductal fibroblasts (Figure 1I).

We then used the transcriptional signatures of each cluster to inform on potential functional differences between these types of fibroblasts. We noticed that peri-TEB fibroblasts were highly enriched in contractility-related genes compared to the other clusters (Figure 1J) but expressed fewer genes encoding for fibrillar collagens and basal membrane proteins (Figure 1K). On the other hand, peri-TEB fibroblasts expressed tenascin C (Figure 1K), a gene encoding an anti-adhesive ECM molecule linked to organ development and cancer invasion[30,31]. Peri-TEB fibroblasts also differed in their expression of ECM remodeling enzymes, such as matrix metalloproteinases (*Mmps*), expressing more membrane-type *Mmps* (*Mmp14, Mmp15, Mmp16*, Supplementary figure 2C) that are important for mammary pubertal branching

morphogenesis[32], and fewer soluble *Mmps* (*Mmp2, Mmp3*). We next sought to computationally predict specific paracrine interactions and signaling networks between different fibroblast clusters and epithelial cells (both basal and luminal cells) using the algorithm CellChat, a bioinformatic tool designed to predict significant ligand-receptor interactions between two cell types from scRNAseq data[33]. Interestingly, this analysis identified peri-TEB fibroblasts as the strongest signaling hub, followed by preadipocytes and periductal fibroblasts (Supplementary figure 3A-C). Analysis of signals emanating from fibroblasts and received by epithelial cells revealed, surprisingly, that FGF ligands were not expressed by peri-TEB fibroblasts but rather by fat-pad associated fibroblasts (*Fgf2* by interstitial progenitors, *Fgf7* by AREGs and *Fgf10* by preadipocytes, Supplementary figure 3D-G). Peri-TEB fibroblasts, on the other hand, expressed higher levels of WNT ligands (*Wnt2, Wnt11*) and the WNT signaling regulator *Rspo1* (Supplementary figure 3D-G).

A spatial atlas of mammary fibroblasts during pubertal branching morphogenesis

To retrieve a more precise information about the spatial distribution of the different fibroblast clusters identified in our scRNAseq dataset, we stained histological sections to analyze the expression of genes that we found to be characteristic of each fibroblast cluster based on the transcriptomic data (Figure 2A; Supplementary figure 4A) and annotated the regional localization of each examined field as containing predominantly ducts, TEBs or epithelium-free fat pad (Figure 2B). Expression of specific markers highly correlated with a defining regionalization of the different fibroblast clusters. Besides finding pan-fibroblastic markers (COL1A1, VIM) in all examined regions, we could detect expression of peri-TEB fibroblast markers (αSMA, NES, TNC, MYH10, SDC1) specifically in fibroblasts around the mammary TEBs, whereas the peri-ductal cluster marker *Mfap4* was found in fibroblasts lining the epithelial ducts (Figure 2C, D). Furthermore, genes enriched in fat pad-associated fibroblasts (CD34 for all of them, *F3* for AREGs, DPP4 and *Pi16* for interstitial progenitors, *Enpep* and *Thbs1* for preadipocytes) were indeed located in the distal fat pad devoid of mammary epithelium (Supplementary figure 4A-C). More specifically, AREGs defined by cluster #2 were identified lining blood vessels as expected from studies in

the male fat pad[29], preadipocytes were dispersed between adipocytes, and interstitial progenitors were found in the fat pad septae and in the interstitial reticulum (Supplementary figure 4D), a loose connective tissue at the fat pad border that creates a continuum with the septae dividing the fat pad lobules[28].

This spatial mapping demonstrated that the 6 fibroblast clusters that we identified by scRNAseq show a high degree of spatial organization within the mammary fat pad.

The peri-epithelial fibroblasts expand during puberty

During pubertal growth, the mammary epithelium expands from a rudimentary tree to form a complex branched ductal system that entirely fills the fat pad[6,27]. To assess the dynamic behavior of the different fibroblast populations identified here during such prominent organ remodeling, we sought to sort different mammary fibroblasts by flow cytometry. To this aim, we first used a negative selection (Lin^{neg}/Ep^{neg} [$CD45^{neg}/CD31^{neg}/CD24^{neg}/CD49f^{neg}$]) to exclude immune, endothelial and mammary epithelial cells[23,34,35]. Then, we designed a FACS gating strategy based on our newly identified markers distinguishing different types of mammary fibroblasts at the RNA level (Supplementary figure 5A) and by immunostaining (Supplementary figure 5B, C), dividing Lin^{neg}/Ep^{neg} stromal cells in $SCA1^{neg}$/CD39+ (encoded by *Entpd1*) peri-epithelial fibroblasts and SCA1+ (encoded by *Ly6a*) fat-pad associated fibroblasts. The latter ones were further separated into SCA1+/$DPP4^{neg}$ cells comprising preadipocytes and AREGs, and SCA1+/DPP4+ interstitial progenitors (Figure 3A, Supplementary figure 5D, E). Immunofluorescence staining of freshly isolated FACS-sorted cells from pubertal mammary glands confirmed the presence of αSMA+ and NES+ peri-TEB fibroblasts in the $SCA1^{neg}$/CD39+ population (Supplementary figure 5F-I). Flow cytometry analysis of mammary glands at 3 weeks of age (pre-puberty), 5 weeks (peak of puberty) and 14 weeks (adult stage) revealed the expansion of peri-epithelial $SCA1^{neg}$/CD39+ fibroblasts relatively to other fibroblast populations (Figure 3B, C), consistent with the prominent increase in epithelial cells due to ductal extension and ramification. In addition, our transcriptomic map hinted to the presence of proliferative fibroblasts in TEB proximity (Figure 1F, G) and indeed a 2-hour EdU pulse revealed EdU+

stromal cells mostly located near TEBs (Supplementary figure 6A, B). Intriguingly, we detected proliferative EdU+/SDC1+/αSMA+ fibroblasts in the peri-TEB niche (Supplementary figure 6C).

These results indicate that, at puberty, peri-epithelial fibroblasts expand alongside the growing ductal epithelium and that proliferating fibroblasts are specifically concentrated around TEBs.

Peri-TEB fibroblasts are trailing behind the growing epithelium

To assess the fate of the peri-TEB fibroblasts and understand whether they contribute to the expansion of peri-epithelial fibroblasts, we used a genetic labeling approach to lineage trace them and to follow their behavior *in vivo*. For this, *Acta2-CreERT2;R26-mT/mG* mice were induced at the peak of puberty to label peri-TEB fibroblasts with permanent and heritable GFP expression (Figure 3D-E). After 24/48 hours (acute labeling) or longer chase times (1, 3, 4, 20 weeks), we analyzed the GFP+ fibroblasts by flow cytometry. Surprisingly, flow cytometry showed no expansion of GFP+ cells within the stromal cell population (Figure 3F). However, the distribution of GFP+ cells in the fibroblast populations considerably changed: while acute labeling and 1 week chase resulted in GFP+ cells only in the peri-epithelial CD39+ population, longer chase times for 3 weeks or 20 weeks resulted in a substantial increase in SCA1+/DPP4^{neg} cells (in purple in Figure 3G, Supplementary figure 7A), suggesting that *Acta2*+ peri-TEB fibroblasts can give rise to preadipocytes.

To visualize the spatial distribution of *Acta2*+ peri-TEB fibroblasts and their progeny, we employed whole-organ imaging of CUBIC-cleared mammary glands[36,37], a method that enables evaluation of a large volume of the organ to facilitate the detection of rare cells or cells with an unconventional 3D shape, like fibroblasts. With a short pulse of labeling, the GFP+ fibroblasts were localized around TEBs, in contact with the epithelial cells (Figure 3H-J; note that the level of GFP expression is considerably lower in fibroblasts than in the epithelial cells and mural cells [Supplementary figure 7B], therefore the epithelial signal is overexposed) whereas we could not detect any GFP+ fibroblasts surrounding the ducts (Figure 3J, Supplementary figure 7C). Immunostaining confirmed that the GFP+ cells found in the peri-TEB stromal

region were indeed αSMA+/VIM+ and CD34^{neg}/DPP4^{ne} peri-TEB fibroblasts (Supplementary figure 8A, B).

After 1 or 3 weeks of chase, however, there were no GFP+ fibroblasts around TEBs anymore and the *Acta2*-labeled fibroblasts appeared to have moved to the subtending epithelial ducts (Figure 3H-J, Supplementary figure 8C), at a distance from the TEBs ranging from 1 to 2 mm after 1 week chase and 2.5 mm to 10 mm after 3 weeks chase (Figure 3K), roughly corresponding to the distance covered by growing TEBs in 1 or 3 weeks[7]. Of interest, after a 1- or 3-week chase, we found GFP+ fibroblasts either sitting right on the mammary epithelial ducts or dispersed in the fat pad (Figure 3L, M) and by immunostaining we demonstrated that the GFP+ fibroblasts (VIM+) located either in the peri ductal stroma or further in the fat pad did not express αSMA (Supplementary figure 8C). This corroborates the flow cytometry results suggesting that both periductal fibroblasts and preadipocytes can arise from *Acta2*+ fibroblasts. Altogether, by lineage tracing analysis we provided evidence indicating that the peri-TEB fibroblasts do not prominently expand during puberty and do not seem to move forward to escort the invading epithelial TEBs, but they rather lag behind the growing ducts and either differentiate or give rise to peri-ductal fibroblasts and later to preadipocytes.

Peri-TEB fibroblasts are recruited from the fat pad stroma by the growing epithelium

The lineage tracing experiments described above drew the important conclusion that the peri-TEB fibroblasts are left behind during the ductal growth, raising the question of the origin of new contractile fibroblasts that must be delivered to TEBs to maintain an equilibrium within the peri-TEB stromal cells and to support epithelial growth and fat pad invasion. We reasoned that the tips of growing TEBs inevitably encounter preadipocytes dispersed within the fat pad on their morphogenetic journey, therefore we aimed to lineage trace preadipocytes to establish whether they can be recruited by growing TEBs and acquire a peri-TEB fate. We observed that the Notch1 receptor was expressed by preadipocytes, although not exclusively since it is also found in peri-epithelial fibroblasts (Figure 4A). We therefore used pubertal *Notch1-CreERT2;R26-mT/mG* mice for lineage tracing (Figure 4B, C) and quantified and visualized the

distribution of labelled fibroblasts by flow cytometry and microscopy. Similar to *Acta2-CreERT2* tracing, *Notch1*-expressing stromal cells did not expand (Figure 4D), but the proportion of labelled fibroblasts in different subsets changed. Upon acute labeling (24 h), most GFP+ fibroblasts were found in the SCA1+/DPP4^{neg} gate (Figure 4E), suggesting an efficient labeling of preadipocytes; however, already after 1 week of chase, the ratio switched, and we detected GFP+ fibroblasts primarily within the SCA1^{neg}/CD39+ population of peri-epithelial fibroblasts (Figure 4E). Consistently, by whole-tissue microscopy, we found GFP+ fibroblasts both dispersed within the fat pad and touching the epithelium at acute labeling, whereas 1 week after labeling the GFP+ cells either formed clusters of adipocytes in the fat pad or they were located around TEBs (Supplementary figure 9).

The switch in *Notch1*-traced cells from SCA1+/DPP4^{neg} to SCA1^{neg}/CD39+ cell subsets may suggest that preadipocytes change state by becoming "activated" and convert into contractile peri-epithelial fibroblasts when they encounter a growing duct. We cannot however exclude the possibility that the small population of SCA1^{neg}/CD39+ cells labeled at 24 h expanded and generated the GFP+ peri-epithelial fibroblasts that we observed at later time points after tracing.

In an attempt to discriminate between these two possibilities, we conducted a transplantation experiment, engrafting tdTomato+ fragments of mammary glands (consisting of epithelium and surrounding stroma both labeled by red fluorescence) into cleared fat pads of immunocompromised host mice (Supplementary figure 10A). Supporting our hypothesis that fibroblasts can be recruited by growing TEBs and they do not migrate alongside the growing mammary tips, 3.5 weeks after transplantation, the tdTomato+ epithelium reconstituted a branched outgrowth (Supplementary figure 10B) presenting red fluorescent TEBs, that were surrounded by tdTomato-negative host-derived stromal cells, while tdTomato+ engrafted stromal cells remained at the original grafting site, corroborating our lineage tracing results (Supplementary figure 10C, D).

Furthermore, we co-cultured GFP+ mammary epithelial organoids with the different subsets of tdTomato-labeled fibroblasts that we can now sort by flow cytometry (SCA1^{neg}/CD39+, SCA1+/DPP4^{neg} and

SCA1+/DPP4+; Figure 4F, G). In such co-cultures, we have recently shown that fibroblasts induce organoid branching in a contractility-dependent manner[17]. Surprisingly, we found that after 5 days of co-culture, fibroblasts of all three populations promoted epithelial organoid budding, although the peri-epithelial SCA1^{neg}/CD39+ fibroblasts displayed the highest morphogenetic potential (Figure 4G-I). Therefore, we probed αSMA expression in fibroblasts co-cultured for 5 days with mammary epithelial organoids and discovered that all fibroblast populations acquired αSMA expression when in direct contact with epithelial organoids (Figure 4G, J). Together these results demonstrate that the growing epithelium can recruit fibroblasts from the fat pad and induce their peri-TEB phenotype and namely contractility.

Discussion

Heterogeneity of mammary fibroblasts

Dissection of fibroblast heterogeneity is a blooming topic of research, thanks to scRNAseq analyses that can now offer unprecedented details into the differences between individual fibroblast subtypes presenting common features as well as organ specific differences[4,5]. In the mammary gland, our recent scRNAseq analyses discriminated two distinct clusters in the embryonic mammary stroma[38]; also, other groups identified four fibroblast clusters in the adult mammary gland[26], revealed changes in fibroblast abundance and ECM expression in the aging mammary glands[25] and compared the profile of normal fibroblasts with breast cancer-associated fibroblasts[23]. We have recently reported the existence of specialized αSMA+ peri-TEB fibroblasts that exist only in the proliferating and branching pubertal mammary gland[17]. In the present study, we employed our newly discovered cluster-specific markers to draw a full picture of the spatial distribution of different fibroblasts within the mammary stroma (Figure 5). We show that three SCA1+ clusters represent fat pad fibroblasts, previously found in the male fat pad[28,29] as well as in the adult mammary gland[26]. In this study, we focused on two clusters of peri-epithelial fibroblasts that reside in the collagen-rich sheath around the epithelium: periductal and contractile peri-TEB fibroblasts, unique to puberty.

Our data thus suggest a strong correlation between spatial organization of stromal cells and fibroblast heterogeneity, that seems to be conserved in other organs. For example in the skin, papillary fibroblasts are close to the epidermis, while SCA1+ reticular fibroblasts are embedded deeper in the dermis, close to the subcutaneous fat pad[39]; likewise, in the liver, SCA1+ periportal fibroblasts sit in the portal area and form a separate scRNAseq cluster, distinguished from hepatic stellate cells that line hepatocytes[40,41]. We thus propose that the spatial patterning of fibroblast subtypes may reflect the niche-specific needs for ECM as ECM-related genes represent the major discriminators of fibroblast subtypes across different organs[5].

Fibroblast hierarchy

Fibroblasts are stromal cells of remarkable plasticity, that has been revealed by genetic lineage tracing and transplantation assays, helping to dissect cellular hierarchies in various tissues. In the skin, papillary and reticular fibroblast lineages split during embryonic development and never overlap in adult homeostasis[39]. In the fat pad, Dpp4+ interstitial progenitors contribute to both preadipocytes and AREGs in a unidirectional way[28,42] in accord with transcriptomic analysis that identified Pi16+/Dpp4+ fibroblasts as a progenitor population sitting at the top of the fibroblast hierarchy[4]. Our lineage tracing experiments show that the newly discovered peri-TEB fibroblasts can contribute to both periductal fibroblasts and preadipocytes, but in accord with aforementioned studies, we never observed them to give rise to Pi16+/Dpp4+ interstitial progenitors. Importantly, we show by transplantation and ex vivo recombination that both preadipocytes and interstitial progenitors can be activated by contact with the epithelium and acquire a peri-TEB contractile phenotype. Thus, our results support the hypothesis that peri-TEB fibroblasts represent a transient cell state associated with epithelial morphogenesis and provide a link between fat pad fibroblasts and peri-epithelial fibroblasts, demonstrating that they are not separate lineages (Figure 5).

Fibroblasts can also differentiate into pericytes and adipocytes in the skin[43,44] and in the interscapular, inguinal[45], mesenteric and gonadal fat pad[42]. In the mammary gland, adipocytes dedifferentiate into fibroblasts during pregnancy and are reestablished from fibroblasts during involution[46,47]. It is yet to be determined which fibroblast clusters can trans-differentiate into adipocytes in homeostasis and during

pregnancy-associated changes of the mammary stroma. Our data showing the remarkable plasticity of these cells, at least in co-cultures, suggest however that both fat pad and peri-epithelial fibroblasts could be able to give rise to adipocytes.

Fibroblasts orchestrate epithelial morphogenesis

Fibroblasts are believed to be critical regulators of mammary branching morphogenesis[2,10], due to their capacity of secreting Fibroblast Growth Factors (FGFs)[11]. FGF10 acts as a chemoattractant in organoids[11] and FGF10-soaked beads locally accelerate branching when implanted *in vivo*[8]. Our transcriptomic analysis shows that FGFs are mostly expressed by fat pad fibroblasts (Figure 5). While most epithelial cells are shielded from the fat pad by a dense collagenous stroma, the leading edge of TEB is in direct contact with FGF10-expressing preadipocytes. Thus, we believe that the spatial organization of fibroblast clusters can explain how FGF10-mediated chemoattraction acts *in vivo*. Also FGF2 induces epithelial proliferation and organoid budding *in vitro*[12], which is reminiscent of mammary side branching[48]. Here we found that FGF2 is produced by interstitial progenitors, located along the septae dividing the fat pad; these stromal cells could stochastically encounter a growing duct however if this impacts the pattern of epithelial branching is an attractive hypothesis that remains to be mechanistically explored. We have also detected cluster-specific Wnt ligand expression (Figure 5), with peri-TEB fibroblasts being the stronger producers of Wnt ligands, suggesting that they may create a stem cell-promoting niche, rich in Wnt ligands, around the TEBs. Other paracrine signals predicted to act between fibroblasts and epithelium by the Cellchat analysis we provide here remain to be functionally addressed.

ECM expression and organization is another critical regulator of mammary epithelial branching[49–51] and our scRNAseq analysis reveals distinct patterns of ECM expression in different fibroblast clusters. Our analysis shows that peri-TEB fibroblasts express low levels of fibrillar collagens, including *Col1a1* and *Col1a2*, suggesting that they may produce the collagen sheath only after their transition into peri-ductal fibroblasts. Similarly, we detected lower expression of basal membrane genes in peri-TEB fibroblasts, in agreement with the well documented reduction in basal membrane thickness around TEBs[27]. Peri-TEB

fibroblasts are also the primary source of membrane bound Matrix Metalloproteases MMPs that can further promote basal membrane thinning and have been shown to facilitate mammary branching *in vivo*[32]. Finally, the peri-TEB fibroblasts we characterize here are the exclusive producers of Tenascin C, another ECM molecule associated with pro-invasive properties[30,31].

A new line of evidence suggest that stromal cells may also regulate epithelial morphogenesis through mechanical forces derived from actomyosin cell contraction, as it was shown for the regulation of lung branching[18,52], the growth of feathers[53] and hair follicles[54] as well as gut vilification[55]. In the mammary gland, we have recently demonstrated that fibroblast contractility drives epithelial organoid branching in a co-culture system[17]. It is conceivable that the contractile fibroblasts positioned around the neck of TEBs that we studied here may create a hoop stress that facilitates the ductal invasion through the fat pad, as previously suggested for myoepithelial cells[56]. Of note, the peculiar localization of contractile peri-TEB fibroblasts correlates with the transition of the cuboidal epithelial cap cells of TEBs into myoepithelial cells lining the subtending ducts, opening an exciting opportunity to test the involvement of contractile fibroblasts in this process in further studies. In conclusion, we have characterized a novel fibroblast population that creates a specialized mechano-chemical niche to facilitate epithelial morphogenesis (Figure 5).

Fibroblasts activation – signals from the epithelium and beyond

The process of fibroblast activation is probably best studied in wound healing, when fibroblast contractility and ECM production is turned on to aid proper wound closure and healing. Excessive fibroblast activation, however, can result in scarring, fibrosis and provide cancer prone microenvironment. Contractile fibroblasts, however, are also found in developing tissues and it is not clear if they are controlled by conserved mechanisms and molecular regulators. Interestingly, we have observed that while peri-TEB fibroblasts are characterized by a signature of contractility, they express lower levels of fibrillar collagens, suggesting that the activation process is either completely different or only partial, when compared to wound healing. Many of the signaling pathways commonly

associated with fibroblast activation have been shown to be involved in mammary fibroblasts regulation, like PDGF[57], FGF[58] or WNT signaling[59–61]. Finally, contact with macrophages can activate myofibroblasts in wounds, via cell-cell adhesion and TGFβ signaling[62], while macrophages are present in the peri-TEB stroma and their depletion impairs mammary outgrowth[63,64]. It is therefore tempting to speculate that TEBs invading the fat pad create a miniature wound-like environment, involving activation of contractile fibroblasts that are recruited to propel epithelial branching in an evolutionary conserved manner. Further research into fibroblast activation during organ development is needed to understand the differences and similarities between morphogenesis, wound-healing, fibrosis and cancer.

Material and methods

Mice

All procedures involving animals were performed under the approval of the Ministry of Education, Youth and Sports of the Czech Republic (license # MSMT-9232/2020-2), supervised by the Expert Committee for Laboratory Animal Welfare of the Faculty of Medicine, Masaryk University, at the Laboratory Animal Breeding and Experimental Facility of the Faculty of Medicine, Masaryk University (facility license #58013/2017-MZE-17214), or under the approval of the ethics committee of the Institut Curie and the French Ministry of Research (reference #34364-202112151422480) in the Animal Facility of Institut Curie (facility license #C75–05–18). ICR mice and nude mice were obtained from the Laboratory Animal Breeding and Experimental Facility of the Faculty of Medicine, Masaryk University. *LifeAct-GFP* mice were created by Wedlich-Söldner team[65], *R26-mT/mG*[66] and *Acta2-CreERT2* mice[67] were acquired from the Jackson Laboratory. *Notch1-CreERT2* mice[68] were created in our laboratory. Transgenic animals were maintained on a C57BL/6 background. Experimental animals were obtained by breeding of the parental strains, the genotypes were determined by genotyping. The mice were housed in individually ventilated or open cages, all with ambient temperature of 22°C, a 12 h:12 h light:dark cycle, and food and water ad

libitum. For induction of *CreERT2* constructs, mice were treated with tamoxifen (Sigma, 2 mg/10 g of mouse) diluted in corn oil (Sigma), delivered via intraperitoneal injection. For EdU incorporation assay, 5 weeks old wild-type females were injected with 10 nmol/1 g of mouse, delivered via intraperitoneal injection 2 h prior to euthanasia. Mice were euthanized by cervical dislocation and mammary gland tissues were collected immediately.

Microdissection of TEB/duct

For microdissection of TEB- and duct-containing regions, 5 weeks old *R26-mT/mG* females were used. Mammary glands #3 and #4 were dissected and spread on 10 cm plastic petri dishes. Under the control of a fluorescent stereoscope (Leica FM165C), 0.5x0.5 mm pieces of tissue containing either TEBs or pieces of ducts (assessed based on tdTomato fluorescence) were dissected and collected in CO_2-independent medium on ice. 5-8 mice were pooled for one experiment.

Single cell RNA sequencing

For scRNAseq experiment, microdissected pieces of mammary gland were digested in a collagenase/hyaluronidase solution [3 mg/ml collagenase A, 100 U/ml hyaluronidase (all Merck), 5% fetal bovine serum (FBS; Hyclone/GE Healthcare) in CO_2 independent medium (Thermo Fisher Scientific)] for 2 hours at 37°C, shaking at 120 rpm. Resulting tissue fragments were treated with 0.25% trypsin, 5 mg/ml dispase II, 100 µg/ml DNase and red blood cell lysis buffer (Sigma) and filtered through a 40 µm cell strainer. Resulting single cell suspension was pooled down, resuspended in freezing medium (10% DMSO in FBS) and frozen by slow freezing at -80°C and moved to liquid nitrogen 24 h thereafter. Sequencing was performed at Single Cell Discoveries BV, Netherlands, using the 10x Genomics platform, at 5,000 target cells/sample and with sequencing depth of 50,000 reads per cell.

scRNAseq data analysis – data preprocessing

The analysis of scRNAseq data was performed in R (R systems) using the Seurat package[69]. The following filters were applied to the data to remove doublets and damaged cells: genes with expression in < 3,

nCount_RNA < 3000 or > 60000, *nFeature_RNA* < 1000 or with a percentage of mitochondrial reads > 20 were removed. The data were normalized with the *SCTransform* function. Uniform Manifold Approximation and Projection and neighbors identification were computed using the *RunUMAP* and *FindNeighbors* function on the first 9 PCs Clusters were defined using the *FindClusters* function with a resolution set to 0.2. Fibroblast, epithelial and leukocyte populations were then identified based on canonical markers (*Col1a1*, *Col3a1*, *Pdgfra* for fibroblasts; *Ptprc* for leukocytes; *Epcam*, *Cdh1* for epithelium).

scRNAseq data analysis – subpopulation analysis

The fibroblast, epithelial and leukocyte subsets of cells were then merged together and reanalyzed using the first 10 PCs for *RunUMAP* and 0.3 resolution for *FindClusters*. Possible lymphocyte-containing doublets within fibroblast cluster were identified by *Ptprc* expression and excluded from the analysis. Cluster markers were calculated using the *FindAllMarkers* function. The expression scores were calculated using the *AddModuleScore* function with genes in supplementary table 1.

scRNAseq data analysis – cell communication analysis

Communication link between cell populations were identified using the CellChat R package[33]. Only epithelial and fibroblast clusters were used for this analysis. Interactions between the different clusters were identified based on the mouse 'Secreted Signaling' internal CellChat database. Interactions identified in less than 5 cells per group were filtered out. Interactions between groups were visualized using the 'netVisual_chord_gene' function.

Immunohistochemistry (IHC)

For IHC, mammary glands #4 were dissected, spread on glass slide and fixed in 4% paraformaldehyde (EM grade; Electron Microscopy Sciences) overnight at 4°C, dehydrated in ethanol solutions with increasing concentration and xylene and embedded in paraffin. 5 µm sections were cut on rotational microtome (Thermo scientific, Microm HM340E). After rehydration, sections were boiled in pH6 citrate buffer or pH9 Tris-EDTA buffer to retrieve antigens, blocked in 1% bovine serum albumin and 5% FBS and incubated

with primary antibodies (supplementary table 2), fluorophore-conjugated secondary antibodies (ThermoFisher Scientific) and 1 µg/ml 4′,6-diamidino-2-phenylindole (DAPI, Merck) , mounted (Aqua Poly/Mount, Polysciences) and imaged on laser scanning confocal microscope (LSM780/800/880/900, Zeiss). For SCA1 staining, slides were first stained for COL1A1 than biotin-conjugated SCA1 primary antibody was followed by incubation with 1 µg/ml Alexafluor633-conjugated streptavidin (ThermoFisher Scientific) for 1 hour before counterstaining with DAPI. EdU detection was performed using Click-iT imaging kit (ThermoFisher Scientific) following the manufacturer's instructions. The quantification of positive cells was done manually in ImageJ, using DAPI signal to count total stromal cell number. Cells of epithelial ducts and blood vessels, recognized by typical morphology, autofluorescence and cell shape, were omitted from analysis. The field of views (FOVs) were all of the same size (212×212 µm) and were scored "duct", "TEB" or "fat" based on morphology and position of the structures (TEBs: stratified epithelium, bulb-like shape and position of the structure at the distal part of the mammary epithelium (invasive front); duct: bi-layered epithelium; fat: no epithelial structures in the FOV).

In situ hybridization (ISH)

For ISH, mammary glands were processed in the same way as for IHC and the staining was performed using RNA Scope kit following manufacturer's instructions, using commercially available probes (supplementary table 2). The quantification of positive cells was done manually in ImageJ similarly to IHC quantification, using DAPI signal to count total stromal cell number. Rules for determining positive cell were unique for each probe, based on the level of expression (3 dots for *Enpep*, *Thbs1* and *Ly6a*; cytoplasm full of dots for *F3*, *Tnc, Pi16* and *Mfap4*).

Fluorescence assisted cell sorting (FACS)

For FACS or flow cytometry, harvested mammary glands #1, #2, #3, #4 and #5 were chopped into 0.5×0.5×0.5 mm^3 pieces and digested in a solution of collagenase and trypsin [2 mg/ml collagenase A, 2 mg/ml trypsin, 5 µg/ml insulin, 50 µg/ml gentamicin (all Merck), 5% FBS (Hyclone/GE Healthcare) in DMEM/F12 (Thermo Fisher Scientific)] for 30-60 min at 37°C. Resulting tissue suspension was treated

with DNase I (20 U/ml; Merck) and red blood cell lysis buffer and filtered through 40 µm cell strainer to achieve single cell solution. The cells were resuspended in staining medium (10% FBS, 100 U/ml of penicillin, and 100 µg/ml of streptomycin in CO_2 independent medium) with antibodies (supplementary table 2) and incubated on ice in dark for 30 min. Then, the cells were washed twice with PBS, resuspended in flow buffer (5 mM EDTA, 1% BSA, 1% FBS in phenol red-free DMEM/F12 with HEPES) and passed through a 40 µm cell strainer. The analysis was done on Aria III or Fusion (both BD), operated by SORP software (BD). The flow cytometry data were analyzed using the FlowJo software (BD).

Immunocytochemistry (ICC)

For immunofluorescent analysis, 10,000 FACS-sorted fibroblasts were plated directly on coverslip-bottom 8 well plates (IBIDI) and cultured in fibroblast medium [10% FBS, 1× ITS (10 µg/ml insulin, 5.5 µg/ml transferrin, 6.7 ng/ml sodium selenite), 100 U/ml of penicillin, and 100 µg/ml of streptomycin in DMEM], fixed with 4% formaldehyde for 15 min, permeabilized with 0.5% Triton X-100 in PBS for 10 min and blocked with PBS with 10% FBS for 30 min. Then the cells were incubated with primary antibodies (supplementary table 2) for 2 h at RT. After washing, the cells were incubated with fluorophore-conjugated secondary antibodies (ThermoFisher Scientific) and phalloidin AlexaFluor 488 and DAPI for 2 h at RT. The cells were photographed using LSM 780/880/900 (Zeiss).

Whole-mount clearing and imaging

Staining and clearing of the mammary glands was done following clear, unobstructed brain imaging cocktails (CUBIC) protocol[36,37]. Briefly, mammary glands #3 or #4 were harvested and fixed in in 4% paraformaldehyde overnight at 4°C, washed and incubated in CUBIC reagent 1 (25% (w/w) urea, 25% (w/w) N,N,N',N'-tetrakis(2-hydroxypropyl)ethylenediamine, 15% (w/w) Triton X-100 in distilled water) for 4 days shaking at RT. After washing, the tissue was blocked using blocking buffer (5% FBS, 2% BSA, 1% Triton X-100, 0.02% sodium azide in PBS) overnight at RT, incubated with primary antibodies (supplementary table 2) diluted in blocking buffer for 3 days at 4°C with rocking, washed three times for 2 h (0.05% Tween 20 in PBS) and incubated with DAPI (1 µg/ml) in blocking buffer. Then the glands were

transferred to CUBIC reagent 2 (50% (w/w) sucrose, 25% (w/w) urea, 10% (w/w) 2,2',2''-nitrilotriethanol, 0.1% (w/w) Triton X-100 in distilled water) for >1 day at RT with rocking. The samples were mounted with CUBIC reagent 2 between two coverslips with double-sided tape as a spacer to enable imaging from both sides and they were imaged on laser scanning confocal microscope LSM780/880 (Zeiss). Non-fibroblastic cells were identified based on their morphology, position in tissue and difference in GFP expression level. Namely, the *Acta2* model induced GFP expression in basal epithelial cells, vascular smooth muscle cells and pericytes; *Notch1* model induced GFP expression in subset of luminal epithelial cells and in endothelium.

Mammary fragment transplantation

For transplantation experiments, mammary gland #4 from 5-week old *R26-mT/mG* females was harvested, spread on a 10 cm plastic petri dish and a 0.5×0.5×0.5 mm^3 piece containing epithelial duct was dissected under a stereoscope using tdTomato fluorescence for guidance (Leica FM165C) and kept in CO2 independent medium on ice until use, but for maximum of 6 h. 3 weeks old nude females were anesthetized with isoflurane, after disinfection of abdominal area, reversed Y shaped incision was made into skin and #4 mammary glands were mobilized from the peritoneum. After cauterization of blood vessel in the connection of #5 and #4 mammary glands, proximal part of #4 mammary gland (from nipple to lymph node) was cut out. Small incision using iris scissors was made in the middle of the remaining fat pad to create a capsule, where a single piece of *R26-mT/mG* tissue was grafted. The skin opening was closed using bio-degradable suture and mice were carefully monitored until full recovery. During first 2 weeks after surgery, mice were supplied with analgesia (0.2 mg/ml of Ibuprofen in drinking water). 3.5 weeks after the surgery, the mice were euthanized and the mammary outgrowth was analyzed.

Mammary organoid-fibroblast co-cultures

3D culture of mammary organoids and fibroblasts was performed as previously described[70]. Briefly, for isolation of primary mammary organoids (fragments), mammary glands were harvested, chopped and enzymatically digested [2 mg/ml collagenase A, 2 mg/ml trypsin, 5 µg/ml insulin, 50 µg/ml gentamicin (all

Merck), 5% FBS (Hyclone/GE Healthcare) in DMEM/F12 (Thermo Fisher Scientific)] for 30 min at 37°C and 120 rpm. Resulting tissue suspension was treated with DNase I (20 U/ml; Merck) and enriched for organoids by 5 rounds of differential centrifugation at 450 × g for 10 s. The collagen/Matrigel gel matrix [MEM 1×, collagen 1 from rat tail (Corning) 2.5 mg/ml, 30% growth factor reduced Matrigel (Corning)] was mixed and pre-incubated for 1 h on ice before mixing with cells. 100 organoids, 80,000 FACS-sorted fibroblasts and 25 µl of collagen/Matrigel gel matrix were mixed well and plated on small patches of Matrigel on 8-well coverslip-bottom dishes (IBIDI) and overlayed with basal organoid medium (1× ITS, 100 U/ml of penicillin, and 100 µg/ml of streptomycin in DMEM/F12).

Co-culture immunofluorescence

For immunofluorescent analysis of 3D co-cultures, the co-cultures were fixed with 4% paraformaldehyde for 40 min at RT, washed, and stored in PBS. The co-cultures were permeabilized with 0.5% Triton X-100 in PBS, blocked with 1% BSA, 5% FBS and 0.1% Triton X-100 in PBS (3D staining buffer, 3SB) and incubated with primary antibodies (supplementary table 2) in 3SB over 1-3 nights at 4°C. Then the co-cultures were washed for 3 h with 0.05% Tween-20 in PBS and incubated with fluorophore-conjugated secondary antibodies (ThermoFisher Scientific) and DAPI (1 µg/ml; Merck) in 3SB overnight at 4°C in dark. Then the co-cultures were washed for 3 h with 0.05% Tween-20 in PBS, cleared with 60% glycerol overnight at RT in dark. The co-cultures were imaged using LSM 880 (Zeiss).

Statistical analysis

Statistical analysis was carried out in R using *stat_compare_means* function or *geom_signif* function of ggplot2 package. For comparing percentage, the *chisq.test* was used. N denotes number of samples used for statistical analysis, n denotes number of independent biological replicates, n.s. means not significant, *p < 0.05, **p < 0.01, ***p < 0.001, ****p < 0.0001. The box plots show median, the box borders are Q2-Q3, the whiskers are minimum to maximum, big points are predicted outliers, dots show single samples.

Author contribution

JS conceptualized the work, performed the experiments, analyzed data and wrote original manuscript, ZSK and SF acquired funding, conceptualized and supervised the work and wrote the manuscript. RJ performed CellChat analysis of scRNAseq data. MMF contributed to experimental work and edited the manuscript.

Funding

Czech Science Foundation (GAČR GA23-04974S) and Ministry of Education, Youth and Sports (ERC CZ LL2323 FIBROFORCE) to ZSK, Barrande Fellowship (Ministry of Education, Youth and Sports); FRM FDM202106013570; Brno PhD Talent Scholarship funded by the Brno City Municipality to JS. This work was supported by the French National Research Agency (ANR) grants number ANR-21-CE13-0047 and ANR-22-CE13-0009, the Medical Research Foundation FRM "FRM Equipes" EQU201903007821, the FSER (Fondation Schlumberger pour l'éducation et la recherche) FSER20200211117, the Association for Research against Cancer (ARC) label ARCPGA2021120004232_4874, the Worldwide Cancer Research Foundation # 24-0216 and by Labex DEEP ANR-Number 11-LBX-0044 to SF.

Acknowledgement

The authors would like to acknowledge the Cell and Tissue Imaging Platform – PICT-IBiSA (member of France–Bioimaging – ANR-10-INBS-04) of the U934/UMR3215 of Institut Curie for help with light microscopy. We acknowledge the core facility CELLIM of CEITEC, supported by the Czech-BioImaging large RI project (LM2023050 funded by MEYS CR), for their support with obtaining scientific data presented in this paper. We acknowledge the Cytometry platform of Institut Curie, The platform of *in vivo* experimentation of Institut Curie and the animal unit of Masaryk University. We thank to Danijela M. Vignijevic and Pavel Tomancak for constructive discussions.

Conflict of interest statement

The authors declare no conflict of interest.

References

1. Plikus, M. V. *et al.* Fibroblasts: Origins, definitions, and functions in health and disease. *Cell* **184**, 3852–3872 (2021).

2. Sumbal, J., Belisova, D. & Koledova, Z. Fibroblasts: The grey eminence of mammary gland development. *Semin Cell Dev Biol* **114**, 134–142 (2021).

3. Tomasek, J. J., Gabbiani, G., Hinz, B., Chaponnier, C. & Brown, R. A. Myofibroblasts and mechano-regulation of connective tissue remodelling. *Nat Rev Mol Cell Biol* **3**, 349–363 (2002).

4. Buechler, M. B. *et al.* Cross-tissue organization of the fibroblast lineage. *Nature* **593**, 575–579 (2021).

5. Muhl, L. *et al.* Single-cell analysis uncovers fibroblast heterogeneity and criteria for fibroblast and mural cell identification and discrimination. *Nat Commun* **11**, 3953 (2020).

6. Macias, H. & Hinck, L. Mammary gland development. *Wiley Interdiscip Rev Dev Biol* **1**, 533–557 (2012).

7. Paine, I. S. *et al.* A Geometrically-Constrained Mathematical Model of Mammary Gland Ductal Elongation Reveals Novel Cellular Dynamics within the Terminal End Bud. *PLoS computational biology* **12**, (2016).

8. Hannezo, E. *et al.* A Unifying Theory of Branching Morphogenesis. *Cell* **171**, (2017).

9. Scheele, C. L. G. J. *et al.* Identity and dynamics of mammary stem cells during branching morphogenesis. *Nature* **542**, (2017).

10. Wiseman, B. S. & Werb, Z. Stromal effects on mammary gland development and breast cancer. *Science* **296**, 1046–1049 (2002).

11. Zhang, X. *et al.* FGF ligands of the postnatal mammary stroma regulate distinct aspects of epithelial morphogenesis. *Development (Cambridge, England)* **141**, (2014).

12. Ewald, A. J., Brenot, A., Duong, M., Chan, B. S. & Werb, Z. Collective Epithelial Migration and Cell Rearrangements Drive Mammary Branching Morphogenesis. *Developmental cell* **14**, 570 (2008).

13. Peuhu, E. *et al.* SHARPIN regulates collagen architecture and ductal outgrowth in the developing mouse mammary gland. *The EMBO Journal* **36**, 165–182 (2017).

14. Nguyen-Ngoc, K.-V. & Ewald, A. J. Mammary ductal elongation and myoepithelial migration are regulated by the composition of the extracellular matrix. *J Microsc* **251**, 212–223 (2013).

15. Brownfield, D. G. *et al.* Patterned Collagen Fibers Orient Branching Mammary Epithelium through Distinct Signaling Modules. *Current Biology* **23**, 703–709 (2013).

16. Nerger, B. A. *et al.* Local accumulation of extracellular matrix regulates global morphogenetic patterning in the developing mammary gland. *Current Biology* **31**, 1903-1917.e6 (2021).

17. Sumbal, J., Fre, S. & Sumbalova Koledova, Z. Fibroblast-induced mammary epithelial branching depends on fibroblast contractility. *PLoS Biol* **22**, e3002093 (2024).

18. Goodwin, K. *et al.* Smooth muscle differentiation shapes domain branches during mouse lung development. *Development* **146**, dev181172 (2019).

19. Heitman, N. *et al.* Dermal sheath contraction powers stem cell niche relocation during hair cycle regression. *Science* **367**, 161–166 (2020).

20. Schuster, R., F, Y., M, E. & B, H. The Role of Myofibroblasts in Physiological and Pathological Tissue Repair. *Cold Spring Harbor perspectives in biology* **15**, (2023).

21. Sahai, E. *et al.* A framework for advancing our understanding of cancer-associated fibroblasts. *Nat Rev Cancer* **20**, 174–186 (2020).

22. Barbazán, J. & Matic Vignjevic, D. Cancer associated fibroblasts: is the force the path to the dark side? *Curr Opin Cell Biol* **56**, 71–79 (2019).

23. Houthuijzen, J. M. *et al.* CD26-negative and CD26-positive tissue-resident fibroblasts contribute to functionally distinct CAF subpopulations in breast cancer. *Nat Commun* **14**, 183 (2023).

24. Kanaya, N. *et al.* Single-cell RNA-sequencing analysis of estrogen- and endocrine-disrupting chemical-induced reorganization of mouse mammary gland. *Commun Biol* **2**, 406 (2019).

25. Li, C. M.-C. *et al.* Aging-Associated Alterations in Mammary Epithelia and Stroma Revealed by Single-Cell RNA Sequencing. *Cell Rep* **33**, 108566 (2020).

26. Yoshitake, R. *et al.* Single-Cell Transcriptomics Identifies Heterogeneity of Mouse Mammary Gland Fibroblasts With Distinct Functions, Estrogen Responses, Differentiation Processes, and Crosstalks With Epithelium. *Frontiers in Cell and Developmental Biology* **10**, (2022).

27. Paine, I. S. & Lewis, M. T. The Terminal End Bud: the Little Engine that Could. *J Mammary Gland Biol Neoplasia* **22**, 93–108 (2017).

28. Merrick, D. *et al.* Identification of a mesenchymal progenitor cell hierarchy in adipose tissue. *Science* **364**, eaav2501 (2019).

552 29. Schwalie, P. C. *et al.* A stromal cell population that inhibits adipogenesis in mammalian fat
553 depots. *Nature* **559**, 103–108 (2018).

554 30. Midwood, K. S., Hussenet, T., Langlois, B. & Orend, G. Advances in tenascin-C biology. *Cell*
555 *Mol Life Sci* **68**, 3175–3199 (2011).

556 31. Inaguma, Y. *et al.* Epithelial induction of stromal tenascin in the mouse mammary gland: from
557 embryogenesis to carcinogenesis. *Developmental biology* **128**, (1988).

558 32. Feinberg, T. Y. *et al.* Divergent Matrix-Remodeling Strategies Distinguish Developmental
559 from Neoplastic Mammary Epithelial Cell Invasion Programs. *Dev Cell* **47**, 145-160.e6
560 (2018).

561 33. Jin, S. *et al.* Inference and analysis of cell-cell communication using CellChat. *Nat Commun*
562 **12**, 1088 (2021).

563 34. Bartoschek, M. *et al.* Spatially and functionally distinct subclasses of breast cancer-associated
564 fibroblasts revealed by single cell RNA sequencing. *Nat Commun* **9**, 5150 (2018).

565 35. Stingl, J. *et al.* Purification and unique properties of mammary epithelial stem cells. *Nature*
566 **439**, 993–997 (2006).

567 36. Lloyd-Lewis, B. *et al.* Imaging the mammary gland and mammary tumours in 3D: optical
568 tissue clearing and immunofluorescence methods. *Breast Cancer Res* **18**, 127 (2016).

569 37. Susaki, E. A. *et al.* Whole-brain imaging with single-cell resolution using chemical cocktails
570 and computational analysis. *Cell* **157**, 726–739 (2014).

571 38. Carabaña, C. *et al.* Positional cues underlie cell fate specification during branching
572 morphogenesis of the embryonic mammary epithelium. 2022.08.30.505826 Preprint at
573 https://doi.org/10.1101/2022.08.30.505826 (2022).

574 39. Driskell, R. R. *et al.* Distinct fibroblast lineages determine dermal architecture in skin
575 development and repair. *Nature* **504**, 277–281 (2013).

576 40. Cordero-Espinoza, L. *et al.* Dynamic cell contacts between periportal mesenchyme and ductal
577 epithelium act as a rheostat for liver cell proliferation. *Cell Stem Cell* **28**, 1907-1921.e8 (2021).

578 41. Lepreux, S. & Desmoulière, A. Human liver myofibroblasts during development and diseases
579 with a focus on portal (myo)fibroblasts. *Frontiers in Physiology* **6**, (2015).

580 42. Stefkovich, M., Traynor, S., Cheng, L., Merrick, D. & Seale, P. Dpp4+ interstitial progenitor
581 cells contribute to basal and high fat diet-induced adipogenesis. *Mol Metab* **54**, 101357 (2021).

582 43. Driskell, R. R., Jahoda, C. A. B., Chuong, C.-M., Watt, F. M. & Horsley, V. Defining dermal
583 adipose tissue. *Experimental Dermatology* **23**, 629–631 (2014).

584 44. Goss, G., Rognoni, E., Salameti, V. & Watt, F. M. Distinct Fibroblast Lineages Give Rise to
585 NG2+ Pericyte Populations in Mouse Skin Development and Repair. *Front Cell Dev Biol* **9**,
586 675080 (2021).

587 45. Sun, C., Berry, W. L. & Olson, L. E. PDGFRα controls the balance of stromal and adipogenic
588 cells during adipose tissue organogenesis. *Development* **144**, 83–94 (2017).

589 46. Wang, Q. A. *et al.* Reversible De-differentiation of Mature White Adipocytes into
590 Preadipocyte-like Precursors during Lactation. *Cell Metabolism* **28**, 282-288.e3 (2018).

591 47. Zwick, R. K. *et al.* Adipocyte hypertrophy and lipid dynamics underlie mammary gland
592 remodeling after lactation. *Nat Commun* **9**, 3592 (2018).

593 48. Sumbal, J., Vranova, T. & Koledova, Z. FGF signaling dynamics regulates epithelial
594 patterning and morphogenesis. 2020.11.17.386607 Preprint at
595 https://doi.org/10.1101/2020.11.17.386607 (2020).

596 49. Fata, J. E., Werb, Z. & Bissell, M. J. Regulation of mammary gland branching morphogenesis
597 by the extracellular matrix and its remodeling enzymes. *Breast Cancer Res* **6**, 1–11 (2004).

598 50. Paramore, S. V., Goodwin, K. & Nelson, C. M. How to build an epithelial tree. *Phys. Biol.* **19**,
599 061002 (2022).

600 51. Schedin, P. & Keely, P. J. Mammary Gland ECM Remodeling, Stiffness, and
601 Mechanosignaling in Normal Development and Tumor Progression. *Cold Spring Harb*
602 *Perspect Biol* **3**, a003228 (2011).

603 52. Li, R., Li, X., Hagood, J., Zhu, M.-S. & Sun, X. Myofibroblast contraction is essential for
604 generating and regenerating the gas-exchange surface. *J Clin Invest* **130**, 2859–2871 (2020).

605 53. Shyer, A. E. *et al.* Emergent cellular self-organization and mechanosensation initiate follicle
606 pattern in the avian skin. *Science* **357**, 811–815 (2017).

607 54. Villeneuve, C. *et al.* Mechanical forces across compartments coordinate cell shape and fate
608 transitions to generate tissue architecture. *Nat Cell Biol* **26**, 207–218 (2024).

609 55. Shyer, A. E. *et al.* Villification: how the gut gets its villi. *Science* **342**, 212–218 (2013).

610 56. Neumann, N. M. *et al.* Coordination of receptor tyrosine kinase signaling and interfacial
611 tension dynamics drive radial intercalation and tube elongation. *Dev Cell* **45**, 67-82.e6 (2018).

612 57. Hammer, A. M. *et al.* Stromal PDGFR-α Activation Enhances Matrix Stiffness, Impedes
613 Mammary Ductal Development, and Accelerates Tumor Growth. *Neoplasia* **19**, 496–508
614 (2017).

615 58. Sumbal, J. & Koledova, Z. FGF signaling in mammary gland fibroblasts regulates multiple
616 fibroblast functions and mammary epithelial morphogenesis. *Development* **146**, dev185306
617 (2019).

618 59. Rajaram, R. D. *et al.* Progesterone and Wnt4 control mammary stem cells via myoepithelial
619 crosstalk. *EMBO J* **34**, 641–652 (2015).

620 60. van Amerongen, R., Bowman, A. N. & Nusse, R. Developmental stage and time dictate the
621 fate of Wnt/β-catenin-responsive stem cells in the mammary gland. *Cell Stem Cell* **11**, 387–
622 400 (2012).

623 61. Wang, J. *et al.* Endothelial Wnts control mammary epithelial patterning via fibroblast
624 signaling. *Cell Reports* **34**, 108897 (2021).

625 62. Lodyga, M. *et al.* Cadherin-11–mediated adhesion of macrophages to myofibroblasts
626 establishes a profibrotic niche of active TGF-β. *Science Signaling* **12**, eaao3469 (2019).

627 63. Gouon-Evans, V., Rothenberg, M. E. & Pollard, J. W. Postnatal mammary gland development
628 requires macrophages and eosinophils. *Development* **127**, 2269–2282 (2000).

629 64. Gyorki, D. E., Asselin-Labat, M.-L., van Rooijen, N., Lindeman, G. J. & Visvader, J. E.
630 Resident macrophages influence stem cell activity in the mammary gland. *Breast Cancer Res*
631 **11**, R62 (2009).

632 65. Riedl, J. *et al.* Lifeact mice for studying F-actin dynamics. *Nat Methods* **7**, 168–169 (2010).

633 66. Muzumdar, M. D., Tasic, B., Miyamichi, K., Li, L. & Luo, L. A global double-fluorescent Cre
634 reporter mouse. *Genesis* **45**, 593–605 (2007).

635 67. Wendling, O., Bornert, J.-M., Chambon, P. & Metzger, D. Efficient temporally-controlled
636 targeted mutagenesis in smooth muscle cells of the adult mouse. *Genesis* **47**, 14–18 (2009).

637 68. Fre, S. *et al.* Notch lineages and activity in intestinal stem cells determined by a new set of
638 knock-in mice. *PLoS One* **6**, e25785 (2011).

639 69. Hao, Y. *et al.* Integrated analysis of multimodal single-cell data. *Cell* **184**, 3573-3587.e29
640 (2021).

641 70. Koledova, Z. & Lu, P. A 3D Fibroblast-Epithelium Co-culture Model for Understanding
642 Microenvironmental Role in Branching Morphogenesis of the Mammary Gland. *Methods Mol*
643 *Biol* **1501**, 217–231 (2017).

644

645

Sumbal et al.

Figures and figure legends

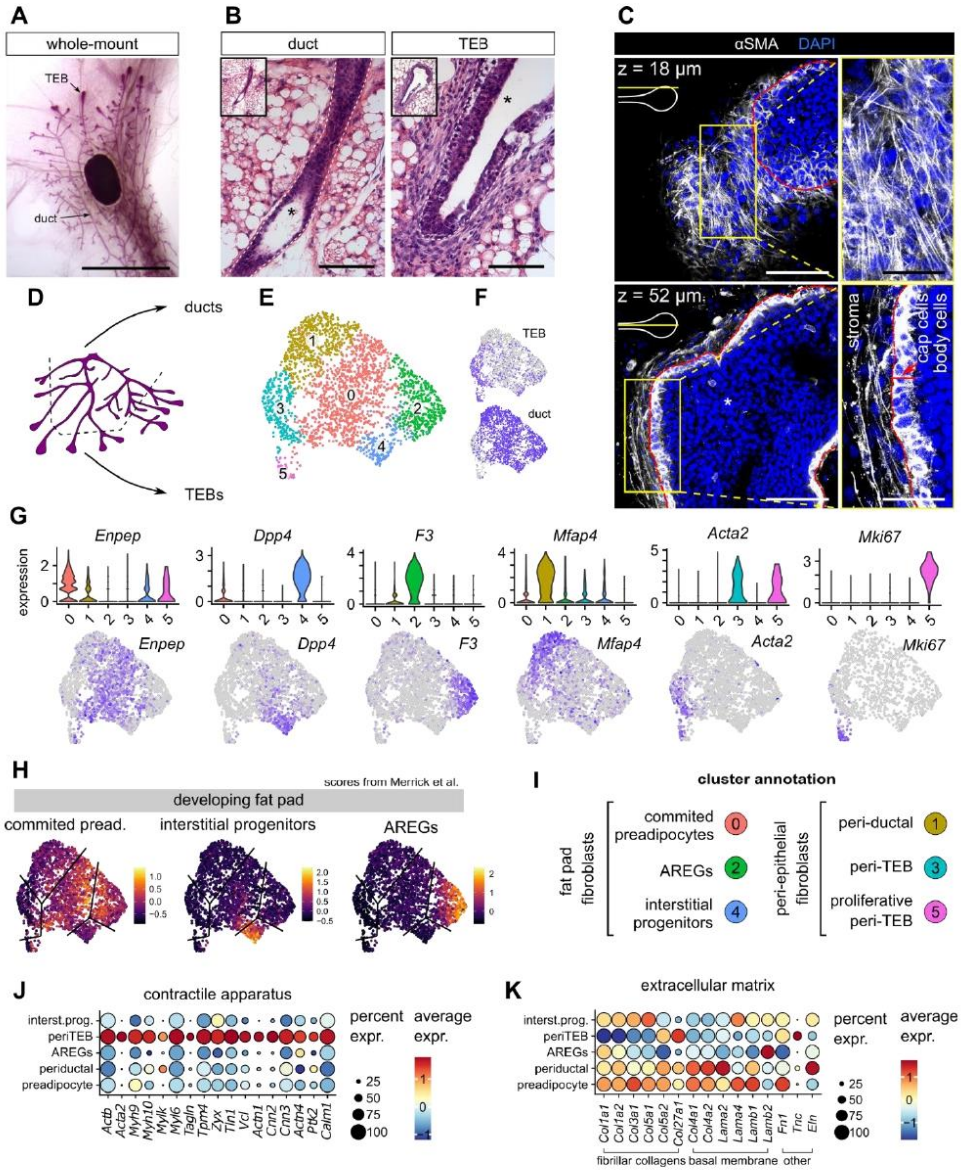

Fig. 1. Single cell RNA sequencing of pubertal mammary fibroblasts

A. A representative image of a pubertal mammary gland from a 5 week old mouse. Scale bar: 1 cm. **B.** Histological detail of epithelial duct and TEB. Scale bar: 100 μm. Ep. marks epithelial compartment. **C.** Immunostaining for αSMA in a cleared mammary gland detects fibroblasts around TEB (TEB borders are delineated by a red line) as well as cap cells of the TEB. Top and middle optical sections of the imaged z stack are presented; their localization according to TEB is indicated by yellow line. The full z-stack is presented in Movie 1. Scale bars: 100 μm, 50 μm in detail. Ep. marks epithelium. **D.** A scheme of microdissected regions of the mammary gland. **E-F.** UMAP of merged mammary fibroblasts showing fibroblast clusters (**E**) and sample of origin (**F**). **G.** Violin plots and UMAPs showing expression of cluster marker genes. **H.** Transcriptomic scores of fibroblasts from developing fat pad (Merrick et al. 2019) plotted over our dataset of mammary fibroblasts. The black lines indicate approximate borders between our 6 clusters. **I.** Annotation of fibroblast clusters. **J, K.** Dot plots showing expression of contractility-related genes (**J**) and genes encoding extracellular matrix (**K**).

Sumbal et al.

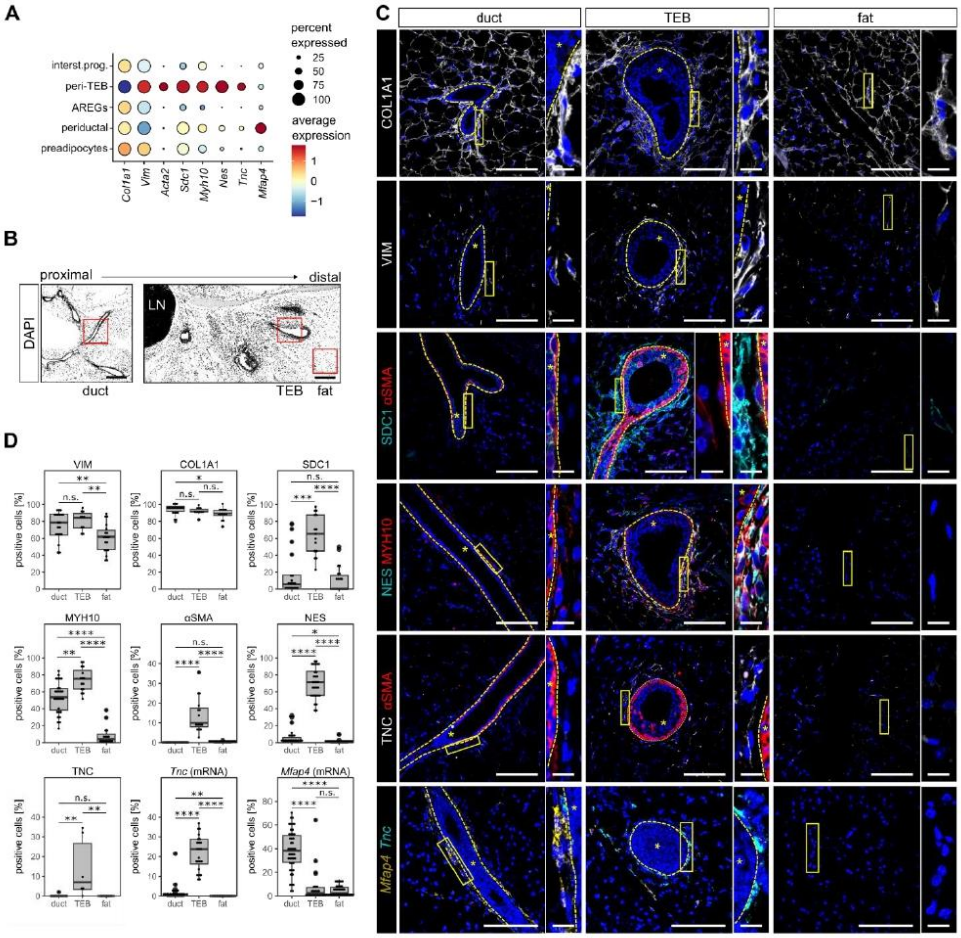

Fig. 2. Spatial atlas of mammary fibroblasts during pubertal morphogenesis

A. A dot plot showing expression of marker genes used for spatial mapping. **B.** An overview of mammary gland on histological slide, red squares show fields of view (FOVs) containing duct, TEB or distal fat pad. Scale bar: 100 µm. **C.** Representative images showing expression of various gene or protein markers in regions containing duct, TEB or distal fat pad, the inset shows detail on fibroblasts. * marks epithelial compartment encircled by yellow dashed line. Scale bar: 100 µm, 10 µm in detail. **D.** Quantification of marker-positive stromal cells in different regions of mammary gland, shown as box plot. Each dot represents a single FOV, n = 3 biological replicates, N = 69 FOVs for VIM, 47 FOVs for COL1A1, 57 FOVs for SDC1, 59 FOVs for MYH10 and αSMA, 83 FOVs for NES, 26 FOVs for TNC, 113 FOVs for *Tnc* and *Mfap4*; statistical analysis: Wilcoxon test.

Sumbal et al.

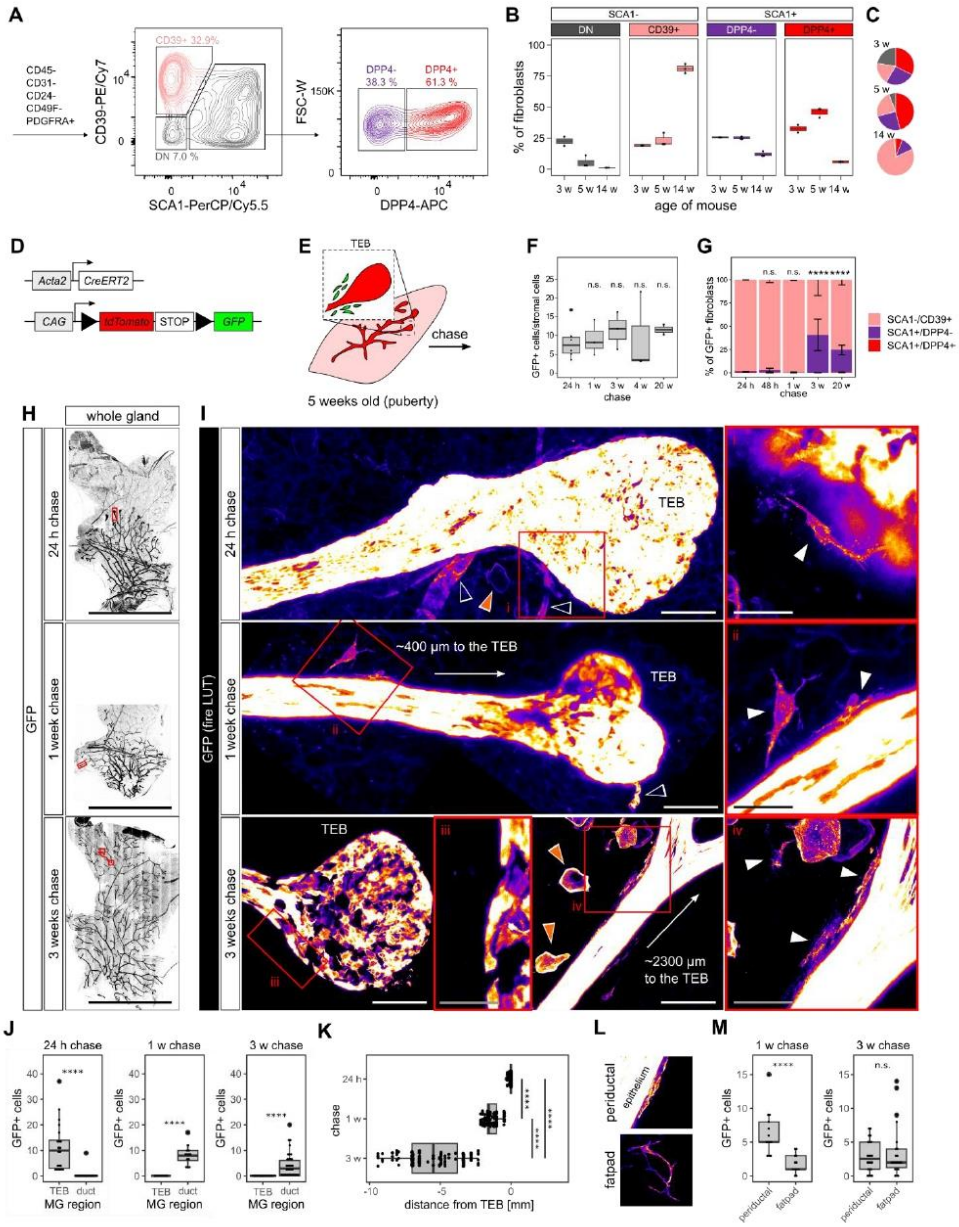
A
CD45-
CD31-
CD24-
CD49F-
PDGFRA+
CD39-PE/Cy7
CD39+ 32.9%
DN 7.0 %
SCA1-PerCP/Cy5.5
FSC-W
DPP4- 38.3 %
DPP4+ 61.3 %
DPP4-APC
B
SCA1-
SCA1+
DN
CD39+
DPP4-
DPP4+
% of fibroblasts
3 w 5 w 14 w
age of mouse
C
3 w
5 w
14 w
D
Acta2
CreERT2
CAG
lsl-tomato
STOP
GFP
E
TEB
chase
5 weeks old (puberty)
F
GFP+ cells/stromal cells
n.s.
24 h 1 w 3 w 4 w 20 w
chase
G
% of GFP+ fibroblasts
24 h 48 h 1 w 3 w 20 w
chase
SCA1-/CD39+
SCA1+/DPP4-
SCA1+/DPP4+
H
whole gland
GFP
24 h chase
1 week chase
3 weeks chase
I
GFP (fire LUT)
TEB
~400 µm to the TEB
~2300 µm to the TEB
J
24 h chase
1 w chase
3 w chase
GFP+ cells
TEB duct
MG region
K
chase
distance from TEB [mm]
L
periductal
epithelium
fatpad
M
1 w chase
3 w chase
GFP+ cells
periductal
fatpad

Sumbal et al.

Fig. 3. Peri-TEB fibroblasts are a transient cell state and do not migrate with the invading epithelium

A. Representative FACS plots dividing mammary fibroblasts into CD39+; SCA1+/DPP4- and SCA1+/DPP4+ populations. **B, C.** Flow cytometry quantification of mammary fibroblast proportions from 3 week, 5 week and 14 week old mice shown as boxplots (**B**) and pie charts (**C**), n = 3 mice per sample. **D.** Schematic representation of the *Acta2-CreERT2;R26-mT/mG* mouse model. **E.** Induction strategy for the chase experiments. **F, G.** Flow cytometry quantification of GFP+ cells out of total stromal cells (**F**) and quantification of the proportion of FACS populations within the GFP+ fibroblasts (**G**); n = 3 mice per time-point, statistical analysis: Wilcoxon (**F**) and chi square test (**G**). **H, I.** Projections of z-stack imaging of whole mammary glands after tamoxifen induction and 24 h-, 1 week- or 3 week-long chase. Red boxes in whole organ overview pictures (**H**) indicate regions presented in **I.** Red boxes in detail pictures of ductal or peri-TEB regions (**I**) indicate magnified regions with GFP+ fibroblasts (i-iv). GFP channel is shown as "fire" lookup table. White arrowheads indicate GFP+ fibroblasts, orange arrowheads indicate GFP+ adipocytes, empty arrowheads indicate GFP+ mural cells. Scale bars: 1 cm in **H**; 100 μm in **I**, 50 μm in detail in **I**. **J.** Quantification of positional distribution of GFP+ fibroblasts after 24 h or 3 weeks of chase; n = 3 mice, N = 38 z-stack for the 24 h chase, 22 z-stacks for 1 week and 51 z-stacks for the 3 weeks chase, statistical analysis: Wilcoxon test. **K.** Quantification of distance of GFP+ fibroblasts from the TEB; n = 3 mice, N = 343 fibroblasts for 24 h, 106 for 1 week and 144 for 3 week-long chase. **L, M.** Representative appearance (**L**) and quantification (**M**) of GFP+ fibroblasts found after 1 or3 weeks of chase. n = 3 mice; N = 22 z-stacks for 1 week and 51 z-stacks for 3 weeks chase (M).

Sumbal et al.

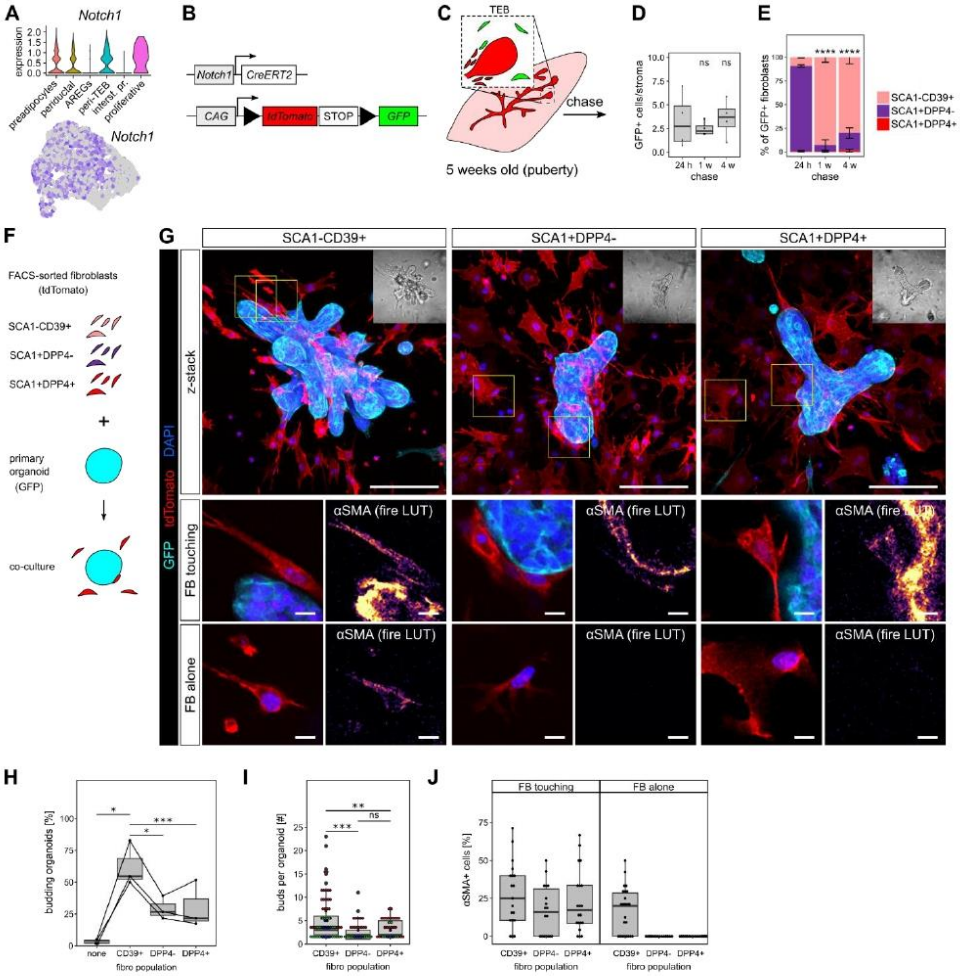

Fig. 4. Growing epithelium recruits peri-TEB fibroblasts from the fat pad

A-E. *Notch1* fibroblast chase experiment. **A.** Violin plot and UMAP expression of *Notch1* in fibroblast clusters. **B.** Schematic representation of the *Notch1-CreERT2;R26-mT/mG* mouse model. **C.** The induction strategy. Flow cytometry quantification of GFP+ cells out of total stromal cells (**D**) and quantification of the proportion of FACS populations within the GFP+ fibroblasts (**E**); n = 3 mice per time-point, statistical analysis: Wilcoxon (D) and chi square test (**E**). **F-J.** Co-culture of sorted fibroblasts with epithelial organoids. **F.** A schematic representation of the experiment. **G.** Representative images of the organoids after 5 days of co-culture with FACS-sorted fibroblasts (organoids in cyan, fibroblasts in red). The inlets show brightfield images of the cultures. The magnified regions (demarcated by yellow lines) provide a detailed view on fibroblasts in contact with the organoid or further away from it in the ECM and their staining for

αSMA. Scale bars: 100 μm and 10 μm in detail. **H.** Quantification of percentage of organoid budding, shown as box plot. Each dot represents a biological replicate, lines connect paired experiments; n = 3 independent experiments, statistical analysis: Student's t-test. **I.** Quantification of the number of buds formed per organoid, each dot represents one organoid, colors code paired experiments; n = 3 independent experiments, N = 91, 40 and 44 organoids for CD39+, DPP4- and DPP4+ population, respectively, statistical analysis: Student's t-test. **J.** Quantification of αSMA+ fibroblasts (FB) in co-cultures, shown as a box plot, each dot shows one organoid; n = 3 independent experiments, N = 24, 18 and 20 organoids for CD39+, DPP4- and DPP4+ population, respectively.

Sumbal et al.

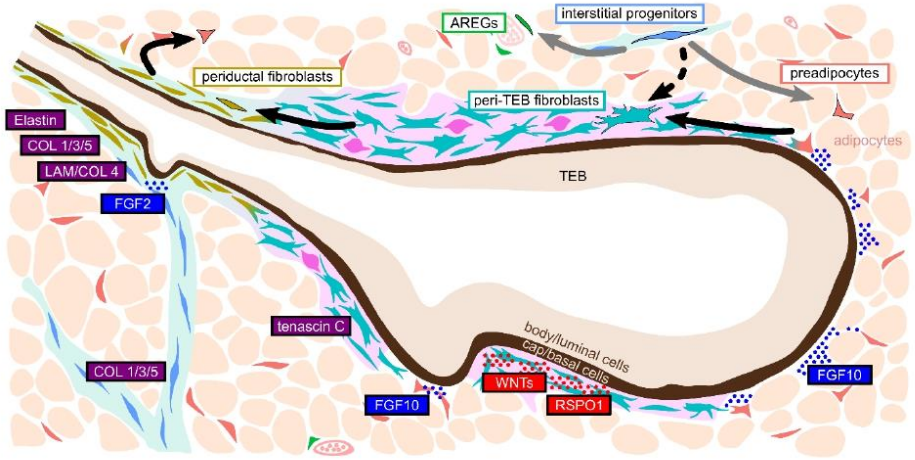

Fig. 5. A scheme: contractile peri-TEB fibroblasts are recruited by the growing epithelium

A schematic representation of our findings. Mammary stroma comprises 5 clusters of fibroblasts (+ proliferative fibroblasts) with distinct spatial locations: peri-TEB fibroblasts surround TEBs, periductal fibroblasts wrap around subtending ducts, interstitial progenitors reside in collagenous fat pad septae, AREGs dwell in blood vessel stroma, and preadipocytes are scattered between adipocytes. Interstitial progenitors have been shown to provide other fat pad fibroblasts (Stefkovic et al. 2021, gray arrows). Our data suggest that fat pad fibroblasts are recruited by the TEB and activated into peri-TEB phenotype, then differentiate into periductal fibroblasts and back to preadipocytes (black arrows). Based on spatial resolution of fibroblast clusters, we predict spatial resolution of ECM (purple), WNT signaling ligands (red) in peri-TEB stroma and FGF signaling ligands (blue) in fat pad and fat pad septae. The dots show expected sites where mammary epithelium encounters FGF/WNT ligands.

Sumbal et al.

Supplementary figures

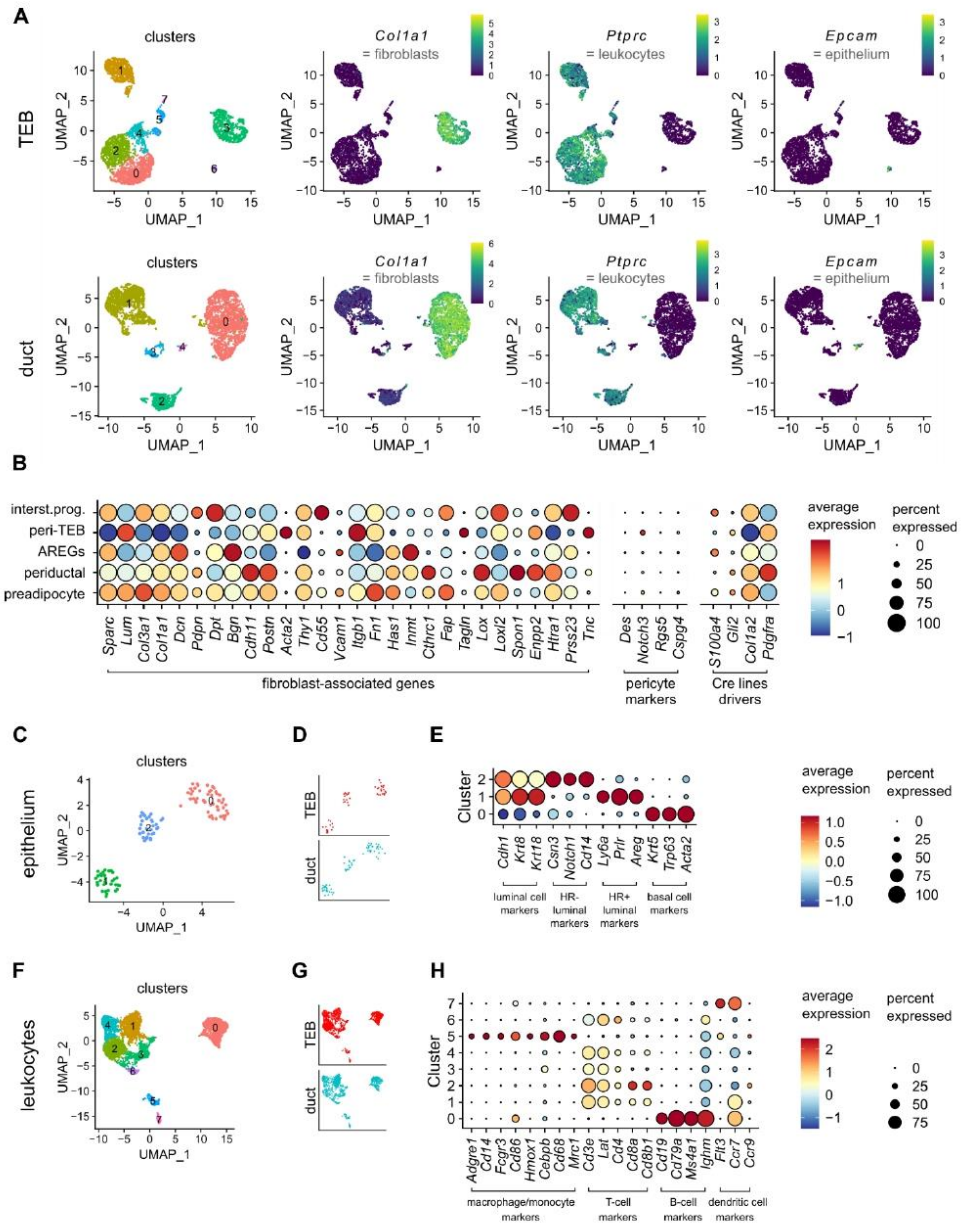

Sumbal et al.

Supplementary figure 1. scRNAseq of pubertal mammary gland

A. UMAP plots showing cell clusters and canonical fibroblast, leukocyte and epithelial cell genes in the micro-dissected samples containing TEBs or ducts. **B.** Dot plot showing expression of fibroblast-associated genes, pericyte maker genes and genes previously used to drive Cre expression in mammary fibroblasts. **C-E.** Analysis of subsets of epithelial cells merged from the TEB and duct samples: UMAPs showing clusters (**C**) and cell origin (**D**), and a dot plot showing expression of epithelial cell type markers (**E**). **F-H.** Analysis of subset of leukocytes merged from TEB and duct sample: UMAPs showing clusters (**F**) and cell origin (**G**), and a dot plot showing expression of immune cell type markers (**H**).

Sumbal et al.

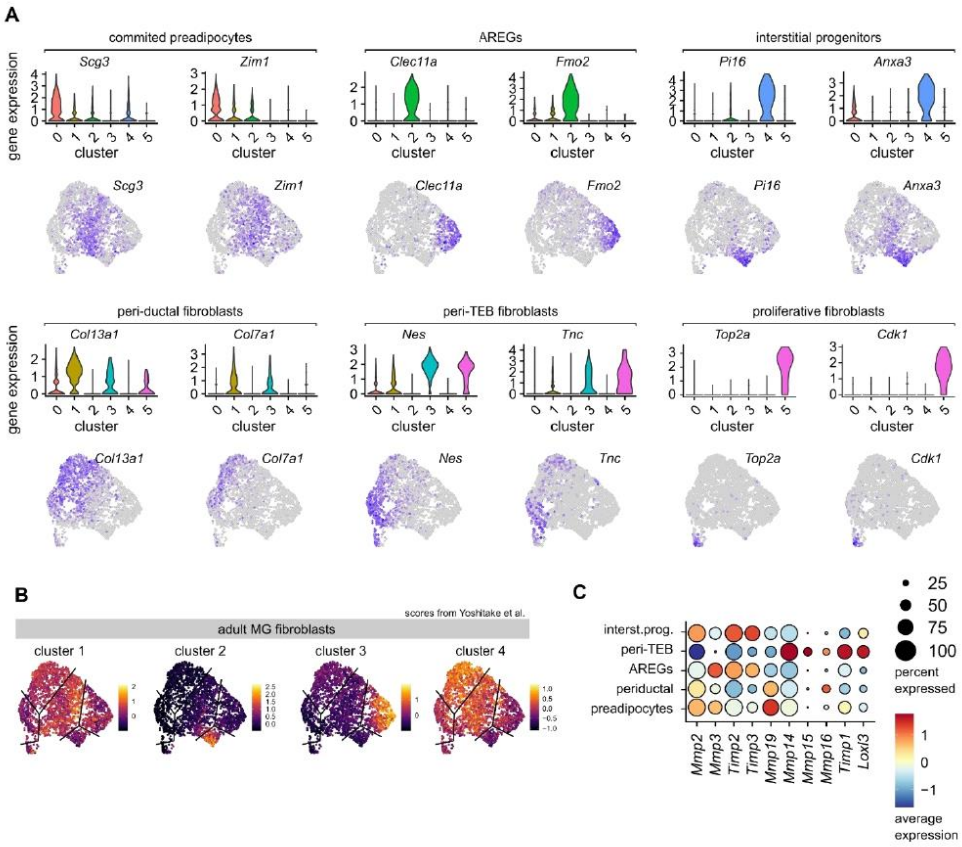

Supplementary figure 2. scRNAseq analysis of pubertal mammary fibroblasts

A. Violin plots and UMAPs showing expression of additional cluster marker genes. **B.** Transcriptomic scores of the 4 clusters of fibroblasts from adult mammary gland (MG) (Yoshitake et al. 2022) plotted over our dataset of mammary fibroblasts. The black lines indicate approximate borders between our 6 fibroblast clusters. **C.** Dot plot showing expression of ECM remodeling genes in our fibroblast clusters.

Sumbal et al.

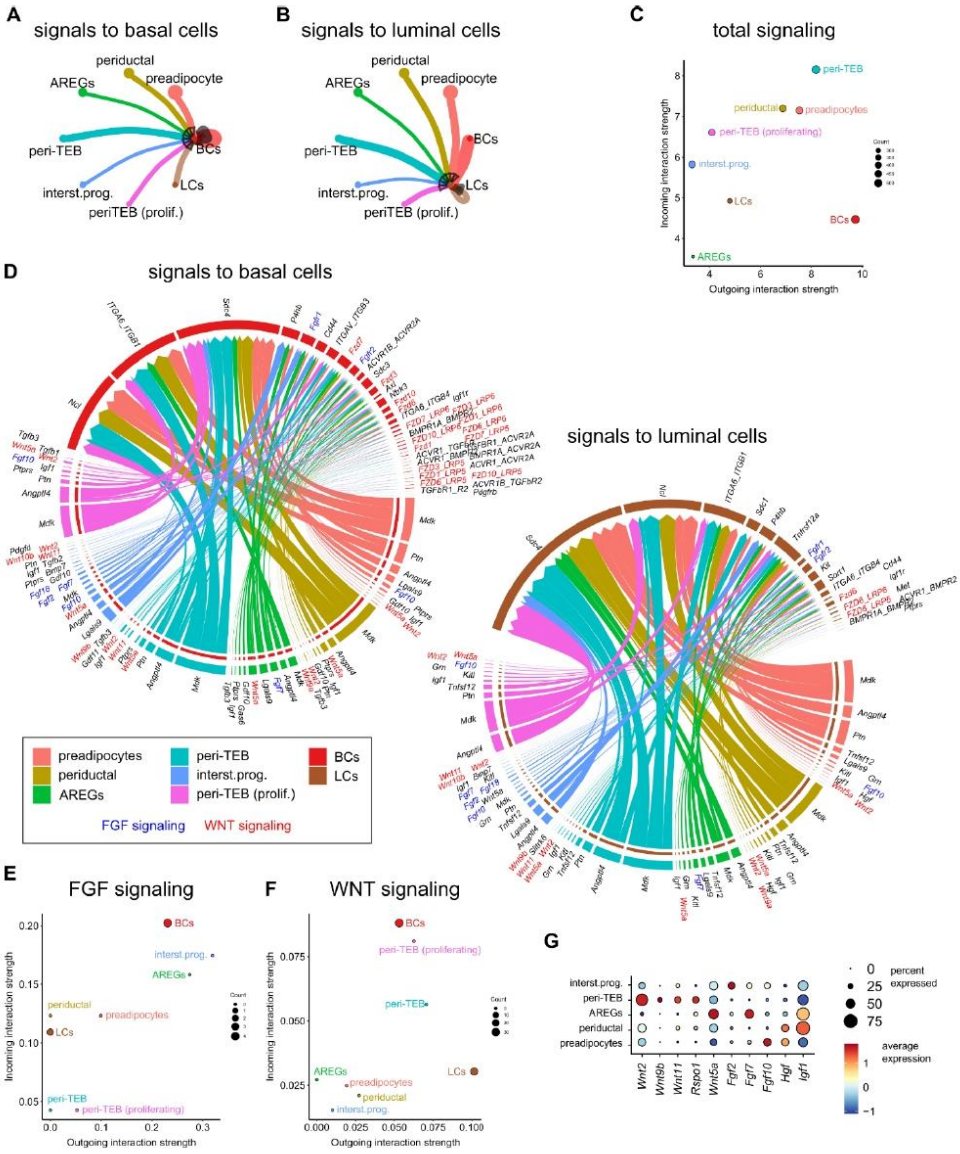

Supplementary figure 3. CellChat analysis of pubertal mammary fibroblast-epithelium interactome

A, B. Quantification of predicted signals originating in fibroblasts and directing into basal (BCs) (**A**) or luminal (LCs) (**B**) epithelial cells. The thickness of the line represents the signal strength.

C. A graph of overall incoming and outgoing signals for single fibroblast clusters and epithelial cells. **D.** Chord diagrams showing predicted signals incoming into basal or luminal epithelial cells from the identified fibroblast clusters. Members of FGF signaling are colored in blue, members of WNT signaling in red. **E, F.** Graphs showing the strength of incoming and outgoing signal of FGF (**E**) and WNT (**F**) signaling. **G.** A dot plot showing expression of selected signaling molecule genes in fibroblast clusters.

Sumbal et al.

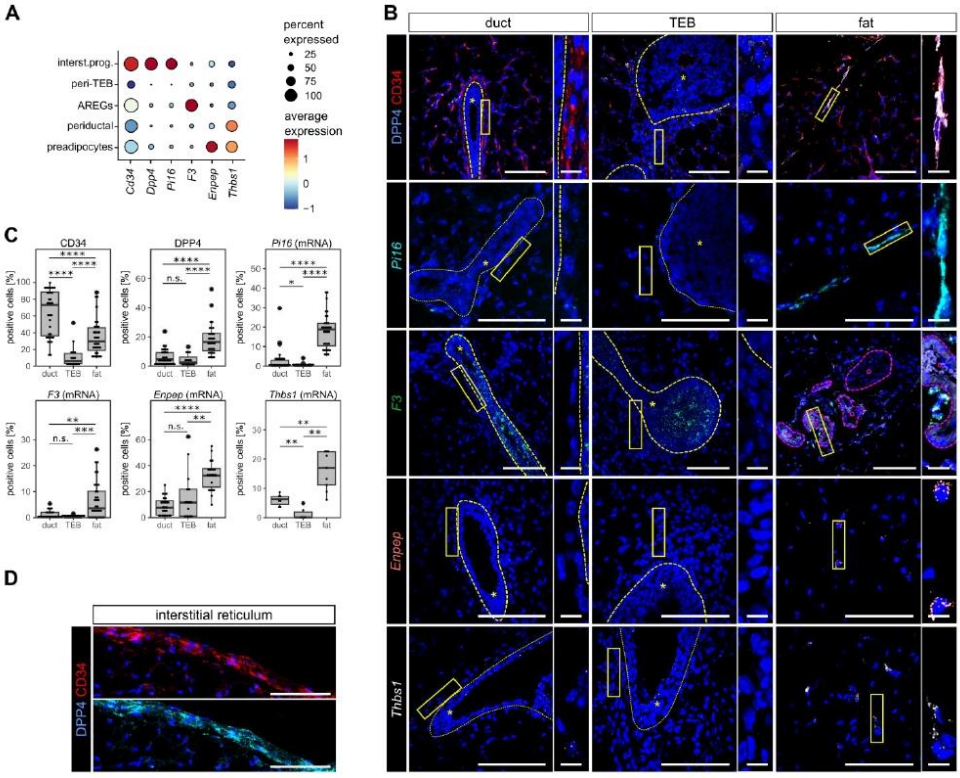

Supplementary figure 4. Detection of fat pad clusters

A. A dot plot showing expression of marker genes used for spatial mapping. **B.** Representative images showing expression of various gene or protein markers in regions containing duct, TEB or distal fat pad. The insets show details on fibroblasts. The dashed yellow line demarcates epithelial compartment, which is indicated by *. The dashed purple line demarcates blood vessel, which is indicated by °. Scale bar: 100 µm, 10 µm in detail. **C.** Quantification of marker-positive stromal cells in different regions of the mammary gland, shown as box plot. The dots show single fields of view (FOV), n = 3 biological replicates, N = 89 FOVs for CD34 and DPP4, 90 FOVs for *Pi16*, 74 FOVs for *F3*, 81 FOVs for *Enpep*, 28 FOVs for *Thbs1*, statistical analysis: Wilcoxon test. **D.** Representative images showing expression of DPP4 and CD34 in interstitial reticulum at the border of the mammary gland (D). Scale bar: 100 µm.

Sumbal et al.

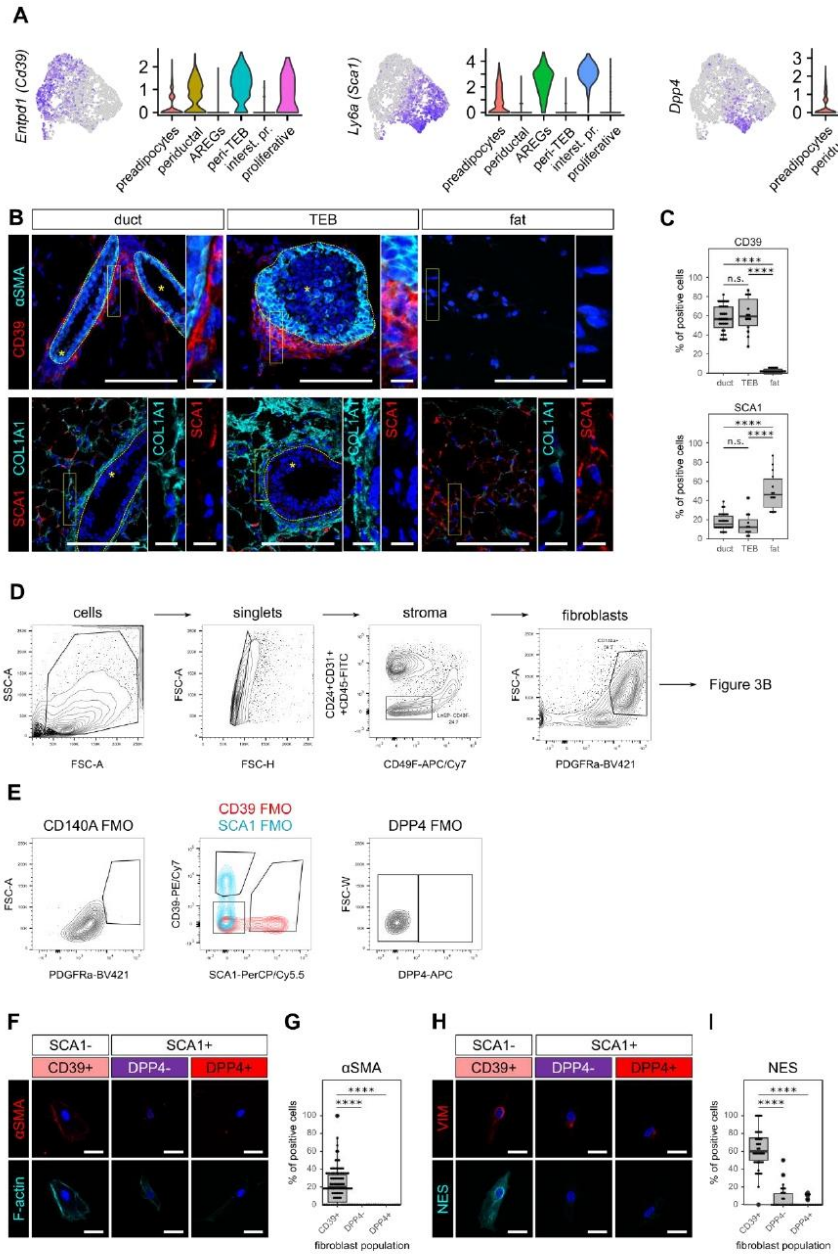
A
Entpd1 (Cd39)
Ly6a (Sca1)
Dpp4
preadipocytes
periductal
AREGs
peri-TEB
interst. pr.
proliferative
B
duct
TEB
fat
CD39
αSMA
COL1A1
SCA1
C
CD39
SCA1
% of positive cells
n.s.
****
D
cells
singlets
stroma
fibroblasts
SSC-A
FSC-A
FSC-H
CD24+CD31+ +CD45-FITC
CD49F-APC/Cy7
PDGFRa-BV421
Figure 3B
E
CD140A FMO
CD39 FMO
SCA1 FMO
DPP4 FMO
FSC-W
CD39-PE/Cy7
SCA1-PerCP/Cy5.5
DPP4-APC
F
SCA1-
SCA1+
CD39+
DPP4-
DPP4+
αSMA
F-actin
G
αSMA
fibroblast population
H
VIM
NES
I
NES

Sumbal et al.

Supplementary figure 5. Flow cytometry analysis of mammary fibroblasts.

A. UMAPs and violin plots showing expression of *Entpd1*, *Ly6a* and *Dpp4* in mammary fibroblasts. **B.** Representative images showing expression of CD39 and SCA1 in regions containing duct, TEB or distal fat pad. The insets show detail on fibroblasts. The dashed yellow line demarcates epithelial compartment, which is indicated by *. Scale bars: 100 μm, 10 μm in detail. **C.** Quantification of marker positive stromal cells in different regions of mammary gland, shown as box plot, the dots show single fields of view (FOV), n = 3 biological replicates, N = 68 FOVs for CD39 and 55 FOVs for SCA1, statistical analysis: Wilcoxon test. **D.** Representative flow cytometry scatter plots showing initial gating of isolated mammary gland cells, further gating of fibroblasts is shown in Figure 3A. **E.** Fluorescence minus one (FMO) controls for the experiment in D and Figure 3A. **F-I.** Characterization of peri-TEB marker expression. Representative images (**F**) and quantification (**G**) of αSMA expression in FACS-sorted populations of mammary fibroblasts. **H, I.** Representative images (**H**) and quantification (**I**) of NES expression in FACS-sorted populations of mammary fibroblasts. The dots of box plots in G and I represent single FOVs, n = 2 and 3 independent experiments for αSMA and NES, respectively; N = 848 cells in CD39+, 147 cells in DPP4- and 237 cells in DPP4+ population for αSMA; N = 479 cells in CD39+, 251 cells in DPP4- and 226 cells in DPP4+ population for NES. Scale bars: 10 μm.

Sumbal et al.

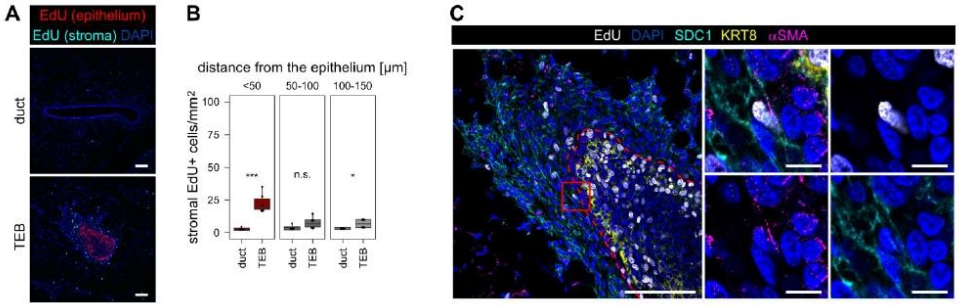

Supplementary figure 6. Detection of proliferation in pubertal mammary stroma

A-C. Detection of EdU incorporation after 2 h pulse on histological sections of the mammary gland. **A.** EdU signal is separated by manually drawing a mask in stromal and epithelial areas. Scale bar: 100 µm. **B.** Quantification of EdU+ stromal cells in relation to distance from the epithelial structures; n = 11 fields of view, statistical analysis: Wilcoxon test. **C.** Micrograph of the TEB from **A** showing an EdU+ αSMA+ SDC1+ peri-TEB fibroblast. Scale bar: 100 µm, 10 µm in detail.

Sumbal et al.

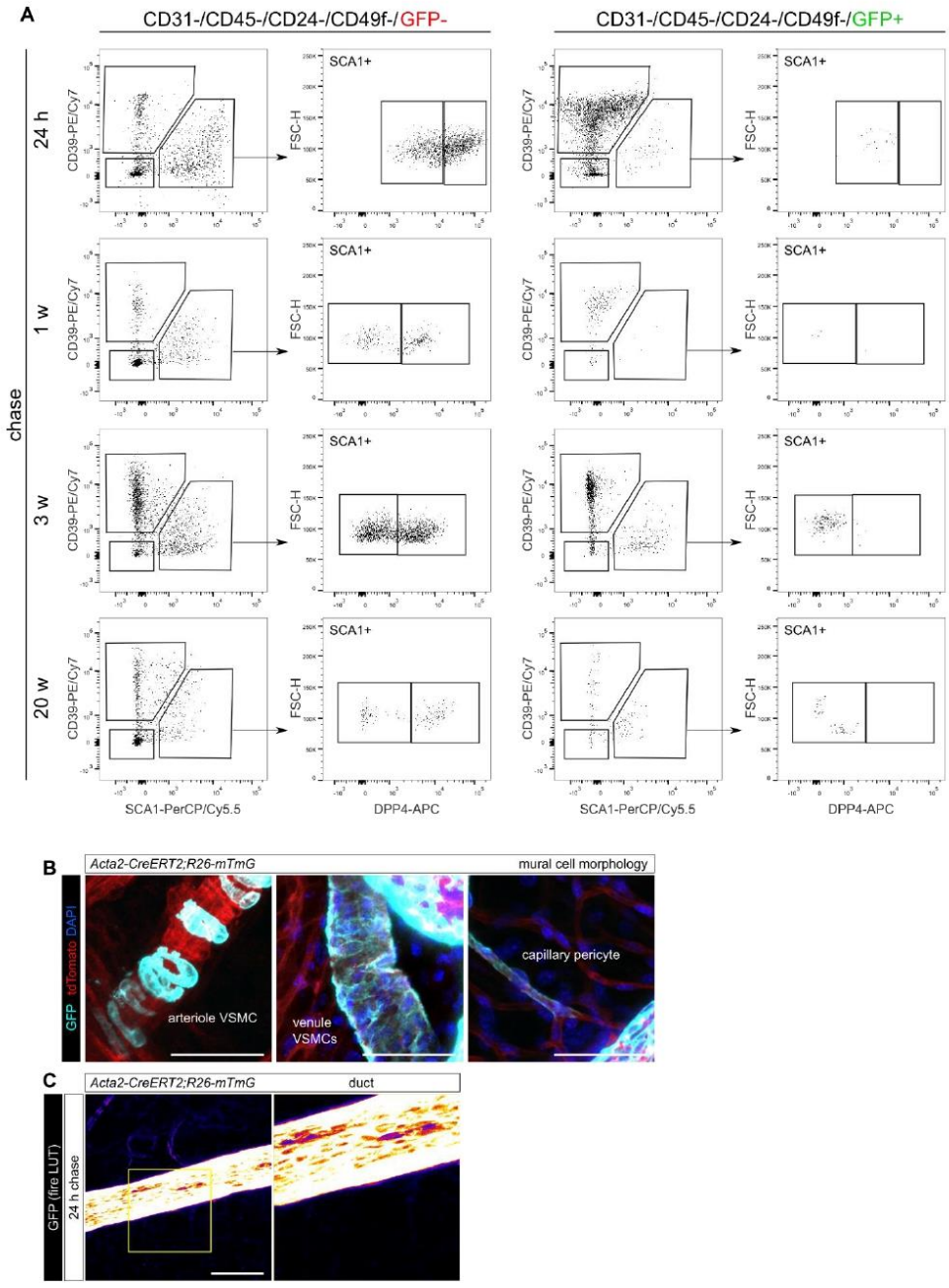
A
CD31-/CD45-/CD24-/CD49f-/GFP-
CD31-/CD45-/CD24-/CD49f-/GFP+
chase
24 h
1 w
3 w
20 w
CD39-PE/Cy7
FSC-H
SCA1+
SCA1-PerCP/Cy5.5
DPP4-APC
B
Acta2-CreERT2;R26-mTmG
mural cell morphology
GFP tdTomato DAPI
arteriole VSMC
venule VSMCs
capillary pericyte
C
Acta2-CreERT2;R26-mTmG
duct
GFP (fire LUT)
24 h chase

Sumbal et al.

Supplementary figure 7. Fibroblast tracing in the Acta2-CreERT2;R26-mTmG mouse model

A. Representative flow cytometry scatter plots showing gating of fibroblast populations in GFP- and GFP+ stromal cells, used in quantification in Figure 3G. **B.** Representative images of mural cells visualized with the *Acta2-CreERT2;R26-mTmG*: vascular smooth muscle cells (VSMCs) and pericytes show characteristic shape and association with blood vessels. **C.** Z-stack and magnification of a duct from *Acta2-CreERT2;R26-mTmG* mouse induced with a 24 h pulse of tamoxifen (shown in Figure 3I). GFP channel is shown as "fire" lookup table (LUT). Scale bar: 100 μm.

Sumbal et al.

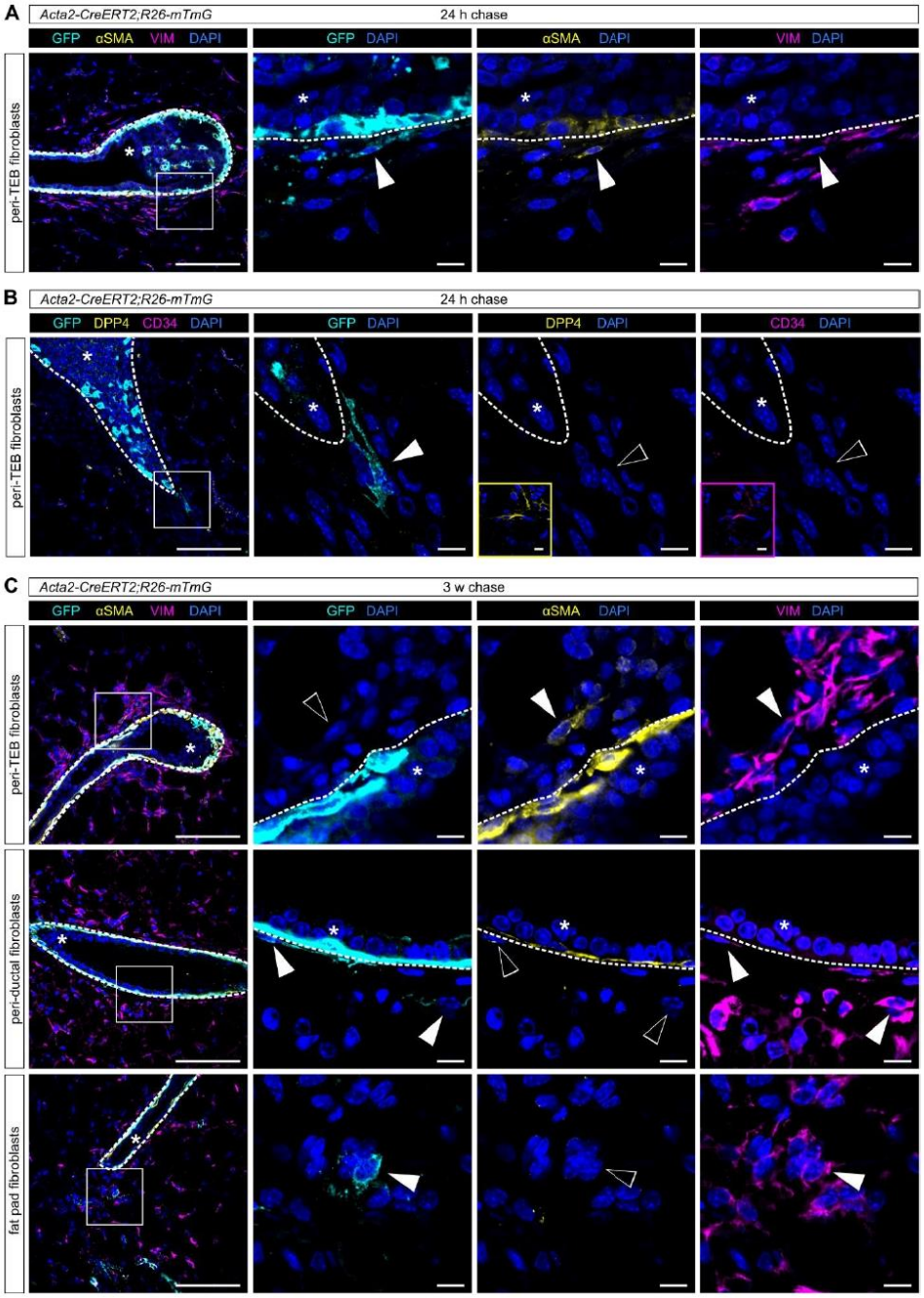

50

Sumbal et al.

Supplementary figure 8. Immuno-histological analysis of traced fibroblasts in the Acta2-CreERT2;R26-mTmG mouse model

A-C. Representative images of mammary TEBs of an *Acta2-CreERT2;R26-mTmG* mouse induced with tamoxifen at 5 weeks of age and after a 24 h (**A, B**) or 3 week (**C**) chase, with details zooming on GFP+ fibroblasts, stained for VIM and αSMA (**A, C**) or CD34 and DPP4 (**B**). The yellow and magenta insets in **B** show positive staining of fat pad fibroblasts photographed in the same section. The dashed white line demarcates epithelial compartment, which is indicated by *. Full white arrowheads point out positive staining, empty arrowheads point out negative staining. Scale bars: 100 μm, 10 μm in detail.

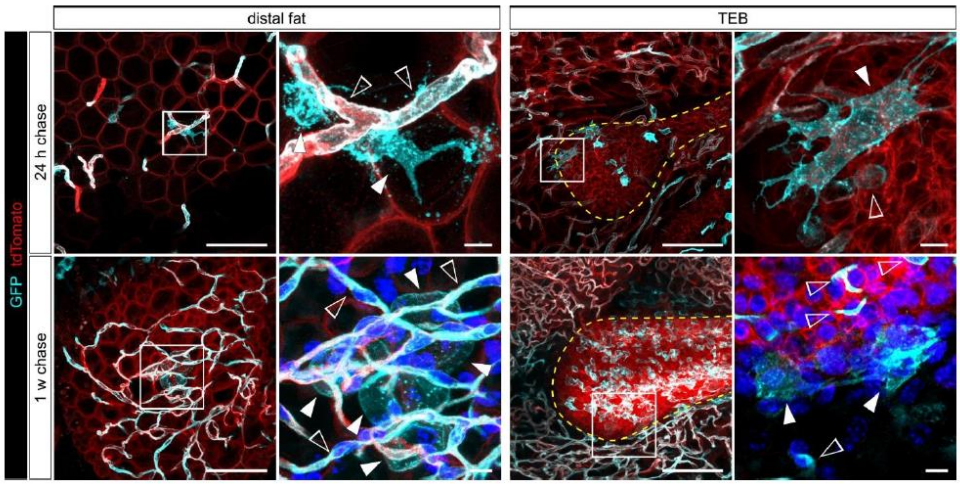

Supplementary figure 9. Fibroblast visualization in the Notch1-CreERT2;R26-mTmG cleared mammary glands

A distal fat pad region and a TEB region of a *Notch1-CreERT2;R26-mTmG* mice induced with a tamoxifen pulse and chased for 24 h (top panel) or 1 week (bottom panel). Full white arrowheads show GFP+ fibroblasts or adipocytes, empty arrowheads show GFP+ epithelial or endothelial cells. Scale bars: 100 μm, 10 μm in detail.

Sumbal et al.

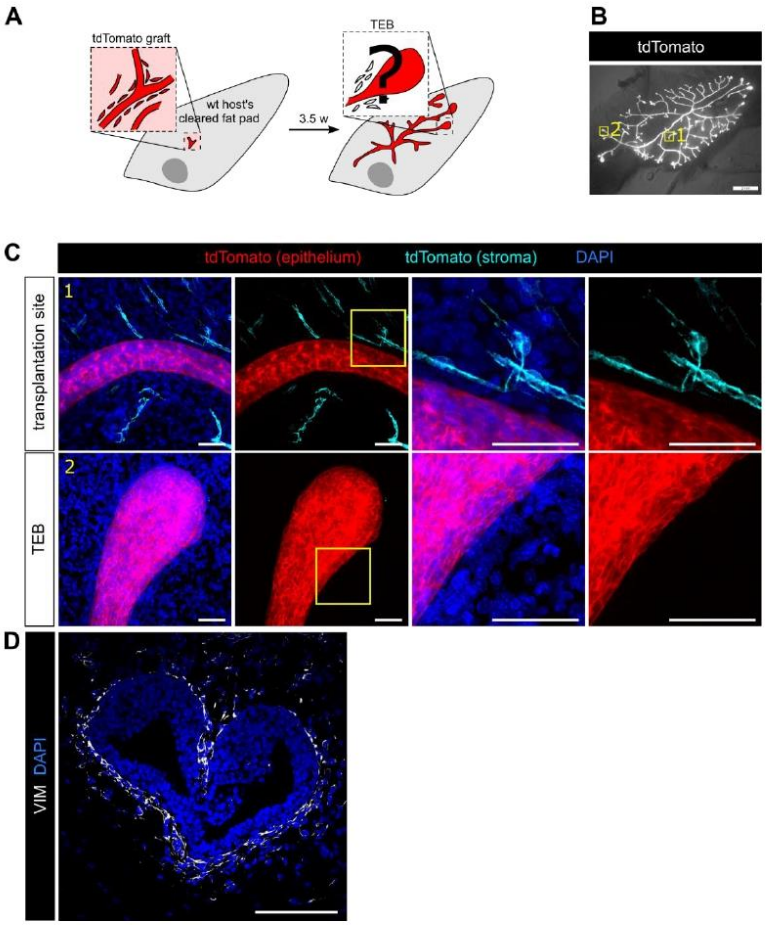

Supplementary figure 10. tdTomato+ mammary fragment transplantation in wild-type host

A. A scheme depicting the transplantation of a tdTomato+ tissue fragment containing epithelial duct with surrounding stroma in a wild-type (wt) host cleared fat pad. **B.** A representative outgrowth of a regenerated gland 3.5 w after transplantation. Areas marked by yellow squares are zoomed-in in **C**. Scale bar: 1 mm. **C**. Z-stacks of the transplantation site (1) and a TEB (2). The tdTomato signal was divided into epithelial (red) and stromal (turquoise) using manually drawn masks based on morphology. The yellow squares indicate magnified areas. Scale bars: 50 μm. **D.** Staining of VIM on histological section of a TEB of a transplanted mammary gland shows the abundant presence of fibroblasts around the TEB. Scale bars: 100 μm.

Sumbal et al.

Supplementary tables

Supplementary table 1: the gene scores

Study	Cluster	Genes									
Merrick et al. 2019	**Group 1**	Ark1c18	Cd55	anxa3	Pi16	Sema3c	Gap43	Bmp7	Dect2	Dpp4	Wnt2
Merrick et al. 2019	**Group 2**	Ggt5	Fabp4	Pparg	Vcam1	Bmper	Cd36	Rarres2	Apoe	Icam1	
Merrick et al. 2019	**Group 3**	Fmo2	Vit	Ifitm1	Gdf10	Clec11a	F3				
Yoshitake et al. 2022	**Fib_0**	Pi16	Anxa3	Sema3c	Myoc	Igfbp5	Akr1c18	Cd55	Smpd3	Ackr3	Dpp4
Yoshitake et al. 2022	**Fib_1**	Fabp4	Lpl	Col4a1	Sparcl1	Cxcl14	Hmgcs1	Col6a3	Smoc2	Col5a3	Col4a2
Yoshitake et al. 2022	**Fib_2**	Postn	Mfap4	Scg3	Penk	Tnc	Apoe	Enpp2	Mdk	Srpx	Thbs1
Yoshitake et al. 2022	**Fib_3**	Gdf10	F3	Gas6	Cxcl12	Cst3	Tmem176b	Fmo2	Inmt	Mgp	Il6

Supplementary table 1. The genes used for transcriptomic scores in Figure 1 and Supplementary figure 2

Sumbal et al.

Supplementary table 2: antibodies and probes used

whole-mount staining (CUBIC)						
target	**manufacturer**	**Reference #**	**species**	**clone**	**concentration**	**conjugate**
ACTA2	Sigma	C6198	mouse	1A4	1/300	Cy3
IHC-IF						
target	**manufacturer**	**Reference #**	**species**	**clone**	**concentration**	**conjugate**
COLA1A	Cell Signaling Technologies	#72026	rabbit	E8F4L	1/100	N/A
VIM	Cell Signaling Technologies	#5741	rabbit	D21H3	1/400	N/A
ACTA2	Sigma	A2547	mouse	1A4	1/300	N/A
SDC1	BD	#553712	rat	281-2	1/400	N/A
NES	Chemicon	MAB353	mouse	rat401	1/100	N/A
MYH10	BioLegend	#909901	rabbit	polyclonal	1/200	N/A
TNC	R&D	MAB2138	rat	#578	1/30	N/A
DPP4	Abcam	ab187048	rabbit	EPR18215	1/200	N/A
CD34	Abcam	ab8185	rat	MEC 14.7	1/50	N/A
CD39	Cell Signaling Technologies	#14481	rabbit	E2X6B	1/200	N/A
KRT8	DSHB	TROMA-I	rat	TROMA-I	1/200	N/A
GFP	Novus Biologicals	NB100-1614	chicken	polyclonal	1/300	N/A
SCA1	A Becton Dickinson co.	553334	rat	E13-161.7	1/100	biotin
ICC-IF						
target	**manufacturer**	**Reference #**	**species**	**clone**	**concentration**	**conjugate**
ACTA2	Sigma	A2547	mouse	1A4	1/300	N/A
VIM	Cell Signaling Technologies	#5741	rabbit	D21H3	1/200	N/A
NES	Chemicon	MAB353	mouse	rat401	1/100	N/A
phalloidin	Sigma		N/A	N/A	1/300	AF488
IF organoids						
target	**manufacturer**	**Reference #**	**species**	**clone**	**concentration**	**conjugate**
ACTA2	Sigma	C6198	mouse	1A4	1/300	Cy3
ACTA2	Sigma	A2547	mouse	1A4	1/300	N/A
flow cytometry/FACS						
target	**manufacturer**	**Reference #**	**species**	**clone**	**concentration**	**conjugate**
CD45	BD	#561037	rat	30-F11	1/200	APC/Cy7
CD31	BioLegend	#102439	rat	390	1/200	APC/Cy7
CD24	BioLegend	#101849	rat	M1/69	1/200	APC/Cy7
CD49f	BioLegend	#313628	rat	GoH3	1/200	APC/Cy7
CD140A	BioLegend	#135923	rat	APA5	1/50	BV421
CD39	eBioscience	25-0391-80	rat	24DMS1	1/200	PE/Cy7
SCA1	BioLegend	#108123	rat	D7	1/200	PerCP/Cy5.5
DPP4	BioLegend	#137807	rat	H194-112	1/200	APC
ISH probes						
Target	**Manufacturer**	**Reference #**	**channel**			
Mfap4	ACD	421391	C1			
Tnc	ACD	465021-C2	C2			
Pi16	ACD	451311-C3	C3			
F3	ACD	448691	C1			
Enpep	ACD	862211-C3	C3			
Thbs1	ACD	457891-C3	C3			

Supplementary figure 2. Antibodies and probes used